بسم الله الرحمن الرحيم

Mathematical Observation for Peristaltic flows of Nanofluid in an Endoscope

By

Nuzhat Irshad

Department of Mathematics
Quaid-I-Azam University
Islamabad, Pakistan
2020

Mathematical Observation for Peristaltic flows of Nanofluid in an Endoscope

By

Nuzhat Irshad

Supervised
Prof. Dr. Sohail Nadeem

Department of Mathematics
Quaid-I-Azam University
Islamabad, Pakistan
2020

Mathematical Observation for Peristaltic flows of Nanofluid in an Endoscope

By

Nuzhat Irshad

A THESIS SUBMITTED IN THE PARTIAL FULFILLMENT OF THE REQUIREMENT FOR THE DEGREE OF

DOCTOR OF PHILOSOPHY

IN

MATHEMATICS

Supervised by

Prof. Dr. Sohail Nadeem

Department of Mathematics
Quaid-I-Azam University
Islamabad, Pakistan
2020

Author's Declaration

I, **Nuzhat Irshad,** hereby state that my PhD thesis titled **Mathematical Observation for Peristaltic flows of Nanofluid in an Endoscope** is my own work and has not been submitted previously by me for taking any degree from the Quaid-I-Azam University Islamabad, Pakistan or anywhere else in the country/world.

At any time if my statement is found to be incorrect even after my graduate the university has the right to withdraw my PhD degree.

Name of Student: **Nuzhat Irshad**

Date: **19-May-2020**

Plagiarism Undertaking

I solemnly declare that research work presented in the thesis titled "**Mathematical Observation for Peristaltic flows of Nanofluid in an Endoscope**" is solely my research work with no significant contribution from any other person. Small contribution/help wherever taken has been duly acknowledged and that complete thesis has been written by me.

I understand the zero tolerance policy of the HEC and **Quaid-i-Azam University** towards plagiarism. Therefore, I as an Author of the above titled thesis declare that no portion of my thesis has been plagiarized and any material used as reference is properly referred/cited.

I undertake that if I am found guilty of any formal plagiarism in the above titled thesis even afterward of PhD degree, the University reserves the rights to withdraw/revoke my PhD degree and that HEC and the University has the right to publish my name on the HEC/University Website on which names of students are placed who submitted plagiarized thesis.

Student/Author Signature

Name: **Nuzhat Irshad**

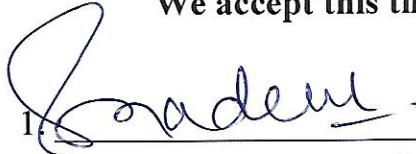# Mathematical Observation for Peristaltic flows of Nanofluid in an Endoscope
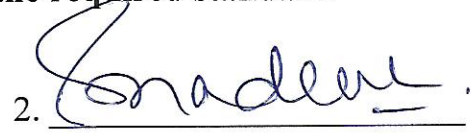
By
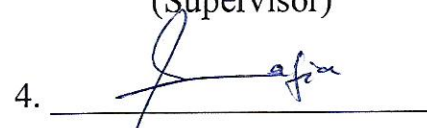
Nuzhat Irshad

CERTIFICATE

A THESIS SUBMITTED IN THE PARTIAL FULFILLMENT OF THE
REQUIREMENTS FOR THE DEGREE OF THE

DOCTOR OF PHILOSOPHY IN MATHEMATICS

We accept this thesis as conforming to the required standard

1. **Prof. Dr. Sohail Nadeem**
   (Chairman)

2. **Prof. Dr. Sohail Nadeem**
   (Supervisor)

3. **Dr. Rahmat Ellahi**
   (External Examiner)

4. **Dr. Safia Akram**
   (External Examiner)

Department of Mathematics & Statistics
International Islamic University, Sector H-10
Islamabad.

Department of Mathematics, Miltary
College of Signals, NUST, Rawalpindi.

Department of Mathematics
Quaid-I-Azam University
Islamabad, Pakistan
2020

Certificate of Approval

This is to certify that the research work presented in this thesis entitled **Mathematical Observation for Peristaltic flows of Nanofluid in an Endoscope** was conducted by **Ms. Nuzhat Irshad** under the kind supervision of **Prof. Dr. Sohail Nadeem**. No part of this thesis has been submitted anywhere else for any other degree. This thesis is submitted to the Department of Mathematics, Quaid-i-Azam University, Islamabad in partial fulfillment of the requirements for the degree of Doctor of Philosophy in field of Mathematics from Department of Mathematics, Quaid-i-Azam University Islamabad, Pakistan.

Student Name: **Nuzhat Irshad**   Signature:_____

External committee:

    a) **External Examiner 1**:   Signature:_____
        Name**: Dr. Rahmat Ellahi**
        Designation: Associate Professor
        Office Address: Department of Mathematics & Statistics, Faculty of Basics Applied Sciences International Islamic University, Islamabad.

    b) **External Examiner 2**:   Signature:_____
        Name: **Dr. Safia Akram**
        Designation: Associate Professor
        Office Address: Department of Mathematics, Miltary College of Signals, NUST, Rawalpindi.

    c) **Internal Examiner**   Signature:_____
        Name: **Prof. Dr. Sohail Nadeem**
        Designation: Professor
        Office Address: Department of Mathematics, QAU Islamabad.

    Supervisor Name: Signature:_____
    Prof. Dr. Sohail Nadeem

    Name of Dean/ HOD   Signature:_____

    Prof. Dr. Sohail Nadeem

In the Name of Allah, The Most Merciful, The most Gracious

Acknowledgement

"O my lord! Open for me my chest, And ease my task for me, And make loose the knot from my tongue, that they understand my speech"

Praise be to **Allah**, his majesty for his uncountable blessings and making me enable to proceed in this dissertation successfully. The best prayers and peace be unto **Holy Prophet Hazrat Muhammad S.A.W.W** the pure descendent, and his family and his noble companions. I express my humble gratitude for his guidance to right path, teachings of patience, motivation and immense knowledge.

NO research is possible without infrastructure and requisite materials and resource. At the very outset, I express my deepest thanks to **Quaid-I-Azam University** for all the academic support to complete my degree as a PhD student.

I owe my gratitude to my esteemed supervisor **Prof. Dr Sohail Nadeem** for providing me this great opportunity to do my doctoral program under his guidance and to learn from his research expertise. His support and advice helped me throughout my research and writing of this thesis. Similar, profound gratitude goes to all my teachers for their valuable support during my student career.

I wish to express my heartiest thanks and gratitude to my Parents **Mr. and Mrs. CH Irshad Ullah**, the ones who can never ever be thanked enough for their overwhelming love, kindness and care they bestow upon me. They supported me financially as well as morally and without their guidance it would not been possible

for me to complete my higher education. I also owe my gratitude to my loving brothers **Aamir Gondal** and **Qaiser Gondal** and their wives **Sana** and **Zainab** for being there for me. **Rameen** and **Ashfa** had been great motivation all the time and **Hashir** played a vital role as well. I would not be who I am today without you all.

Special mention goes to my dear husband **Rashid Javed** for his guidance support and encouragement during this work. His presence taught me to get through the hardship and frustration. He helped me keep things in perspective. I am indebted to him for giving me this feeling of fulfillment in life. A heartiest thanks to my daughter **Eshaal Fatima** for having patience with me in this time.

I have great pleasure in acknowledging my gratitude to my friends, colleagues and fellow research scholars at QAU. My profound thanks and best wishes go to my friends **Saima Mehboob, Madiha Bibi, Humera** and **Sadia**. I also want to thank **D. Iqra Shahzadi, Dr Tanzila Hayat, Dr Maryam, Dr Madiha** And **Dr Noor** for their help and suggestions.

Finally my heart felt regard goes to my father in law and mother in law **Mr. and Mrs. Javed Ahmed** for their love and moral support.

I thank Allah Almighty for giving me the strength and patience to work through all these years so that I can stand proudly with my head held high.

Nuzhat Irshad

19.05.2020

Contents

Nomenclature

English words	
d	Darcy number
c	wave speed
R^*	radius
n	power law index
W_e	Weissenberg number
M	Hartmann number
p	pressure
a_1	half width of endoscope
a_2	half width of tube
q	flow rate
E_3	viscous damping force parameter
E_2	stiffness parameter
E_1	rigidity parameter
N_T	thermophoresis parameter
N_b	Brownian motion parameter
R_e	Reynolds number
G_r	Grashof number
B_r	local nanoparticle Grashof number
J_o	current density distribution
R_m	magnetic Reynolds number
b	wave amplitude
T_o, T_1	constant temperature on walls
u, v, w	components of velocity
r, z	radial and axial directions
k	curvature parameter
C_o, C_1	nanoparticles concentration on walls
S	Strommer's number

Greek words	
γ	heat source parameter
δ	wave number
α	viscosity parameter
ζ	curvature parameter
ς	magnetic diffusivity
ϕ	radius of the endoscopic tube
λ	wavelength
φ	nanoparticle volume
κ	thermal slip
ε	amplitude ratio
σ	nanoparticle concentration
θ	temperature
μ_{hnf}	Hybrid nanofluid viscosity
μ_{nf}	Nanofluid viscosity
μ_f	Base fluid viscosity
k_{hnf}	thermal conductivity of the hybrid nanofluid
k_{nf}	thermal conductivity of the nanofluid
k_f	thermal conductivity of the fluid
$(\rho c_p)_{nf}$	heat capacity of nanofluid
σ_{nf}	electrical conductivity of nanofluid
$(\rho c_p)_f$	heat capacity of fluid
σ_f	electrical conductivity of basefluid
k_s	thermal conductivity of the solid particle
$(\rho c_p)_s$	heat capacity of solid particle
σ_s	electrical conductivity of solid particle

Chapter 1

Introduction

The continuous process of wave contraction and relaxation along the boundary causing the fluid to flow is termed as peristaltic pumping. This is an eminent mechanism in physiology of fluid flows. Peristaltic phenomena is quite significant in engineering and applied mathematics as well, because of its huge involvement in real life it has gained limelight among many researchers. It is tracked back to 1966 when Latham [1] did the inaugural work in this direction and studied peristaltic pumping. Afterwards number of researchers are inspired by the topic and they analyzed peristaltic phenomena of different situations $[2-6]$. It has many applications in biological field when there is no direct contact of transmitting matter with any other part except the inner surface of walls, which makes it very effective for transmitting the fluid to short distance without infecting it . Some medical examples are passage of food through esophagus, movement of ovum in the fallopian tube, transport of urine from kidney to bladder, movement of spermatozoa in the ductus efferents of reproductive tract, blood vessels vasomotion, chyme movement in intestines and many more. Numerous advanced mechanical applications are invented on the pumping principle of peristalsis for the transportation of fluid in the absence of internal operational components. Such devices include peristaltic transport of treacherous fluid in nuclear reactors, heart lung machine, finger and roller pumps, cell separation etc. A variety of hose pumps also follow the working essence of peristalsis.

Non-Newtonian fluid, is the class of fluids that do not follow Newton's law of viscosity e.g. shampoos, soaps, sugar solutions, honey, tomato ketchup etc. A single constitutive equation is not enough to completely characterize the diverse rheological properties of such fluids. Because

of the significance of non-Newtonian fluids, numerous researchers have examined peristaltic transport in distinct flow configuration in several aspects. Kalantan et al. [7] studied peristaltic transport in curved channel for non-Newtonian fluid by numerical technique. Ali et al. [8] analyzed peristaltic transport through curved channel by considering the micropolar fluid. Peristaltic flow of couple stress fluid in an asymmetric channel with hall effects was examined by Hayat et al. [9]. Singh [10] presented the Rabinowitsch fluid model for curved slider bearings and deduced the results for shear thickening, shear thinning and Newtonian fluids. Jothi at el. [11] analyzed the Prandtl fluid in a symmetric channel under magnetic field impact by using long wavelength and low Reynolds number approximation. Nadeem and Maraj [12] studied the hyperbolic tangent fluid in curved channel. Moreover some studies relevant to the topic are given in [13 − 15].

Properties of electrically conducting fluids can be summarized with the help of Magnetohydrodynamic (MHD) qualities. Major applications of MHD are applicable in the disciplines like cosmology, geophysics, astrophysics, sensors, engineering and magnetic drug targeting. Study of complex rheology of biological fluids within the range of magnetic field known as Biomagnetic fluid dynamics (BFD) is generally a new region in fluid mechanics. It has numerous utilizations in medicine and bioengineering. Research work in this field is being multiplied so considerably [16 − 22]. Due to the movement of fluid (conducting) magnetic filed creates electric current which in result modify the magnetic field and henceforth mechanical forces are produced which alter the flow stream. Initially such analysis was done by Vishnyakow and Pavlov [23]. In their work, viscous fluids had been discussed.

Darcy's Law is responsible for fluid flow in porous region meanwhile fluid in the free flow region is represented by Navier Stokes equation. In 1967, Beavers and Joseph considered permeable surface with couple flow motion [24, 25]. Several pragmatic practices experience the flow in the occupancy of permeable medium especially in the dynamics of geophysical fluid. Sandstones, limestones, beach sands, blood vessels with stones in gall bladder, human lungs and filter paper are some of the remarkable examples of natural permeable surfaces. Akbar et al. [26] examined the nanofluid flow through permeable walls of stenosed arteries. An excellent biological example of the porous media is the placement of gallstones in bile ducts when they close them completely or partially. Rapits et al. [27] considered infinite vertical plates with

fluid crossing through permeable medium. Effects of magnetic field and porous media in a vertical tube are examined by Vasudev et al. [28]. Mekheimer [29] considered the porous inclined channel for nonlinear peristaltic flow.

Parenthetically, it is more reasonable to consider curved tube/channel for the development of mathematical models related to fluid flow domains such as blood arteries, turbine blades, turbo-compressor devices, pumps and fluid machinery. As most of the natural flows in biological courses and glandular pipes are designed in curved tubes [30, 31]. In addition, the wall compliance is found more active regarding rigidity, solidness and mass per unit area for tubes having thinner span (<0.05cm). Medically, the biddable sort of walls have huge role in respiratory and cardiovascular procedures where vessels stretch out because of pressure and accordingly impacts pumping and blood pressure. It implies that under similar circumstances vessels with greater compliance contort easily than lower compliant vessels. During the previous decades, number of studies have taken place on compliant walls but its working phenomena in reducing skin friction still needs a lot of work to understand [32 − 34]. In view of blood flow, study on peristalsis with wall properties in complex geometry has moved toward becoming subject of enthusiasm these days. To study these wall properties, the contribution of Kramer [35, 36] is notable. Kramer published many experimental studies in which he covers the considered entity with rubber and significant reduction is found in the drag. To study the flows through compliant boundaries experiments have been performed i.e. dolphin propulsion , blood flow in arteries, etc. Mittra and Prasad [37] extended the idea of compliant wall for peristaltic flows given by Kramer .Heat transfer analysis of Jaffery fluid in a porous media was analyzed by Dheia et al. [38] under compliant walls effects. Sreenadh et al. [39] examined the peristaltic movement of bolus through esophagus with wall properties and heat transfer effects. Further analyzed by many investigators as [40 − 42].

In the majority of the given references, viscosity of the fluid is viewed to be consistent. The change in radius and temperature can impressively change the physical properties of the fluid. Viscosity of the fluid get influenced due to the calefaction produced by the internal retarding force that corresponds to rise in temperature, so the fluid viscosity can not be assumed to be constant any longer. Subsequently, to inspect the flow behavior precisely it is adequate to consider the variation of viscosity for incompressible fluids [43 − 45]. Hakeem et al. [46]

considered the hydromagnetic flow of fluid in a tube under the influence of variable viscosity. Abbasi et al. [47] discussed the impact of viscosity depending upon temperature for magneto hydrodynamic peristaltic flows.

Endoscopy, from the very beginning has dramatically affected the execution of modern examination. It has created new ways of diagnostic possibilities that are still growing rapidly. Inclusion of a long attenuated tube specifically into the body to watch an interior tissue or organ in particular is called endoscopy. Its simultaneous usage is to perform different tasks such as imaging and minor surgery. From dynamic viewpoint there is no contrast amongst catheter and endoscope. Catheters can be adjusted for cardiovascular, neurovascular, urological, gastrointestinal and ophthalmic applications by amending the material and refining the strategy catheters are produced. Administration of fluid and gases, drainage, access of surgical instruments and wide range of different tasks are fundamental elements of catheters depending upon its classification. Furthermore flow field and pressure distribution will be altered due to lodged catheter. Number of examinations are completed to breakdown the effect of endoscope over peristalsis. Mekheimer et al. [48] discussed the application of an endoscope by considering the couple stress fluid model in an annulus. There are many investigations to examine the impact of endoscope/annulus on the peristaltic flow of Newtonian and non-Newtonian fluids [49 − 51]. An important utilization of fluid dynamics is in infusion of fluid in the body by needles or syringes. In the surgical procedure of thread lift infusion, an expert imbues fluid or various medical supplements in the body. Lip augmentation is one of the most popular and used thread lift injection in modern

plastic surgery. Many investigators have theoratically studied the peristaltic fluid flow through annular cylinders [52 − 54].

Currently, the heat transfer phenomena in peristalsis has picked up a lot of consideration because to its innumerable applications in the field of engineering and biomedical science. Heat transfer includes different complex procedure such as destruction of unwanted cancer tissues, assessing skin burns, vasodilation, making of paper, food processing, hyperthermia, metabolic heat generation and in the treatment of tissue coagulation. It is noticed that when a person does some intense physical exercise or when body uncovered its exorbitant heat to the surrounding environment then the flow of blood stream increases. The elements of artery should be adjusted

in such a way the increase in blood flow should be controlled. It is evident that the heat transfer happens through skin surface by the procedure of evaporation via perspiring when temperature exceeds 20^0C and heat of person's body drop by both radiation and conduction when the temperature is less then 20^0C. Eldabe et al. [55] discussed the heat and mass transfer analysis of couple stress fluid in a porous media with MHD. Sinha et al. [56] analyzed the transfer of heat in the asymmetric channel with the impact of velocity and thermal slip with variable viscosity.

Scientists are motivated to investigate increasingly in thermal engineering due to rising needs of modern technology driven world. Right now, a standout amongst most crucial quest is to give attention on new kind of heat transfer fluids. Scientists found that expansion of solid particles to base fluid can enhance the thermal exchange ability. In view of this idea, a new fluid named as "nanofluid" is introduced and it has hold the attention of scientists and kept them passionate through the last two decades and word "nanofluid" was first introduced by Choi [57]. In the study of nanofluids, thermophoresis and Brownian motion shows vital importance as proposed by Buongiorno [58]. The term nanofluid is used to represent the suspension of ultrafine elements with diameter upto 50nm. These elements may be nonmetals (graphite, carbon nanotubes) or metals (oxides, carbides, nitrides). Ordinarily, water, ethylene glycol, oil etc. are utilized as base liquids, which have naturally low thermal conductivity. As metals have greater thermal conductivity, thus their inclusion in conventional fluids give the possibility to enhance the substantially higher thermal conductivity of base fluids. Modern research uncovers that nanofluid based frameworks have a broad potential zone, for example, electronics cooling, nuclear reactor cooling, modulators, optical gratings, sink float separations, heat exchangers, refrigerators and solar collectors [59 − 61]. Very significant and intriguing use of nanoparticles in medicine is drug delivery. In this process nanoparticles are engineered that they only attract to malignant cells which allow coordinate treatment of these cells. This procedure is mostly utilized in cancer treatment so that it cause less harm to healthy cells. The prospective usage to such mixture fluids for different systems have showed the importance of meticulous examination on properties of nanofluids [62 − 64]. Since the size and the shape of nanoparticles plays an effective part in improving the thermal conductivity of base fluid therefore, Timofeeva et al. [65] exhibit a research where shape effect of nanofluid parcticles is considered.

Magnetic properties of nanoparticles include another scope, where they can improve the utilization of an external magnetic field. Infact, magnetic nanofluids have the prospects for both of liquid and magnetic field. Some of the useful applications are optical gratings, switches, adjustable optical fiber filters and modulators. Magnetic nanoparticles show critical significance in the treatment of cancer where medicine and the nanoparticles are instructed to move with the circulation system towards the malignant cells with magnets. The influence of these nanoparticles on the malignancy are found in more adhesive than the invigorating cells. Mody et al. [66] discussed that the magnetic nanoparticles are used as a drug agent to treat the tumor cells. Abbasi et al. [67] studied the hydromagnetic peristaltic flow of nanofluid under the influence of temperature dependent viscosity.

Keeping an eye on above literature, the purpose of the present thesis is to study the theoretical analysis of peristaltic transport of nanofluid in different flow configurations under different effects. Dimensionless parameters and assumptions of long wavelength and low Reynolds number are used to present the significant modeling. The resulting equations are then solved exactly and by using HPM techniques [68]. Physical clarification of results is given with the help of tables and graphs. The thesis consists of six chapters that are prepared by the author and is published in international journal. **Chapter 1** is devoted to the introduction while the other five are mainly the study and analysis of peristaltic flow of nanofluid in the presence of endoscope.

The unit wise division of the thesis is presented as below.

Chapter 2 reveals the study of peristaltic transport of nano hyperbolic tangent fluid in an annulus. The motivation behind the current examination is to concentrate on the impacts of induced magnetic field on the peristaltic flow of non-Newtonian fluid. The flow is explored in a wave frame of reference which is moving with velocity c. Nanoparticle and temperature conditions are comprehended analytically by utilizing Homotopy Perturbation Method and exact solutions are calculated for velocity, axial induced magnetic field, current distribution, pressure gradient and stream functions. The impacts of various rising parameters are examined for sinusoidal wave. The phenomenon of trapping has additionally been talked about toward the end of chapter.

In **chapter 3**, we deal with the peristaltic transport of Au-nanoparticles in curved tube

having biddable walls. Governing equations have been derived for curved tube by using toroidal coordinate system. Long wavelength and low Reynolds number approximation are utilised to tackle the nonlinear partial differential equation. Furthermore, perturbation approximation is used in the form of variant curvature parameter to get the analytical solutions such as axial velocity and streamlines. Graphs are drawn to understand the physical features of dominant parameters such as Grashoff's number, heat source/sink parameter, amplitude ratio and elastic parameters. Also temperature tables are subsumed for varying values of mentioned parameters. This chapter summarised that there is a critical contrast amongst curvature and non-curvature flow across the catheterised tube.

The purpose of **chapter 4** is to summarize the effects of different shaped Ag-nanoparticles on peristaltic flow through a curved tube having permeable walls.The different shaped Ag-nanoparticles are cylinders,bricks and platelets.To study the behaviour of these Ag-nanoparticles mathematically, system of toroidal coordinate for viscous fluid is utilized. Furthermore, the analysis is carried out under the assumptions of low Reynolds number and long wavelength approximation. The method of Perturbation approximation is utilized to simplify the problem and get the results for pressure gradient, pressure rise, axial velocity and stream functions. The effects of several parameters have been discussed graphically. We percieve from present analysis that the temperature profile exhibits a decline for larger shape factor of Ag-nanoparticles. Also the trapped bolus is observed to have larger size for bigger shape factor.

Nanofluids are classified as a class of fluids that enhance the thermal conductivity and serve as a modern drug delivery technique. The main motivation of **chapter 5** is to illustrate the effects of variable viscosity on peristaltic flow of Au-nanoparticles. The geometry under consideration is a curved tube with an endoscope inserted into it. The constructed mathematical differential system is solved by perturbation method. The comparison between curvature and non-curvature tube over velocity, pressure gradient and pressure rise are visualized graphically. For better comprehension of flow and heat characteristics, streamlines for flow and contour map for temperature are plotted. The contemporary investigstion has revealed that non-curvature tube exhibits larger velocity, pressure gradient and pressure rise in the presence of nanoparticles.

Chapter 6 is the study of hybrid nanofluid, which is considered to be a new class of nanofluids and getting famous due to its thermal properties and possible utilities to further

ameliorates the heat transfer rate. Main objective of this analysis is to represent a comparison between conventional nanofluid and hybrid nanofluid when fluid passes through curved tube with an endoscope inserted in it while flow behavior is peristaltic. Cu/water nanofluid and $Cu - Fe_2O_4$/water hybrid nanofluid are considered for this problem. Results for pressure gradient, velocity, pressure rise and streamlines are given graphically. Tables for temperature and heat transfer rate are also mentioned. Present study concludes that heat transfer rate for hybrid nanofluid is higher in comparison to nanofluid.

Chapter 2

Consequences of induced magnetic field on peristaltic flow of nano hyperbolic tangent fluid in an annulus

The objective of this present chapter is to investigate the peristaltic transport of nano hyperbolic tangent fluid in an endoscope. The motivation behind this examination is to concentrate on the impacts of induced magnetic field on the peristaltic flow of non-Newtonian fluid. The flow is explored in a moving wave frame of velocity c. Nanoparticle and temperature conditions have been comprehended analytically by using Homotopy Perturbation Method while exact solutions are calculated for velocity, axial induced magnetic field, current distribution, pressure gradient and stream functions. The impacts of various rising parameters are examined for sinusoidal wave. The phenomenon of trapping has additionally been talked about toward the end of chapter.

2.1 Mathematical formulation

The basic equations for magnetohydrodynamics, abandoning the free charges and displacement currents are defined as [22]

(i) Maxwell's equation

$$\boldsymbol{\nabla} \cdot \mathbf{H}'^{+} = 0 \ , \tag{2.1}$$

$$\boldsymbol{\nabla} \cdot \mathbf{E}' = 0 \ , \tag{2.2}$$

$$\boldsymbol{\nabla} \times \mathbf{H}'^{+} = \mathbf{J}' \quad \text{with } \mathbf{J}' = \sigma \left\{ \mathbf{E}' + \mu_e \left(\mathbf{V}' \times \mathbf{H}'^{+} \right) \right\}, \tag{2.3}$$

$$\boldsymbol{\nabla} \times \mathbf{E}' = -\mu_e \frac{\partial \mathbf{H}'^{+}}{\partial t'}. \tag{2.4}$$

(ii) The continuity equation

$$\boldsymbol{\nabla} . \mathbf{V}' = 0 \ . \tag{2.5}$$

(iii) The Navier-Stokes equation

$$\rho \frac{\mathbf{D} \mathbf{V}'}{\mathbf{D} t'} = -\boldsymbol{\nabla} p' + \boldsymbol{\nabla} . \boldsymbol{\tau}' + \mu_e (\mathbf{J}' \times \mathbf{H}'^{+}) + \rho \mathbf{f}, \tag{2.6}$$

where $\mathbf{V}'$ defines velocity vector, $\mathbf{J}'$ represents electric current density, $\mathbf{E}'$ is an induced electric field, μ_e denotes magnetic permeability while σ represent electrical conductivity, $\mathbf{D}/\mathbf{D}t'$ is the material derivative and $\boldsymbol{\tau}'$ is giving stress tensor. The stress tensor is given as

$$\boldsymbol{\tau}' = [\eta_\infty + (\eta_{0+}\eta_\infty) \tanh(\Gamma\gamma)^n]\gamma_i], \tag{2.7}$$

in which η_0, η_∞, m, Γ, denote the zero shear rate viscosity, infinite rate of shear viscosity, power law index, and time constant. γ is now defined as

$$\gamma = \sqrt{\frac{1}{2} \sum_i \sum_j \boldsymbol{\gamma}_{ij} \boldsymbol{\gamma}_{ji}} = \sqrt{\frac{1}{2}\boldsymbol{\pi}}, \tag{2.8}$$

where

$$\boldsymbol{\pi} = trace(\text{grad}\,\mathbf{V}' + (\text{grad}\,\mathbf{V}')^T)^2, \tag{2.9}$$

π is representing second invariant strain tensor. Here we discuss Eq. (2.7) for $\eta_\infty = 0$ and $\Gamma\gamma$

‹ 1. The element of extra stress tensor so inscribed as

$$\boldsymbol{\tau} = \eta_0[(\Gamma\gamma)^n]\gamma_i = \eta_0[(1 + \Gamma\gamma - 1)^n]\gamma_i = [1 + n(\Gamma\gamma - 1)]\eta_0\gamma_i, \tag{2.10}$$

$$\gamma_i = \mathbf{L} + \mathbf{L}^T. \tag{2.11}$$

(iv) The energy equation

$$(\rho c)_f \frac{\mathbf{D}T}{\mathbf{D}t'} = k\boldsymbol{\nabla}^2 T + [(\frac{d_T}{T_1})\boldsymbol{\nabla}T.\boldsymbol{\nabla}T + d_b\boldsymbol{\nabla}C.\boldsymbol{\nabla}T](\rho c)_p, \tag{2.12}$$

(v) The mass concentration

$$\frac{\mathbf{D}C}{\mathbf{D}t'} = d_b\boldsymbol{\nabla}^2 C + (\frac{d_T}{T_1})\boldsymbol{\nabla}^2 T, \tag{2.13}$$

(iv) On combining Maxwell's equations, we get induction equation as follow

$$\frac{\partial \mathbf{H'}^+}{\partial t'} = \nabla \times \left\{ \mathbf{V'} \times \mathbf{H'}^+ \right\} + \zeta\nabla^2\mathbf{H'}^+. \tag{2.14}$$

where magnetic diffusitivity is given as $\varsigma = \frac{1}{\sigma\mu_e}$.

2.2 Problem formulation

Consider electrically conducting and incompressible nanofluid across the cavity among two coaxial tubes. The internal tube is uniform, and is sustained at the temperature T_0 and nanoparticle velocity C_0 while outer tube experiences a sinusoidal wave travelling down its walls having temþerature T_1 and nanoparticle velocity C_1. Here we consider cylindrical co-ordinates (R', Z') such as R' is the radial coordinates and Z' is axial coordinates. Uniform magnetic field of strength $H_0 R'_2/R'$ is applied externally in radial direction which results in an induced magnetic field $\mathbf{H'}\left(h'_{R'}\left(R', Z', t'\right), 0, h_{z'}\left(R', Z', t'\right)\right)$. So the total magnetic field will be $\mathbf{H'}^+(\frac{H_0 R'_2}{R'} + h'_{R'}, 0, h'_{Z'})$.

The tube walls are taken to be non-conductive and walls surface geometry is shown in Fig.

2.1.
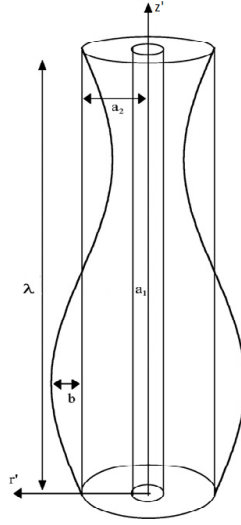
Fig. 2.1 Geometry of problem

The surfaces of the wall satisfy:

$$R_1' = a_1, \tag{2.15}$$

$$R_2' = b\sin\frac{2\pi}{\lambda}\left(Z' - ct'\right) + a_2, \tag{2.16}$$

here b is representing wave amplitude, a_1 and a_2 are the radius of two tubes, λ represent the wavelength and c is denoting propagation velocity.

By assuming the flow parameters independent of the azimuthal coordinates, the velocity is given as $\mathbf{V}' = (U', 0, W')$ where U' and W' are the components of velocity in R' and Z' direction, respectively. Temperature and concentration fields take the form

$$\mathbf{T} = \mathbf{T}\left(R', Z', t'\right), \ \mathbf{C} = \mathbf{C}(R', Z', t'). \tag{2.17}$$

The governing equations along with nanoparticles in the fixed frame are given as

$$\frac{\partial h_R'}{\partial R'} + \frac{h_{R'}'}{R'} + \frac{\partial h_{Z'}'}{\partial Z'} = 0, \tag{2.18}$$

16

$$\frac{\partial U'}{\partial R'} + \frac{U'}{R'} + \frac{\partial W'}{\partial Z'} = 0, \tag{2.19}$$

$$\rho\left(\frac{\partial U'}{\partial t'} + U'\frac{\partial U'}{\partial R'} + W'\frac{\partial U'}{\partial Z'}\right) = -\frac{\partial p'}{\partial R'} + \frac{1}{R'}\frac{\partial(R\tau'_{RR})}{\partial R'} + \frac{\partial(\tau'_{RZ})}{\partial Z'} - \frac{\tau'_{\theta\theta}}{R'}$$
$$+ \mu_e h'_Z\left[\frac{\partial}{\partial Z'}\left(H'_o\frac{R'_2}{R'} + h'_R\right) - \frac{\partial h'_Z}{\partial R'}\right], \tag{2.20}$$

$$\rho\left(\frac{\partial U'}{\partial t'} + U'\frac{\partial W'}{\partial R'} + W'\frac{\partial W'}{\partial Z'}\right) = -\frac{\partial p'}{\partial Z'} + \frac{1}{R'}\frac{\partial(R'\tau'_{RR})}{\partial R'} + \frac{\partial(\tau'_{ZZ})}{\partial Z'}$$
$$+ \mu_e\left[\frac{\partial h'_Z}{\partial R'} - \frac{\partial}{\partial Z'}\left(H'_o\frac{R'_2}{R'} + h'_{R'}\right)\right]\left(H'_o\frac{R'_2}{R'} + h'_{R'}\right)$$
$$+ \rho g\alpha_T(T - T_1) + \rho g\alpha_C(C - C_1). \tag{2.21}$$

Energy and mass concentration equations are given as

$$\left(U'\frac{\partial T}{\partial R'} + W'\frac{\partial T}{\partial Z'}\right) = \quad \alpha_2\left(\frac{\partial^2 T}{\partial R'^2} + \frac{1}{R'}\frac{\partial T}{\partial R'} + \frac{\partial^2 T}{\partial Z'^2}\right) + \tau_1\{d_b\left(\frac{\partial C}{\partial R'}\frac{\partial T}{\partial R'} + \frac{\partial C}{\partial Z'}\frac{\partial T}{\partial Z'}\right)$$
$$+ \frac{d_T}{T_1}\left[\left(\frac{\partial T}{\partial R'}\right)^2 + \left(\frac{\partial T}{\partial Z'}\right)^2\right]\}, \tag{2.22}$$

$$\left(U'\frac{\partial C}{\partial R'} + W'\frac{\partial C}{\partial Z'}\right) = d_b\left(\frac{\partial^2 C}{\partial Z'^2} + \frac{1}{R'}\frac{\partial C}{\partial R'} + \frac{\partial^2 C}{\partial R'^2}\right) + \frac{d_T}{T_1}\left(\frac{\partial^2 T}{\partial Z'^2} + \frac{1}{R'}\frac{\partial T}{\partial R'} + \frac{\partial^2 T}{\partial R'^2}\right), \tag{2.23}$$

$\tau_1 = \frac{(\rho c)_p}{(\rho c)_f}$ is the proportion of the effective heat capacity. The magnetic induction equations in component form is given as

$$\left[\frac{\partial}{\partial t'} + \left(U'\frac{\partial}{\partial R'} + W'\frac{\partial}{\partial Z'}\right) - \frac{\partial U'}{\partial R'}\right]\left(H'_o\frac{R'_2}{R'} + h'_R\right) - \frac{\partial U'}{\partial R'}h'_Z$$
$$= \zeta\frac{\partial}{\partial Z'}\left[\left(\frac{\partial}{\partial Z'}\left(H'_o\frac{R'_2}{R'} + h'_R\right)\right) - \left(\frac{\partial h'_Z}{\partial R'}\right)\right], \tag{2.24}$$

$$\left[\frac{\partial}{\partial t'} + \left(U'\frac{\partial}{\partial R'} + W'\frac{\partial}{\partial Z'}\right) - \frac{\partial W'}{\partial Z'}\right]h'_z - \frac{\partial W'}{\partial R'}\left(H'_o\frac{R'_2}{R'} + h'_R\right)$$
$$= \zeta\left[\frac{1}{R'}\frac{\partial}{\partial R'}\left(R'\frac{\partial h'_Z}{\partial R'}\right) - \frac{\partial}{\partial Z'}\left(\frac{\partial}{\partial R'} + \frac{1}{R'}\right)\left(H'_o\frac{R'_2}{R'} + h'_R\right)\right]. \tag{2.25}$$

In the non moving coordinates (R', Z'), the flow among the two cylinders is not steady. Flow becomes steady in a wave structure (r', z') that moves with similar speed as the wave movement in the Z' direction. Both structures are connected through the following transformations

$$r' = R', \ z' = Z' - ct', U' = u', w' = W' - c, \tag{2.26}$$

where u', w' are the velocity components in the wave structure. Suitable boundary limits in wave structures stands

$$
\begin{aligned}
w' &= -c, \ \text{at } r' = r_1', h_z' = 0, h_{r'}' = 0, \\
w' &= -c, \ \text{at } r' = r_2' = a_2 + b \sin \frac{2\pi}{\lambda}(z'),
\end{aligned}
\tag{2.27}
$$

$$T = T_0 \text{ at } r' = r_1', \ T = T_1 \text{ at } r' = r_2', \tag{2.28}$$

$$C = C_0 \text{ at } r' = r_1', \ C = C_1 \text{ at } r' = r_2'. \tag{2.29}$$

Introducing the dimensionless parameters

$$
\begin{aligned}
R &= \frac{R'}{a_2}, \ Z = \frac{Z'}{\lambda}, \ r = \frac{r'}{a_2}, \ z = \frac{z'}{\lambda}, \ W = \frac{W'}{c}, \ U = \frac{\lambda U'}{a_2 c}, \ w = \frac{w'}{c}, \ u = \frac{\lambda u'}{a_2 c}, \\
p &= \frac{a_2^2 p'}{c \lambda \mu}, \ \theta = \frac{T - T_1}{T_0 - T_1}, \ t = \frac{ct'}{\lambda}, \ \delta = \frac{a_2}{\lambda}, \ R_y = \frac{\rho c a_2}{\mu}, \ \sigma = \frac{C - C_1}{C_0 - C_1}, \\
r_1 &= \frac{r_1'}{a_2} = \epsilon, \ r_2 = \frac{r_2'}{H_2} = 1 + \varepsilon \sin 2\pi z, \varepsilon = \frac{b}{a_2}, \ \epsilon = \frac{a_1}{a_2}, \ h_r = \frac{h_r'}{H_0}, \ h_z = \frac{h_z'}{H_0}, \\
G_r &= \frac{\rho g \alpha_T H_2^2 (T_0 - T_1)}{c \mu}, \ b_r = \frac{\rho g \alpha_C H_2^2 (C_0 - C_1)}{c \mu}, \ N_b = \frac{(\rho c)_p \, d_b (C_0 - C_1)}{\alpha_2 (\rho c)_f}, \\
N_t &= \frac{(\rho c)_p \, (T_0 - T_1) d_T}{T_1 \, \alpha_2 (\rho c)_f}, \ \alpha_2 = \frac{k}{(\rho c)_f}, W_e = \frac{\Gamma c}{a_2},
\end{aligned}
\tag{2.30}
$$

The parameters N_b, N_t, G_r, b_r, R_y, δ are representing the Brownian motion parameter, thermophoresis parameter, local temperature Grashof number, local nanoparticle Grashof number, Reynolds number and wave number respectively. ϵ is the radius ratio and amplitude ratio is represented by ε. W_e as Weissenberg number.

Making use of above non-dimensional parameters Eqs. (2.18) to (2.25) with conditions (2.27)

to (2.29) become

$$\frac{\partial h_{\mathrm{r}}}{\partial \mathrm{r}} + \delta \frac{\partial h_{\mathrm{z}}}{\partial \mathrm{z}} + \frac{h_{\mathrm{r}}}{\mathrm{r}} = 0, \tag{2.31}$$

$$\frac{\partial \mathrm{w}}{\partial \mathrm{z}} + \frac{\mathrm{u}}{\mathrm{r}} + \frac{\partial \mathrm{u}}{\partial \mathrm{r}} = 0, \tag{2.32}$$

$$\delta^3 R_{\mathrm{y}}(\mathrm{u}\frac{\partial \mathrm{u}}{\partial \mathrm{r}} + \frac{\partial \mathrm{u}}{\partial \mathrm{z}}\mathrm{w}) = -\frac{\partial \mathrm{p}}{\partial \mathrm{r}} + \delta^2 \frac{\partial}{\partial \mathrm{z}}(\boldsymbol{\tau}_{\mathrm{rz}}) + \frac{\delta}{\mathrm{r}}\frac{\partial}{\partial \mathrm{r}}(\mathrm{r}\boldsymbol{\tau}_{\mathrm{rr}}) - \frac{\delta}{\mathrm{r}}\boldsymbol{\tau}_{\theta\theta} + S^2 R_{\mathrm{y}}\left[\delta\left(\frac{1}{\mathrm{r}}\frac{\partial \mathrm{r}_2}{\partial \mathrm{z}} + \frac{\partial h_{\mathrm{r}}}{\partial \mathrm{r}}\right)\right.$$
$$\left. -\frac{\partial h_{\mathrm{z}}}{\partial \mathrm{r}}h_{\mathrm{z}}\right], \tag{2.33}$$

$$\delta R_{\mathrm{y}}(\mathrm{w}\frac{\partial \mathrm{w}}{\partial \mathrm{z}} + \mathrm{u}\frac{\partial \mathrm{w}}{\partial \mathrm{r}}) = -\frac{\partial \mathrm{p}}{\partial \mathrm{z}} + \delta\frac{\partial}{\partial \mathrm{z}}(\boldsymbol{\tau}_{\mathrm{zz}}) + \frac{1}{\mathrm{r}}\frac{\partial}{\partial \mathrm{r}}(\mathrm{r}\boldsymbol{\tau}_{\mathrm{rz}}) + S^2 R_{\mathrm{y}}\left[\frac{\partial h_{\mathrm{z}}}{\partial \mathrm{r}} - \delta\left(\frac{1}{\mathrm{r}}\frac{\partial \mathrm{r}_2}{\partial \mathrm{z}} + \frac{\partial h_{\mathrm{r}}}{\partial \mathrm{r}}\right)\right]$$
$$\left(\frac{\mathrm{r}_2}{\mathrm{r}} + h_{\mathrm{r}}\right) + g_{\mathrm{r}}\theta + b_{\mathrm{r}}\sigma, \tag{2.34}$$

where

$$\boldsymbol{\tau}_{\mathrm{rr}} = \frac{\partial \mathrm{u}}{\partial \mathrm{r}}[1 + n(W_e\boldsymbol{\gamma} - 1)]2\delta,$$

$$\boldsymbol{\tau}_{\mathrm{rz}} = (\frac{\partial \mathrm{w}}{\partial \mathrm{r}} + \frac{\partial \mathrm{u}}{\partial \mathrm{z}}\delta^2)[1 + n(W_e\boldsymbol{\gamma} - 1)],$$

$$\boldsymbol{\tau}_{\mathrm{zz}} = \frac{\partial \mathrm{w}}{\partial \mathrm{z}}[1 + n(W_e\boldsymbol{\gamma} - 1)]2\delta,$$

$$\boldsymbol{\tau}_{\theta\theta} = \frac{\mathrm{u}}{\mathrm{r}}[1 + n(W_e\boldsymbol{\gamma} - 1)]2\delta, \tag{2.35}$$

$$\boldsymbol{\gamma} = [2(\frac{\partial \mathrm{u}}{\partial \mathrm{r}})^2\delta^2 + (\frac{\partial \mathrm{w}}{\partial \mathrm{r}} + \frac{\partial \mathrm{u}}{\partial \mathrm{z}}\delta^2)^2 + 2(\frac{\partial \mathrm{w}}{\partial \mathrm{z}})^2\delta^2 + 2\frac{\mathrm{u}^2}{\mathrm{r}^2}\delta^2]^{\frac{1}{2}}. \tag{2.36}$$

Energy, mass and induction equations become

$$\delta a_2 c\left[\mathrm{u}\frac{\partial T}{\partial \mathrm{r}} + \mathrm{w}\frac{\partial T}{\partial \mathrm{z}}\right] = \alpha_2\left(\frac{\partial^2 T}{\partial r^2} + \frac{1}{r}\frac{\partial T}{\partial r} + \delta^2\frac{\partial^2 T}{\partial z^2}\right) + \tau_1\{d_b(\frac{\partial C}{\partial r}\frac{\partial T}{\partial r}$$
$$+\delta^2\frac{\partial C}{\partial z}\frac{\partial T}{\partial z}) + \frac{d_{\mathrm{T}}}{T_1}[(\frac{\partial T}{\partial r})^2 + \delta^2(\frac{\partial T}{\partial z})^2]\}, \tag{2.37}$$

$$\delta a_2 c\left[u\frac{\partial C}{\partial r} + w\frac{\partial C}{\partial z}\right] = d_b(\frac{\partial^2 C}{\partial r^2} + \frac{1}{r}\frac{\partial C}{\partial r} + \delta^2\frac{\partial^2 C}{\partial z^2}) + \frac{d_{\mathrm{T}}}{\mathrm{T}_1}(\frac{\partial^2 T}{\partial r^2} + \frac{1}{r}\frac{\partial T}{\partial r} + \delta^2\frac{\partial^2 T}{\partial z^2}), \tag{2.38}$$

$$\delta\left[\frac{\partial}{\partial t} + (u\frac{\partial}{\partial r} + w\frac{\partial}{\partial z}) - \frac{\partial u}{\partial r}\right]\left(\frac{r_2}{r} + h_r\right) - \delta\frac{\partial u}{\partial r}h_z = \frac{\delta}{R_m}\frac{\partial}{\partial z}\left[\delta\left(\frac{1}{r}\frac{\partial r_2}{\partial z} + \frac{\partial h_r}{\partial z}\right) - \frac{\partial h_z}{\partial r}\right], \tag{2.39}$$

19

$$\delta \left[\frac{\partial}{\partial t} + (u\frac{\partial}{\partial r} + w\frac{\partial}{\partial z}) - \frac{\partial w}{\partial z} \right] h_z - \frac{\partial w}{\partial r} \left(\frac{r_2}{r} + h_r \right) = \frac{1}{R_m}[\frac{1}{r}\frac{\partial}{\partial r} \left(r\frac{\partial h_z}{\partial r} \right)$$

$$-\delta\frac{\partial}{\partial z} \left(\frac{\partial}{\partial r} + \frac{1}{r} \right) \left(\frac{r_2}{r} + h_r \right)]. \tag{2.40}$$

Utilizing the long wavelength approximation and neglecting terms of order δ and higher, Eqs. (2.31) to (2.40) take the form

$$\frac{\partial h_r}{\partial r} + \frac{hr}{r} = 0, \tag{2.41}$$

$$\frac{\partial u}{\partial r} + \frac{u}{r} + \frac{\partial w}{\partial z} = 0, \tag{2.42}$$

$$\frac{\partial p}{\partial r} = 0, \tag{2.43}$$

$$\frac{\partial p}{\partial z} = \frac{1}{r}\frac{\partial}{\partial r} \left(r \left(1 + n \left(W_e \frac{\partial w}{\partial r} - 1 \right) \right) \frac{\partial w}{\partial r} \right) + S^2 R_m \frac{\partial h_z}{\partial r} \left(\frac{r_2}{r} + h_r \right) + g_r \theta + b_r \sigma, \tag{2.44}$$

$$N_b \frac{\partial \sigma}{\partial r} \frac{\partial \theta}{\partial r} + \frac{1}{r}\frac{\partial}{\partial r}(r\frac{\partial \theta}{\partial r}) + N_t (\frac{\partial \theta}{\partial r})^2 = 0, \tag{2.45}$$

$$(\frac{1}{r}\frac{\partial}{\partial r}(r\frac{\partial \sigma}{\partial r})) + \frac{N_t}{N_b}(\frac{1}{r}\frac{\partial}{\partial r}(r\frac{\partial \theta}{\partial r})) = 0, \tag{2.46}$$

$$\frac{\partial w}{\partial r} \left(\frac{r_2}{r} + h_r \right) = -\frac{1}{R_m} \left[\frac{1}{r}\frac{\partial}{\partial r} \left(r\frac{\partial h_z}{\partial r} \right) \right], \tag{2.47}$$

where $R_m = \frac{a_2}{\varsigma}$, and $S^2 = \frac{H_o^2 \mu_e}{\rho c^2}$ are magnetic Reynolds number and Strommer's number(magnetic force number) respectively. Eq. (2.43) displays that p is independent of r.

Rate of volume flow and boundary conditions

In the fixed coordinates volume flow rate in the instantaneous position is specified by

$$\bar{Q} = 2\pi \int_{R_1'}^{R_2'} R'W'dR', \tag{2.48}$$

where R_2' is a function of Z' and t'. Invoking Eq. (2.26) into Eq. (2.48) and integrating produces

$$\bar{Q} = \bar{q} + \pi c(r_2'^2 - r_1'^2), \tag{2.49}$$

20

where

$$\bar{q} = 2\pi \int_{r_1'}^{r_2'} r'w'dr'. \tag{2.50}$$

In the moving coordinates system the volume flow rate is independent of time as mention in Eq. (2.50). Here r_2' is the function of z' only. Now utilizing dimensionless variables, we find

$$F = \frac{\bar{q}}{\pi a_2^2 c} = 2 \int_{r_1'}^{r_2'} \mathrm{r w} dr. \tag{2.51}$$

Over a period $T = \lambda/c$ the time-mean flow at a fixed z is given as

$$q' = \frac{1}{T} \int_0^T \bar{Q} dt'. \tag{2.52}$$

Invoking Eq. (2.49) into Eq. (2.52) and integrating, we attain

$$q' = \bar{q} + \pi c \left(a_2^2 - a_1^2 + \frac{b^2}{2} \right), \tag{2.53}$$

which can be inscribed as

$$\frac{q'}{\pi a_2^2 c} = \frac{\bar{q}}{\pi a_2^2 c} + 1 + \frac{\varepsilon^2}{2} - \epsilon^2. \tag{2.54}$$

Dimensionless time-mean flow can be given as

$$q = \frac{q'}{\pi c a_2^2}. \tag{2.55}$$

With the aid of Eqs. (2.51) and (2.55), Eq. (2.54) become

$$q = F + 1 + \frac{\varepsilon^2}{2} - \epsilon^2. \tag{2.56}$$

The consistent dimensionless boundary conditions for the problem under consideration are

defined as

$$
\begin{aligned}
w &= -1 \ at \ \mathrm{r} = \mathrm{r}_1 = \epsilon, \ w = -1 \ at \ \mathrm{r} = \mathrm{r}_2 = 1 + \varepsilon \sin(2\pi z), \\
h_r &= 0, h_z = 0 \ at \ \mathrm{r} = \mathrm{r}_1, \\
\sigma &= 1 \quad at \ \mathrm{r} = \mathrm{r}_1, \quad \sigma = 0 \qquad at \ \mathrm{r} = \mathrm{r}_2, \\
\theta &= 1 \quad at \ \mathrm{r} = \mathrm{r}_1, \quad \theta = 0 \qquad at \ \mathrm{r} = \mathrm{r}_2.
\end{aligned}
\tag{2.57}
$$

2.3 Solution of the problem

From Eq. (2.41), and boundary condition (2.57), we come to know that $h_r = 0$. Eqs. (2.44) and (2.47) are given as

$$
\frac{\partial \mathrm{p}}{\partial \mathrm{z}} = \frac{1}{\mathrm{r}} \frac{\partial}{\partial \mathrm{r}} (\mathrm{r} \left(1 + n \left(W_e \frac{\partial \mathrm{w}}{\partial r} - 1 \right) \right) \frac{\partial w}{\partial r}) + S^2 R_y \frac{\partial h_z}{\partial r} \left(\frac{r_2}{r} \right) + g_r \theta + b_r \sigma,
\tag{2.58}
$$

$$
-R_m r_2 \frac{\partial w}{\partial r} = \frac{\partial}{\partial r} \left(r \frac{\partial h_z}{\partial r} \right).
\tag{2.59}
$$

Homotopy perturbation method is utilized to solve the above equations. This advises that we write Eqs. (2.37) to (2.38), as [68]

$$
\begin{aligned}
H(w, \ x) &= (1 - x) \left[\pounds(w) - \pounds(w_{20}) \right] + j \left[\pounds(w) - \frac{\partial p}{\partial z} - \frac{M^2 r_2^2}{r^2} \right. \\
&\quad \left. + \frac{1}{r} n W_e \left(\frac{\partial w}{\partial r} \right)^2 + 2n W_e \left(\frac{\partial w}{\partial r} \right) \left(\frac{\partial^2 w}{\partial r^2} \right) \right] + g_r \theta + b_r \sigma,
\end{aligned}
\tag{2.60}
$$

$$
H(\sigma, \ x) = (1 - x) \left[\pounds(\sigma) - \pounds(\sigma_{10}) \right] + x \left[\pounds(\sigma) + \frac{N_t}{N_b} (\frac{1}{\mathrm{r}} \frac{\partial}{\partial \mathrm{r}} (\mathrm{r} \frac{\partial \theta}{\partial r})) \right],
\tag{2.61}
$$

$$
H(\theta, x) = (1 - x)[\pounds(\theta) - \pounds(\theta_{10})] + x \left[\pounds(\theta) + N_b \frac{\partial \theta}{\partial \mathrm{r}} \frac{\partial \sigma}{\partial \mathrm{r}} + N_t (\frac{\partial \theta}{\partial \mathrm{r}})^2 \right],
\tag{2.62}
$$

22

Initial guess and the linear operator are given as

$$\mathcal{L}_{\theta r} = \frac{1}{r}\frac{\partial}{\partial r}\left(r\frac{\partial}{\partial r}\right), \ \mathcal{L}_{\sigma r} = \frac{1}{r}\frac{\partial}{\partial r}\left(r\frac{\partial}{\partial r}\right),$$

$$\mathcal{L}_{wr} = \frac{1}{r}\frac{\partial}{\partial r}\left(r\left(1-n\right)\frac{\partial}{\partial r}\right) - \frac{M^2 r_2^2}{r^2},$$

$$\sigma_{10}(r,z) = \left(\frac{r-r_2}{r_1-r_2}\right), \ \theta_{10}(r,z) = \left(\frac{r-r_2}{r_1-r_2}\right),$$

$$w_{20}(r,z) = \frac{\partial p_0'}{\partial z}\left(a4r^k + a5r^{-k} + a2r^2\right) - 1. \tag{2.63}$$

According to Homotopy Perturbation Method, we write

$$\theta = \theta_0 + x\theta_1 + x^2\theta_2 + ...,$$

$$\sigma = \sigma_0 + x\sigma_1 + x^2\sigma_2 + ...$$

$$w = w_0 + xw_1 + x^2 w_2 + ...,$$

$$p = p_0 + xp_1 + x^2 p_2 + ..., \tag{2.64}$$

Utilizing these equations in Eqs. (2.61) and (2.62), the expression for temperature and concentration field can be written as

$$\sigma = s_{28}r^2 + rs_{36} + s_{37}\ln r + s_{38}, \tag{2.65}$$

$$\theta = s_{39}r^3 + r^2 s_{46} + s_{41}r + s_{47}\ln r + s_{48}. \tag{2.66}$$

The expressions (2.65) and (2.66) finally make it convenient to give the velocity

$$
\begin{aligned}
w = {} & \frac{\partial p}{\partial z}\left(b_4 r^k + b_5 r^{-k} + b_2 r^2\right) + b_{105}r^k + b_{106}r^{-k} + b_{107}r^2 + b_{108}r^{2k-1} \\
& + b_{109}r^{-(2k+1)} + b_{110}r^3 + b_{111}r^{-1} + b_{112}r^{k+1} + b_{113}r^{-k+1} - b_{85}r^{3k-2} \\
& - b_{86}r^{-k-2} - b_{87}r^{k+2} - b_{88}r^{k-2} - b_{89}r^{-k+2} - b_{90}r^{2k} - b_{91}r^{-2k} \\
& - b_{92}r^{-3k-2} - b_{96}r^4 + b_{100}r^2\ln r - 1.
\end{aligned}
\tag{2.67}
$$

and pressure gradient is given as

$$\frac{\partial p}{\partial z} = b_{114} \left[\theta - \left(1 + \frac{\varepsilon^2}{2} \right) + \epsilon^2 \right] + b_{115}. \tag{2.68}$$

Integration of Eq. (2.59) with respect to r takes the form

$$\frac{\partial h_z}{\partial r} = -\frac{R_m r_2}{r} w - \frac{c_1}{r_1}, \tag{2.69}$$

where c_1 is constant.

To find the constant c_1, we used Eqs. (2.3) and (2.69)

$$J_0 = -\frac{\partial h_z}{\partial r} = \frac{R_m r_2}{r} w + \frac{c_1}{r_1}, \tag{2.70}$$

since $J_0 = 0$ at $r = r_2$, so $c_1 = R_m r_2$, which gives

$$J_0 = -\frac{\partial h_z}{\partial r} = \frac{R_m r_2}{r} (w + 1). \tag{2.71}$$

The axial induced magnetic field is given as

$$
\begin{aligned}
h_z &= R_m r_2 [\frac{\partial p}{\partial z} \left(b_4 \left(\frac{r_2^k - r^k}{k} \right) - b_5 \left(\frac{r_2^{-k} - r^{-k}}{k} \right) + b_2 \left(\frac{r_2^2 - r^2}{2} \right) \right) \\
&+ b_{105} \left(\frac{r_2^k - r^k}{k} \right) - b_{106} \left(\frac{r_2^{-k} - r^{-k}}{k} \right) + b_{107} \left(\frac{r_2^2 - r^2}{2} \right) \\
&+ b_{108} \left(\frac{r_2^{2k-1} - r^{2k-1}}{2k-1} \right) - b_{109} \left(\frac{r_2^{-(2k+1)} - r^{-(2k+1)}}{2k+1} \right) \\
&+ b_{110} \left(\frac{r_2^3 - r^3}{3} \right) - b_{111} \left(\frac{r_2^{-1} - r^{-1}}{1} \right) + b_{112} \left(\frac{r_2^{k+1} - r^{k+1}}{k+1} \right) \\
&+ b_{113} \left(\frac{r_2^{-k+1} - r^{-k+1}}{-k+1} \right) - b_{85} \left(\frac{r_2^{3k-2} - r^{3k-2}}{3k-2} \right) - b_{86} \left(\frac{r_2^{-k-2} - r^{-k-2}}{-k-2} \right) \\
&- b_{87} \left(\frac{r_2^{k+2} - r^{k+2}}{k+2} \right) - b_{88} \left(\frac{r_2^{k-2} - r^{k-2}}{k-2} \right) - b_{89} \left(\frac{r_2^{-k+2} - r^{-k+2}}{-k+2} \right) \\
&- b_{90} \left(\frac{r_2^{2k} - r^{2k}}{2k} \right) + b_{91} \left(\frac{r_2^{2k} - r^{2k}}{2k} \right) + b_{92} \left(\frac{r_2^{-(3k+2)} - r^{-(3k+2)}}{3k+2} \right) \\
&- b_{96} \left(\frac{r_2^4 - r^4}{4} \right) + b_{100} \left(\frac{r_2^2 \ln r_2 - r^2 \ln r}{2} - \frac{r_2^2 - r^2}{4} \right)].
\end{aligned}
\tag{2.72}
$$

From Eqs. (2.71) and (2.72), the current density distribution become

$$
\begin{aligned}
J_o &= R_m r_2 [\frac{\partial p}{\partial z} \left(b_4 r^{k-1} + b_5 r^{-k-1} + b_2 r \right) + b_{105} r^{k-1} + b_{106} r^{-k-1} + b_{107} r \\
&+ b_{108} r^{2k-2} + b_{109} r^{-(2k+2)} + b_{110} r^2 + b_{111} r^{-2} + b_{112} r^k + b_{113} r^{-k} \\
&- b_{85} r^{3k-3} - b_{86} r^{-k-3} - b_{87} r^{k+1} - b_{88} r^{k-3} - b_{89} r^{-k+1} - b_{90} r^{2k-1} \\
&- b_{91} r^{-2k-1} - b_{92} r^{-3k-3} - b_{96} r^3 + r \ln r b_{100}].
\end{aligned}
\tag{2.73}
$$

The pressure rise, ΔP, and the frictional forces on the outer and inner tubes, $F^{(0)}$ and $F^{(i)}$, in non-dimensional form are given as

$$
\Delta P = \int_0^1 \frac{\partial p}{\partial z} dz, \quad F^{(0)} = \int_0^1 r_2^2 (-\frac{\partial p}{\partial z}) dz, \quad F^{(i)} = \int_0^1 r_1^2 (-\frac{\partial p}{\partial z}) dz.
\tag{2.74}
$$

The pressure rise ΔP and the friction forces are calculated numerically by mathematica, where

25

as appendix is given to define constants.The velocities and stream functions are related as [1]

$$u = \frac{-\delta}{r}\left(\frac{\partial \Psi}{\partial z}\right) \text{ and } w = \frac{1}{r}\left(\frac{\partial \Psi}{\partial r}\right).$$ (2.75)

Using Eq. (2.67) into Eq. (2.75), we get stream function as

$$
\begin{aligned}
\Psi =\ & \frac{\partial p}{\partial z}\left(b_4\left(\frac{r^{k+2} - r_1^{k+2}}{k+2}\right) + b_5\left(\frac{r^{-k+2} - r_1^{-k+2}}{-k+2}\right) + b_2\left(\frac{r^4 - r_1^4}{4}\right)\right) \\
& - \left(\frac{r^2 - r_1^2}{2}\right) + b_{105}\left(\frac{r^{k+2} - r_1^{k+2}}{k+2}\right) + b_{106}\left(\frac{r^{-k+2} - r_1^{-k+2}}{-k+2}\right) \\
& + b_{107}\left(\frac{r^4 - r_1^4}{4}\right) + b_{108}\left(\frac{r^{2k+1} - r_1^{2k+1}}{2k+1}\right) + b_{109}\left(\frac{r_2^{-2k+1} - r^{-2k+1}}{-2k+1}\right) \\
& + b_{110}\left(\frac{r^5 - r_1^5}{5}\right) + b_{111}(r - r_1) + b_{112}\left(\frac{r^{k+3} - r_1^{k+3}}{k+3}\right) \\
& + b_{113}\left(\frac{r^{-k+3} - r_1^{-k+3}}{-k+3}\right) - b_{85}\left(\frac{r^{3k} - r_1^{3k}}{3k}\right) - b_{86}\left(\frac{r^{-k} - r_1^{-k}}{-k}\right) \\
& - b_{87}\left(\frac{r^{k+4} - r_1^{k+4}}{k+4}\right) - b_{88}\left(\frac{r^k - r_1^k}{k}\right) - b_{89}\left(\frac{r^{-k+4} - r_1^{-k+4}}{-k+4}\right) \\
& - b_{90}\left(\frac{r^{2k+2} - r_1^{2k+2}}{2k+2}\right) - b_{91}\left(\frac{r_2^{-2k+2} - r^{-2k+2}}{-2k+2}\right) - b_{92}\left(\frac{r^{-3k} - r_1^{-3k}}{3k}\right) \\
& - b_{96}\left(\frac{r^6 - r_1^6}{6}\right) + b_{100}\left(\frac{r^4 \ln r - r_1^4 \ln r_1}{4} - \frac{r^4 - r_1^4}{16}\right)].
\end{aligned}
$$ (2.76)

2.4   Results and discussion

2.4.1   Pumping characteristics

This section deals with the effects of different parameters involved in the study of pressure gradient $\frac{\partial p}{\partial z}$, frictional forces $F^{(i)}$ and $F^{(0)}$ and pressure rise ΔP. $Figs$ $2.2 - 2.13$ depicts these effects. In Fig 2.2, pressure gradient variations are given against axial coordinates z for values of Hartmann number M and keeping other parameters fixed. As M elevates, maximum amplitude of pressure gradient rises. Fig 2.3 describes that by elevating Brownian motion parameter N_b, the amplitude of pressure gradients drops. Fig 2.4 depicts a decline in pressure gradient with elevating values of thermophoresis parameter N_t. It is evident from figures that pressure gradient

26

is compact in extensive part of annulus $z \; \epsilon \; [0, 0.5]$ and in the shrinked section $z \; \epsilon \; [0.5, 1]$ the pressure gradient is significantly greater i.e. in the extensive portion, fluid can smoothly flow without interference of huge pressure gradient whereas in the shrinked section, massive pressure gradient is required to sustain the flux primarily at the narrowest point $z = 0.75$. This even satisfies the physical situation. $Figs \; 2.5 - 2.7$ gives the variation of pressure rise with the volume flow rate with varying M, N_b, N_t. These figures depict an inverse relation among pressure rise and flow rate i.e. a rise in flow rate drops the pressure rise which describes that maximum pressure results in zero flow rate and elevating flow rate reduces the pressure rise. Retrograde pumping region $(\Delta P > 0, q < 0)$, augmented pumping region $(\Delta P < 0, q > 0)$ and peristaltic pumping region $(\Delta P > 0, q > 0)$ are the pumping regions which are displayed in the $Fig \; 2.5$ within the intervals $q \; \epsilon \; [0, 0.5]$, $q \; \epsilon \; [0.5, 0.7]$ and $q \; \epsilon \; [0.7, 1]$ respectively. It is also evident that by increasing Hartmann number M, the pressure rise elevates in the retrograde pumping region and opposite behaviors are observed in augmented pumping. Also $Fig \; 2.5$ reveals free pumping region for $\Delta P = 0$, $q = 0$. It can be seen in $Fig \; 2.6$ that by elevating Brownian motion parameter N_b, pressure rise decreases whereas for increasing thermophoresis parameter N_t pressure rise show an increase which is revealed in $Fig \; 2.7$.

Frictional forces for inner and outer wall against flow rate are shown in $Fig \; 2.8 - 2.13$. Behavior of these forces is entirely opposite to that of pressure rise whereas both behave likewise for maintaining the values of different parameters. Also outer wall friction is observed to be dominant as compared to inner wall friction.

2.4.2 Magnetic field characteristics

The variations of axial induced magnetic field h_z at $r = 0.22$ with other settled arrangement of parameters with various estimations of Hartmann number M along axial coordinate z is shown in $Fig \; 2.14$. It is revealed that by expanding the values of M, the axial induced magnetic field h_z show an increment. Behaviour of h_z for several values of q is described in $Fig \; 2.17$. As q elevates, h_z show decreasing behavior. In $Fig \; 2.17$, variation of R_m is taken to investigate the induced magnetic field along z coordinate. By increasing R_m, h_z first increases in the region $[0, 0.1]$ then decreasing behavior is observed in region $[0.1, 0.4]$ and again a sharp increasing behavior is seen in the region $[0.4, 1]$.

In Fig 2.17, different values of M are taken for induced magnetic field across annulus. It declines in region $[0, 0.4]$ whereas elevates in region $[0.4, 1]$ for increasing values of M. A rise in magnetic Reynolds number R_m results in rise of induced magnetic field h_z as depicted in Fig 2.18. Similar behavior is observed for flow rate q which can be seen in Fig 2.18. By increasing Weisenberg number We , induced magnetic field h_z first decreases in region $[0, 0.5]$ and then follows an increasing attitude in region $[0.5, 1]$ as plotted in Fig 2.20. Current density J_o across annulus is discussed in Fig $2.21 - 2.22$. It is observed that current density for increasing M initially declines and then elevates for increasing R_m.

2.4.3   Nanofluid characteristics

It is seen that the temperature profile θ elevates with the increasing value of Brownian motion parameter N_b as can be seen in Fig 2.23. Exactly same behavior is found for thermophoresis parameter N_t in Fig 2.24. Now by increasing N_b, concentration profile σ is found to be increasing as seen in Fig 2.25 whereas for increasing N_t opposite trend is noticed i.e. σ shows decline as depicted in Fig 2.26.

2.4.4   Fluid trapping

When an internal circulating bolus of fluid is formed along closed streamline and moves forward with peristaltic wave then such phenomenon is said to be trapping. Trapping situation is described by plotting the streamlines in $Figs$ $2.27 - 2.29$.
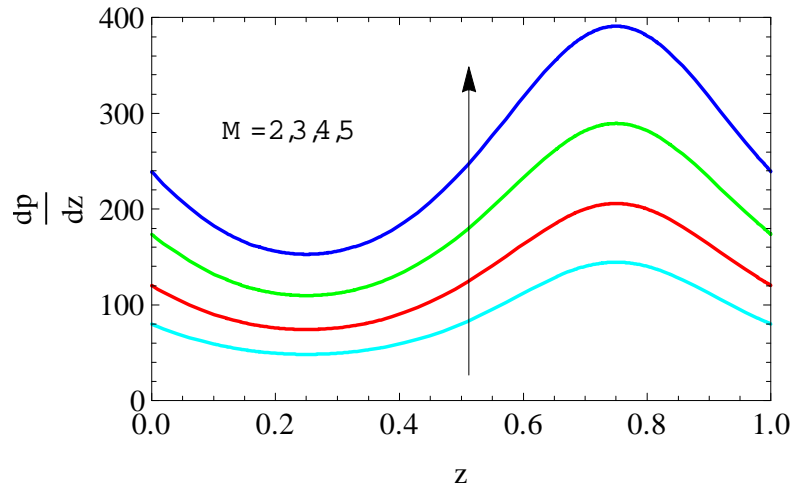
$Fig.\ 2.2$: Pressure gradient dp/dz with z for different values of M.
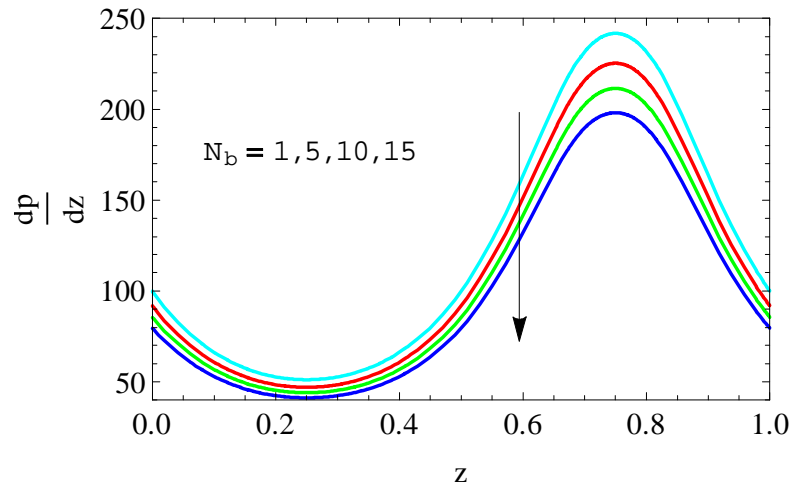
$Fig.\ 2.3$: Pressure gradient dp/dz with z for different values of N_b.
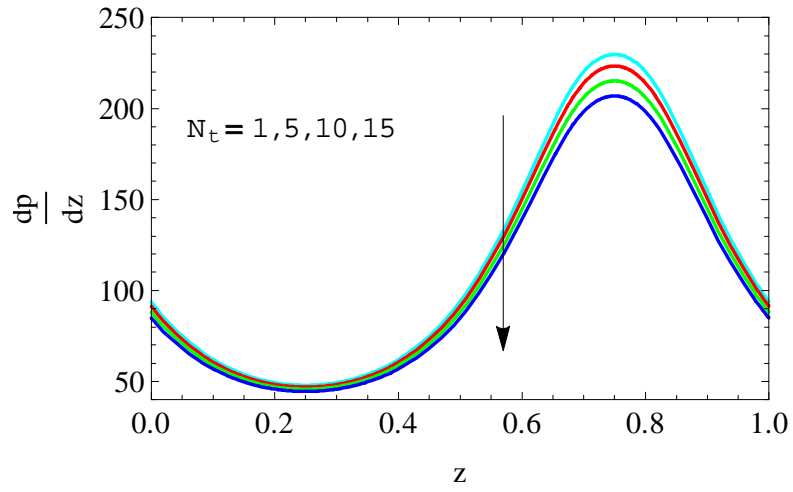
$Fig.\ 2.4$: Pressure gradient dp/dz with z for different values of N_t.
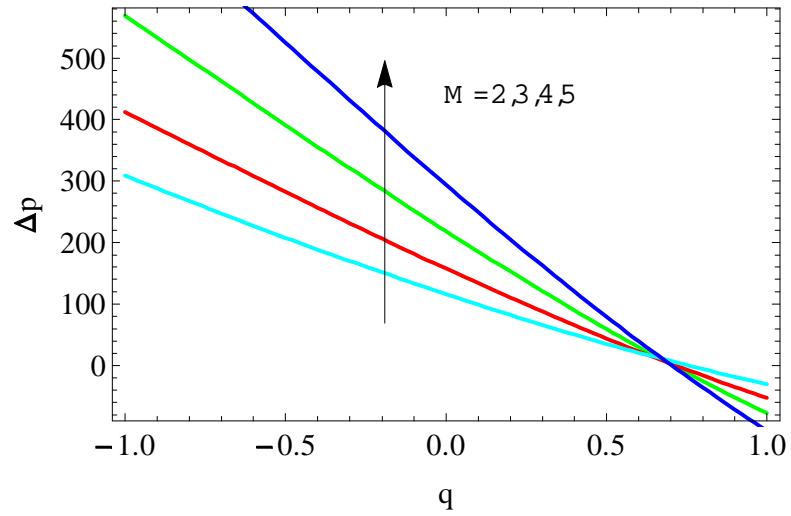
$Fig.\ 2.5$: Pressure rise Δp with q for different values of M.
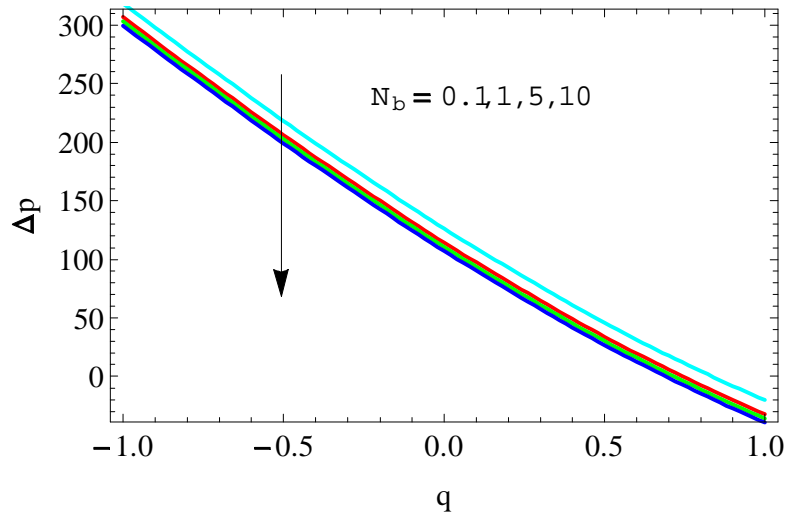
$Fig.$ 2.6 : Pressure rise Δp with q for different values of N_b.
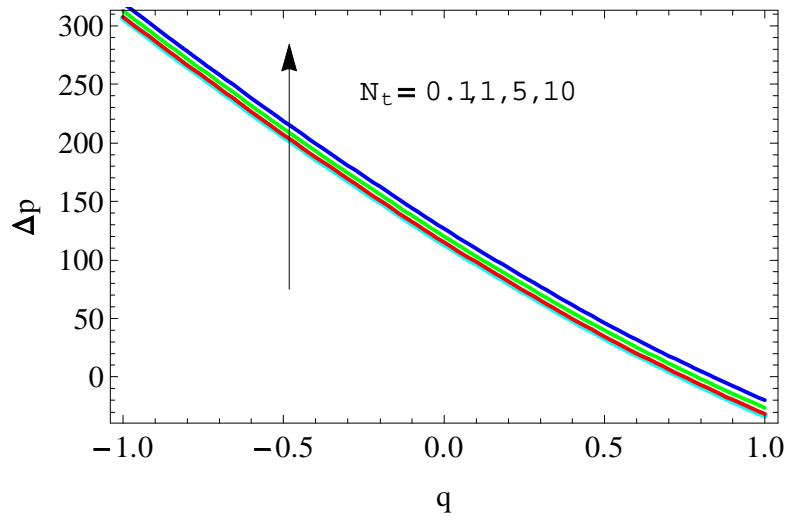
$Fig.$ 2.7 : Pressure rise Δp with q for different values of N_t.

31
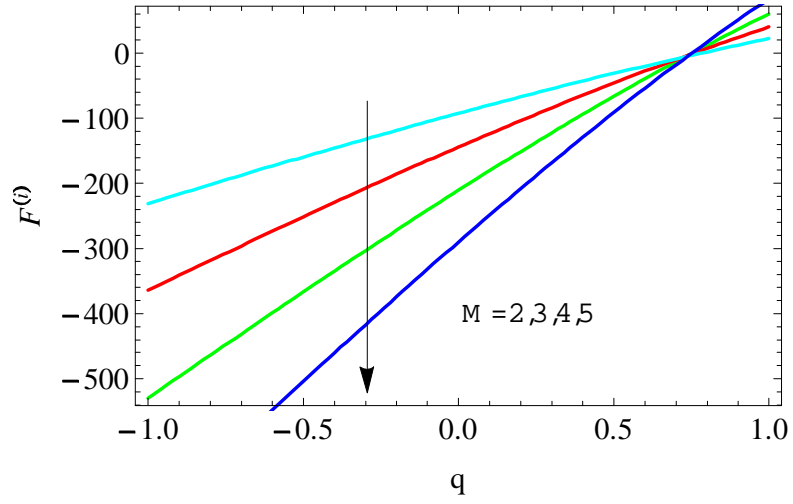
Fig. 2.8: Friction force $F(i)$ (on inner wall) with q for different values of M.
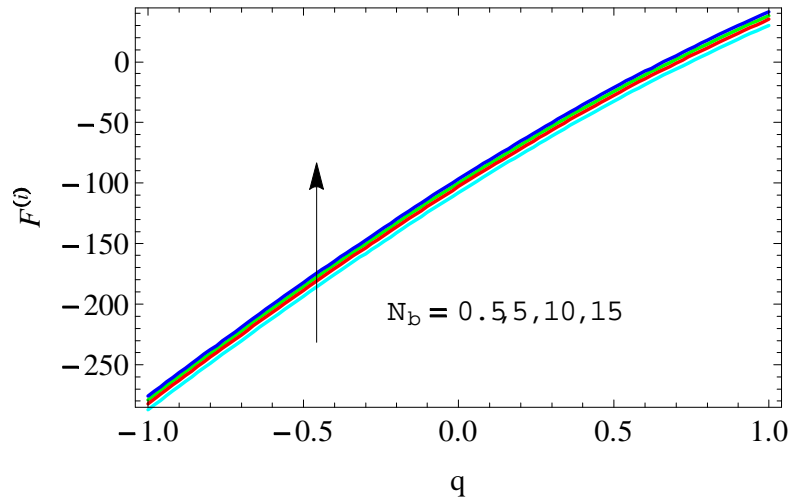
Fig. 2.9: Friction force $F(i)$ (on inner wall) with q for different values of N_b.
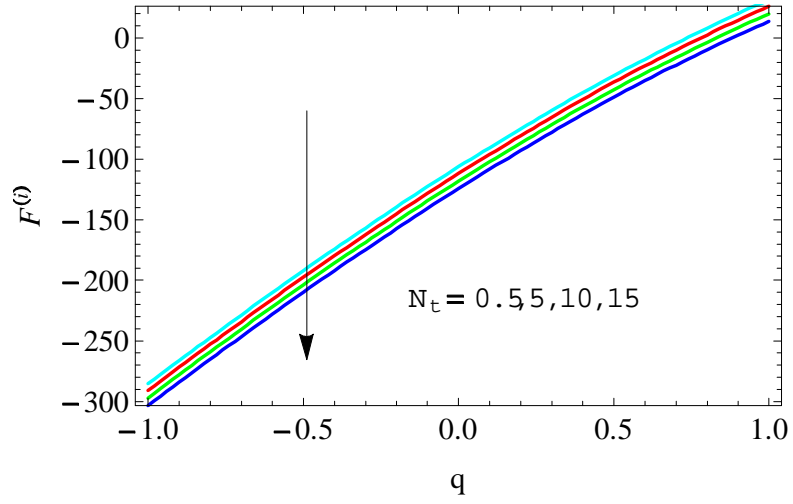
$Fig.$ 2.10: Friction force $F(i)$ (on inner wall) with q for different values of N_t.
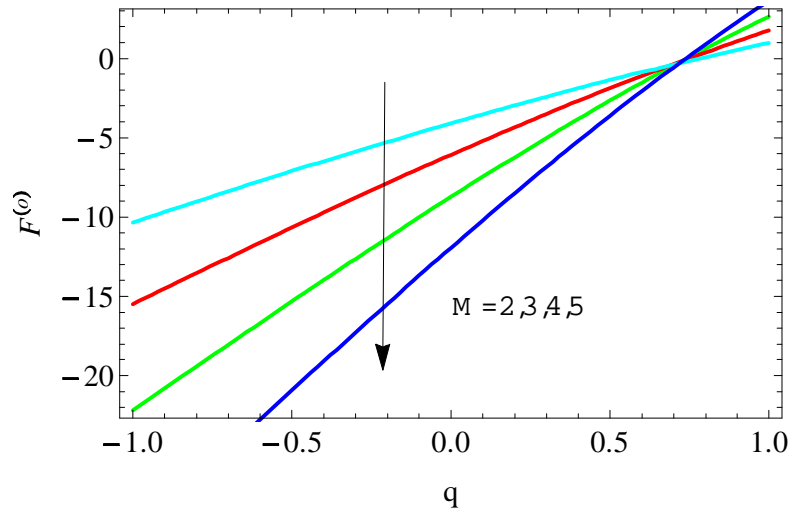
$Fig.$ 2.11: Friction force $F(o)$ (on outer wall) with q for different values of M.
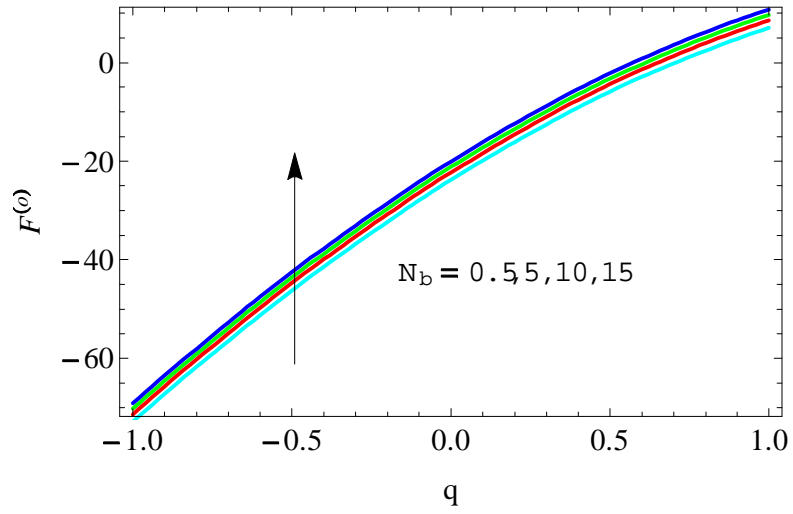
Fig. 2.12: Friction force $F(o)$ (on outer wall) with q for different values of N_b.
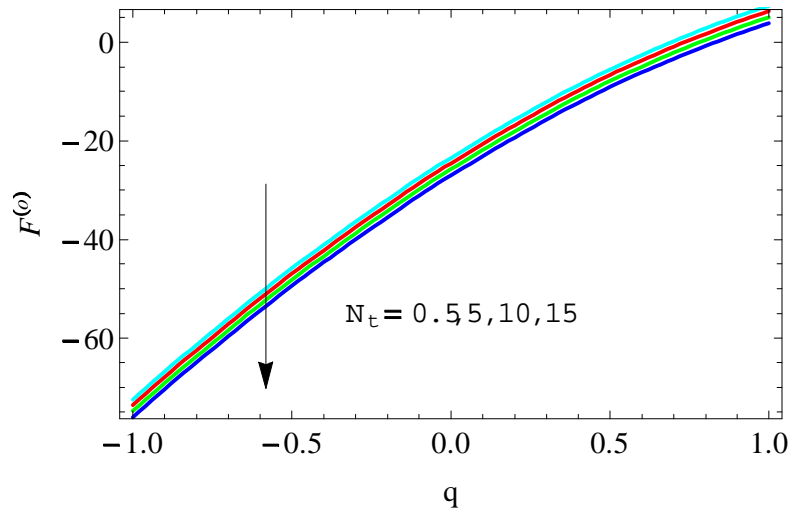
Fig. 2.13: The variation of friction force $F(o)$ (on outer wall) with q for different values of N_t.
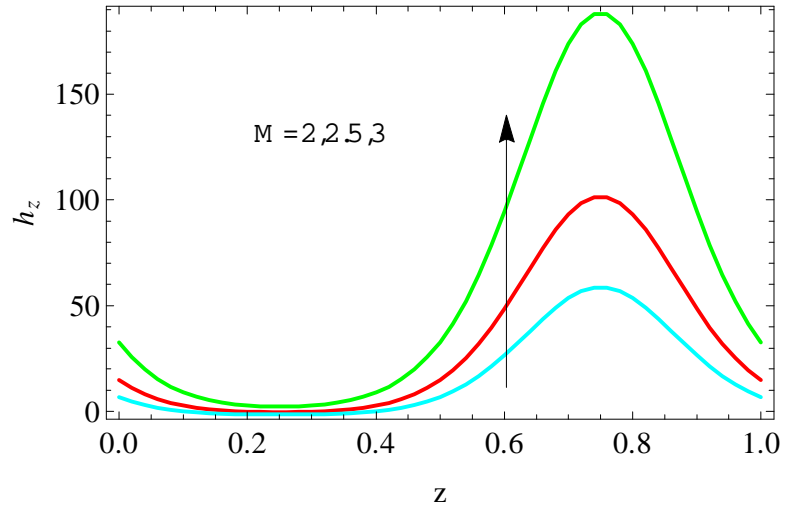
$Fig.$ 2.14: Axial induced magnetic field h_z with z for different values of M.
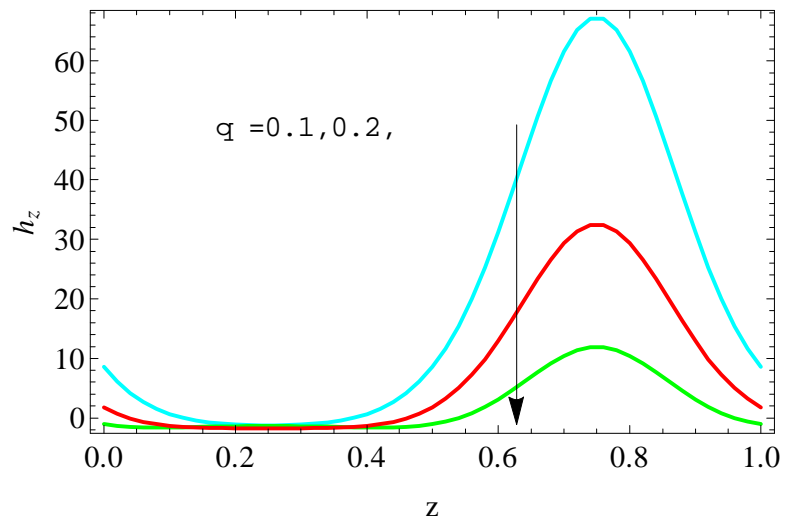
$Fig.$ 2.15: Axial induced magnetic field h_z with z for different values of q.
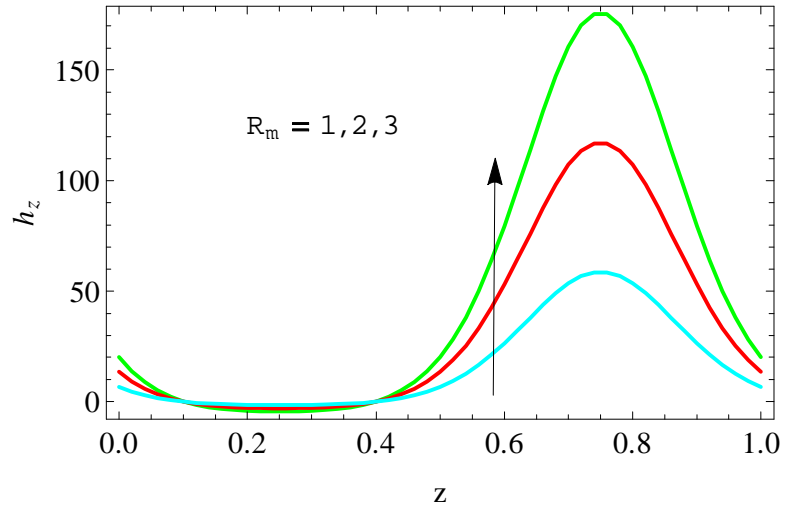
$Fig.$ 2.16: Axial induced magnetic field h_z with the z for different values of R_m.
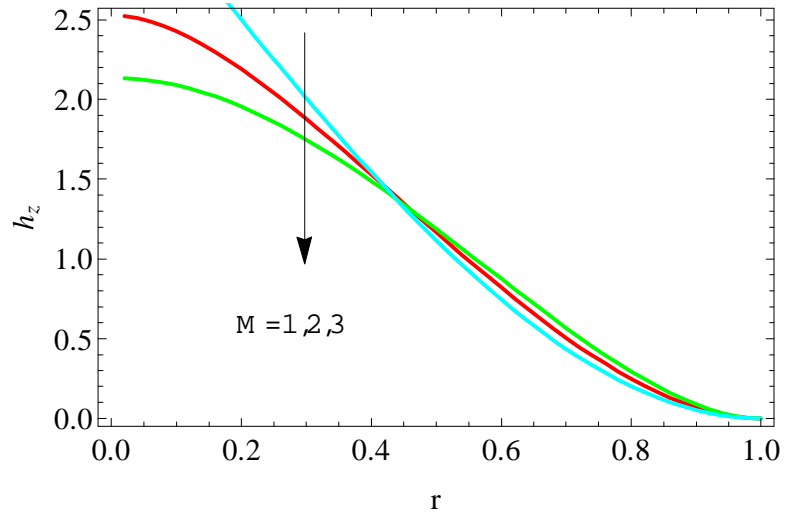
$Fig.$ 2.17: The modifications of axial induced magnetic field h_z with the radial coordinate r for different values of M where $r \in [\epsilon, r_2]$.
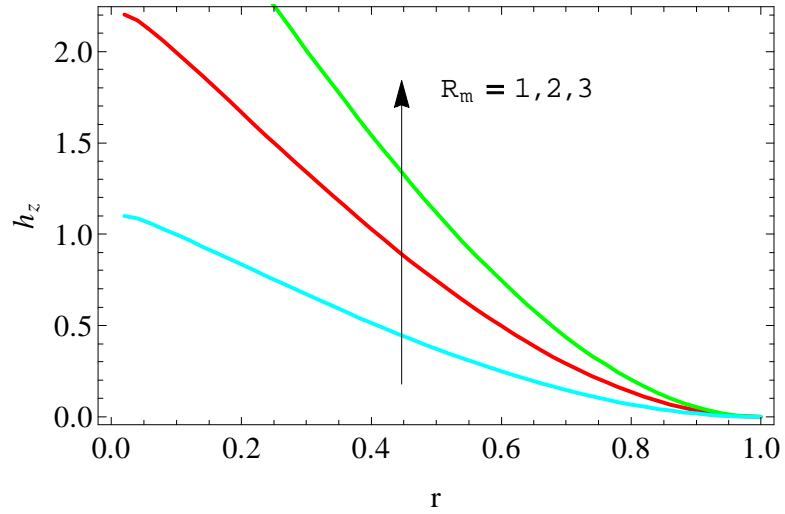
Fig. 2.18: The modifications of axial induced magnetic field h_z with the radial coordinate r for different values of R_m where $r \in [\epsilon, r_2]$.
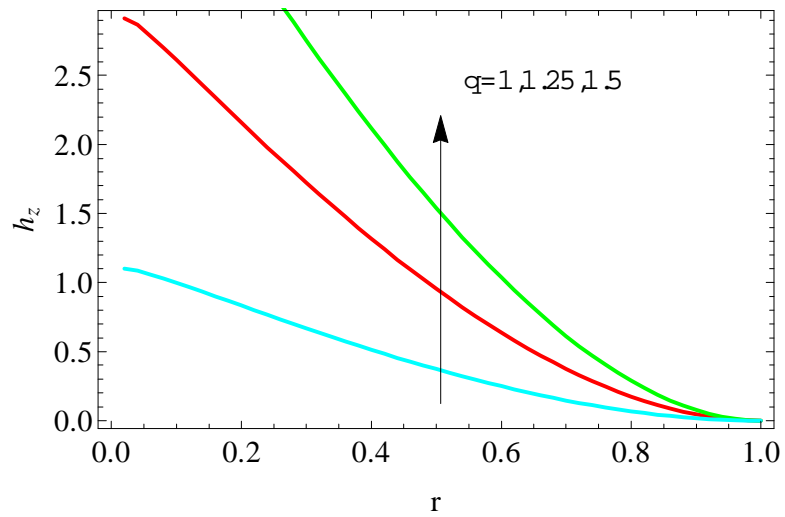
Fig. 2.19: The modifications of axial induced magnetic field h_z with the radial coordinate r for different values of q where $r \in [\epsilon, r_2]$.
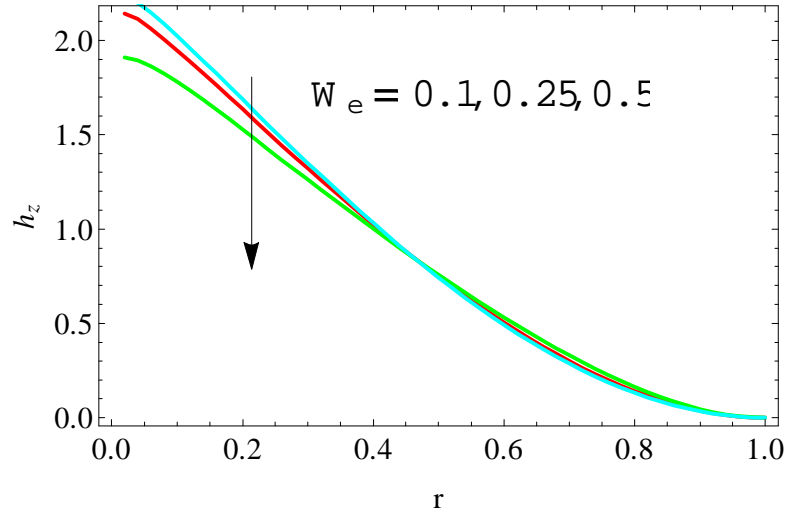
$Fig.$ 2.20: The modification of axial induced magnetic field h_z with the radial coordinate r for different values of W_e where $r \in [\epsilon, r_2]$.
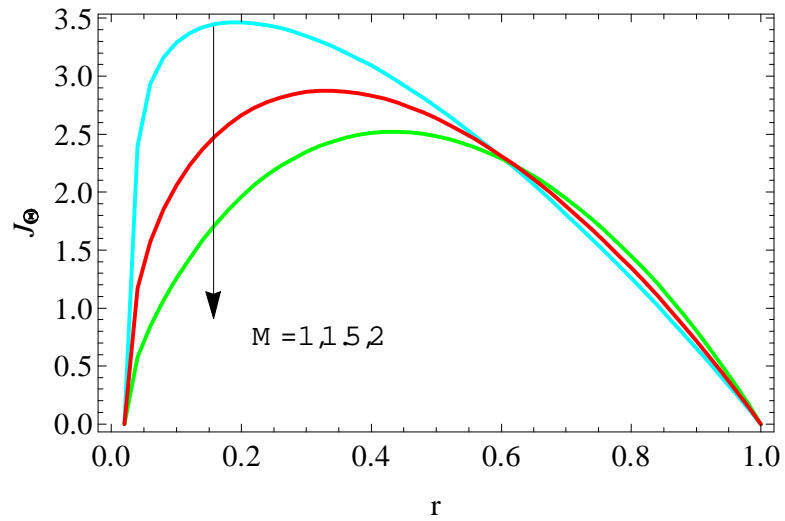
$Fig.$ 2.21: The modification of current density J_o across the annulus for different values of M where $r \in [\epsilon, r_2]$.
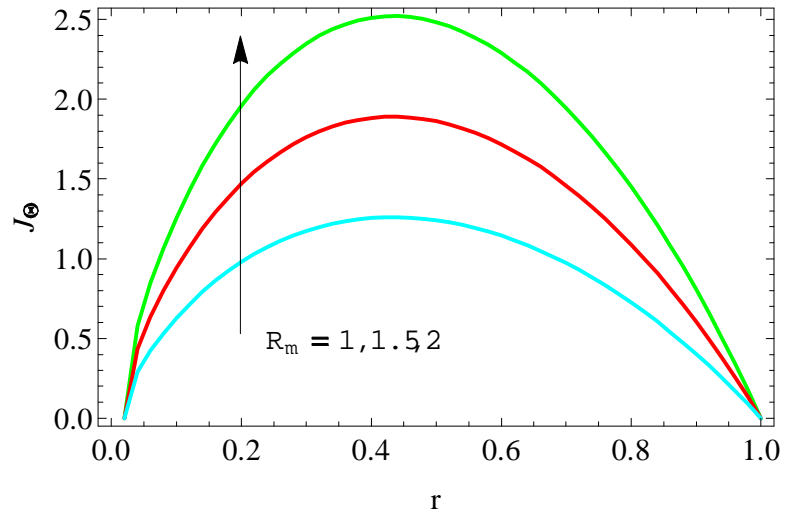
Fig. 2.22: The variation of current density J_o with the radial coordinate r for different values of R_m where $r \in [\epsilon, r_2]$.
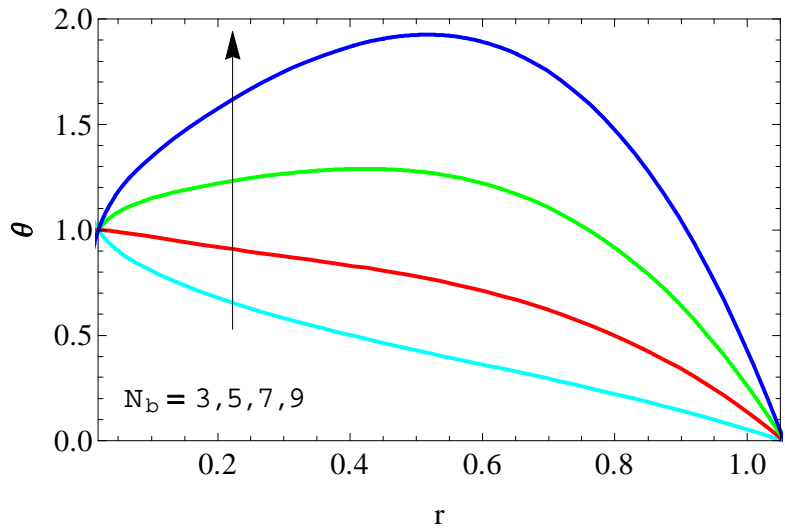
Fig. 2.23: Temperature profile for modifications of N_b.
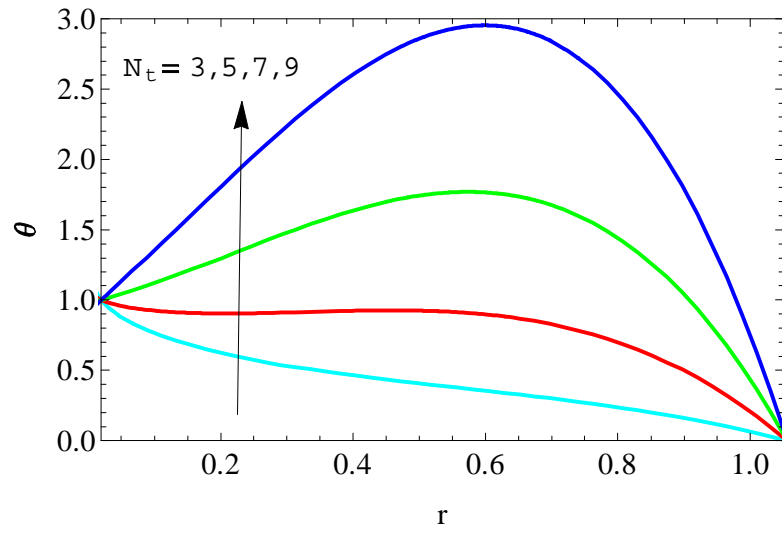
Fig. 2.24: Temperature profile for modifications of N_t.
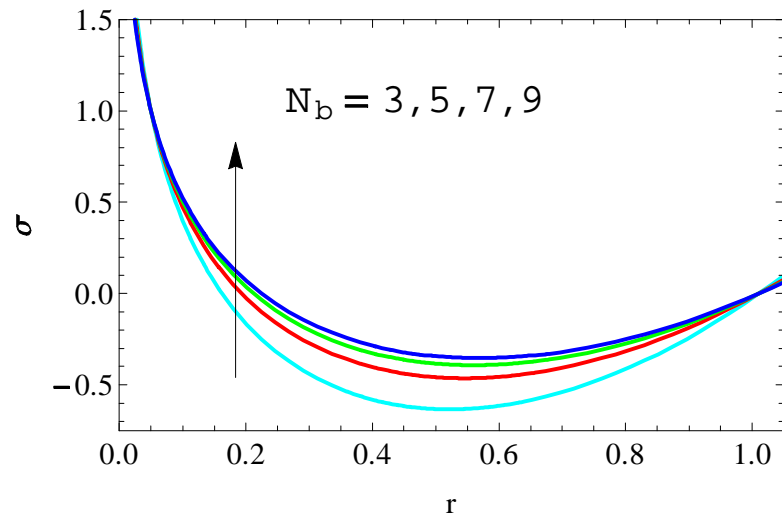
Fig. 2.25: Concentration profile for modifications of N_b.
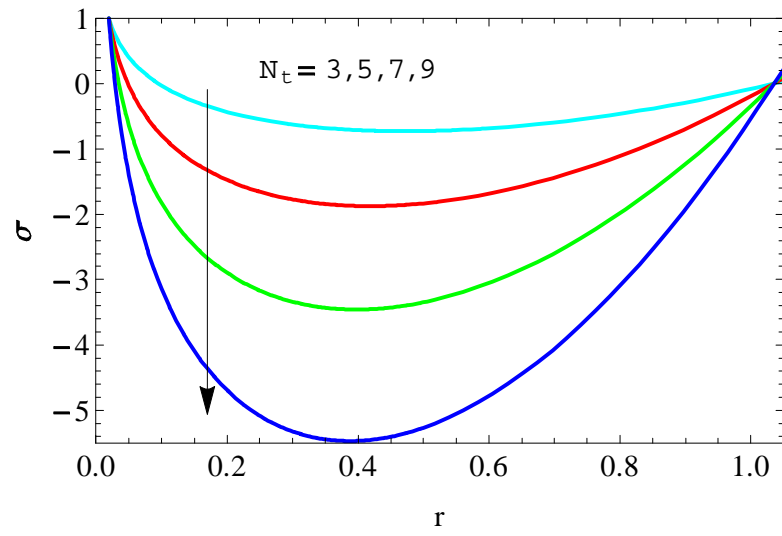
$Fig.$ 2.26: Concentration profile for modifications of N_t.
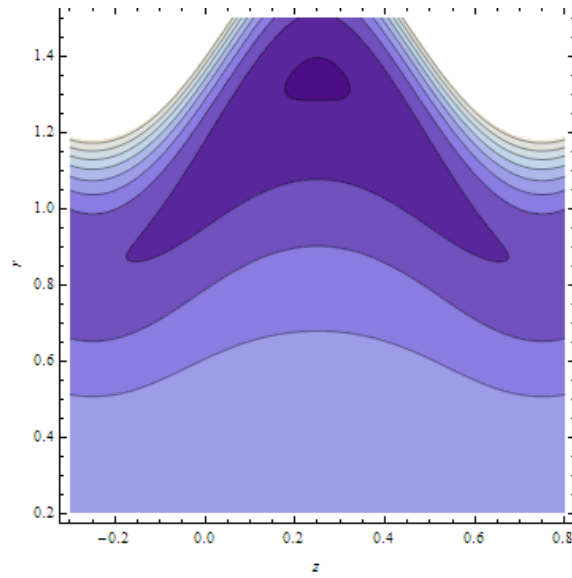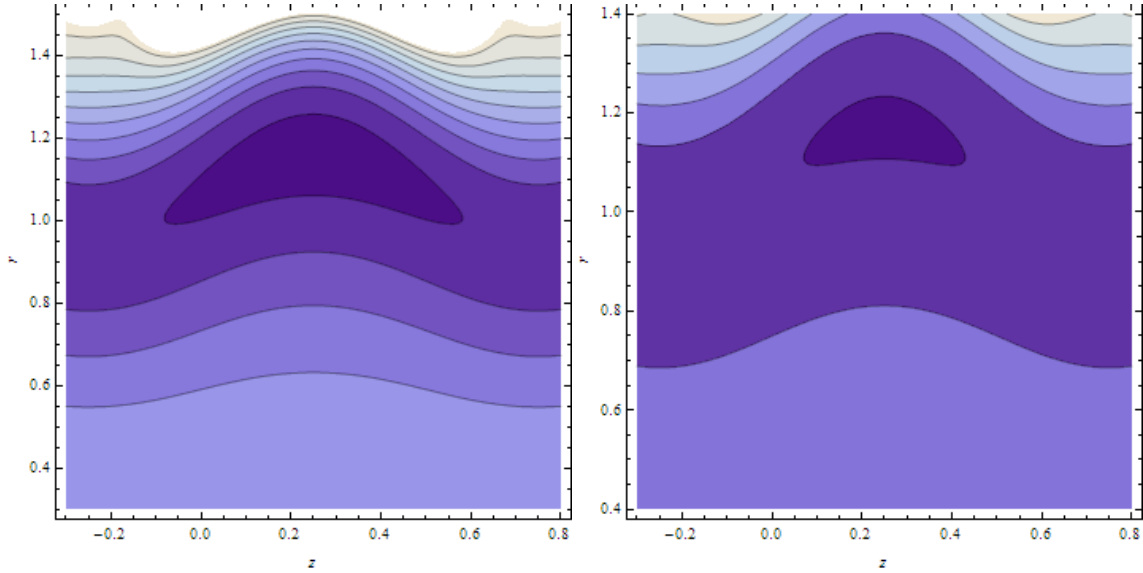
$Fig.2.27$: Streamlines for $\epsilon = 0.2,\ \ \epsilon = 0.3, \epsilon = 0.4$.

2.5   Conclusions

This study observes the impact of induced magnetic filed on peristaltic flow of nano hyperbolic tangent fluid in an endoscope. The main findings of the examination are given beneath.

- The greatest amplitude of pressure gradient boosts as the Hartmann number elevate while it drops for expanding values of N_b and N_t.

- For rising values of N_b and N_t retrograde, peristaltic and augmented pumping grows.

- There is a contrarily linear relation among Δp and q that is pressure rise falls off with rising flow rate.

- The outer and inner friction forces carry on by an opposite manner contrasted with pressure rise Δp.

- The induced magnetic field h_z boosts by aggravating Magnetic Reynolds number across the endoscope.

- Expansion in values of Magnetic Reynolds number results in larger current density J_o.

- Temperature profile gives increasing behavior with rising values of N_b and N_t.

- Nanoparticles concentration decline with the rise of N_t and elevates with increasing N_b.

2.6   Appendix

$$s_{11} = r_1 - r_2, \ s_{12} = \frac{r_2}{s_{11}}, \ s_{13} = N_b + N_t, \ s_{13\prime} = 2N_t + N_b, \ s_{14} = \ln r_1 - \ln r_2,$$

$$s_{15} = r_2^2 - r_1^2, \ s_{16} = \frac{-s_{13}}{4s_{11}^2}, \ s_{17} = \frac{1}{s_{14}} + \frac{s_{15}s_{16}}{s_{14}}, \ s_{18} = r_2^2 \ln r_1 - r_1^2 \ln r_2,$$

$$s_{19} = \frac{-\ln r_2}{s_{14}} - \frac{s_{16}s_{18}}{s_{14}}, \ s_{20} = s_{12} + s_{19}, \ s_{21} = \frac{-s_{13}}{N_b s_{11}}, \ s_{22} = \frac{s_{12}s_{13}}{N_b},$$

$$s_{23} = \frac{-s_{21}s_{11}}{s_{14}}, \ s_{24} = r_1 \ln r_2 - r_2 \ln r_1, \ \ell_{25} = \frac{s_{21}s_{24}}{s_{14}} - s_{22}, \ s_{26} = s_{22} + s_{25},$$

$$s_{27} = \frac{-N_t}{N_b}, \ s_{28} = s_{16}s_{27}, \ s_{29} = \frac{s_{27}}{s_{11}}, \ s_{30} = s_{17}s_{27}, \ s_{31} = s_{20}s_{27},$$

$$s_{32} = \frac{s_{15}s_{28} + s_{11}s_{29} - s_{14}s_{30}}{s_{14}}, \ s_{33} = -\frac{s_{18}s_{28} + s_{24}s_{29} + s_{14}s_{31}}{s_{14}}, s_{34} = s_{30} + s_{32},$$

$$s_{35} = s_{31} + s_{33}, \ s_{36} = \frac{1}{s_{11}} + s_{21} - s_{29}, \ s_{37} = s_{23} + s_{34}, s_{38} = s_{26} - s_{12} + s_{35},$$

$$s_{39} = \frac{-2s_{13\prime}s_{16}}{9s_{11}}, s_{40} = \frac{-s_{13\prime}}{4s_{11}^2} + \frac{N_b s_{21}}{4s_{11}}, \ s_{41} = \frac{-s_{13\prime}s_{17}}{s_{11}} - \frac{N_b s_{23}}{s_{11}}, \ s_{42} = r_1^3 - r_2^3,$$

$$s_{43} = \frac{-s_{39}s_{42} - s_{15}s_{40} - s_{11}s_{41}}{s_{14}}, \ s_{44} = r_1^3 \ln r_2 - r_2^3 \ln r_1, \ s_{45} = \frac{s_{39}s_{44} + s_{18}s_{40} + s_{24}s_{41}}{s_{14}},$$

$$s_{46} = s_{16} - s_{40}, \ s_{47} = s_{17} + s_{43}, \ s_{48} = -s_{12} + s_{20} + s_{45},$$

$$b_1 = \frac{r_1^2 r_2^k - r_1^k r_2^2}{r_1^k r_2^{-k} - r_1^{-k} r_2^k}, \ b_2 = \frac{1}{4\,(1-n) - M^2 r_2^2}, \ b_3 = \frac{r_1^2 r_2^{-k} - r_1^{-k} r_2^2}{r_1^{-k} r_2^k - r_1^k r_2^{-k}},$$

$$b_4 = b_2 b_3, \ b_5 = b_1 b_2, b_6 = \frac{(r_2^2 - r_1^2)}{2},$$

$$b_7 = 2b_4 \frac{\left(r_2^{k+2} - r_1^{k+2}\right)}{k+2} + 2b_5 \frac{\left(r_2^{-k+2} - r_1^{-k+2}\right)}{-k+2} + 2b_2 \frac{(r_2^4 - r_1^4)}{4},$$

$$b_8 = \frac{1}{k^2\,(1-n) - M^2 r_2^2}, \ b_9 = \frac{1}{(1-n)\,(2k-1)^2 - M^2 r_2^2},$$

$$b_{10} = \frac{1}{(1-n)\,(2k+1)^2 - M^2 r_2^2}, b_{11} = \frac{1}{(1-n)\,9 - M^2 r_2^2},$$

$$b_{12} = \frac{1}{(1-n) - M^2 r_2^2}, \ b_{13} = \frac{1}{(1-n)\,(k+1)^2 - M^2 r_2^2},$$

$$b_{14} = \frac{1}{(1-n)\,(-k+1)^2 - M^2 r_2^2}, \ b_{15} = kb_4 b_8, \ b_{18} = kb_5 b_8,$$

$$b_{19} = 2b_2^2, b_{20} = k\,(k-1)\,b_4 b_8, b_{21} = k\,(k+1)\,b_5 b_8, b_{22} = 2b_2^2,$$

$$b_{23} = b_4 b_8, \ b_{24} = b_5 b_8, b_{25} = b_2^2, \ b_{26} = k^2 b_4^2 b_9, b_{27} = k^2 b_5^2 b_{10},$$

$$b_{28} = 4b_2^2 b_{11}, \ b_{29} = 2k^2 b_4 b_5 b_{12}, b_{30} = 4kb_2 b_4 b_{13}, \ b_{31} = 4kb_2 b_5 b_{14},$$

$$b_{32} = k^2\,(k-1)\,b_4^2 b_9, b_{33} = k^2\,(k+1)\,b_5^2 b_{10}, b_{34} = 2kb_2 b_5 b_{14},$$

$$b_{35} = k^2\,(k-1)\,b_4 b_5 b_{12}, b_{36} = k^2\,(k+1)\,b_5^2 b_{10}, \ b_{37} = 2kb_2 b_5 b_{14},$$

$$b_{38} = 2k(k-1)b_2b_4b_{13}, \; b_{39} = 2k(k+1)b_2b_5b_{14},$$

$$b_{40} = 4b_2^2b_{11}, b_{41} = -(1-n)\frac{\partial p_o}{\partial z}b_{17} - (1-n)\frac{\partial p_o}{\partial z}b_{20} + M^2r_2^2\frac{\partial p_o}{\partial z}b_{23},$$

$$b_{42} = (1-n)\frac{\partial p_o}{\partial z}b_{18} - (1-n)\frac{\partial p_o}{\partial z}b_{21} + M^2r_2^2\frac{\partial p_o}{\partial z}b_{24},$$

$$b_{43} = -(1-n)\frac{\partial p_o}{\partial z}b_{19} - (1-n)\frac{\partial p_o}{\partial z}b_{22} + M^2r_2^2\frac{\partial p_o}{\partial z}b_{25} + \left(\frac{g_r + b_r}{r_1 - r_2}\right)r_2b_2,$$

$$b_{44} = -nW_e\left(\frac{\partial p_o}{\partial z}\right)^2 b_{26} - 2nW_e\left(\frac{\partial p_o}{\partial z}\right)^2 b_{32},$$

$$b_{45} = -nW_e\left(\frac{\partial p_o}{\partial z}\right)^2 b_{27} + 2nW_e\left(\frac{\partial p_o}{\partial z}\right)^2 b_{36},$$

$$b_{46} = -nW_e\left(\frac{\partial p_o}{\partial z}\right)^2 b_{28} - 2nW_e\left(\frac{\partial p_o}{\partial z}\right)^2 b_{40} - \left(\frac{g_r + b_r}{r_1 - r_2}\right)b_{11},$$

$$b_{47} = [nW_eb_{29} - 2nW_e(b_{33} - b_{35})]\left(\frac{\partial p_o}{\partial z}\right)^2,$$

$$b_{48} = [-nW_eb_{30} - 2nW_eb_{34} - 2nW_eb_{38}]\left(\frac{\partial p_o}{\partial z}\right)^2,$$

$$b_{49} = \left(\frac{\partial p_o}{\partial z}\right)^2 [nW_eb_{31} + 2nW_eb_{37} - 2nW_eb_{39}], b_{50} = b_2\left(\frac{r_1^2 r_2^k - r_1^k r_2^2}{r_1^{-k} r_2^k - r_1^k r_2^{-k}}\right),$$

$$b_{51} = b_{42} + \frac{1}{r_1^{-k} r_2^k - r_1^k r_2^{-k}}[b_{43}\left(r_1^2 r_2^k - r_1^k r_2^2\right) + b_{44}\left(r_1^{2k-1} r_2^k - r_1^k r_2^{2k-1}\right)$$

$$+ b_{45}\left(r_1^{-(2k+1)} r_2^k - r_1^k r_2^{-(2k+1)}\right) b_{46}\left(r_1^3 r_2^k - r_1^k r_2^3\right) + b_{47}\left(r_1^{-1} r_2^k - r_1^k r_2^{-1}\right)$$

$$+ b_{48}\left(r_1^{k+1} r_2^k - r_1^k r_2^{k+1}\right) + b_{49}\left(r_1^{-k+1} r_2^k - r_1^k r_2^{-k+1}\right),$$

$$b_{52} = b_2\left(\frac{r_1^2 r_2^{-k} - r_1^{-k} r_2^2}{r_1^k r_2^{-k} - r_1^{-k} r_2^k}\right), b_{53} = b_{41} + \frac{1}{r_1^{-k} r_2^k - r_1^k r_2^{-k}}\left[b_{43}\left(r_1^2 r_2^{-k} - r_1^{-k} r_2^2\right)\right.$$

$$+ b_{44}\left(r_1^{2k-1} r_2^{-k} - r_1^{-k} r_2^{2k-1}\right) + b_{45}\left(r_1^{-(2k+1)} r_2^{-k} - r_1^{-k} r_2^{-(2k+1)}\right)$$

$$+ b_{46}\left(r_1^3 r_2^{-k} - r_1^{-k} r_2^3\right) + b_{47}\left(r_1^{-1} r_2^{-k} - r_1^{-k} r_2^{-1}\right) + b_{48}\left(r_1^{k+1} r_2^{-k} - r_1^{-k} r_2^{k+1}\right)$$

$$+ b_{49}\left(r_1^{-k+1} r_2^{-k} - r_1^{-k} r_2^{-k+1}\right),$$

$$b_{54} = b_{41} - b_{53}, \; b_{55} = b_{42} - b_{51},$$

$$b_{56} = 2\left[-b_{52}\left(\frac{r_2^{k+2} - r_1^{k+2}}{k+2}\right) - b_{50}\left(\frac{r_2^{-k+2} - r_1^{-k+2}}{-k+2}\right) + b_2\left(\frac{r_2^4 - r_1^4}{4}\right)\right],$$

45

$$b_{57} = 2[b_{44}\left(\frac{r_2^{2k+1} - r_1^{2k+1}}{2k+1}\right) + b_{45}\left(\frac{r_2^{-2k+1} - r_1^{-2k+1}}{-2k+1}\right) + b_{46}\left(\frac{r_2^5 - r_1^5}{5}\right)$$

$$+ b_{47}\left(r_2 - r_1\right) + b_{48}\left(\frac{r_2^{k+3} - r_1^{k+3}}{k+3}\right) + b_{49}\left(\frac{r_2^{-k+3} - r_1^{-k+3}}{-k+3}\right)$$

$$+ b_{54}\left(\frac{r_2^{k+2} - r_1^{k+2}}{k+2}\right) + b_{55}\left(\frac{r_2^{-k+2} - r_1^{-k+2}}{-k+2}\right) + b_{43}\left(\frac{r_2^4 - r_1^4}{4}\right),$$

$$b_{58} = \frac{1}{b_7} + \frac{1}{b_{56}}, b_{59} = \frac{b_6}{b_7} - \frac{b_{57}}{b_{56}},$$

$$b_{60} = 2nW_e\left(\frac{\partial p_o}{\partial z}\frac{\partial p_1}{\partial z}k^2\left(2k-1\right)b_4^2 + \frac{\partial p_o}{\partial z}k^2\left(2k-1\right)b_4b_{54}\right),$$

$$b_{61} = 2nW_e\left(\frac{\partial p_o}{\partial z}\frac{\partial p_1}{\partial z}2k^2b_4b_5 + \frac{\partial p_o}{\partial z}\left(k^2b_5b_{54} + k^2b_4b_{55}\right)\right),$$

$$b_{62} = 2nW_e\frac{\partial p_o}{\partial z}\left(\frac{\partial p_1}{\partial z}4k\left(k+1\right)b_2b_4 + 2k\left(k+1\right)b_4b_{43} + 2k\left(k+1\right)b_2b_{54}\right),$$

$$b_{63} = 2nW_e\frac{\partial p_o}{\partial z}\left(-\frac{\partial p_1}{\partial z}k^2\left(2k+1\right)b_5^2 - k^2\left(2k+1\right)b_5b_{55}\right),$$

$$b_{64} = 2nW_e\frac{\partial p_o}{\partial z}\left(\frac{\partial p_1}{\partial z}4k\left(k-1\right)b_2b_5 + 2k\left(k-1\right)b_5b_{43} + 2k\left(k-1\right)b_2b_{55}\right),$$

$$b_{65} = 2nW_e\frac{\partial p_o}{\partial z}k(2k-1)(3k-2)a_4a_{44},$$

$$b_{66} = 2nW_e\frac{\partial p_o}{\partial z}\left(k\left(2k+1\right)\left(k+2\right)b_4b_{45} - k\left(k+2\right)b_5b_{47}\right),$$

$$b_{67} = 2nW_e\frac{\partial p_o}{\partial z}\left(3k\left(k+2\right)\left(k+2\right)b_4b_{46} + 2\left(k+1\right)\left(k+2\right)b_2b_{48}\right),$$

$$b_{68} = 2nW_e\frac{\partial p_o}{\partial z}\left(k(-k+2)b_4b_{47} - k\left(k-2\right)\left(2k-1\right)b_5b_{44}\right),$$

$$b_{69} = 2nW_e\frac{\partial p_o}{\partial z}\left(3k(k-2)b_5b_{46} + 2\left(-k+2\right)\left(2-k\right)b_2b_{49}\right),$$

$$b_{70} = 2nW_e\frac{\partial p_o}{\partial z}\left(4k(2k-1)b_2b_{44} + 2k^2(k+1)b_4b_{48}\right),$$

$$b_{71} = 2nW_e\frac{\partial p_o}{\partial z}\left(4k(2k+1)b_2b_{45} + 2k^2\left(-k+1\right)b_5b_{49}\right),$$

$$b_{72} = 2nW_e\frac{\partial p_o}{\partial z}k(2k+1)(-3k-2)b_5b_{45}, b_{76} = 2nW_e\frac{\partial p_o}{\partial z}(24b_2b_{46}) + g_rs_{16},$$

$$b_{77} = 2nW_e(12\frac{\partial p_o}{\partial z}b_2b_{43} + 12\frac{\partial p_o}{\partial z}\frac{\partial p_1}{\partial z}b_2^2) + \frac{g_r}{s_{11}} + b_rs_{21}, b_{78} = g_rs_{20} + b_rs_{26},$$

$$b_{79} = g_rs_{17} + b_rs_{23}, b_{80} = b_9b_{60}, b_{81} = b_{12}b_{61}, b_{82} = b_{13}b_{62}, b_{83} = b_{10}b_{63},$$

$$b84 = b_{14}b_{64}, b_{85} = \frac{b_{65}}{(3k-2)^2\left(1-n\right) - M^2r_2^2},$$

$$b_{86} = \frac{b_{66}}{(k+2)^2\left(1-n\right) - M^2r_2^2}, b_{87} = \frac{b_{67}}{(k+2)^2\left(1-n\right) - M^2r_2^2},$$

$$b_{88} = \frac{b_{68}}{(k-2)^2 (1-n) - M^2 r_2^2}, b_{89} = \frac{b_{69}}{(-k+2)^2 (1-n) - M^2 r_2^2},$$

$$b_{90} = \frac{b_{70}}{(2k)^2 (1-n) - M^2 r_2^2}, b_{91} = \frac{b_{71}}{(2k)^2 (1-n) - M^2 r_2^2},$$

$$b_{92} = \frac{b_{72}}{(3k+2)^2 (1-n) - M^2 r_2^2}, b_{96} = \frac{b_{76}}{16 (1-n) - M^2 r_2^2},$$

$$b_{97} = b_{11} b_{77}, b_{98} = b_2 b_{78}, b_{99} = -b_{98} + \frac{2 b_{79} (1-n)}{(M^2 r_2^2)^2},$$

$$b_{100} = \frac{b_{79}}{M^2 r_2^2} + \frac{4 b_{79} (1-n)}{(M^2 r_2^2)^2},$$

$$\begin{aligned}
b_{101} = \ & \frac{1}{-r_1^k r_2^{-k} + r_1^{-k} r_2^k} (-b_{80}(r_1^{-1+2k} r_2^{-k} - r_1^{-k} r_2^{-1+2k}) - b_{81}(r_1^{-1} r_2^{-k} - r_1^{-k} r_2^{-1}) \\
& -b_{82}(r_1^{k+1} r_2^{-k} - r_1^{-k} r_2^{k+1}) - b_{83}(r_1^{-1-2k} r_2^{-k} - r_1^{-k} r_2^{-1-2k}) \\
& -b_{84}(r_1^{-k+1} r_2^{-k} - r_1^{-k} r_2^{-k+1}) - b_{85}(r_1^{3k-2} r_2^{-k} - r_1^{-k} r_2^{3k-2}) \\
& -b_{86}(r_1^{-k-2} r_2^{-k} - r_1^{-k} r_2^{-k-2}) - b_{87}(r_1^{k+2} r_2^{-k} - r_1^{-k} r_2^{k+2}) \\
& -b_{88}(r_1^{k-2} r_2^{-k} - r_1^{-k} r_2^{k-2}) - b_{89}(r_1^{-k+2} r_2^{-k} - r_1^{-k} r_2^{-k+2}) \\
& -b_{90}(r_1^{2k} r_2^{-k} - r_1^{-k} r_2^{2k}) - b_{91}(r_1^{-2k} r_2^{-k} - r_1^{-k} r_2^{-2k}) \\
& -b_{92}(r_1^{-3k-2} r_2^{-k} - r_1^{-k} r_2^{-3k-2}) - b_{96}(r_1^4 r_2^{-k} - r_1^{-k} r_2^4) \\
& -b_{97}(r_1^3 r_2^{-k} - r_1^{-k} r_2^3) + b_{99}(r_1^2 r_2^{-k} - r_1^{-k} r_2^2) \\
& +b_{100}(r_1^2 \ln r_1 r_2^{-k} - r_1^{-k} r_2^2 \ln r_2)),
\end{aligned}$$

$$\begin{aligned}
b_{102} = \ & \frac{1}{r_1^k r_2^{-k} - r_1^{-k} r_2^k} (-b_{80}(r_1^{-1+2k} r_2^k - r_1^k r_2^{-1+2k}) - b_{81}(r_1^{-1} r_2^k - r_1^k r_2^{-1}) \\
& -b_{82}(r_1^{k+1} r_2^k - r_1^k r_2^{k+1}) - b_{83}(r_1^{-1-2k} r_2^k - r_1^k r_2^{-1-2k}) \\
& -b_{84}(r_1^{-k+1} r_2^k - r_1^k r_2^{-k+1}) - b_{85}(r_1^{3k-2} r_2^k - r_1^k r_2^{3k-2}) \\
& -b_{86}(r_1^{-k-2} r_2^k - r_1^k r_2^{-k-2}) - b_{87}(r_1^{k+2} r_2^k - r_1^k r_2^{k+2}) \\
& -b_{88}(r_1^{k-2} r_2^k - r_1^k r_2^{k-2}) - b_{89}(r_1^{-k+2} r_2^k - r_1^k r_2^{-k+2}) \\
& -b_{90}(r_1^{2k} r_2^k - r_1^k r_2^{2k}) - b_{91}(r_1^{-2k} r_2^k - r_1^k r_2^{-2k}) \\
& -b_{92}(r_1^{-3k-2} r_2^k - r_1^k r_2^{-3k-2}) - b_{96}(r_1^4 r_2^k - r_1^k r_2^4) \\
& -b_{97}(r_1^3 r_2^k - r_1^k r_2^3) + b_{99}(r_1^2 r_2^k - r_1^k r_2^2) \\
& +b_{100}(r_1^2 \ln r_1 r_2^k - r_1^k r_2^2 \ln r_2)),
\end{aligned}$$

$$b_{103} = 2(b_{101}\frac{r_2^{k+2} - r_1^{k+2}}{k+2} + b_{102}\frac{r_2^{-k+2} - r_1^{-k+2}}{-k+2} - b_{80}\frac{r_2^{2k+1} - r_1^{2k+1}}{2k+1}$$

$$-b_{81}\frac{r_2 - r_1}{1} - b_{82}\frac{r_2^{k+3} - r_1^{k+3}}{k+3} - b_{83}\frac{r_2^{-2k+1} - r_1^{-2k+1}}{-2k+1}$$

$$-b_{84}\frac{r_2^{-k+3} - r_1^{-k+3}}{-k+3} - b_{85}\frac{r_2^{3k} - r_1^{3k}}{3k} - b_{86}\frac{r_2^{-k} - r_1^{-k}}{-k}$$

$$-b_{87}\frac{r_2^{k+4} - r_1^{k+4}}{k+4} - b_{88}\frac{r_2^k - r_1^k}{k} - b_{89}\frac{r_2^{-k+4} - r_1^{-k+4}}{-k+4}$$

$$-b_{90}\frac{r_2^{2k+2} - r_1^{2k+2}}{2k+2} - b_{91}\frac{r_2^{-2k+2} - r_1^{-2k+2}}{-2k+2} - b_{92}\frac{r_2^{-3k} - r_1^{-3k}}{-3k}$$

$$-b_{96}\frac{r_2^6 - r_1^6}{6} - b_{97}\frac{r_2^5 - r_1^5}{5} - b_{99}\frac{r_2^4 - r_1^4}{4}$$

$$+b_{100}(\frac{r_2^4 \ln r_2 - r_1^4 \ln r_2}{4} - \frac{r_2^4 - r_1^4}{16}))$$

$$b_{104} = 2(b_2\frac{r_2^4 - r_1^4}{4} + b_4\frac{r_2^{k+2} - r_1^{k+2}}{k+2} + b_{15}\frac{r_2^{-k+2} - r_1^{-k+2}}{-k+2}),$$

$$b_{105} = b_{54} + b_{101}, b_{106} = b_{55} + b_{102}, b_{107} = b_{43} + b_{99},$$

$$b_{108} = b_{44} - b_{80}, b_{109} = b_{95} - b_{83}, b_{110} = b_{46} - b_{97},$$

$$b_{111} = b_{47} - b_{81}.b_{112} = b_{48} - b_{82}, b_{113} = b_{49} - b_{84}.$$

Chapter 3

Au-nanoparticles analysis of catheterised curved tube with biddable walls

In the extant analysis, we have analyzed the peristaltic transport of Au-nanoparticles in curved tube having biddable walls. Governing equations have been derived for curved tube by using toroidal coordinate system. Long wavelength and low Reynolds number approximation are utilised to tackle the nonlinear partial differential equation. Furthermore, perturbation approximation is used to achieve the analytical solutions such as axial velocity and streamlines. Graphs are plotted to understand the physical features of dominant parameters such as Grashoff's number, heat source/sink parameter, amplitude ratio and elastic parameters. Also temperature tables are subsumed for varying values of mentioned parameters. This chapter summarised that there is a critical contrast amongst curvature and non-curvature flow across the catheterised tube.

3.1 Mathematical formulation

The movement of blood for peristaltic transport is modelled in a region between two annular curved tubes. Fluid under consideration is incompressible, laminar and viscous. Gold nanoparticles are considered along with blood. Outer tube walls are flexible and also assumed to be

biddable on which mobile waves are inflicted with small amplitude. While inner tube is firm and maintains temperature T_o. The flow is generated by sinusoidal wave of range b moving with speed c through the outer biddable walls of tube. The formulated model for curved tube is, a flexible circular tube of sweep a_2 wrapped as a hover of radius k and an endoscope as a coaxial tube with span a_1. Because of the bent idea of tube, curvature is likewise considered.

Mathematically, two wall surfaces are delineated as follow

$$\bar{R}_1 = a_1,$$
$$\bar{R}_2 \quad = \quad \eta = b \sin \frac{2\pi}{\lambda} \left(Z' - ct' \right) + a_2, \tag{3.1}$$
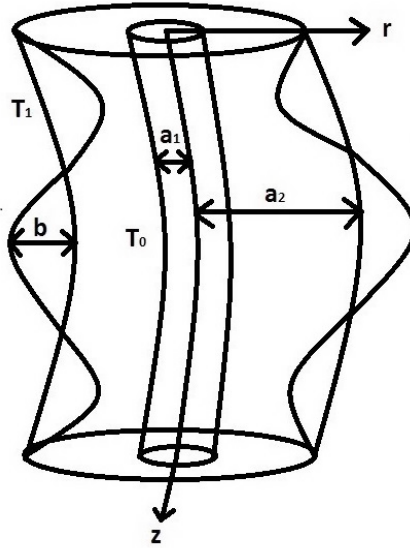
Fig.3.1(a). Geometry of problem

50
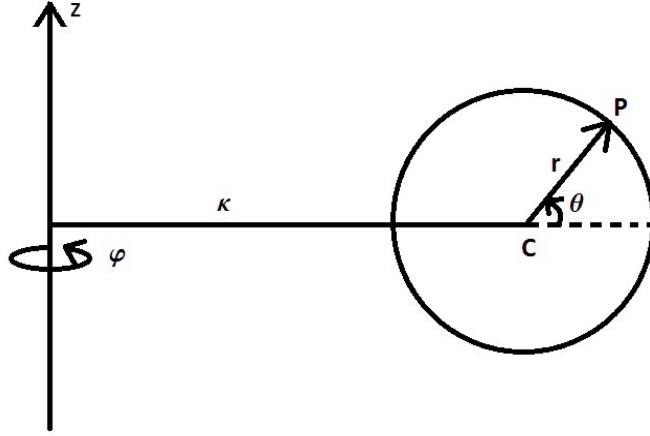
Fig.3.1(b)

Fig. 3.1 uncovers that the toroidal coordinates system (r, θ, φ) is utilized to study the stream field of the mentioned geometry. To ignore the impact of torsion, flow geometry is considered to lie in a plane. C is representing the focal point of cross area of the tube that is making an angle φ with axial plane and (r, θ) is representing polar coordinates of arbitrary point P. Radius of curvature of this curved tube is given as $OC = k$ while $z = k\varphi$ is representing axial coordinate.

For incompressible fluid, continuity equation in the toroidal coordinates is characterized below

$$\frac{\partial \bar{U}}{\partial \bar{R}} + \frac{1}{\bar{R}} \frac{\partial \bar{V}}{\partial \bar{\theta}} + \frac{k}{k + \bar{R}\cos\bar{\theta}} \frac{\partial \bar{W}}{\partial \bar{Z}} + \frac{\bar{U}}{\bar{R}} + \frac{\bar{U}\cos\bar{\theta} - \bar{V}\sin\bar{\theta}}{k + \bar{R}\cos\bar{\theta}} = 0. \tag{3.2}$$

The $\bar{R}$, $\bar{\theta}$ and $\bar{Z}$ components of momentum equation using toroidal coordinate are written as

51

$$\rho_{nf}\left(\frac{\partial \bar{U}}{\partial \bar{t}} + \bar{U}\frac{\partial \bar{U}}{\partial \bar{R}} + \frac{\bar{V}}{\bar{R}}\frac{\partial \bar{U}}{\partial \bar{\theta}} + \frac{k\bar{W}}{k + \bar{R}\cos\bar{\theta}}\frac{\partial \bar{U}}{\partial \bar{Z}} - \frac{\bar{V}^2}{\bar{R}} - \frac{\bar{W}^2\cos\bar{\theta}}{k + \bar{R}\cos\bar{\theta}}\right)$$

$$= \mu_{nf}\left(\left(\frac{\partial^2 \bar{U}}{\partial \bar{R}^2} + \frac{1}{\bar{R}}\frac{\partial \bar{U}}{\partial \bar{R}} + \frac{1}{\bar{R}^2}\frac{\partial^2 \bar{U}}{\partial \bar{\theta}^2}\right) + \frac{k^2}{(k + \bar{R}\cos\bar{\theta})^2}\frac{\partial^2 \bar{U}}{\partial \bar{Z}^2} - \frac{2}{\bar{R}^2}\frac{\partial \bar{V}}{\partial \bar{\theta}}\right.$$

$$-\frac{\bar{U}}{\bar{R}^2} + \frac{1}{k + \bar{R}\cos\bar{\theta}}\left(\cos\bar{\theta}\frac{\partial \bar{U}}{\partial \bar{R}} + \frac{\bar{V}\sin\bar{\theta}}{\bar{R}} - \frac{\sin\bar{\theta}}{\bar{R}}\frac{\partial \bar{U}}{\partial \bar{\theta}}\right)$$

$$\left.+\frac{2k\sin\bar{\theta}}{(k + \bar{R}\cos\bar{\theta})^2}\frac{\partial \bar{W}}{\partial \bar{Z}} - \frac{\cos\bar{\theta}}{(k + \bar{R}\cos\bar{\theta})^2}\left(\bar{U}\cos\bar{\theta} - \bar{V}\sin\bar{\theta}\right)\right) - \frac{\partial \bar{P}}{\partial \bar{R}}, \qquad (3.3)$$

$$\rho_{nf}\left(\frac{\partial \bar{V}}{\partial \bar{t}} + \bar{U}\frac{\partial \bar{V}}{\partial \bar{R}} + \frac{\bar{V}}{\bar{R}}\frac{\partial \bar{V}}{\partial \bar{\theta}} + \frac{k\bar{W}}{k + \bar{R}\cos\bar{\theta}}\frac{\partial \bar{V}}{\partial \bar{Z}} + \frac{\bar{U}\bar{V}}{\bar{R}} + \frac{\bar{W}^2\cos\bar{\theta}}{k + \bar{R}\cos\bar{\theta}}\right)$$

$$= \mu_{nf}\left(\left(\frac{\partial^2 \bar{V}}{\partial \bar{R}^2} + \frac{1}{\bar{R}}\frac{\partial \bar{V}}{\partial \bar{R}} + \frac{1}{\bar{R}^2}\frac{\partial^2 \bar{V}}{\partial \bar{\theta}^2}\right) + \frac{k^2}{(k + \bar{R}\cos\bar{\theta})^2}\frac{\partial^2 \bar{V}}{\partial \bar{Z}^2} - \frac{\bar{V}}{\bar{R}^2} + \frac{2}{\bar{R}^2}\frac{\partial \bar{U}}{\partial \bar{\theta}}\right.$$

$$+\frac{\cos\bar{\theta}}{k + \bar{R}\cos\bar{\theta}}\frac{\partial \bar{V}}{\partial \bar{R}} - \frac{\sin\bar{\theta}}{k + \bar{R}\cos\bar{\theta}}\left(\frac{\bar{U}}{\bar{R}} + \frac{1}{\bar{R}}\frac{\partial \bar{V}}{\partial \bar{\theta}}\right) + \frac{2k\sin\bar{\theta}}{(b + \bar{R}\cos\bar{\theta})^2}\frac{\partial \bar{W}}{\partial \bar{Z}}$$

$$\left.+\frac{\sin\bar{\theta}}{(k + \bar{R}\cos\bar{\theta})^2}\left(\bar{U}\cos\bar{\theta} - \bar{V}\sin\bar{\theta}\right)\right) - \frac{1}{\bar{R}}\frac{\partial \bar{P}}{\partial \bar{\theta}}, \qquad (3.4)$$

$$\rho_{nf}\left(\frac{\partial \bar{W}}{\partial \bar{t}} + \bar{U}\frac{\partial \bar{W}}{\partial \bar{R}} + \frac{\bar{V}}{\bar{R}}\frac{\partial \bar{W}}{\partial \bar{\theta}} + \frac{k\bar{W}}{k + \bar{R}\cos\bar{\theta}}\frac{\partial \bar{W}}{\partial \bar{Z}} + \frac{\bar{W}\left(\bar{U}\cos\bar{\theta} - \bar{V}\sin\bar{\theta}\right)}{k + \bar{R}\cos\bar{\theta}}\right)$$

$$= \mu_{nf}\left(\left(\frac{\partial^2 \bar{W}}{\partial \bar{R}^2} + \frac{1}{\bar{R}}\frac{\partial \bar{W}}{\partial \bar{R}} + \frac{1}{\bar{R}^2}\frac{\partial^2 \bar{W}}{\partial \bar{\theta}^2}\right) + \frac{k^2}{(k + \bar{R}\cos\bar{\theta})^2}\frac{\partial^2 \bar{W}}{\partial \bar{Z}^2} - \frac{\bar{W}}{(k + \bar{R}\cos\bar{\theta})^2}\right.$$

$$\left.+\frac{1}{k + \bar{R}\cos\bar{\theta}}\left(\cos\bar{\theta}\frac{\partial \bar{W}}{\partial \bar{R}} - \frac{\sin\bar{\theta}}{\bar{R}}\frac{\partial \bar{W}}{\partial \bar{\theta}}\right) + \frac{2k\sin\bar{\theta}}{(k + \bar{R}\cos\bar{\theta})^2}\left(\cos\bar{\theta}\frac{\partial \bar{U}}{\partial \bar{Z}} - \sin\bar{\theta}\frac{\partial \bar{V}}{\partial \bar{Z}}\right)\right)$$

$$+(\rho\beta)_{nf}g(T - T_1) - \frac{k}{k + \bar{R}\cos\bar{\theta}}\frac{\partial \bar{P}}{\partial \bar{Z}}. \qquad (3.5)$$

Energy equation for the curved tube and considering the effects of heat generation for nanofluid is described as

$$(\rho c_p)_{nf} \left(\frac{\partial \bar{T}}{\partial \bar{t}} + \bar{U} \frac{\partial \bar{T}}{\partial \bar{R}} + \frac{k\bar{W}}{k + \bar{R}\cos\bar{\theta}} \frac{\partial \bar{T}}{\partial \bar{Z}} + \frac{\bar{U}}{\bar{R}} \frac{\partial \bar{T}}{\partial \bar{\theta}} \right) = K_{nf} \left(\frac{\partial^2 \bar{T}}{\partial \bar{R}^2} + \frac{1}{\bar{R}} \frac{\partial \bar{T}}{\partial \bar{R}} + \frac{\cos\bar{\theta}}{k + \bar{R}\cos\bar{\theta}} \frac{\partial \bar{T}}{\partial \bar{R}} \right.$$

$$+ \frac{1}{\bar{R}^2} \frac{\partial^2 \bar{T}}{\partial \bar{\theta}^2} + \frac{k^2}{(k + \bar{R}\cos\bar{\theta})^2} \frac{\partial^2 \bar{T}}{\partial \bar{Z}^2}$$

$$\left. - \frac{\sin\bar{\theta}}{k + \bar{R}\cos\bar{\theta}} \frac{\partial \bar{T}}{\partial \bar{\theta}} \right) + Q_0. \tag{3.6}$$

The appropriate boundary conditions are given as

$$\bar{W} = 0, \ \bar{T} = \bar{T}_0, \ \text{at} \quad \bar{R} = \bar{R}_1 = a_1,$$

$$\bar{W} = 0, \ \bar{T} = \bar{T}_1, \ \text{at} \quad \bar{R} = \bar{R}_2 = \eta = b\sin\frac{2\pi}{\lambda}\left(Z' - ct'\right) + a_2. \tag{3.7}$$

Mathematically, wall compliance may be given as

$$L\left(\bar{\eta}\right) = \bar{P} - \bar{P}_0,$$

here $\bar{P}_0$ is representing the pressure on the wall surface from outside which is a consequence of muscle tension and is considered zero. L is an operator that is utilized to depict the movement of the stretched membrane with viscous retarding forces, given as

$$L = -\tau \frac{\partial^2}{\partial \bar{Z}^2} + m \frac{\partial^2}{\partial \bar{t}^2} + d_1 \frac{\partial}{\partial t},$$

here τ is representing elastic tension per unit width of the membrane, m is denoting mass per unit area and d_1 is representing coefficient of viscous damping forces.

Introducing the following dimensionless quantities

$$
\begin{aligned}
w &= \frac{\bar{w}}{c}, \; u = \frac{\lambda \bar{u}}{a_2 c}, \; z = \frac{\bar{z}}{\lambda}, \; r = \frac{\bar{r}}{a_2}, \; r_2 = \frac{\bar{r}_2}{a_2} = 1 + \varepsilon \sin(2\pi z), \\
t &= \frac{c\bar{t}}{\lambda}, \; \varepsilon = \frac{b}{a_2}, \; G_r = \frac{a_2^2 (T_1 - T_0)\rho_f \beta_f g}{c\mu_f}, \; \tilde{\theta} = \frac{T - T_1}{T_0 - T_1}, \; \bar{\theta} = \theta, \\
\zeta &= \frac{a_2}{k}, \; r_1 = \frac{\bar{r}_1}{a_2} = \epsilon, \; \gamma = \frac{a_2^2 Q_0}{(T_1 - T_0)k_f}, \; R_e = \frac{a_2 c \rho_f}{\mu_f}, \; \delta = \frac{a_2}{\lambda}, \\
d &= \frac{\kappa^*}{a_2^2}, \; p = \frac{a_2^2 \bar{p}}{c\lambda \mu_f}, \; E_1 = \frac{-\tau a^3}{\lambda^3 c \mu_f}, \; E_2 = \frac{m a^3 c}{\lambda^3 \mu_f}, \; E_3 = \frac{d_1 a^3}{\lambda^2 \mu_f}.
\end{aligned}
\tag{3.13}
$$

After employing the lubrication approach, Eqs. $(3.2) - (3.6)$ take the form

$$
\frac{\partial p}{\partial r} = 0,
\tag{3.14}
$$

$$
\frac{\partial p}{\partial \theta} = 0,
\tag{3.15}
$$

$$
\begin{aligned}
\frac{1}{1 + \zeta r \cos\theta}\frac{\partial p}{\partial z} &= \frac{\mu_{nf}}{\mu_f}\left(\frac{\partial^2 w}{\partial r^2} + \frac{1}{r}\frac{\partial w}{\partial r} + \frac{1}{r^2}\frac{\partial^2 w}{\partial \theta^2} - \frac{\zeta^2(w+1)}{(1 + \zeta r \cos\theta)^2} + \frac{\zeta \cos\theta}{1 + \zeta r \cos\theta}\frac{\partial w}{\partial r} \right. \\
&\left. - \frac{\zeta \sin\theta}{r(1 + \zeta r \cos\theta)}\frac{\partial w}{\partial \theta} + G_r \frac{(\rho\beta)_{nf}}{(\rho\beta)_f}\frac{\mu_f}{\mu_{nf}}\tilde{\theta} \right),
\end{aligned}
\tag{3.16}
$$

$$
\frac{\partial^2 \tilde{\theta}}{\partial r^2} + \frac{1}{r}\frac{\partial \tilde{\theta}}{\partial r} + \frac{\zeta \cos\theta}{1 + \zeta r \cos\theta}\frac{\partial \tilde{\theta}}{\partial r} + \frac{1}{r^2}\frac{\partial^2 \tilde{\theta}}{\partial \theta^2} + \gamma \frac{K_f}{K_{nf}} = 0,
\tag{3.17}
$$

$$
\frac{1}{1 + \zeta r \cos\theta}\frac{\partial p}{\partial z} = \frac{\partial L(\eta)}{\partial z} = E_1 \frac{\partial^3 \eta}{\partial z^3} + E_2 \frac{\partial^3 \eta}{\partial z \partial t^2} + E_3 \frac{\partial^2 \eta}{\partial z \partial t} = M.
\tag{3.18}
$$

3.2 Solution of the problem

To get the expressions for velocity and temperature according to the given boundary condition, we consider the following

$$\tilde{\theta}(r(z,t),\ \theta) \quad = \quad \tilde{\theta}_0(r) + \zeta \cos(\theta)\tilde{\theta}_1(r) + \dots$$

$$w(r(z,t),\ \theta) \quad = \quad w_0(r) + \zeta \cos(\theta)w_1(r) + \dots \tag{3.19}$$

Substituting Eq. (3.19) into Eqs. (3.16) to (3.18) and equating the same powers of $\zeta \cos(\theta)$, we obtain the written below system and their solutions.

3.2.1   Zeroth order system and solution

$$\frac{\partial^2 \tilde{\theta}_0}{\partial r^2} + \frac{1}{r}\frac{\partial \tilde{\theta}_0}{\partial r} + \gamma \frac{K_f}{K_{nf}} = 0, \tag{3.20}$$

$$\frac{\partial^2 w_0}{\partial r^2} + \frac{1}{r}\frac{\partial w_0}{\partial r} + G_r \frac{(\rho\beta)_{nf}}{(\rho\beta)_f}\frac{\mu_f}{\mu_{nf}}\tilde{\theta}_0 = \frac{\mu_f}{\mu_{nf}}\frac{dp}{dz}, \tag{3.21}$$

$$\tilde{\theta}_0(r_1) = 1,\ w_0(r_1) = 0, \tag{3.22}$$

$$\tilde{\theta}_0(r_2) = 0,\ w_0(r_2) = 0. \tag{3.23}$$

The exact solution at this order can be directly written as

$$\tilde{\theta}_0(r) = C_1 \ln r + C_2 - \frac{\gamma \frac{K_f}{K_{nf}}}{4}r^2, \tag{3.24}$$

$$\begin{aligned}
w_0(r) \quad = \quad & \frac{M}{4\frac{\mu_{nf}}{\mu_f}}r^2 - G_r \frac{(\rho\beta)_{nf}}{(\rho\beta)_f}\frac{\mu_f}{\mu_{nf}}\left(-\frac{\gamma \frac{K_f}{K_{nf}}}{64}r^4 + \frac{C_1}{2}\left(\frac{r^2 \ln r}{2} - \frac{r^2}{2}\right) + \frac{C_2}{4}r^2\right) \\
& + C_5 \ln r + C_6. \tag{3.25}
\end{aligned}$$

3.2.2 First order system and solution

$$\frac{\partial^2 \tilde{\theta}_1}{\partial r^2} + \frac{1}{r}\frac{\partial \tilde{\theta}_1}{\partial r} - \frac{\tilde{\theta}_1}{r^2} + r\frac{\partial^2 \tilde{\theta}_0}{\partial r^2} + 2\frac{\partial \tilde{\theta}_0}{\partial r} + r\gamma\frac{K_f}{K_{nf}} = 0 \ , \tag{3.26}$$

$$\frac{\partial^2 w_1}{\partial r^2} + \frac{1}{r}\frac{\partial w_1}{\partial r} - \frac{w_1}{r^2} + r\frac{\partial^2 w_0}{\partial r^2} + 2\frac{\partial w_0}{\partial r} + G_r\frac{(\rho\beta)_{nf}}{(\rho\beta)_f}\frac{\mu_f}{\mu_{nf}}(r\tilde{\theta}_0 + \tilde{\theta}_1) = 0, \tag{3.27}$$

$$\tilde{\theta}_1(r_1) = 0, \ w_1(r_1) = 0, \tag{3.28}$$

$$\tilde{\theta}_1(r_2) = 0, \ w_1(r_2) = 0. \tag{3.29}$$

Solution is obtained by substituting Eqs. $(3.24 - 3.25)$ into Eqs. $(3.26 - 3.27)$ and is given as follow

$$\bar{\theta}_1(r) = rC_3 + \frac{C_4}{r} + r\left(\frac{\gamma\frac{K_f}{K_{nf}}r^2}{8} - \frac{C_1\ln r}{2}\right) - \frac{1}{r}\left(\gamma\frac{K_f}{K_{nf}}\frac{r^4}{16} - \frac{C_1 r^2}{4}\right), \tag{3.30}$$

$$
\begin{aligned}
w_1(r) \ = \ & rC_7 + \frac{C_8}{r} + \frac{r}{2}\left(-\frac{3M}{4\frac{\mu_{nf}}{\mu_f}}r^2 + G_r\frac{(\rho\beta)_{nf}}{(\rho\beta)_f}\frac{\mu_f}{\mu_{nf}}\left(-\frac{\gamma\frac{K_f}{K_{nf}}}{32}r^4 + \frac{C_1}{2}r^2\ln r - \frac{C_1}{4}r^2 + \frac{C_2}{4}r^2\right.\right. \\
& \left.\left. -\frac{C_3}{2}r^2 - C_4\ln r\right) - C_5\ln r\right) - \frac{1}{2r}\left(-\frac{3M}{8\frac{\mu_{nf}}{\mu_f}}r^4 + G_r\frac{(\rho\beta)_{nf}}{(\rho\beta)_f}\frac{\mu_f}{\mu_{nf}}\left(-\frac{\gamma\frac{K_f}{K_{nf}}}{48}r^6 + \frac{C_1}{4}r^4\ln r\right.\right. \\
& \left.\left. -\frac{3C_1}{16}r^4 + \frac{C_2}{8}r^4 - \frac{C_3}{4}r^4 - \frac{C_4}{2}r^2\right) - \frac{C_5}{2}r^2\right). \tag{3.31}
\end{aligned}
$$

here all the C's are constants and defined in appendix.

3.3 Results and discussion

Fluid velocity and streamlines are graphically explained for the effects of various parameters i.e. G_r, γ, φ, E_1, E_2 and E_3. Gold nanoparticles with brick shape factor n=3.7 are used to study these effects. Figs $3.2-3.7$ are plotted to elucidate the sequel of apposite parameters for velocity field. Furthermore, these figures also depict the difference of velocity profile for non-curvature tube and curvature tube. In the region between tube having sinusoidal curve and endoscope, parabolic behavior is observed for axial velocity w against all the involved parameters. Effect of

Grashoff's number G_r is discussed in Fig 3.2(a), magnitude of axial velocity is small for small values of G_r. As G_r increases, an increase in magnitude of velocity profile is seen. It is seen that the maximum velocity is attained closer to the inner tube as compared to the outer tube i.e. at $r = 0.38$. It is also evident from the figure that the velocity for non-curvature tube is lower in comparison to curvature tube for varying G_r. Three dimensional velocity profile is shown in Fig.3.2(b) for brick Au nanoparticles for pertinent values of G_r. Fig 3.3(a) gives the influence of γ, heat source(sink) parameter, on the velocity. It is noticed that the velocity declines with rise in the magnitude of γ. Non-curvature tube experiences low velocity as that of tube having non-zero curvature. Fig 3.3(b) is depicting the 3D graph for the velocity profile with variation of γ for brick Au nanoparticle. Fig 3.4(a) is plotted to display the effect of amplitude ratio on velocity profile. Small variations are taken into consideration and it is clear from the graph that an increase in φ gives rise to the magnitude of velocity profile. The variation gets more small for big values of φ. Non-curvature tube and curvature tube exhibit same behavior for variations of φ with the only difference that magnitude of velocity for curvature tube is higher than non-curvature tube. Fig 3.4(b) is sketched to give a 3D view of axial velocity for different amplitude ratios.

Fig 3.5(a) emphasizes that as rigidity parameter E_1 increases there is a remarkable rise in the velocity profile. Physically, it means that wall elastins is helpful to the fluid flow. Tube having greater curvature experiences larger velocity. The 3D description for the effects of E_1 on velocity is given in Fig 3.5(b). Effects of stiffness parameter E_2 over axial velocity are highlighted in Fig 3.6(a) and 3.6(b) for both 2D and 3D respectively. A rise in velocity is seen for elevating values of E_2 i.e. increase in E_2 reduces tension in the walls of the tube which in result pace up the fluid flow. Variation of damping coefficient E_3 effecting the velocity profile can be observed in Fig 3.7(a) and 3.7(b). It is found that higher values of E_3 results in diminishing velocity . This is due to the fact that E_3 has oscillating resistance to the fluid flow and that is the reason for decrease in velocity for wall damming coefficient E_3. It may also be seen that this behavior of velocity for E_3 remain unaltered for both non-curvature and curvature tube.

Trapping is an imperative phenomena in peristaltic motion. For the most part, the state of streamline demonstrates the impact of boundary wall on flow pattern. Here pattern of flow

in the area between endoscope and tube wall is discussed. Amazingly, the streamlines split to shape recirculating closed streamlines, called bolus, inside the tube. This internally circulating fluid pushes the peristaltic wave ahead. Arbitrary response of encased bolus is seen for variety of G_r alongside closed streamlines and is depicted in Fig 3.8. From Fig it is seen that the quantity of caught bolus increases when G_r shifts from 2 to 3 and size is likewise seen to boost as G_r additionally changes from 3 to 4. Impacts of γ over enclosed bolus is considered in Fig 3.9. It is seen that as γ changes from 0.1 to 0.5, number of caught bolus elevates and the size likewise increases as γ bounces to 0.9 from 0.5. Fig 3.10 is utilized to demonstrate the effect of φ over trapped bolus. As φ is expanded from 0.03 to 0.05, number of bolus increments and on additionally expanding φ from 0.05 to 0.07 a further increment in number of bolus is seen. Fig 3.11 is used to study the bolus phenomena for variation of E_1. As value of E_1 increases an increase in size of trapped bolus is seen. From Fig $3.11 - 3.12$, it is clear that the change in bolus appearance is similar for both E_1 and E_2. Effects of E_3 are elaborated in Fig 3.13 and it is noted that appearance of bolus mitigates with its increase.

Temperature profile for curved tube having elastic walls presented in Table 3.1 and 3.2. It is witnessed that for greater value of source parameter i.e. for larger γ the temperature of the fluid increases. Also it is interesting to see that the variation in curvature effects the temperature profile. With larger curvature parameter ζ low temperature is noticed as can be seen in comparison of tables.
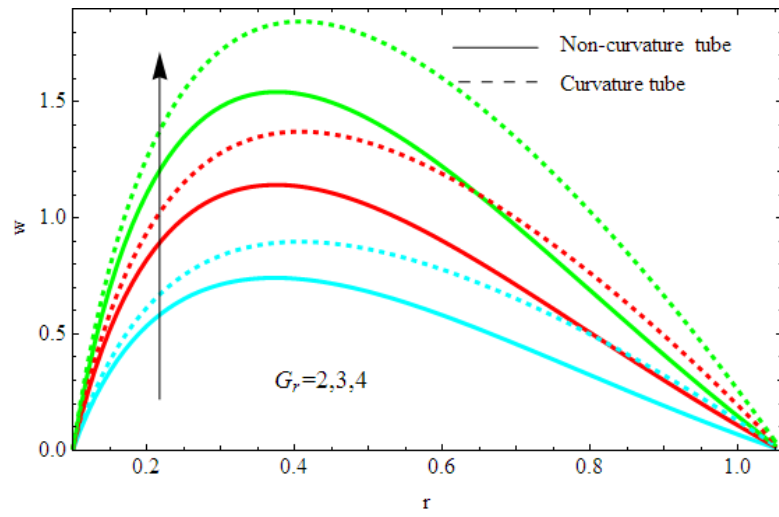
(a)
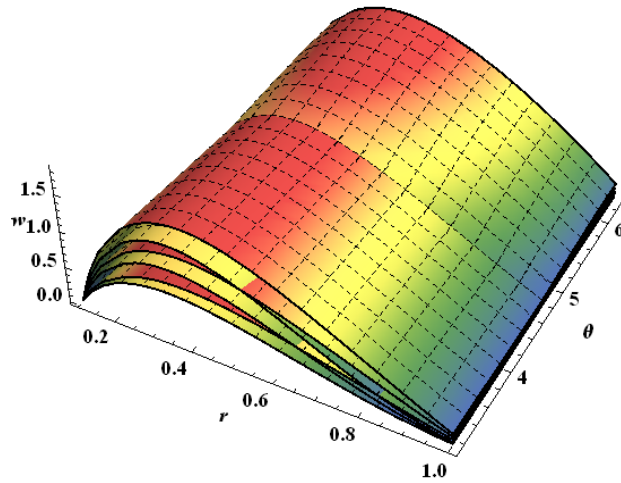
(b)

$Figs.$ $3.2(a, b)$, Velocity profile for distinct Grashroff number G_r

59
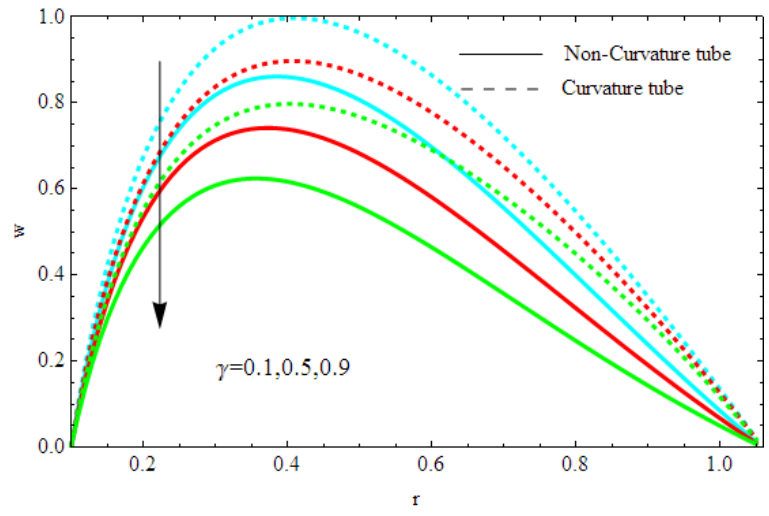
(a)
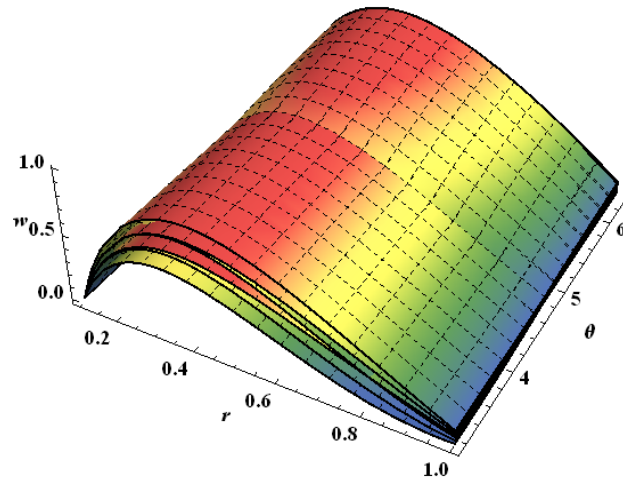
(b)

$Figs.$ $3.3(a, b)$, Velocity profile for distinct heat source(sink) parameter γ
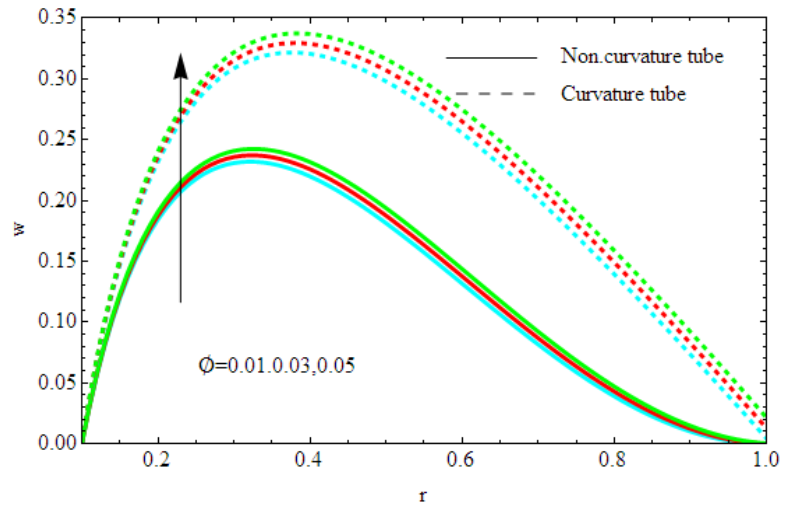
(a)
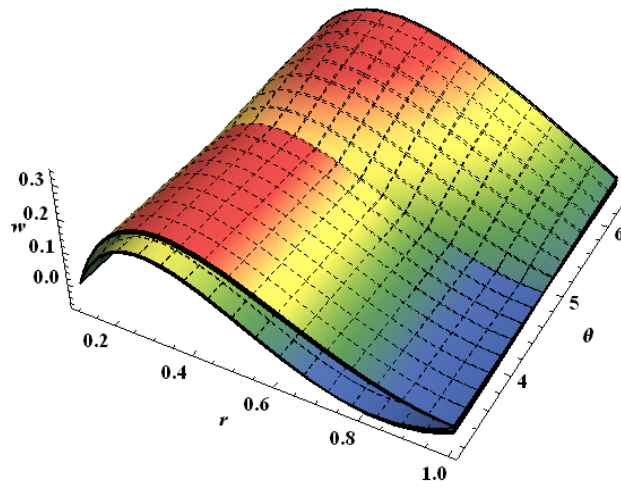
(b)

$Figs.$ 3.4(a, b), Velocity profile for distinct amplitude ratio φ
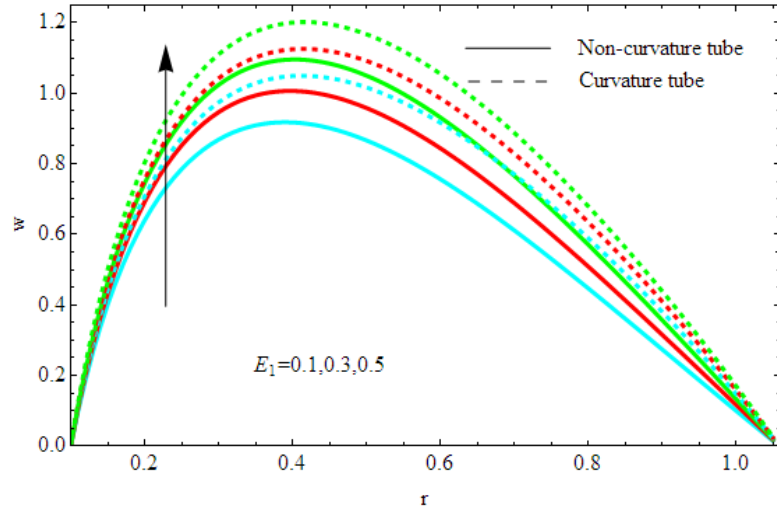
(a)
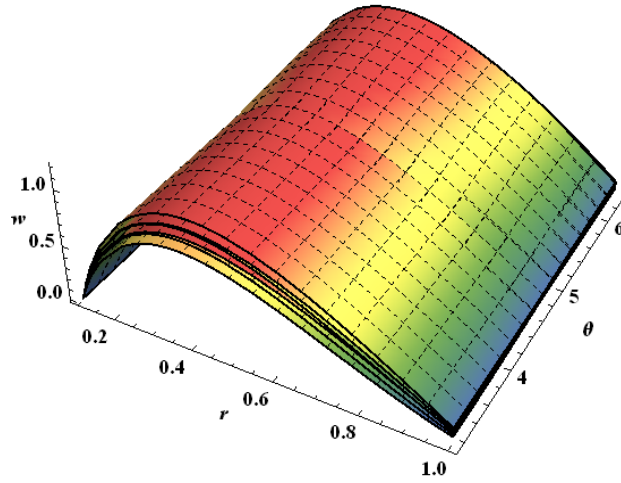
(b)

Figs. 3.5(*a*, *b*), Velocity profile for distinct rigidity parameter E_1
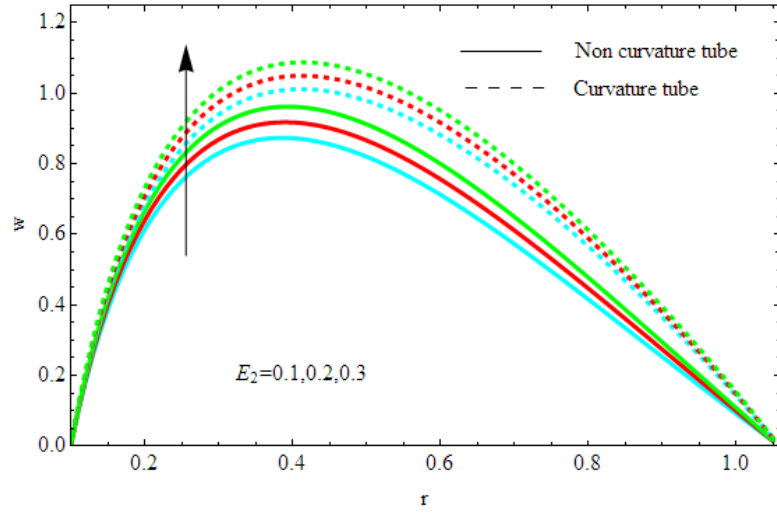
(a)
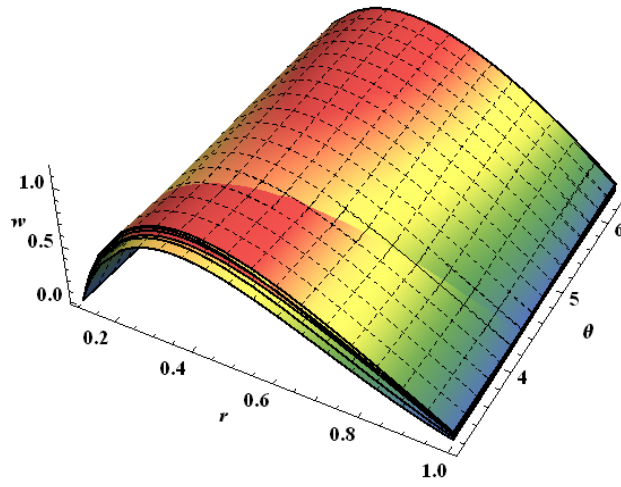
(b)

$Figs.$ $3.6(a, b)$, Velocity profile for distinct stiffness parameter E_2

63
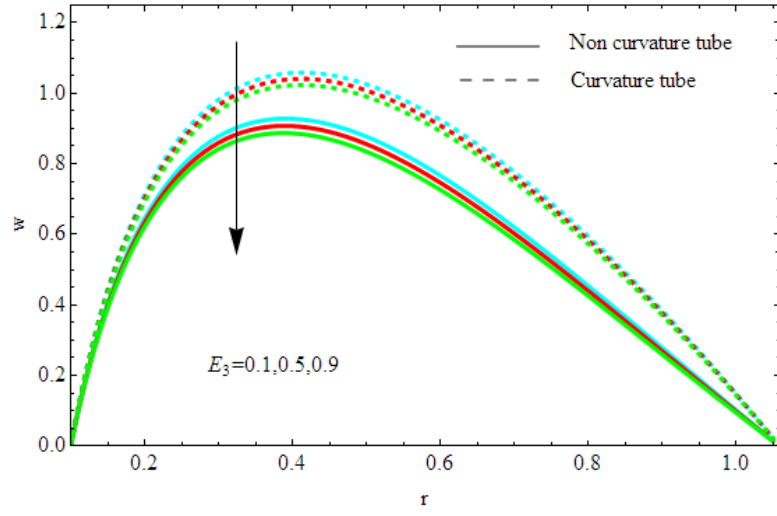
(a)
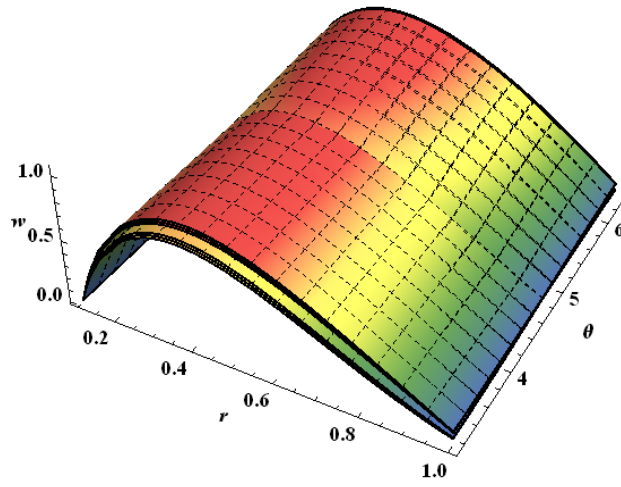
(b)

$Figs.$ 3.7(a, b), Velocity profile for distinct damping force E_3.
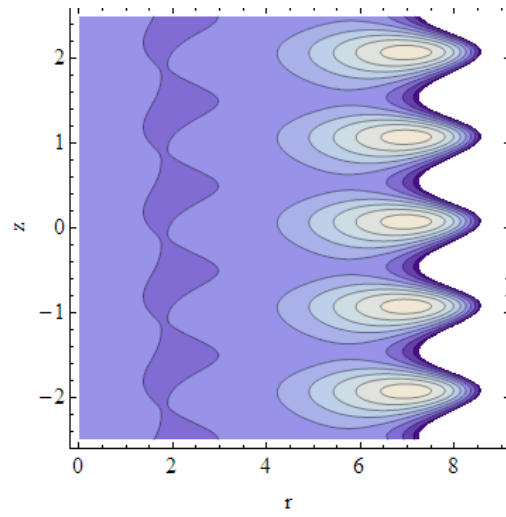
(a)
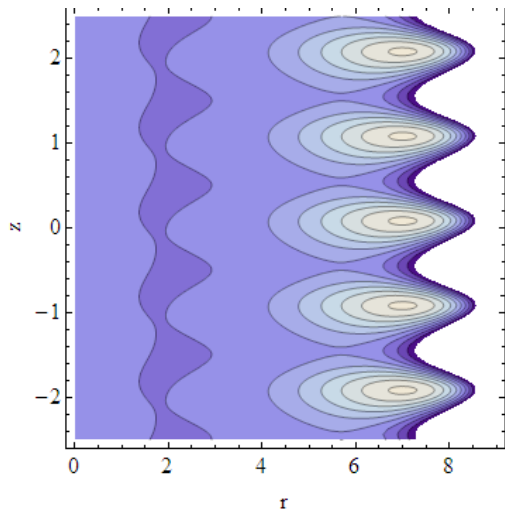
(b)
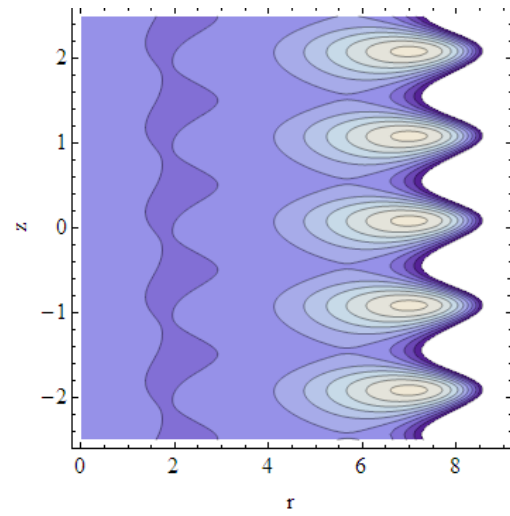
(c)

Figs. 3.8(*a*, *b*, *c*), Streamlines for Gold nanoparticle for (**a**) $G_r = 3.8$, (**b**) $G_r = 4.2$, (**c**) $G_r = 4.4$.

(b)

(c)
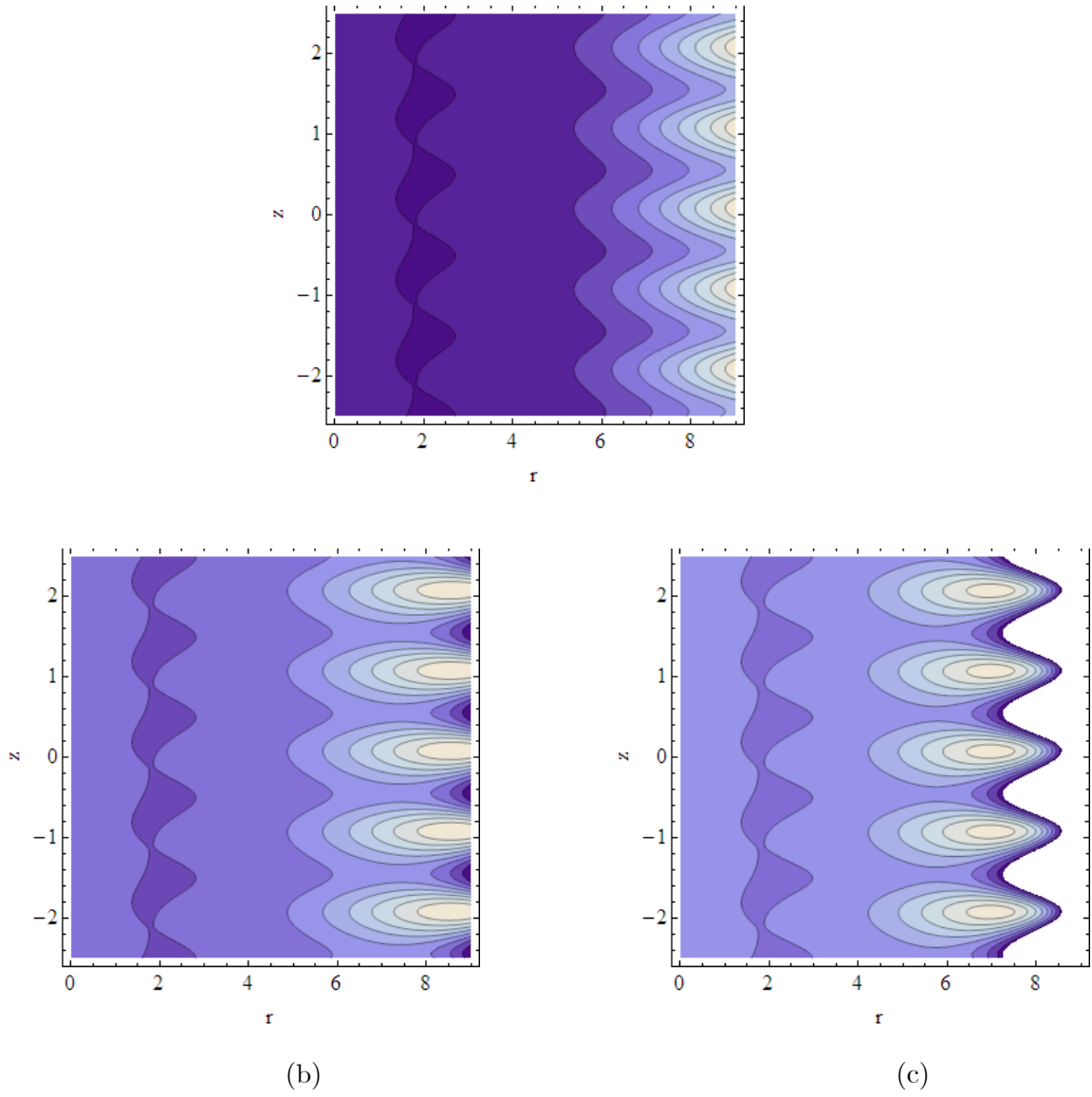
$Figs.$ $3.9(a, b, c)$, Streamlines for Gold nanoparticle for (**a**) $\gamma = 0.1$, (**b**) $\gamma = 0.15$, (**c**) $\gamma = 0.2$.
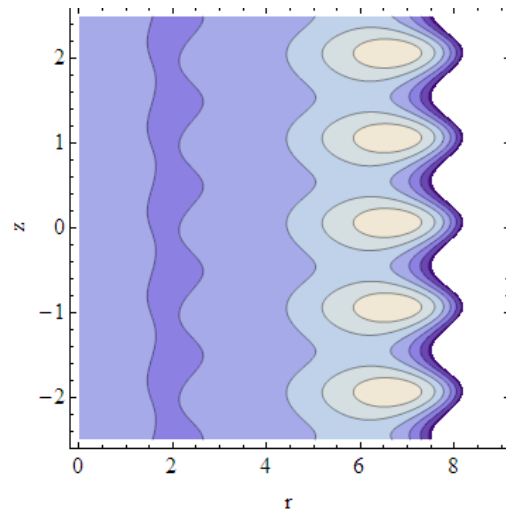
(a)
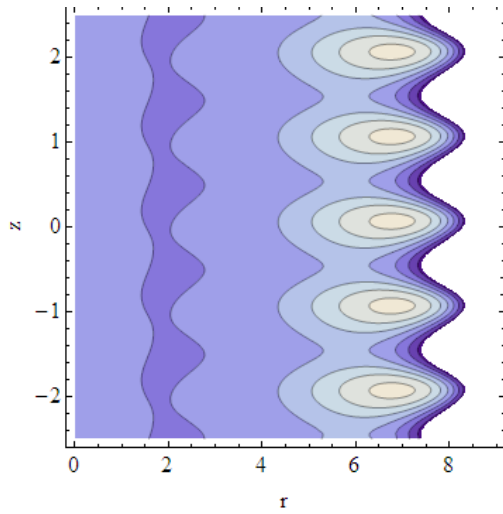
(b)
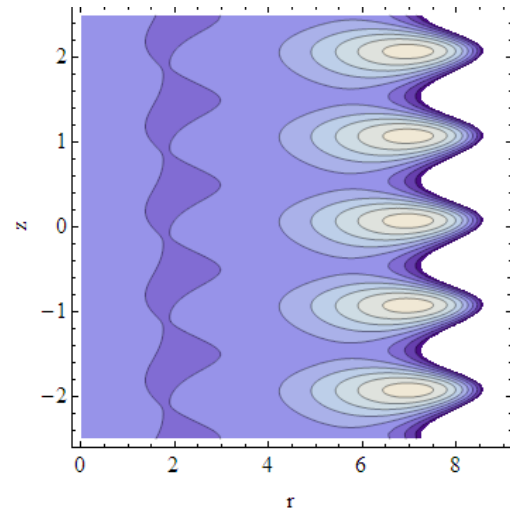
(c)

Figs. 3.10(*a, b, c*), Streamlines for Gold nanoparticles for (**a**) $\phi = 0.05$, (**b**) $\phi = 0.07$, (**c**) $\phi = 0.1$.
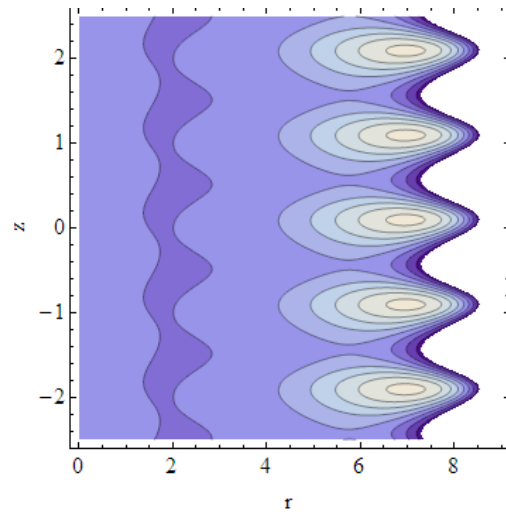
(a)
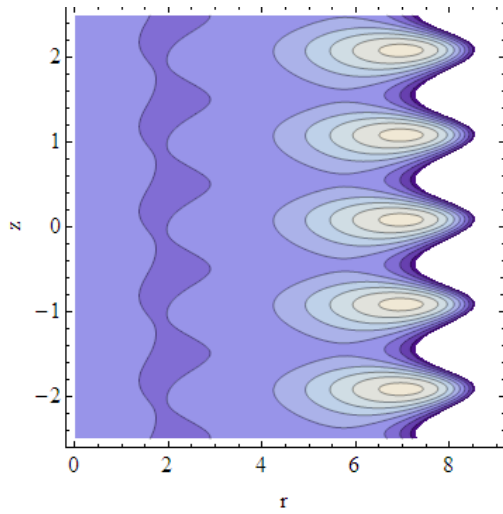
(b)
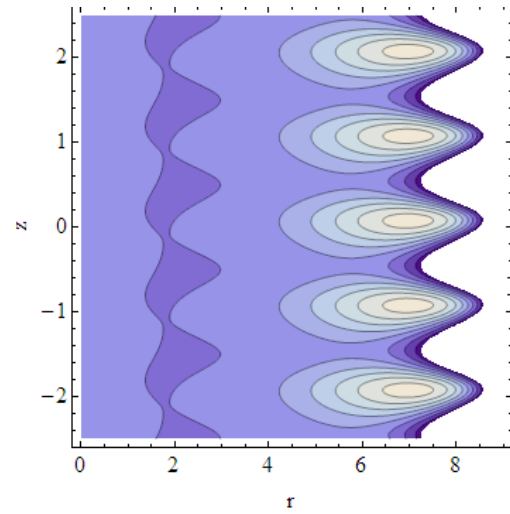
(c)

$Figs.$ 3.11(a, b, c), Streamlines for Gold nanoparticles for (**a**) $E_1 = 0.01$, (**b**) $E_1 = 0.05$, (**c**) $E_1 = 0.1$.
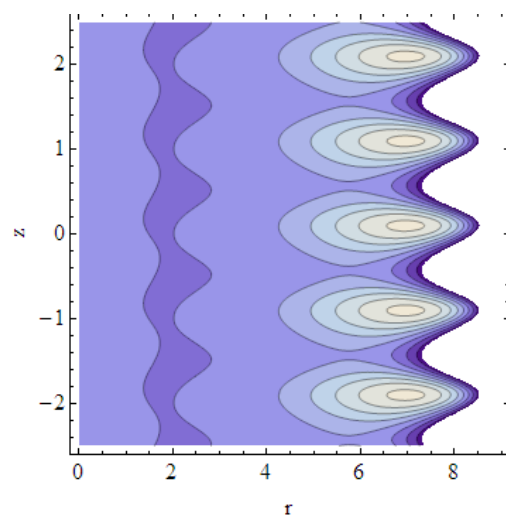
(a)
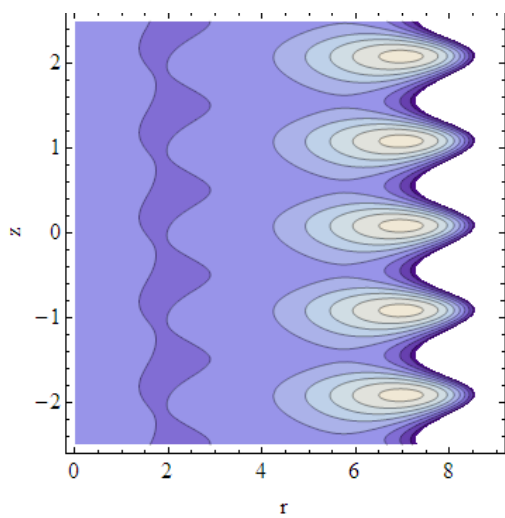
(b)
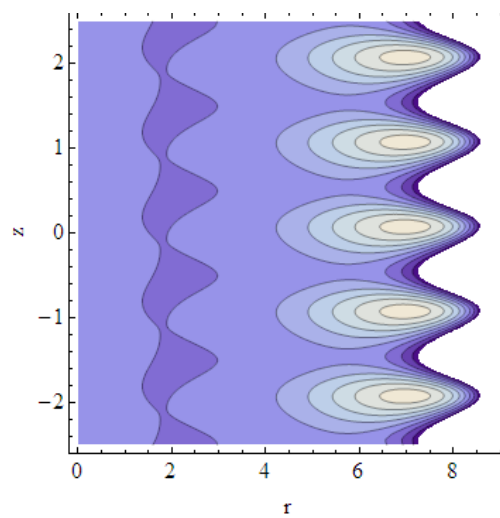
(c)

Figs. 3.12(*a*, *b*, *c*), Streamlines for Gold nanoparticles for (**a**) $E_2 = 0.1$, (**b**) $E_2 = 0.15$, (**c**) $E_2 = 0.2$.
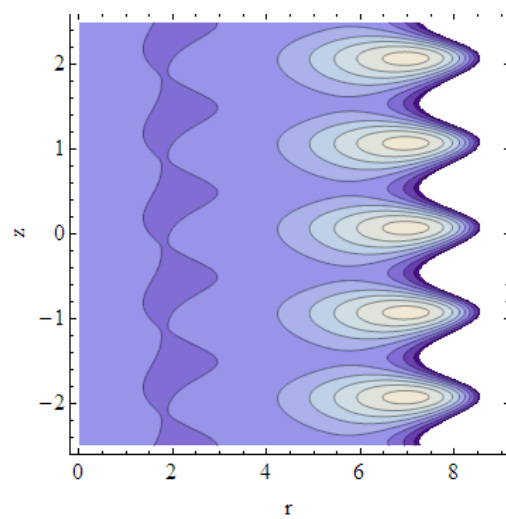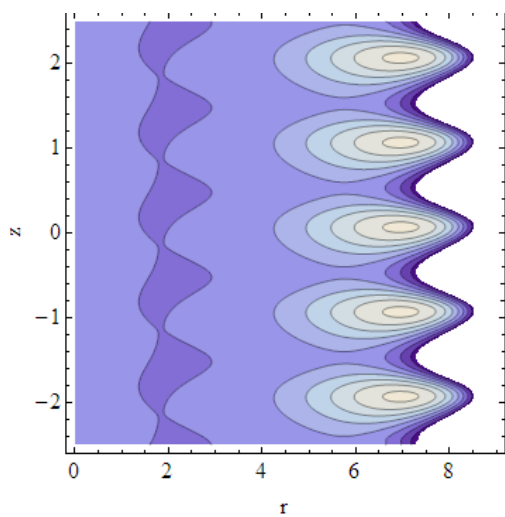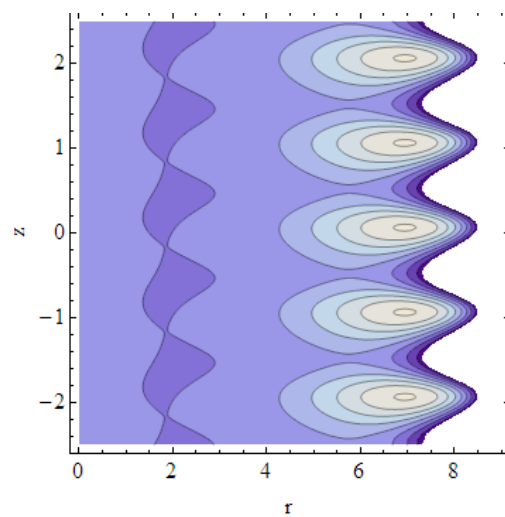
$Figs.$ $3.13(a, b, c)$, Streamlines for Gold nanoparticles for (**a**) $E_3 = 0.4$, (**b**) $E_3 = 0.6$, (**c**) $E_3 = 0.8$.

"r"	"$\gamma = 0.1$"	"$\gamma = 0.5$"	"$\gamma = 0.9$"
r_1=0.1	1.000000	1.000000	1.000000
0.2	0.711671	0.733329	0.754988
0.3	0.542416	0.574373	0.606329
0.4	0.421698	0.458437	0.495177
0.5	0.327408	0.365249	0.403089
0.6	0.249702	0.285777	0.321852
0.7	0.183327	0.215205	0.247083
0.8	0.125147	0.150657	0.176167
0.9	0.073139	0.090278	0.107418
"h"=1	0.025924	0.032803	0.039817

Table. (3.1), Temperature profile for variant source parameters with curvature $\zeta = 0$.

"r"	"$\gamma = 0.1$"	"$\gamma = 0.5$"	"$\gamma = 0.9$"
r_1=0.1	1.00000	1.000000	1.000000
0.2	0.688735	0.71079	0.732845
0.3	0.510258	0.542328	0.574399
0.4	0.385937	0.422296	0.458656
0.5	0.291537	0.328471	0.365406
0.6	0.216283	0.251008	0.285734
0.7	0.154407	0.184667	0.214927
0.8	0.102449	0.126326	0.150203
0.9	0.0581672	0.073982	0.089797
"h"=1	0.0200189	0.026275	0.032531

Table. (3.2), Temperature profile for variant source parameters with curvature $\zeta = 0.5$.

3.4   Conclusions

This study investigates Au-nanoparticles in an elastic curved tube with endoscope.Perturbation method is utilized to get the analytical solution.On the basis of graphical results, some observations are made which are given below

- Non-curvature tube experiences low velocity as compared to curved tube.

- Axial velocity profile is observed to be higher for greater Grashoff's number.

- Large damping force parameter E_3 results in lower velocity field.

- An increase in source parameter results in higher temperature.

- Trapped bolus grow bigger with larger E_1 and E_2 and reduces for larger E_3.

3.5 Appendix

$$C_1 = -\frac{4 + \gamma \frac{K_f}{K_{nf}} r_1^2 - \gamma \frac{K_f}{K_{nf}} r_2^2}{4 \left(\ln r_1 - \ln r_2 \right)}, C_2 = -\left(\frac{4 \ln r_2 + \gamma \frac{K_f}{K_{nf}} r_1^2 \ln r_2 - \gamma \frac{K_f}{K_{nf}} r_2^2 \ln r_1}{4 \left(\ln r_1 - \ln r_2 \right)} \right),$$

$$C_3 = \frac{1}{16(r_1^2 - r_2^2)} \left(-4C_1 r_1^2 + 8C_1 r_1^2 \ln r_1 - \gamma \frac{K_f}{K_{nf}} r_1^4 + 4C_1 r_2^2 - +8C_1 r_2^2 \ln r_2 - \gamma \frac{K_f}{K_{nf}} r_2^4 \right),$$

$$C_4 = -\frac{r_2^2}{16(r_1^2 - r_2^2)} \left(8C_1 r_1^2 \ln r_1 - 8C_1 r_1^2 \ln r_2 - \gamma \frac{K_f}{K_{nf}} r_1^4 + \gamma \frac{K_f}{K_{nf}} r_1^2 r_2^2 \right),$$

$$C_5 = \frac{1}{a_6} \left(a_4 + \frac{1}{\frac{\zeta \cos \theta}{1 + \zeta r \cos \theta}} \left(\frac{\alpha}{\sqrt[2]{d}} a_4 - a_5 \right) \right), C_6 = -1 - a_3 - \frac{\ln r_1}{a_6} \left(a_4 + \frac{1}{\frac{\zeta \cos \theta}{1 + \zeta r \cos \theta}} \left(\frac{\alpha}{\sqrt[2]{d}} a_4 - a_5 \right) \right),$$

$$C_7 = \frac{a_{11}}{a_{12}}, C_8 = -r_1 \left(a_7 + r_1 \frac{a_{11}}{a_{12}} \right), b_1 = -S \left(\frac{C_2 r_2}{2} - \frac{Br_2^3}{16} + C_1 \left(-\frac{r_2}{4} + \frac{r_2 \ln r_2}{2} \right) \right), b_2 = -S \left(\frac{C_2 r_1^2}{4} \right.$$

$$\left. -\frac{Br_2^4}{64} + \frac{C_1}{2} \left(-\frac{r_2^2}{2} + \frac{r_2^2 \ln r_2}{2} \right) \right), b_3 = -S \left(\frac{C_2 r_1^2}{4} - \frac{Br_1^4}{64} + \frac{C_1}{2} \left(-\frac{r_1^2}{2} + \frac{r_1^2 \ln r_1}{2} \right) \right),$$

$$b_7 = S \left(-\frac{Br_1^4}{32} + C_1 \left(-\frac{r_1^2}{4} + \frac{r_1^2 \ln r_1}{2} \right) + \frac{C_2 r_1^2}{4} - \frac{C_3 r_1^2}{2} - C_4 \ln r_1 \right),$$

$$b_8 = S \left(-\frac{Br_1^6}{48} + C_1 \left(-\frac{3r_1^4}{16} + \frac{r_1^4 \ln r_1}{4} \right) + \frac{C_2 r_1^4}{8} - \frac{C_3 r_1^4}{4} - \frac{C_4}{2} r_1^2 \right),$$

$$b_9 = S \left(-\frac{Br_2^4}{32} + C_1 \left(-\frac{r_2^2}{4} + \frac{r_2^2 \ln r_2}{2} \right) + \frac{C_2 r_2^2}{4} - \frac{C_3 r_2^2}{2} - C_4 \ln r_2 \right), \ b_{10} = S \left(-\frac{Br_2^6}{48} \right.$$

$$+C_1(-\frac{3r_2^4}{16}+\frac{r_2^4\ln r_2}{4})+\frac{C_2 r_2^4}{8}-\frac{C_3 r_2^4}{4}-\frac{C_4}{2}r_2^2),\ b_{11}=S(-\frac{5Br_2^4}{32}+\frac{C_1}{2}\left(-r_2^2+3r_2^2\ln r_2\right)$$

$$-\frac{3C_1 r_2^2}{4}+\frac{3C_2 r_2^2}{4}-\frac{3C_3 r_2^2}{2}-C_4(\ln r_2+1),\ b_{12}=S(-\frac{5Br_2^4}{48}+\frac{C_1}{4}\left(r_2^2+3r_2^2\ln r_2\right)$$

$$-\frac{9C_1 r_2^2}{16}+\frac{3C_2 r_2^2}{8}-\frac{3C_3 r_2^2}{4}-\frac{C_4}{2}),\ b_{13}=1+\zeta r_2\cos\theta,\ b_{14}=\frac{\zeta\cos\theta}{1+\zeta r_2\cos\theta},$$

$$a_1=b_1+\frac{Lr_2}{2A},\ a_2=b_2+\frac{Lr_2^2}{4A},\ a_3=b_3+\frac{Lr_1^2}{4A}, a_4=a_2-a_3,\ a_5=a_1-1-\frac{AdL}{b_{13}},$$

$$a_6=(\ln r_1-\ln r_2)(1+\frac{\zeta r_2\cos\theta\alpha}{\zeta\cos\theta\sqrt[2]{d}})+\frac{1+\zeta r_2\cos\theta}{\zeta r_2\cos\theta},\ a_7=\frac{r_1}{2}(-\frac{3Lr_1^2}{4A}+b_7-C_5\ln r_1)$$

$$-\frac{1}{2r_1}(-\frac{3Lr_1^4}{8A}+b_8-\frac{C_5 r_1^2}{2}),\ a_8=\frac{r_2}{2}(-\frac{3Lr_2^2}{4A}+b_9-C_5\ln r_2)-\frac{1}{2r_2}(-\frac{3Lr_2^4}{8A}+b_{10}-\frac{C_5 r_2^2}{2}),$$

$$a_9=\frac{1}{2}(-\frac{9Lr_2^2}{4A}+b_{11}-\frac{C_5}{r_2})-\frac{1}{2}(-\frac{9Lr_2^4}{4A}+b_{12}-\frac{C_5}{2}),\ a_{10}=-1-\frac{AdL}{b_{13}},\ a_{11}=-a_8+\frac{r_1}{r_2}a_7$$

$$\frac{\sqrt[2]{d}}{\alpha}(-r_1 a_7\ln r_2+a_9-b_{14}a_8+\frac{b_{14}a_7}{r_2}-b_{14}+a_{10}),\ a_{12}=r_2-\frac{r_1^2}{r_2}-\frac{\sqrt[2]{d}}{\alpha}+r_1^2\ln r_2\frac{\sqrt[2]{d}}{\alpha}$$

$$+\frac{\sqrt[2]{d}}{\alpha}\frac{r_2\zeta\cos\theta}{1+\zeta r_2\cos\theta}-\frac{\sqrt[2]{d}}{\alpha}\frac{r_1^2\zeta\cos\theta}{r_2\left(1+\zeta r_2\cos\theta\right)}.$$

Chapter 4

Endoscopic analysis of wave propagation with Ag-nanoparticles in curved tube having permeable walls

The purpose of present chapter is to summarize the effects of different shaped Ag-nanoparticles on peristaltic flow through a curved tube having permeable walls.The different shaped Ag-nanoparticles are cylinders,bricks and platelets.To study the behaviour of these Ag-nanoparticles mathematically, system of toroidal coordinate for viscous fluid is utilized. Furthermore, the analysis is carried out under the assumptions of low Reynolds number and long wavelength approximation. The method of Perturbation approximation is utilized to simplify the problem and get the results for pressure gradient, pressure rise, axial velocity and stream functions. The effects of several parameters have been discussed graphically. We percieve from present analysis that the temperature profile exhibits a decline for larger shape factor of Ag-nanoparticles. Also the trapped bolus is observed to have larger size for bigger shape factor.

4.1 Formulation of the problem

We are interested to examine the peristaltic transport of incompressible, laminar and viscous nanofluid in the region between two curved annular tubes. A sinusoidal wave of speed c travels along the walls of outer tube with wave amplitude b and wavelength λ. Inner tube is considered to be rigid and have constant temperature T_o while outer tube maintains temperature T_1. The mathematical formulation model for curved tube is, an inflexible circular tube of radius a_2 wrapped as a circle of radius k and endoscope in the form of coaxial tube with radius a_1. In view of the fact that tube is curved, the curvature parameter is also taken into account. Gold nanoparticles with shape factors brick, cylinder and platelet are considered along with blood.

Mathematically, two wall surfaces can be given as

$$\bar{R}_1 = a_1,$$
$$\bar{R}_2 = a_2 + b\sin\left[\frac{2\pi}{\lambda}(Z - ct)\right], \tag{4.1}$$
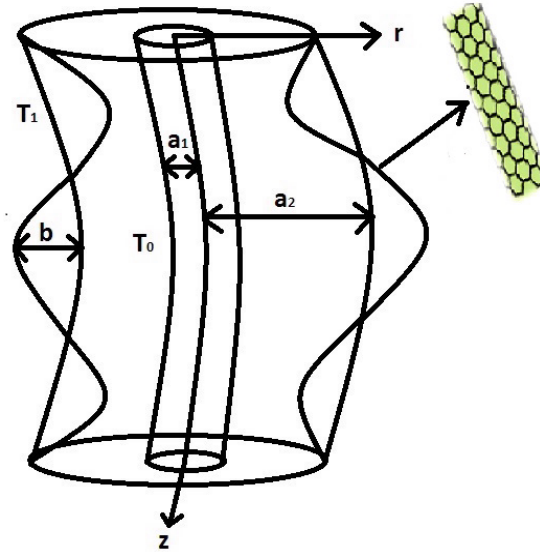
Fig.4.1. Geometry of problem

Fig. 4.1 reveals that the system of toroidal coordinates (r, θ, φ) is utilized to investigate the flow field in the mentioned geometry. Flow geometry is considered to lie in a plane so torsion impact is ignored. C is representing centre of the cross section of the tube that is making an angle φ with the fixed axial plane and (r, θ) is representing polar coordinates of an arbitrary point P in the cross section. Radius of the curvature of this curved tube is given as $OC = k$ while axial coordinate is defined as $z = k\varphi$.

The continuity equation for incompressible fluid in the toroidal coordinates is given below

$$\frac{\partial \bar{U}}{\partial \bar{R}} + \frac{\bar{U}}{\bar{R}} + \frac{1}{\bar{R}}\frac{\partial \bar{V}}{\partial \bar{\theta}} + \frac{\bar{U}\cos\bar{\theta} - \bar{V}\sin\bar{\theta}}{k + \bar{R}\cos\bar{\theta}} + \frac{k}{k + \bar{R}\cos\bar{\theta}}\frac{\partial \bar{W}}{\partial \bar{Z}} = 0. \tag{4.2}$$

The $\bar{R}$, $\bar{\theta}$ and $\bar{Z}$ components of momentum equation using toroidal coordinate are given as

$$
\rho_{nf}\left(\frac{\partial \bar{U}}{\partial \bar{t}} + \bar{U}\frac{\partial \bar{U}}{\partial \bar{R}} + \frac{\bar{V}}{\bar{R}}\frac{\partial \bar{U}}{\partial \bar{\theta}} + \frac{k\bar{W}}{k + \bar{R}\cos\bar{\theta}}\frac{\partial \bar{U}}{\partial \bar{Z}} - \frac{\bar{V}^2}{\bar{R}} - \frac{\bar{W}^2\cos\bar{\theta}}{k + \bar{R}\cos\bar{\theta}}\right)
$$
$$
= \mu_{nf}\left(\left(\frac{\partial^2 \bar{U}}{\partial \bar{R}^2} + \frac{1}{\bar{R}}\frac{\partial \bar{U}}{\partial \bar{R}} + \frac{1}{\bar{R}^2}\frac{\partial^2 \bar{U}}{\partial \bar{\theta}^2}\right) + \frac{k^2}{(k + \bar{R}\cos\bar{\theta})^2}\frac{\partial^2 \bar{U}}{\partial \bar{Z}^2} - \frac{2}{\bar{R}^2}\frac{\partial \bar{V}}{\partial \bar{\theta}}\right.
$$
$$
- \frac{\bar{U}}{\bar{R}^2} + \frac{1}{k + \bar{R}\cos\bar{\theta}}\left(\cos\bar{\theta}\frac{\partial \bar{U}}{\partial \bar{R}} + \frac{\bar{V}\sin\bar{\theta}}{\bar{R}} - \frac{\sin\bar{\theta}}{\bar{R}}\frac{\partial \bar{U}}{\partial \bar{\theta}}\right)
$$
$$
\left. + \frac{2k\sin\bar{\theta}}{(k + \bar{R}\cos\bar{\theta})^2}\frac{\partial \bar{W}}{\partial \bar{Z}} - \frac{\cos\bar{\theta}}{(k + \bar{R}\cos\bar{\theta})^2}\left(\bar{U}\cos\bar{\theta} - \bar{V}\sin\bar{\theta}\right)\right) - \frac{\partial \bar{P}}{\partial \bar{R}} \tag{4.3}
$$

$$
\rho_{nf}\left(\frac{\partial \bar{V}}{\partial \bar{t}} + \bar{U}\frac{\partial \bar{V}}{\partial \bar{R}} + \frac{\bar{V}}{\bar{R}}\frac{\partial \bar{V}}{\partial \bar{\theta}} + \frac{k\bar{W}}{k + \bar{R}\cos\bar{\theta}}\frac{\partial \bar{V}}{\partial \bar{Z}} + \frac{\bar{U}\bar{V}}{\bar{R}} + \frac{\bar{W}^2\cos\bar{\theta}}{k + \bar{R}\cos\bar{\theta}}\right)
$$
$$
= \mu_{nf}\left(\left(\frac{\partial^2 \bar{V}}{\partial \bar{R}^2} + \frac{1}{\bar{R}}\frac{\partial \bar{V}}{\partial \bar{R}} + \frac{1}{\bar{R}^2}\frac{\partial^2 \bar{V}}{\partial \bar{\theta}^2}\right) + \frac{k^2}{(k + \bar{R}\cos\bar{\theta})^2}\frac{\partial^2 \bar{V}}{\partial \bar{Z}^2} - \frac{\bar{V}}{\bar{R}^2} + \frac{2}{\bar{R}^2}\frac{\partial \bar{U}}{\partial \bar{\theta}}\right.
$$
$$
+ \frac{\cos\bar{\theta}}{k + \bar{R}\cos\bar{\theta}}\frac{\partial \bar{V}}{\partial \bar{R}} - \frac{\sin\bar{\theta}}{k + \bar{R}\cos\bar{\theta}}\left(\frac{\bar{U}}{\bar{R}} + \frac{1}{\bar{R}}\frac{\partial \bar{V}}{\partial \bar{\theta}}\right) + \frac{2k\sin\bar{\theta}}{(b + \bar{R}\cos\bar{\theta})^2}\frac{\partial \bar{W}}{\partial \bar{Z}}
$$
$$
\left. + \frac{\sin\bar{\theta}}{(k + \bar{R}\cos\bar{\theta})^2}\left(\bar{U}\cos\bar{\theta} - \bar{V}\sin\bar{\theta}\right)\right) - \frac{1}{\bar{R}}\frac{\partial \bar{P}}{\partial \bar{\theta}} \tag{4.4}
$$

76

$$
\rho_{nf} \left(\frac{\partial \bar{W}}{\partial \bar{t}} + \bar{U} \frac{\partial \bar{W}}{\partial \bar{R}} + \frac{\bar{V}}{\bar{R}} \frac{\partial \bar{W}}{\partial \bar{\theta}} + \frac{k\bar{W}}{k + \bar{R}\cos\bar{\theta}} \frac{\partial \bar{W}}{\partial \bar{Z}} + \frac{\bar{W} \left(\bar{U}\cos\bar{\theta} - \bar{V}\sin\bar{\theta} \right)}{k + \bar{R}\cos\bar{\theta}} \right)
$$

$$
= \mu_{nf} \left(\left(\frac{\partial^2 \bar{W}}{\partial \bar{R}^2} + \frac{1}{\bar{R}} \frac{\partial \bar{W}}{\partial \bar{R}} + \frac{1}{\bar{R}^2} \frac{\partial^2 \bar{W}}{\partial \bar{\theta}^2} \right) + \frac{k^2}{(k + \bar{R}\cos\bar{\theta})^2} \frac{\partial^2 \bar{W}}{\partial \bar{Z}^2} - \frac{\bar{W}}{(k + \bar{R}\cos\bar{\theta})^2} \right.
$$

$$
\left. + \frac{1}{k + \bar{R}\cos\bar{\theta}} \left(\cos\bar{\theta} \frac{\partial \bar{W}}{\partial \bar{R}} - \frac{\sin\bar{\theta}}{\bar{R}} \frac{\partial \bar{W}}{\partial \bar{\theta}} \right) + \frac{2k\sin\bar{\theta}}{(k + \bar{R}\cos\bar{\theta})^2} \left(\cos\bar{\theta} \frac{\partial \bar{U}}{\partial \bar{Z}} - \sin\bar{\theta} \frac{\partial \bar{V}}{\partial \bar{Z}} \right) \right)
$$

$$
+ (\rho\beta)_{nf} g(T - T_1) - \frac{k}{k + \bar{R}\cos\bar{\theta}} \frac{\partial \bar{P}}{\partial \bar{Z}}. \tag{4.5}
$$

Energy equation in the presence of heat generation for a nanofluid is given as,

$$
(\rho c_p)_{nf} \left(\frac{\partial \bar{T}}{\partial \bar{t}} + \bar{U} \frac{\partial \bar{T}}{\partial \bar{R}} + \frac{k\bar{W}}{k + \bar{R}\cos\bar{\theta}} \frac{\partial \bar{T}}{\partial \bar{Z}} + \frac{\bar{U}}{\bar{R}} \frac{\partial \bar{T}}{\partial \bar{\theta}} \right) = K_{nf} \left(\frac{\partial^2 \bar{T}}{\partial \bar{R}^2} + \frac{1}{\bar{R}} \frac{\partial \bar{T}}{\partial \bar{R}} + \frac{\cos\bar{\theta}}{k + \bar{R}\cos\bar{\theta}} \frac{\partial \bar{T}}{\partial \bar{R}} \right.
$$

$$
+ \frac{1}{\bar{R}^2} \frac{\partial^2 \bar{T}}{\partial \bar{\theta}^2} + \frac{k^2}{(k + \bar{R}\cos\bar{\theta})^2} \frac{\partial^2 \bar{T}}{\partial \bar{Z}^2}
$$

$$
\left. - \frac{\sin\bar{\theta}}{k + \bar{R}\cos\bar{\theta}} \frac{\partial \bar{T}}{\partial \bar{\theta}} \right) + Q_0. \tag{4.6}
$$

For the fixed frame, the boundary conditions are given as

$$
\bar{W} = 0, \ \bar{T} = \bar{T}_0, \ \text{at} \quad \bar{R} = \bar{R}_1 = a_1,
$$

$$
\bar{W} = \bar{W}_B, \ \bar{T} = \bar{T}_1, \ \text{at} \quad \bar{R} = \bar{R}_2 = b\sin\left[\frac{2\pi}{\lambda} \left(\bar{Z} - ct \right) \right] + a_2, \tag{4.7}
$$

here $\bar{W}_B$ is the slip velocity at $\bar{R}_2$ as suggested in [29]

$$
\tau_{rz} = \beta_1^*(\bar{W}_B - Q), \tag{4.8}
$$

where Q is the Darcy's velocity given by

$$
Q = -\frac{\kappa^*}{\mu_{nf}} (\nabla \bar{P} - (\rho\beta)_{nf} g(\bar{T} - \bar{T}_1), \tag{4.9}
$$

where κ^* is the permeability constant.

For the stated nanofluid model, the nanofluid viscosity μ_{nf}, specific heat and density are defined as mentioned in [5]

$$\mu_{nf} = \frac{\mu_f}{(1-\varphi)^{2.5}}, \ (\rho c_p)_{nf} = \varphi(\rho c_p)_s + (1-\varphi)(\rho c_p)_f, \ \alpha_{nf} = \frac{K_{nf}}{(\rho C_p)_{nf}},$$
$$(\rho\beta)_{nf} = \varphi(\rho\beta)_s + (1-\varphi)(\rho\beta)_f, \ \rho_{nf} = \varphi\rho_s + (1-\varphi)\rho_f. \tag{4.10}$$

The expression for thermal heat conductivity of nanofluids is expressed as

$$\frac{K_{nf}}{K_f} = \frac{(n-1)k_f + k_s - (n-1)(k_f - k_s)\varphi}{k_s + (n-1)k_f + \varphi(k_f - k_s)}. \tag{4.11}$$

Here n signify shape factor of nanoparticles given by $3/\psi$, where ψ represents sphericity of the particle and is determined by the formation of nanoparticle. For cylindrical nanoparticle $n = 6$ or $\psi = 1/2$ while for spherical nanoparticle $\psi = 1$ or $n = 6$. Here, in this investigation we have taken $n = 6$ i.e. considered spherical shape.

Since the active velocity component is axial velocity so we assume the velocity vector in the form $(0, 0, \bar{W})$. The written below transformation is used to shift from $(\bar{R}, \bar{Z}, \bar{t})$ fixed frame to $(\bar{r}, \bar{z})$ wave frame,

$$\bar{z} = \bar{Z} - c\bar{t}, \ \bar{p}(\bar{z}, \bar{r}) = \bar{P}(\bar{Z}, \bar{R}, \bar{t}), \ \bar{r} = \bar{R}, \ \bar{w} = \bar{W} - c, \ \bar{u} = \bar{U}. \tag{4.12}$$

Bring out the following dimensionless quantities

$$w = \frac{\bar{w}}{c}, \ r = \frac{\bar{r}}{a_2}, \ u = \frac{\lambda\bar{u}}{a_2 c}, \ z = \frac{\bar{z}}{\lambda}, \ r_2 = \frac{\bar{r}_2}{a_2} = 1 + \varepsilon\sin(2\pi z),$$
$$\varepsilon = \frac{b}{a_2}, \ t = \frac{c\bar{t}}{\lambda}, \ G_r = \frac{a_2^2(T_1 - T_0)\rho_f\beta_f g}{c\mu_f}, \ \tilde{\theta} = \frac{T - T_1}{T_0 - T_1}, \ \bar{\theta} = \theta,$$
$$\zeta = \frac{a_2}{k}, \ r_1 = \frac{\bar{r}_1}{a_2} = \epsilon, \ \gamma = \frac{a_2^2 Q_0}{(T_1 - T_0)k_f}, \ R_e = \frac{a_2 c\rho_f}{\mu_f}, \ \delta = \frac{a_2}{\lambda},$$
$$p = \frac{a_2^2\bar{p}}{c\lambda\mu_f}, \ d = \frac{\kappa^*}{a_2^2}, \ w = \frac{1}{r}\frac{\partial\psi}{\partial r}, \ u = -\frac{1}{r}\frac{\partial\psi}{\partial z}. \tag{4.13}$$

In these expressions, p is representing the pressure, G_r represents the Grashrof number, $\tilde{\theta}$ is

78

dimensionless temperature,R_e is Reynolds number,γ is dimensionless heat source parameter, ζ is curvature parameter, d is the darcy number and δ represent wave number. After employing the lubrication approach, Eqs. $(4.2) - (4.6)$ take the form:

$$\frac{\partial p}{\partial r} = 0, \tag{4.14}$$

$$\frac{\partial p}{\partial \theta} = 0, \tag{4.15}$$

$$\frac{1}{1+\zeta r \cos\theta}\frac{\partial p}{\partial z} = \frac{\mu_{nf}}{\mu_f}\left(\frac{\partial^2 w}{\partial r^2} + \frac{1}{r}\frac{\partial w}{\partial r} + \frac{1}{r^2}\frac{\partial^2 w}{\partial \theta^2} - \frac{\zeta^2(w+1)}{(1+\zeta r \cos\theta)^2} + \frac{\zeta \cos\theta}{1+\zeta r \cos\theta}\frac{\partial w}{\partial r}\right.$$
$$\left. -\frac{\zeta \sin\theta}{r(1+\zeta r \cos\theta)}\frac{\partial w}{\partial \theta} + G_r\frac{(\rho\beta)_{nf}}{(\rho\beta)_f}\frac{\mu_f}{\mu_{nf}}\tilde{\theta}\right) \tag{4.16}$$

$$\frac{\partial^2 \tilde{\theta}}{\partial r^2} + \frac{1}{r}\frac{\partial \tilde{\theta}}{\partial r} + \frac{\zeta \cos\theta}{1+\zeta r \cos\theta}\frac{\partial \tilde{\theta}}{\partial r} + \frac{1}{r^2}\frac{\partial^2 w}{\partial \theta^2} + \gamma\frac{K_f}{K_{nf}} = 0. \tag{4.17}$$

In wave frame, the suitable boundary conditions are defined as

$$\tilde{\theta} = 1, \ w = -1, \qquad \text{at} \quad r = r_1 = \epsilon,$$
$$\tilde{\theta} = 0, \ w = w_B - 1, \ \text{at} \quad r = r_2 = 1 + \varepsilon \sin(2\pi z), \tag{4.18}$$

Dimensionless volume flow rate is given as

$$q = F + \frac{1}{2} - \frac{\epsilon^2}{2} + \frac{\varepsilon^2}{4}, \tag{4.19}$$

$$F = \int_{r_1}^{r_2} rw dr. \tag{4.20}$$

4.2 Solution of the problem

In order to get the expression for velocity and temperature according to the given boundary condition, we consider the following forms

$$
\begin{aligned}
\tilde{\theta}(r(z,t),\ \theta) &= \tilde{\theta}_0(r) + \zeta \cos(\theta)\tilde{\theta}_1(r) + \dots \\
w(r(z,t),\ \theta) &= w_0(r) + \zeta \cos(\theta)w_1(r) + \dots
\end{aligned}
\tag{4.21}
$$

Substituting Eq. (4.21) into Eqs. (4.16) to (4.18) and equating like powers of $\zeta \cos(\theta)$, we obtain the following systems and their solutions

4.2.1 Zeroth order system and solution

$$
\frac{\partial^2 \tilde{\theta}_0}{\partial r^2} + \frac{1}{r}\frac{\partial \tilde{\theta}_0}{\partial r} + \gamma \frac{K_f}{K_{nf}} = 0,
\tag{4.22}
$$

$$
\frac{\partial^2 w_0}{\partial r^2} + \frac{1}{r}\frac{\partial w_0}{\partial r} + G_r \frac{(\rho\beta)_{nf}}{(\rho\beta)_f}\frac{\mu_f}{\mu_{nf}}\tilde{\theta}_0 = \frac{\mu_f}{\mu_{nf}}\frac{dp}{dz},
\tag{4.23}
$$

$$
\tilde{\theta}_0(r_1) = 1,\ w_0(r_1) = -1,
\tag{4.24}
$$

$$
\tilde{\theta}_0(r_2) = 0,\ w_0(r_2) = w_B - 1.
\tag{4.25}
$$

The exact solution at this order is given as

$$
\tilde{\theta}_0(r) = C_1 \ln r + C_2 - \frac{\gamma \frac{K_f}{K_{nf}}}{4} r^2,
\tag{4.26}
$$

$$
\begin{aligned}
w_0(r) &= \frac{\frac{dp}{dz}}{4\frac{\mu_{nf}}{\mu_f}}r^2 - G_r \frac{(\rho\beta)_{nf}}{(\rho\beta)_f}\frac{\mu_f}{\mu_{nf}}\left(-\frac{\gamma \frac{K_f}{K_{nf}}}{64}r^4 + \frac{C_1}{2}\left(\frac{r^2 \ln r}{2} - \frac{r^2}{2}\right) + \frac{C_2}{4}r^2\right) \\
&\quad + C_5 \ln r + C_6.
\end{aligned}
\tag{4.27}
$$

80

4.2.2 First order system and solution

$$\frac{\partial^2 \tilde{\theta}_1}{\partial r^2} + \frac{1}{r}\frac{\partial \tilde{\theta}_1}{\partial r} - \frac{\tilde{\theta}_1}{r^2} + r\frac{\partial^2 \tilde{\theta}_0}{\partial r^2} + 2\frac{\partial \tilde{\theta}_0}{\partial r} + r\gamma\frac{K_f}{K_{nf}} = 0 , \tag{4.28}$$

$$\frac{\partial^2 w_1}{\partial r^2} + \frac{1}{r}\frac{\partial w_1}{\partial r} - \frac{w_1}{r^2} + r\frac{\partial^2 w_0}{\partial r^2} + 2\frac{\partial w_0}{\partial r} + G_r\frac{(\rho\beta)_{nf}}{(\rho\beta)_f}\frac{\mu_f}{\mu_{nf}}(r\tilde{\theta}_0 + \tilde{\theta}_1) = 0, \tag{4.29}$$

$$\tilde{\theta}_1(r_1) = 0, \ w_1(r_1) = 0, \tag{4.30}$$

$$\tilde{\theta}_1(r_2) = 0, \ w_1(r_2) = w_B, \tag{4.31}$$

Solution is obtained by substituting Eqs. $(4.26 - 4.27)$ into Eqs. $(4.28 - 4.29)$ as follow

$$\bar{\theta}_1(r) = rC_3 + \frac{C_4}{r} + r\left(\frac{\gamma\frac{K_f}{K_{nf}}r^2}{8} - \frac{C_1\ln r}{2}\right) - \frac{1}{r}\left(\gamma\frac{K_f}{K_{nf}}\frac{r^4}{16} - \frac{C_1 r^2}{4}\right), \tag{4.32}$$

$$
\begin{aligned}
w_1(r) \ = \ & rC_7 + \frac{C_8}{r} + \frac{r}{2}\left(-\frac{3\frac{dp}{dz}}{4\frac{\mu_{nf}}{\mu_f}}r^2 + G_r\frac{(\rho\beta)_{nf}}{(\rho\beta)_f}\frac{\mu_f}{\mu_{nf}}\left(-\frac{\gamma\frac{K_f}{K_{nf}}}{32}r^4 + \frac{C_1}{2}r^2\ln r - \frac{C_1}{4}r^2 + \frac{C_2}{4}r^2\right.\right. \\
& \left.\left. - \frac{C_3}{2}r^2 - C_4\ln r\right) - C_5\ln r\right) - \frac{1}{2r}\left(-\frac{3\frac{dp}{dz}}{8\frac{\mu_{nf}}{\mu_f}}r^4 + G_r\frac{(\rho\beta)_{nf}}{(\rho\beta)_f}\frac{\mu_f}{\mu_{nf}}\left(-\frac{\gamma\frac{K_f}{K_{nf}}}{48}r^6 + \frac{C_1}{4}r^4\ln r\right.\right. \\
& \left.\left. - \frac{3C_1}{16}r^4 + \frac{C_2}{8}r^4 - \frac{C_3}{4}r^4 - \frac{C_4}{2}r^2\right) - \frac{C_5}{2}r^2\right).
\end{aligned}
\tag{4.33}
$$

here all the C's are constants and defined in appendix at the end of this chapter.

The pressure gradient is defined as

$$\frac{dp}{dz} = \frac{F - t_1}{t_2}. \tag{4.34}$$

where t_1 and t_2 are calculated by Mathematica.

4.3 Results and discussion

This section represents the discussion for the graphical results of velocity, pressure gradient, pressure rise and streamlines. These graphs are obtained by restricting the included parameters such as $G_r = 2-4$, $\gamma =$, $d =$, $\theta =$. Axial velocity w demonstrates parabolic behavior against all the involved parameters in the region between tube having sinusoidal curve and endoscope. Figs 4.2 (a) and (b) depict the impact of Grashoff's number on velocity profile while keeping other parameters fixed. Shape factor of bricks for Ag nanoparticles are considered and it is evident from the figure that axial velocity shows increasing attitude in the region $[0.1-0.66]$ for growing Grashoff's number but opposite trend is noticed in region $[0.66-1]$. Three dimensional axial velocity profile can be seen in Fig 4.2 b for brick Ag nanoparticles for the variation of Grashoff;'s number. Figs 4.3(a, b) indicate how the velocity profile behaves for cylindrical Ag nanoparticles for varying Grashoff's number. It is viewed that velocity elevates in region $[0.1-0.66]$ and diminishes in region $[0.66-1]$. Fig 4.3 (b) gives the 3 dimensional view of variation of velocity profile for cylindrical nanoparticles with modifying G_r . Similar trend is seen for both brick and cylindrical nanoparticles. Impact of platelet nanoparticles with different G_r on velocity profile is captured in Figs 4.4 (a) and (b) for both 2 and 3 dimensional flow. Variation is noticed to be alike as that of brick and cylindrical nanoparticles. Influence of heat source(sink) parameter γ on axial velocity profile for shape factor of bricks for Ag nanoparticles can be seen in Figs 4.5 (a) and (b) for 2D and 3D respectively. Velocity profile shows a decrease in magnitude for increasing γ. Figs 4.6 (a) and (b) are plotted to exhibit the trends followed by velocity profile for cylindrical Ag particles. Identical behavior is observed for cylindrical and brick nanoparticles i.e. velocity profile shows a decline in its magnitude both for bricks and cylinders. Fig 4.6 (b) portraits the 3D velocity for cylindrical Ag nanoparticles. Platelet nanoparticles with varying γ are plotted in Figs 4.7 (a) and (b) for both 2 and 3 dimensions respectively. Bricks, cylinders and platelets are observed to give the same trend. Velocity is also influenced by amplitude ratio φ. Figs 4.8(a, b) describe the behavior of velocity profile for different φ with brick Ag nanoparticles. It is seen that velocity decreases in the region $[0.1, 0.62]$ and increases in the region $[0.62, 1]$ by increasing φ. An increase is noticed as we move from inner tube to the center of the region enclosed by the two tubes which is depicted in Figs 4.9(a, b) for cylindrical Ag nanoparticles giving both 2D and 3D velocity graphs with increasing amplitude

ratio. Platelets nanoparticles show the same behavior for amplitude ratio as that of cylindrical and brick nanoparticles and this behavior is captured in Figs 4.10(a, b). Variation of Darcy's number d effecting the velocity profile can be seen in Figs 4.11(a, b). Initially velocity increases for increasing d but as we move towards the porous tube, velocity decreases for elevating d. In region $[0.1, 0.74]$ velocity experiences a rise and then a decline is noticed in region $[0.74, 1]$. Figs 4.11(a, b) is 2 and 3-dimensional graph plotted to describe velocity profile for shape factor of brick Ag nanoparticles. Figs 4.12(a, b) portrays 2D and 3D view of axial velocity for cylindrical nanoparticles. Velocity boosts as we move from endoscope to central region i.e.$0.1 < r < 0.74$ and a decline is noticed in the region $0.74 < r < 1$. Figs 4.13(a, b) give the effects of platelet Ag nanoparticles for different values of darcy's number and they behave likely as bricks and cylinders.

Figs $(4.14 - 4.17)$ are sketched to describe the change in pressure gradient for different G_r, γ, φ and d. Figs 4.14(a, b, c) depicts the behavior of pressure gradient effected by Grashoff's number G_r. It the observed that the growth of buoyancy forces results in decrease of pressure gradient. Shape factor of bricks, cylinders and platelets for Ag nanoparticle all give the same behavior. Figs 4.15(a, b, c) describes the behavior of dp/dz against z for variational heat source(sink) parameter γ. The amplitude of pressure is noticed to decrease as γ gets higher values with shape factors of bricks,cylinders and platelets. The variational change in pressure gradient due to amplitude ratio φ with bricks, cylinders and platelets in shown in Figs 4.16(a, b, c) respectively. Pressure gradient is noticed to decrease in region $[-1, -0.5]$ and $[0, 0.5]$ and increase is observed in region $[-0.5, 0]$ and $[0.5, 1]$ for elevating amplitude ratio φ. Figs 4.17(a, b, c) is plotted to give the influence of darcy's number d on dp/dz by taking bricks, cylinders and platelets. An increase in darcy number d give rise to amplitude of pressure gradient.

To explain the pumping properties, it is crucial to know pressure rise per wavelength. Thus Figs $(4.18 - 4.20)$ are plotted to depict the pressure rise for varying different parameters such as Grashoff's number G_r, heat source parameter γ, amplitude ratio and darcy's number d. With expansion in flow rate,on common observation from these figures, pressure rise per wavelength decreases. Figs 4.19(a, b, c) is used to analyze the behavior of pressure rise for different values of G_r. It is observed that pressure rise experiences a decline with elevating G_r through annulus. This trend is followed in both retrograde pumping region$(q < 0, \Delta p > 0)$ and

augmented pumping region ($q > 0, \Delta p < 0$). Also shape factor of bricks, cylinders and platelet Ag nanoparticle behave likely i.e. pressure rise drops for all these nanoparticles with increase in G_r. Figs 4.20(a, b, c) is plotted to the effects of heat source (sink) parameter γ on Δp. It can be seen from fig that Δp decreases in retrograde pumping region as well as in augmented pumping region when γ has been increased. The impact of brick, cylinder and platelet nanoparticles is similar for Δp for different γ.Figs 4.21(a, b, c) give the effects of amplitude ratio φ over Δp. As the value of parameter increases, Δp decreases in retrograde and augmented pumping region. This behavior is seen for brick, cylinder and platelet Ag nanoparticles.

An engrossing phenomena of trapping for peristaltic flow with an endoscope is described in Figs (4.21 − 4.33). Ag nanoparticles with different shape factors are taken into consideration for this discussion. pattern of flow in the region enclosed by catheter and curved tube is studied by plotting streamlines. Random behavior of enclosed bolus is seen for variation of G_r along with closed streamlines and is portrayed in Figs 4.21. From Fig it is seen that the number of trapped bolus decreases when G_r shifts from 2 to 3 and size is also observed to decrease as G_r further changes from 3 to 4. From Figs 4.21 − 4.23 it is evident that the change in bolus appearance is concordant for all different shape factors considered. Effects of γ over trapping phenomena is studied in Fig 4.24. It is witnessed that as γ changes from 0.1 to 0.5, number of trapped bolus decreases and the size also recedes as γ jumps to 0.9 from 0.5. Different shape factors considered give the harmonious behavior for variation of γ and this argument is supported by Figs 4.24 − 4.26. Fig 4.27 is used to show the impact of φ over trapping phenomena. As φ is increased from 0.03 to 0.05, number of bolus increases and on further increasing φ from 0.05 to 0.07 a decrease in number of bolus is seen. Brick, cylinder and platelet Ag Nanoparticles give the same trend which can be verified with the help of Figs 4.27 − 4.29. Decrease in size of bolus in more noticeable in cylinder and platelet particles as compared to brick nanoparticles. Variation of darcy's number is studied in Figs 4.30 − 4.32. Initially, number of trapped bolus increases for increasing darcy's number then their size also increases with similar trend of darcy's number. Visual study has revealed that all the considered shape factors of nanoparticles have shown likely behavior. Fig 4.33 is used to compare the effects of different shape factors of nanoparticles used. Temperature profile for curved channel with permeable walls having shape factor m is presented in Table 4.1. It is witnessed that for greater value of shape factor i.e.

for larger m the temperature of the base fluid decreases. Also it is interesting to see that the variation in curvature effects the temperature profile. With larger curvature parameter ζ low temperature is noticed as can be seen in Table 4.2.
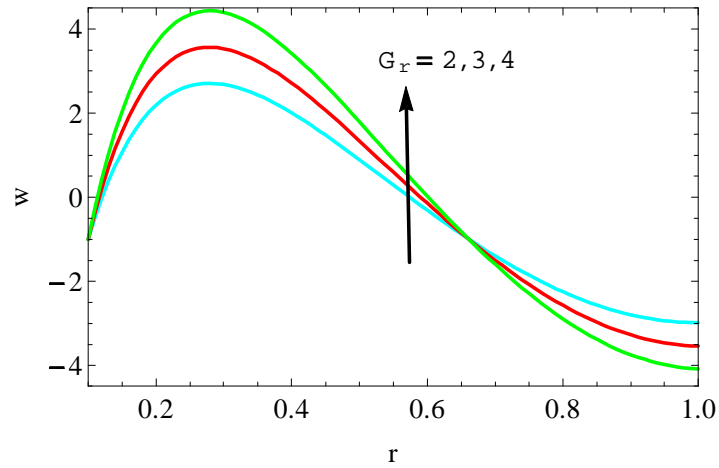
(a)
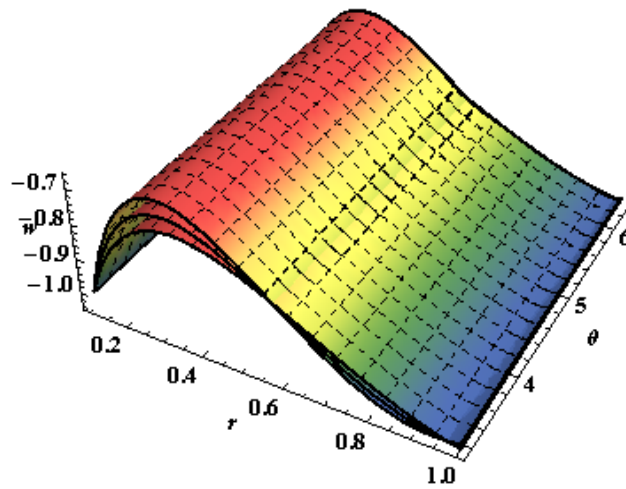
(b)

Figs. 4.2(a, b), velocity profile for distinct values of Grashroff number G_r with shape factor

85

of bricks
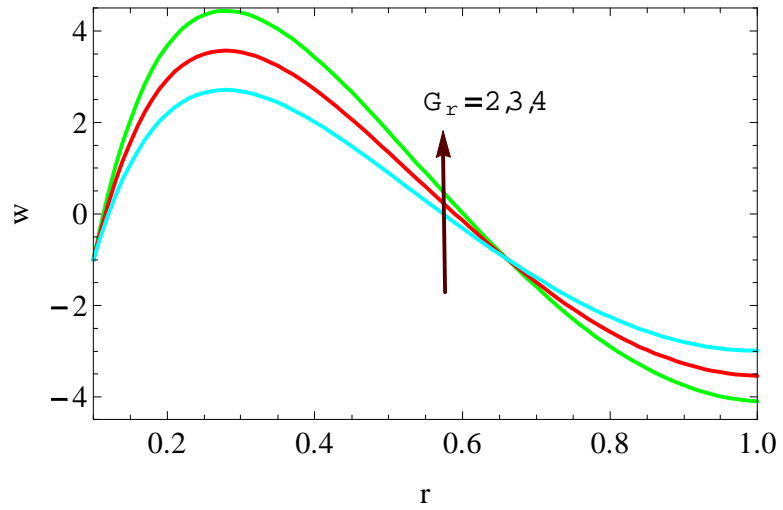
(a)
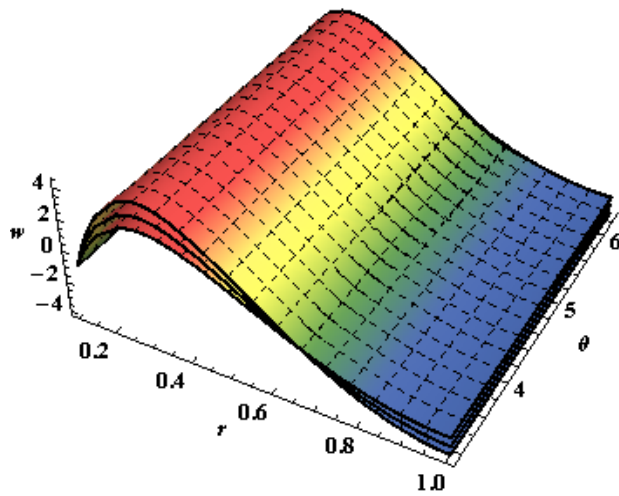
(b)

$Figs.$ 4.3(a, b), velocity profile for distinct values of Grashroff number G_r with shape factor of cylinders
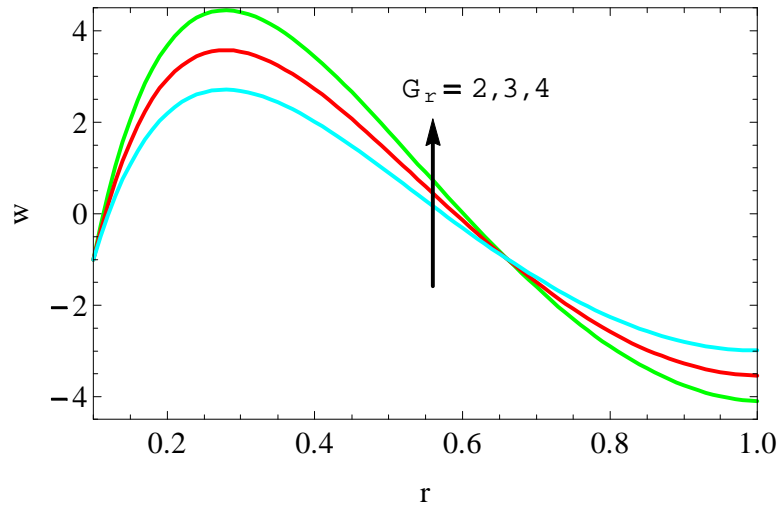
(a)
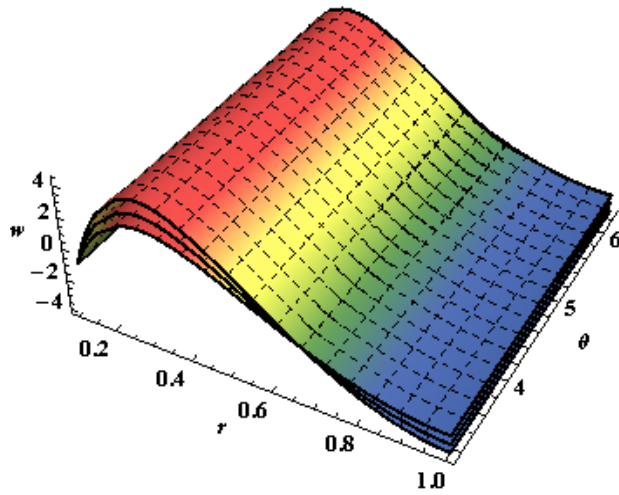
(b)

$Figs.$ 4.4(a, b), velocity profile for distinct values of Grashroff number G_r with shape factor of platelets
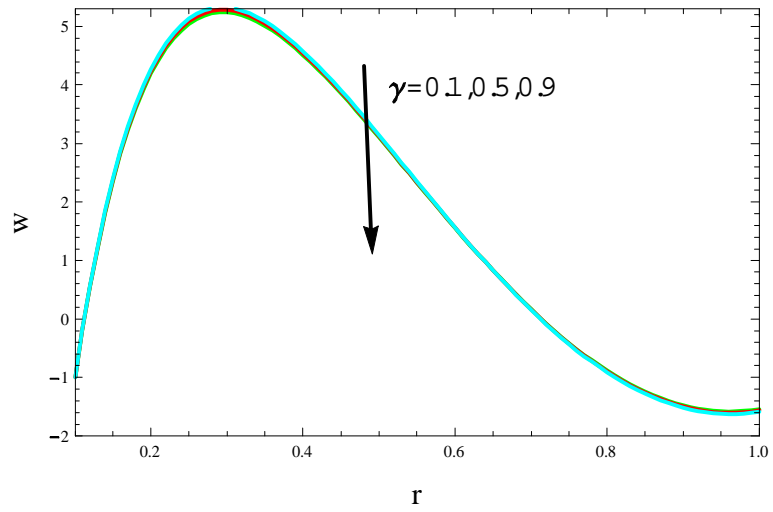
(a)
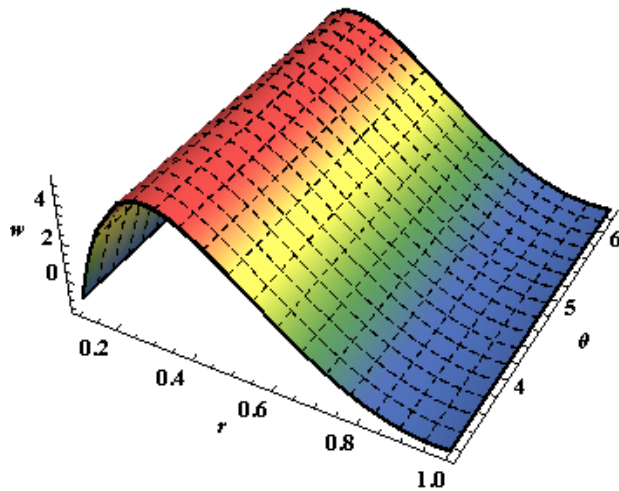
(b)

Figs. 4.5(*a*, *b*), velocity profile for distinct values of heat source(sink) γ with shape factor of bricks
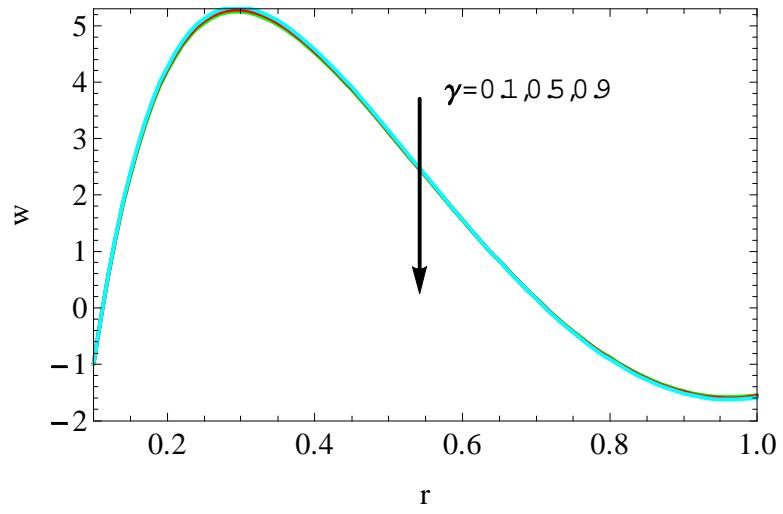
(a)
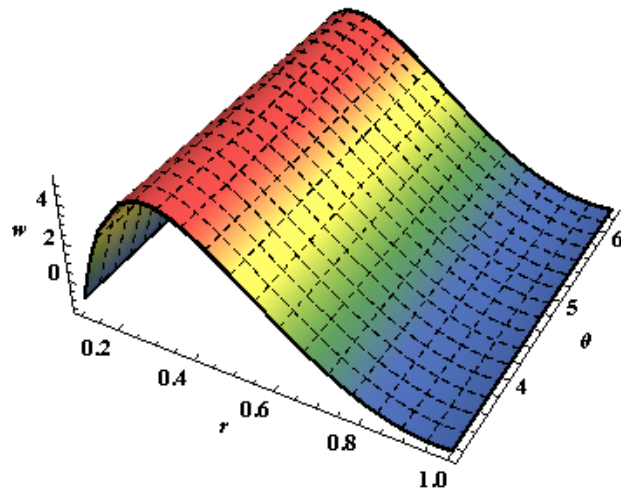
(b)

Figs. 4.6(a, b), velocity profile for distinct values of heat source(sink) γ with shape factor of cylinders
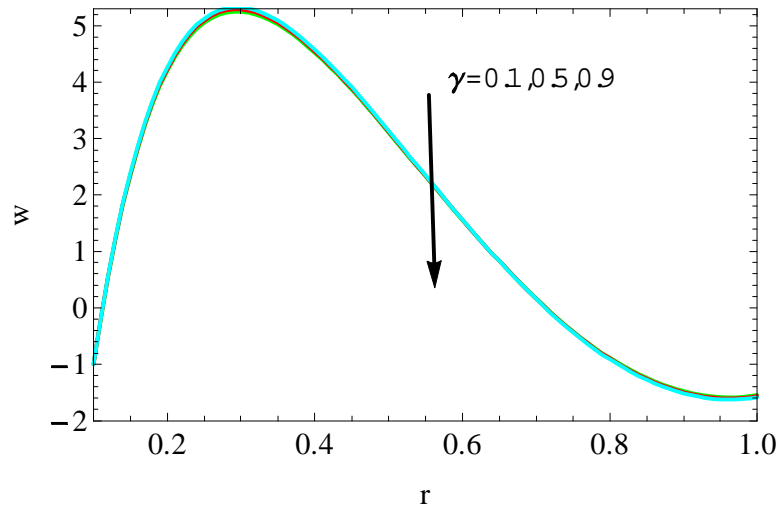
(a)
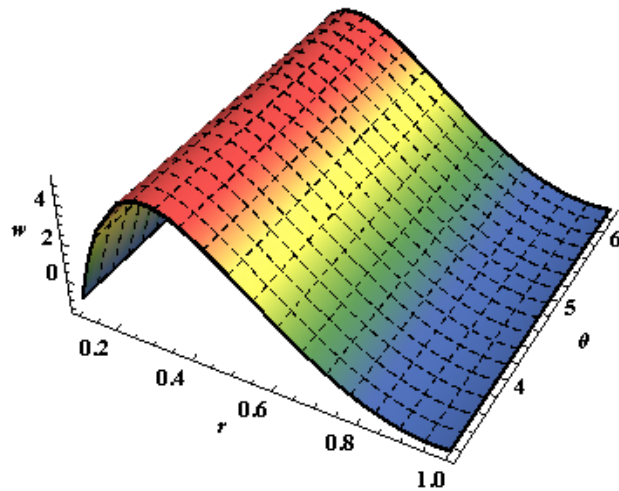
(b)

Figs. 4.7(a, b), velocity profile for distinct values of heat source(sink) γ with shape factor of platelets
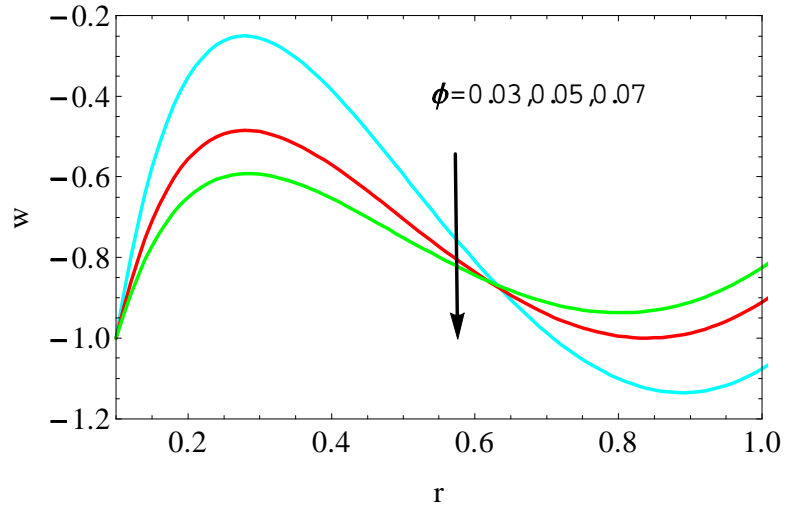
(a)
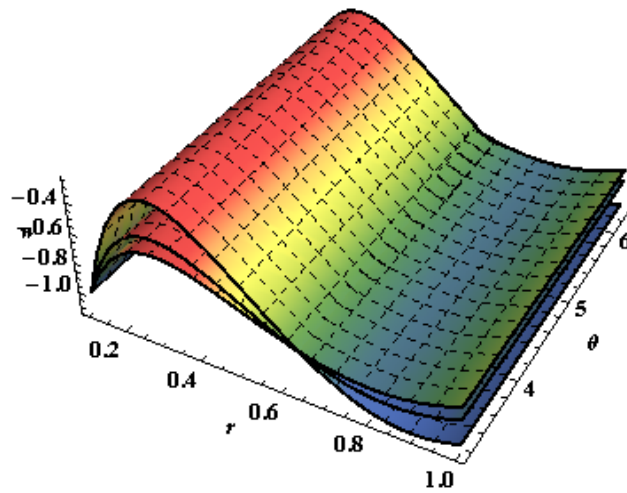
(b)

Figs. 4.8(a, b), velocity profile for distinct values of amplitude ratio φ with shape factor of bricks

91
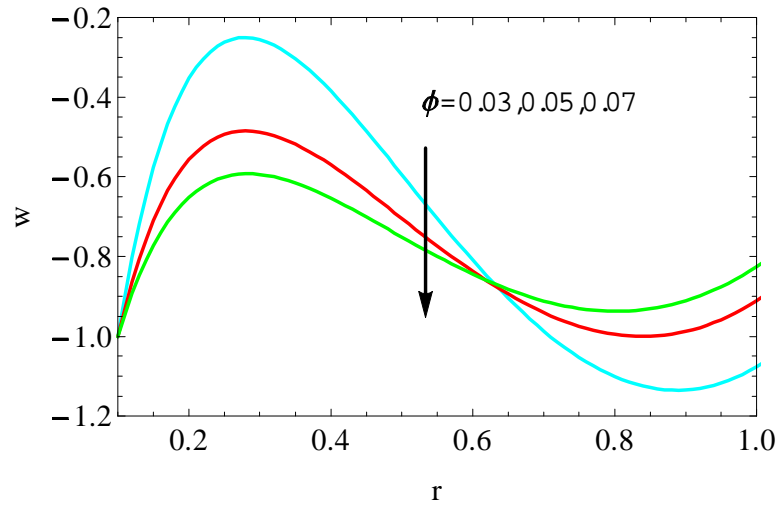
(a)
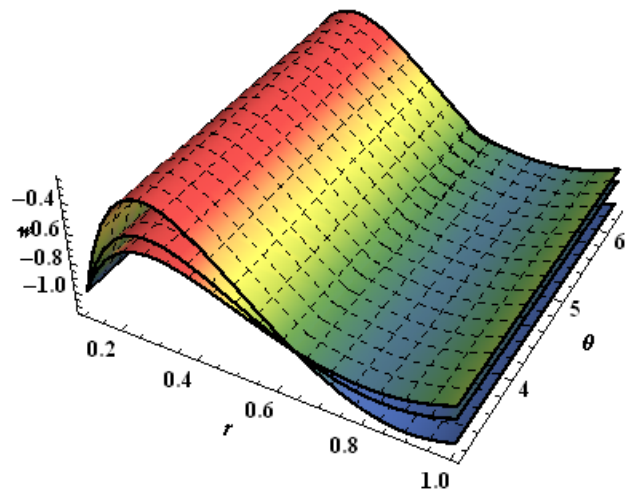
(b)

Figs. 4.9(a, b), velocity profile for distinct values of amplitude ratio φ with shape factor of cylinders
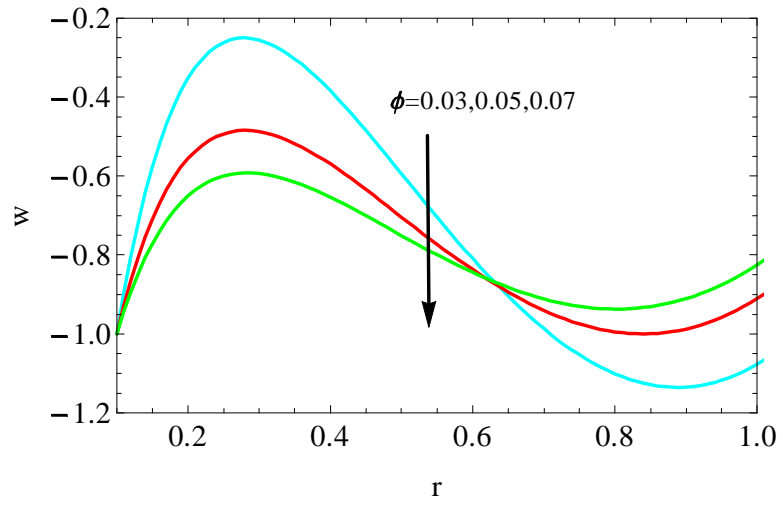
(a)
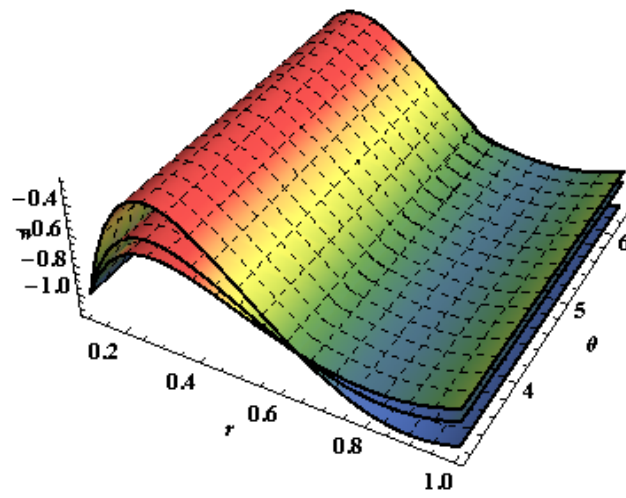
$Figs.$ $4.10(a, b)$, velocity profile for distinct values of amplitude ratio φ with shape factor of platelets
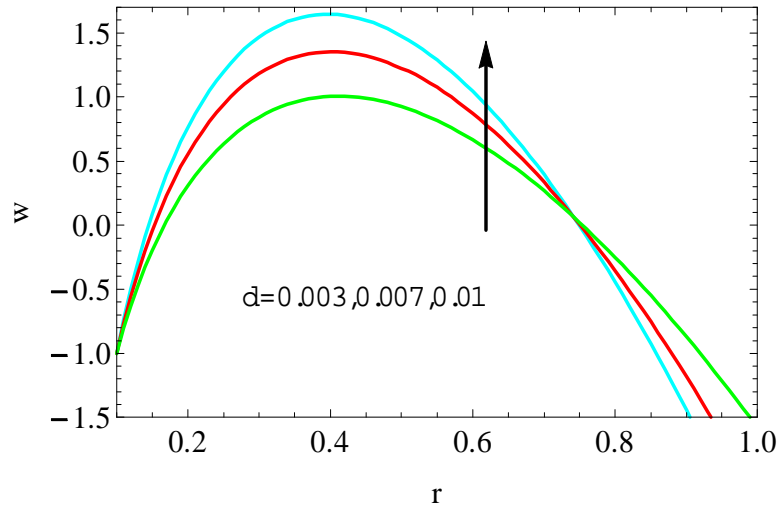
(a)
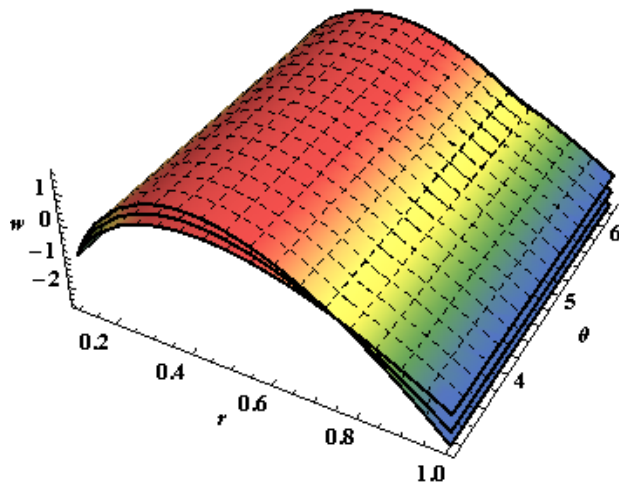
(b)

$Figs.$ 4.11(a, b), velocity profile for distinct values of darcy's number d with shape factor of bricks
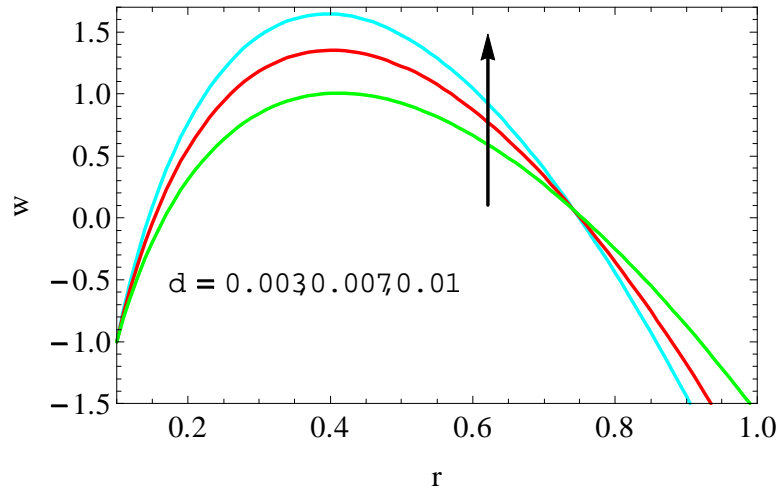
(a)
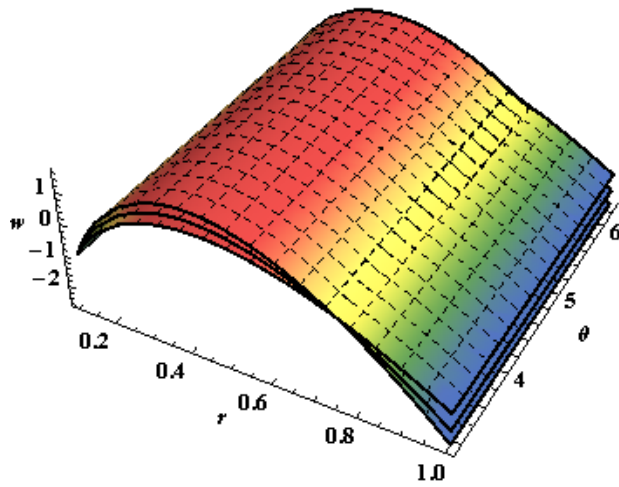
(b)

Figs. 4.12(*a, b*), velocity profile for distinct values of darcy's number *d* with shape factor of cylinders
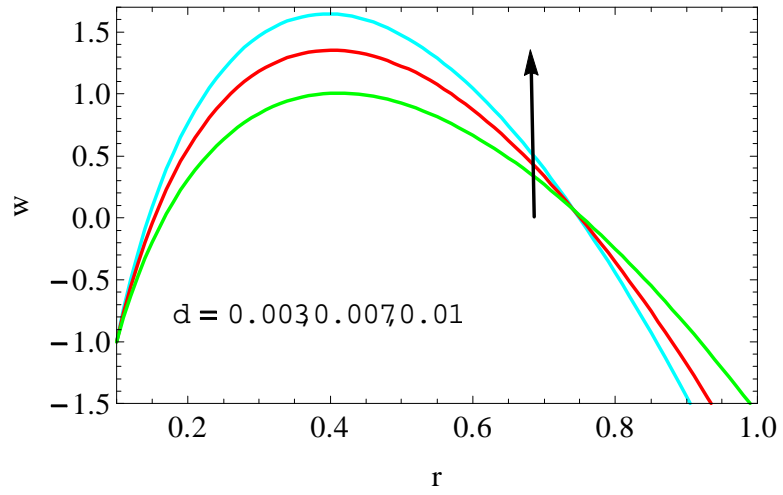
(a)
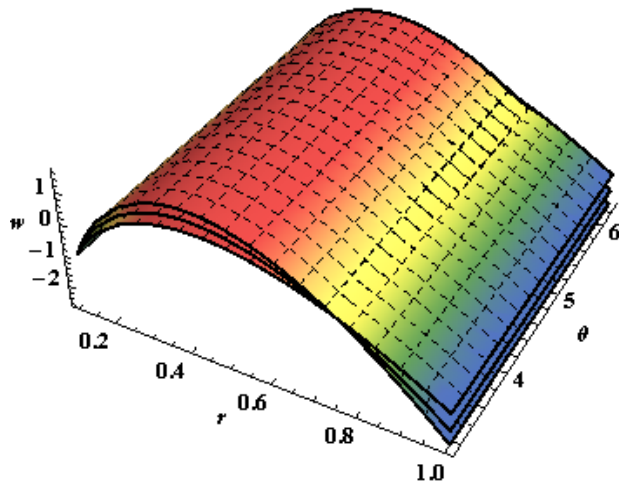
(b)

Figs. 4.13(a, b), velocity profile for distinct values of darcy's number d with shape factor of platelets
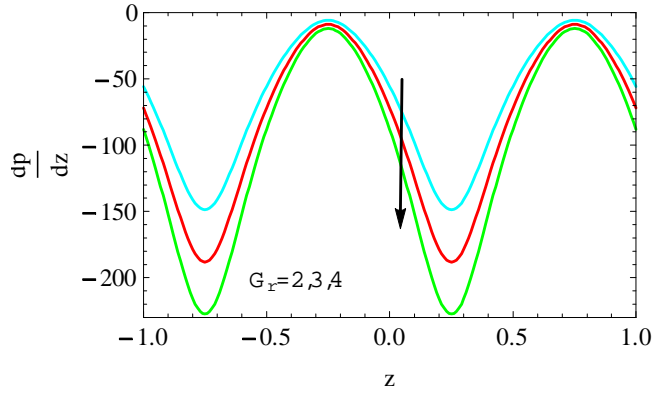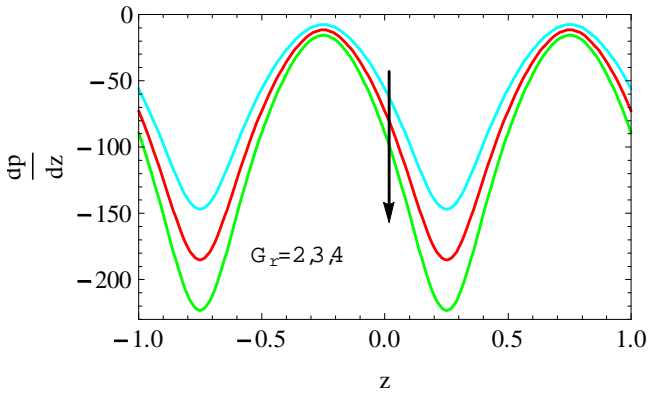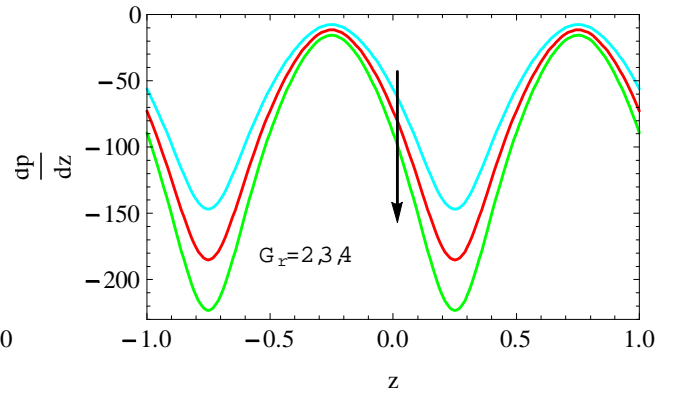
$Figs.$ 4.14(a, b, c), Pressure gradient for different values of Grashroff number G_r for (**a**) bricks (**b**) cylinders (**c**) platelets.
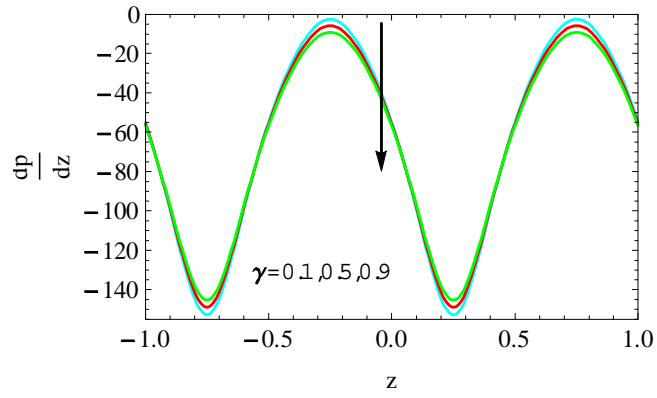
(a)
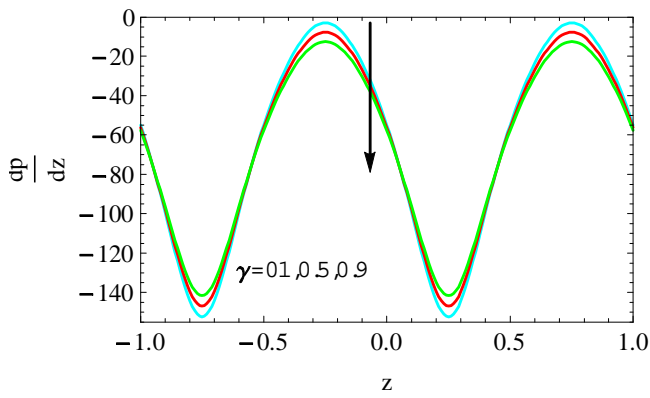
(b)
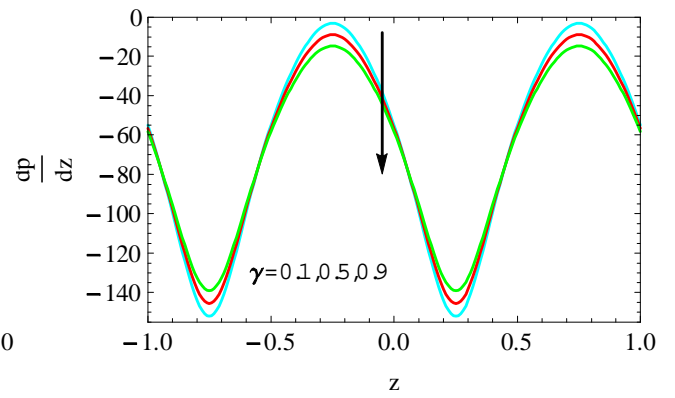
(c)

Figs. 4.15(a, b), Pressure gradient for different values of heat source(sink) parameter γ for **(a)** bricks (**b**) cylinders (**c**) platelets.
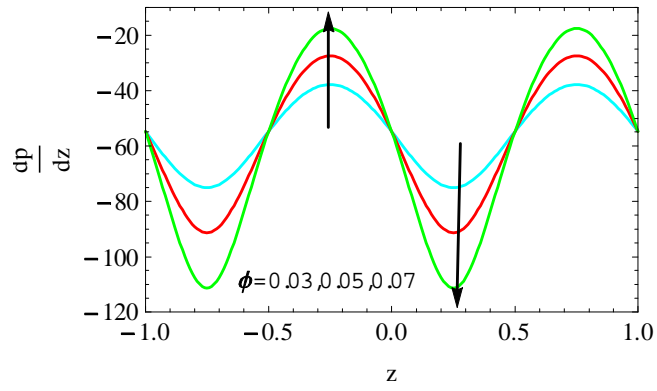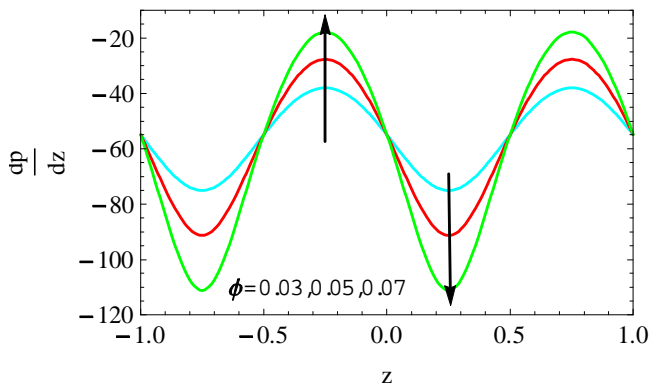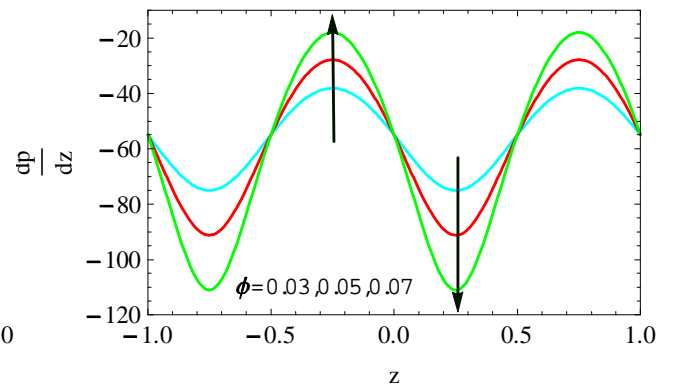
Figs. 4.16(*a, b, c*), Pressure gradient for different values of amplitude ratio φ for **(a)** bricks **(b)** cylinders **(c)** platelets.
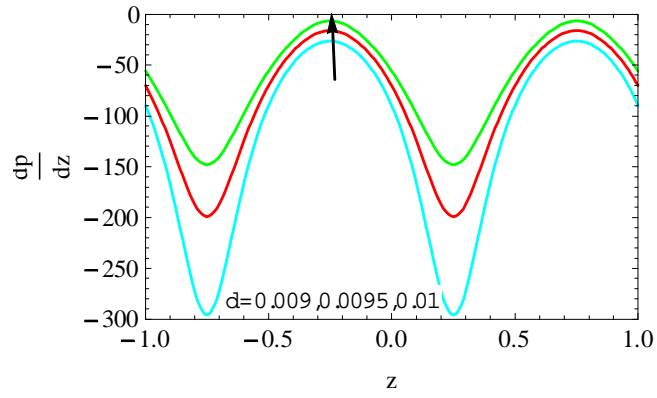
(a)
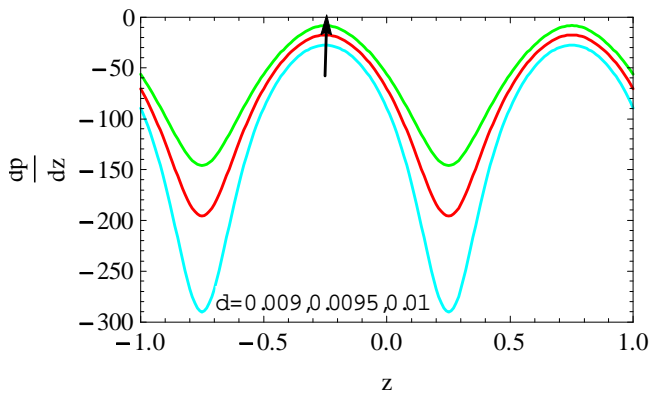
(b)
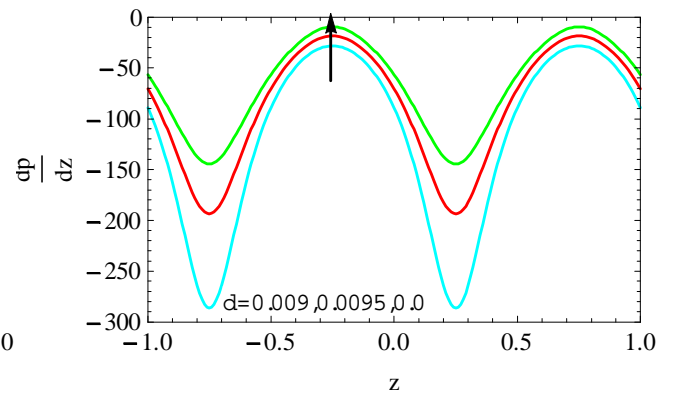
(c)

$Figs.$ 4.17(a, b, c), Pressure gradient for different values of darcy's number d for **(a)** bricks **(b)** cylinders **(c)** platelets.
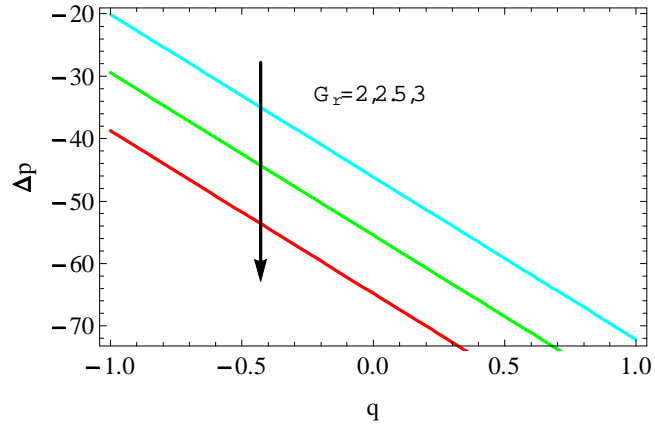
(a)
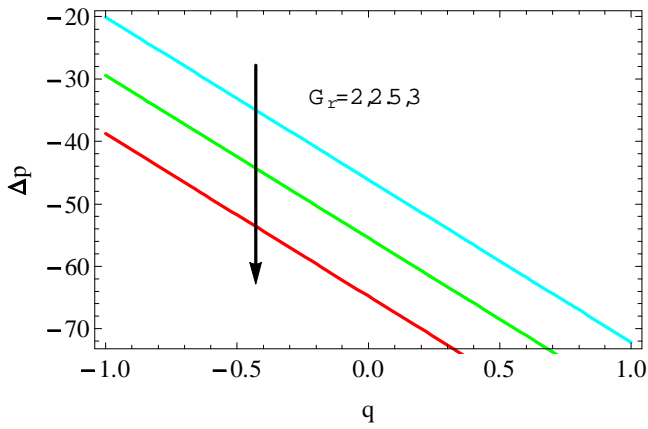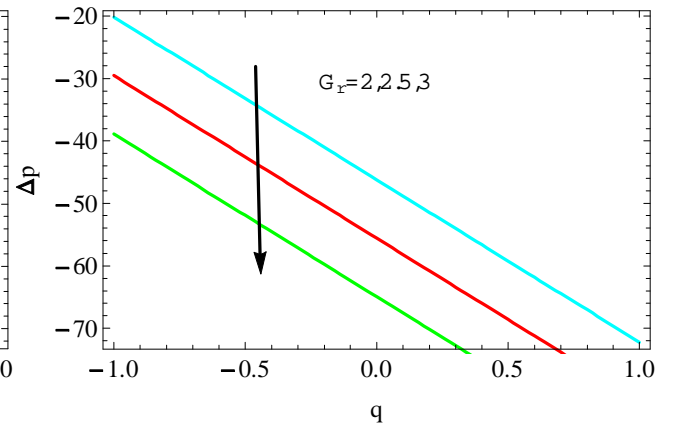
(b)   (c)

Figs. 4.18(*a*, *b*, *c*), Pressure rise for different values of Grashroff number G_r for **(a)** bricks **(b)** cylinders **(c)** platelets.
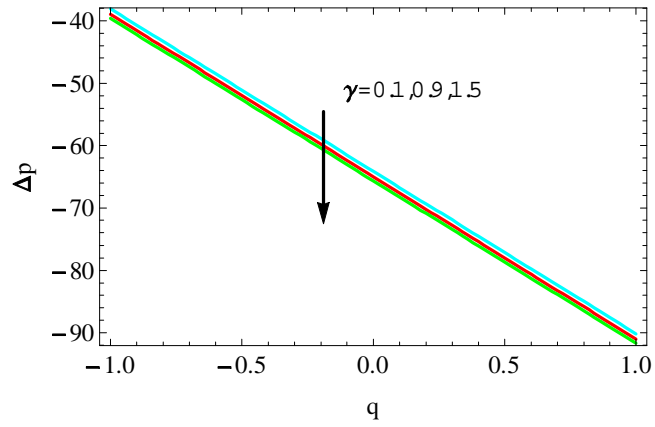
(a)
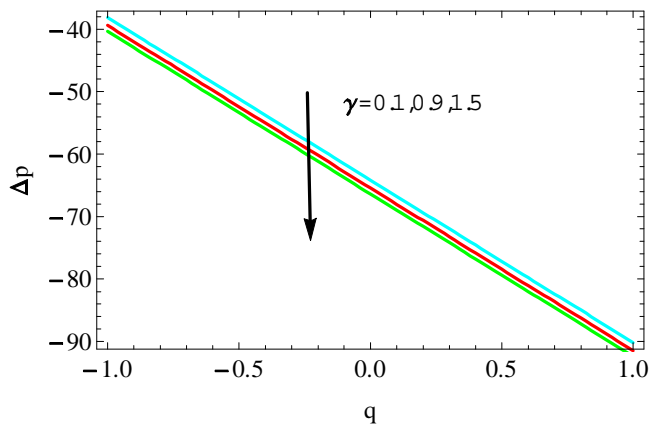
(b)
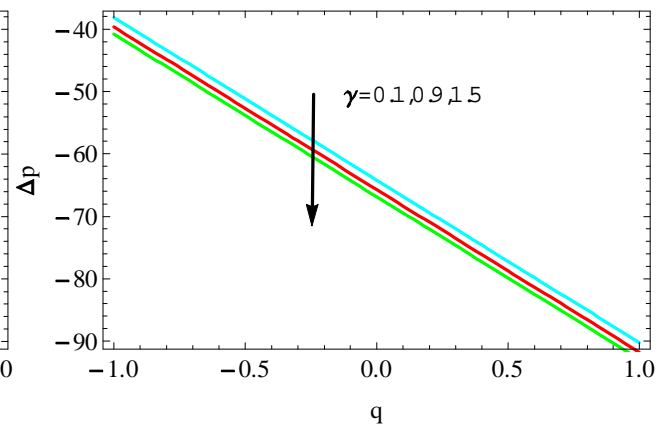
(c)

$Figs.$ 4.19(a, b, c), Pressure rise for different values of heat source (sink) parameter γ for **(a)** bricks **(b)** cylinders **(c)** platelets.
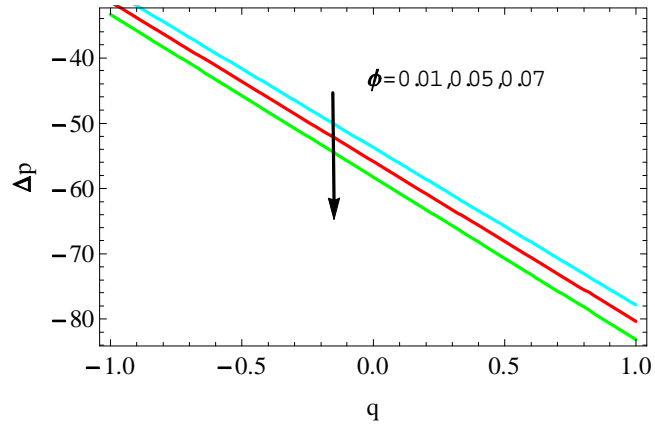
(a)
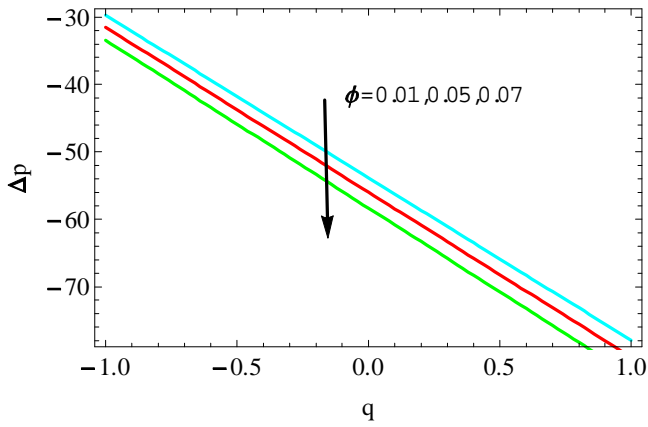
(b)
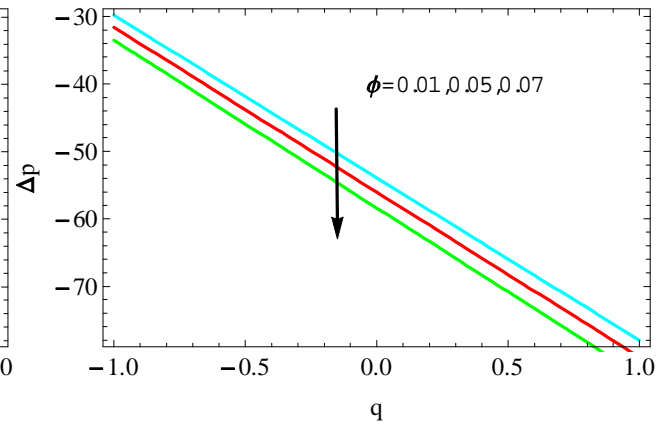
(c)

$Figs.$ 4.20(a, b, c), Pressure rise for distinct values of amplitude ratio φ for (**a**) bricks (**b**) cylinders (**c**) platelets.
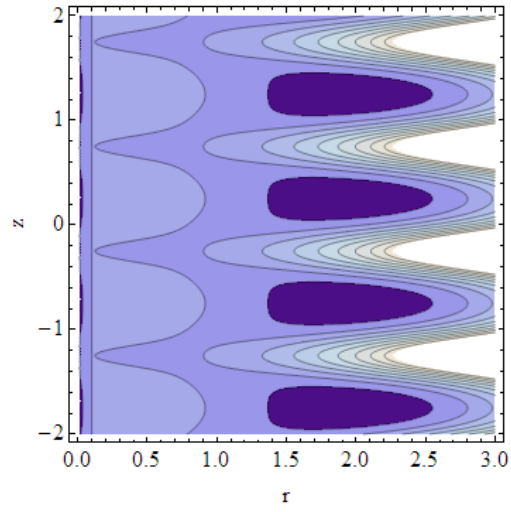
(a)
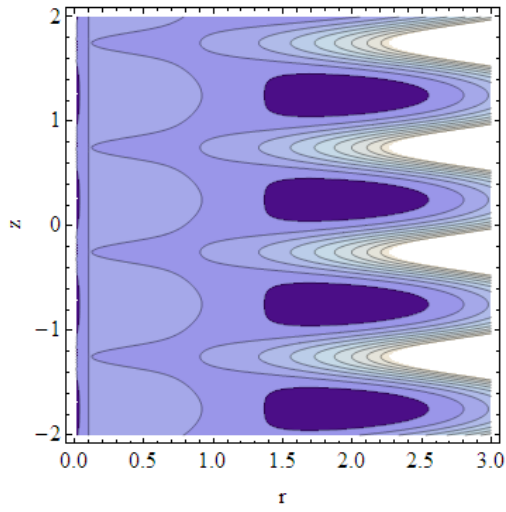
(b)
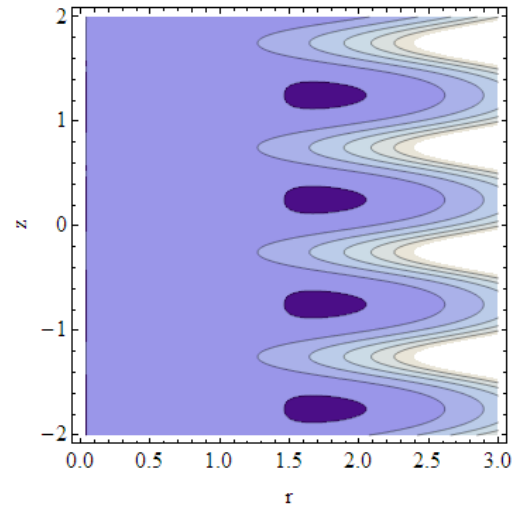
(c)

$Figs.4.21(a, b, c)$, Streamlines for Gold nanoparticle with shape factor of bricks for Grashoff's number (**a**) $G_r = 2$, (**b**) $G_r = 3$, (**c**) $G_r = 4$.
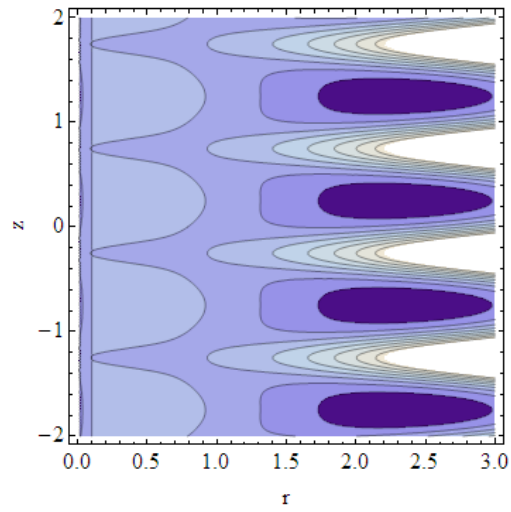
(a)
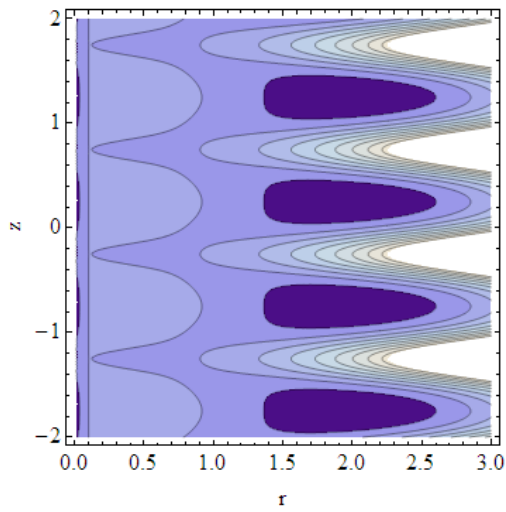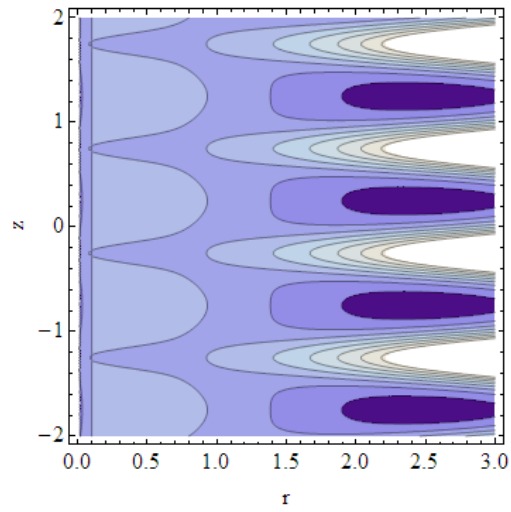

(b)
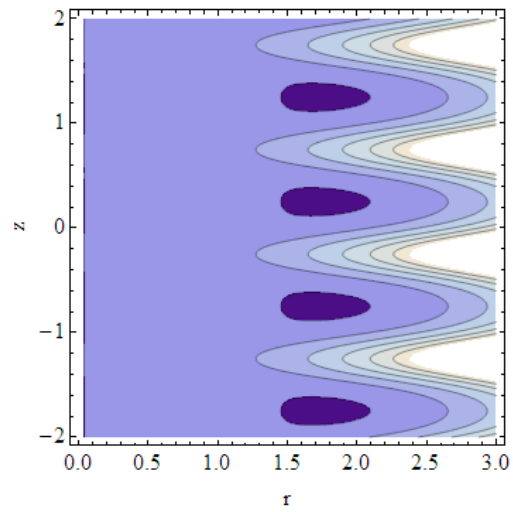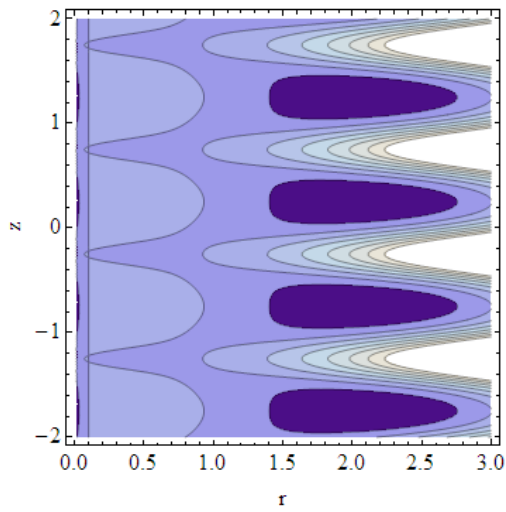

(c)

$Figs.4.22(a, b, c)$, Streamlines for Gold nanoparticle with shape factor of cylinders for distinct values of (**a**) $G_r = 2$, (**b**) $G_r = 3$, (**c**) $G_r = 4$.
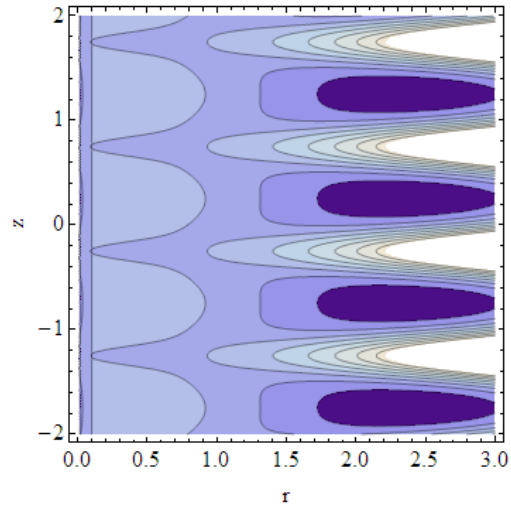
(a)
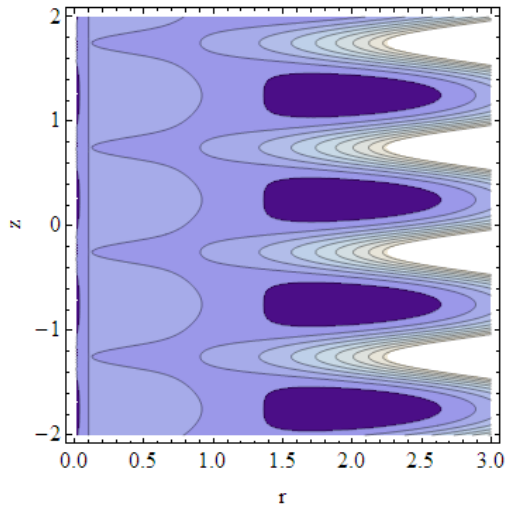
(b)
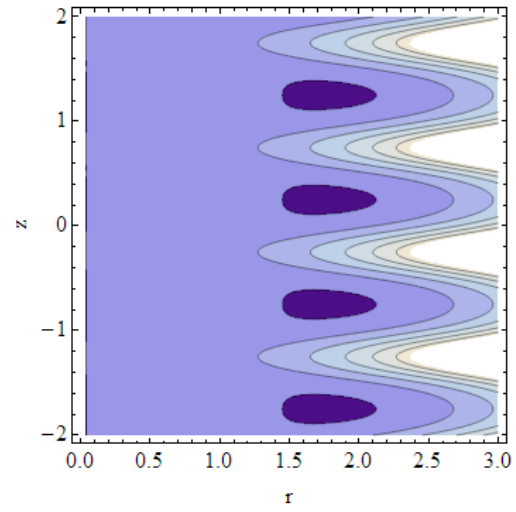
(c)

$Figs.4.23(a, b, c)$, Streamlines for Gold nanoparticle with shape factor of platelets for distinct values of (**a**) $G_r = 2$, (**b**) $G_r = 3$, (**c**) $G_r = 4$.
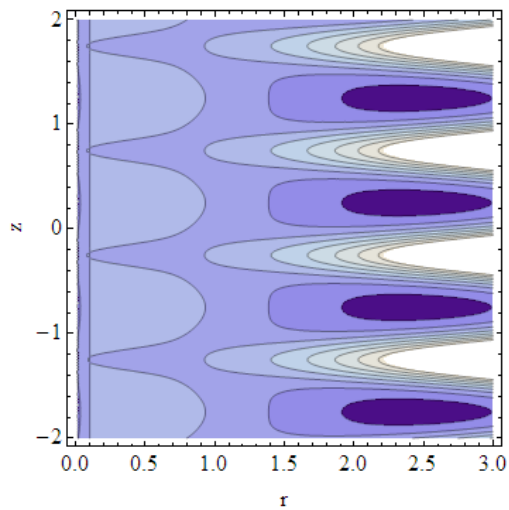
(a)
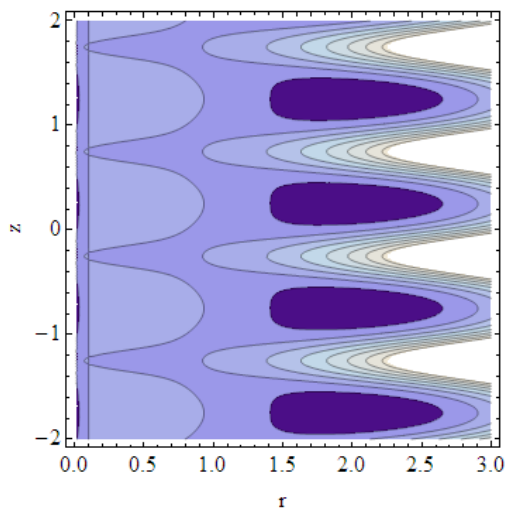
(b)
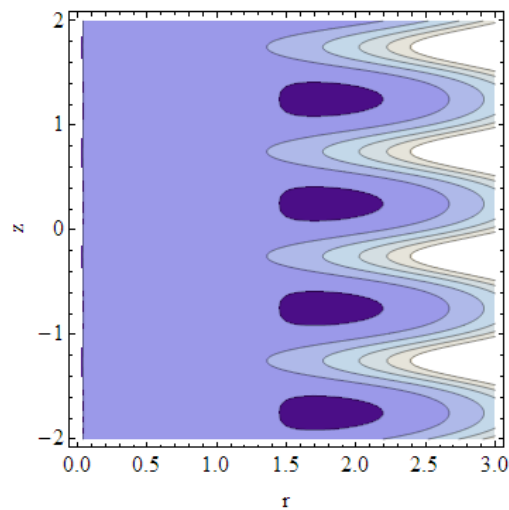
(b)

$Figs.4.24(a, b, c)$, Streamlines for Gold nanoparticle with shape factor of bricks for distinct values of (**a**) $\gamma = 0.1$, (**b**) $\gamma = 0.5$, (**c**) $\gamma = 0.9$.
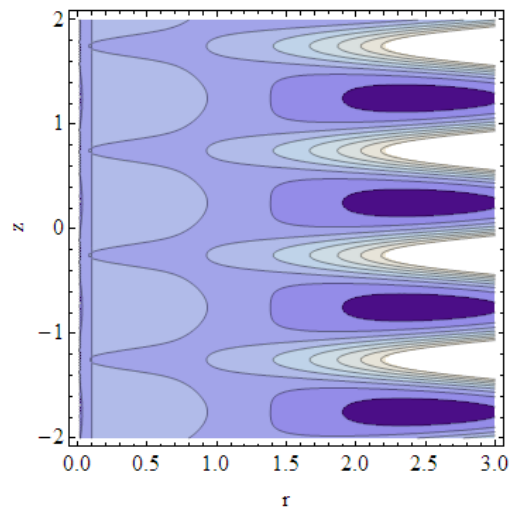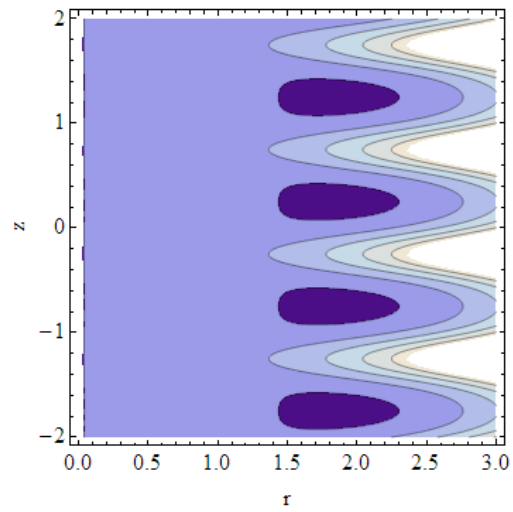
(a)
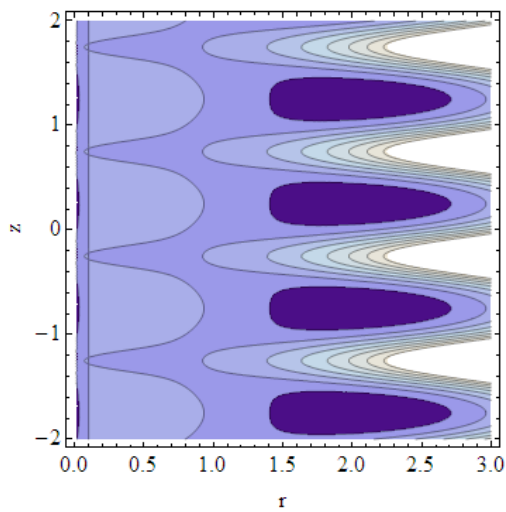
(b)
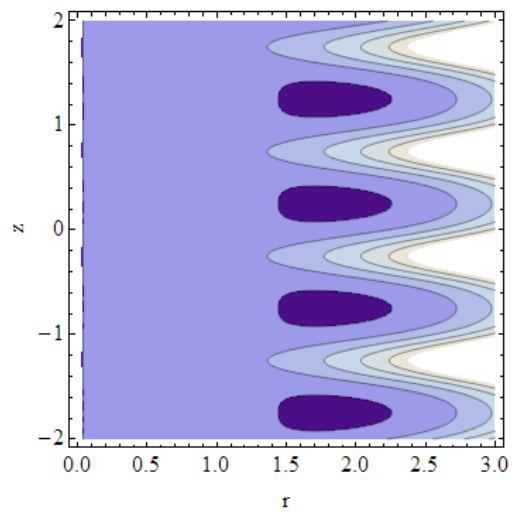
(c)

$Figs.4.25(a, b, c)$, Streamlines for Gold nanoparticle with shape factor of cylinders for distinct values of (**a**) $\gamma = 0.1$, (**b**) $\gamma = 0.5$, (**c**) $\gamma = 0.9$.
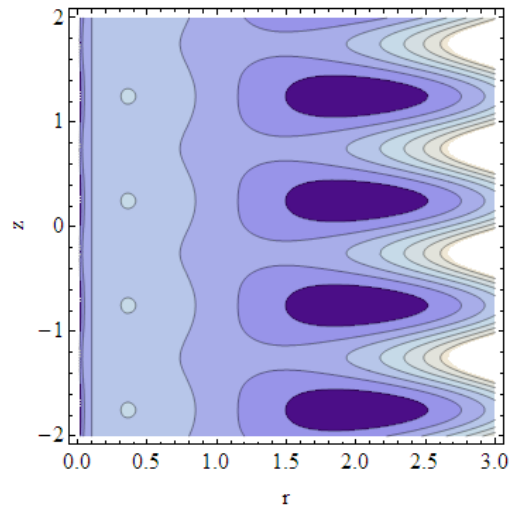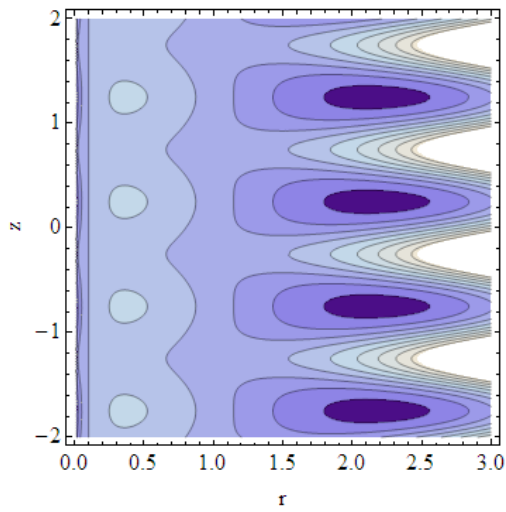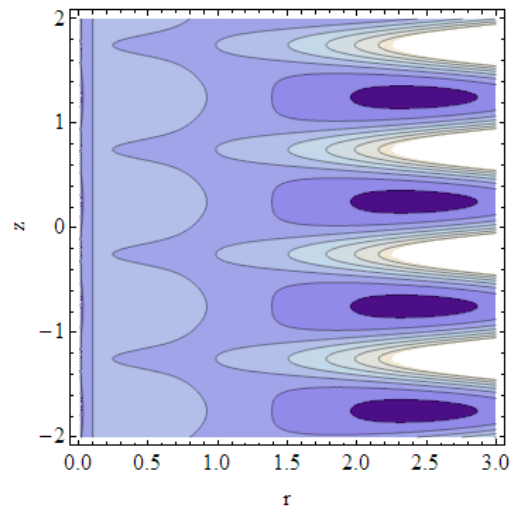
(a)

(b)

(c)

$Figs.$ $4.26(a, b, c)$, Streamlines for Gold nanoparticle with shape factor of platelets for distinct values of (**a**) $\gamma = 0.1$, (**b**) $\gamma = 0.5$, (**c**) $\gamma = 0.9$.
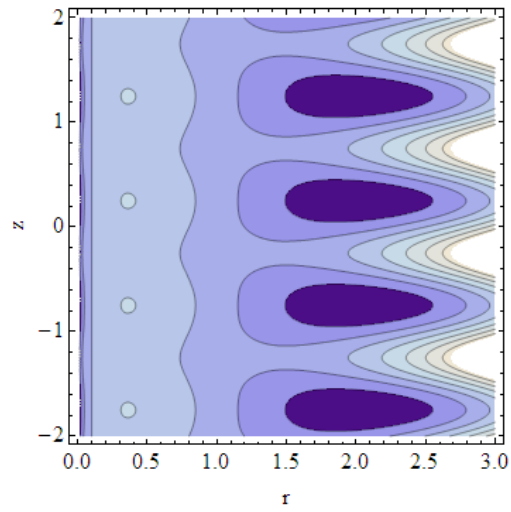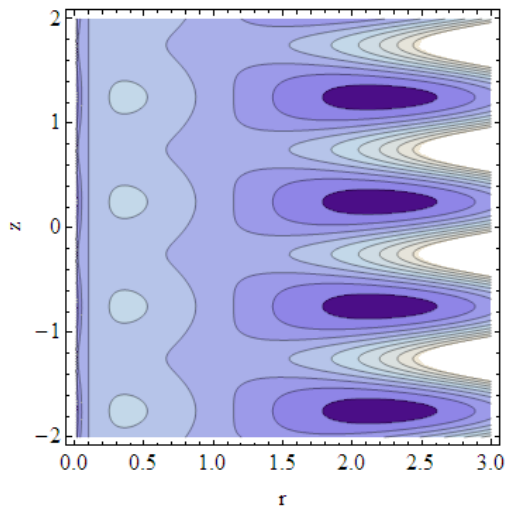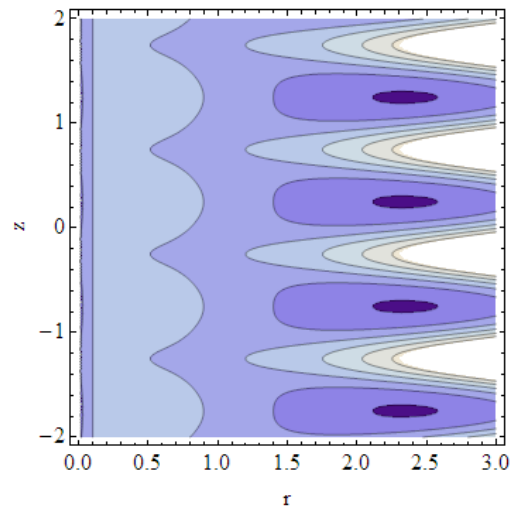
Figs. 4.27(*a, b, c*), Streamlines for Gold nanoparticle with shape factor of bricks for distinct values of (**a**) $\phi = 0.03$, (**b**) $\phi = 0.05$, (**c**) $\phi = 0.07$.

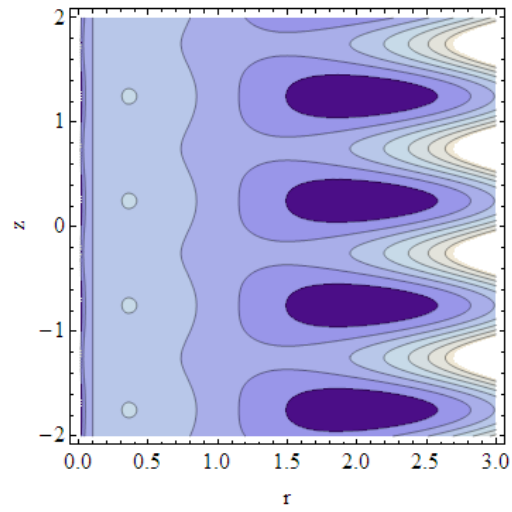(a)

(b)

(c)

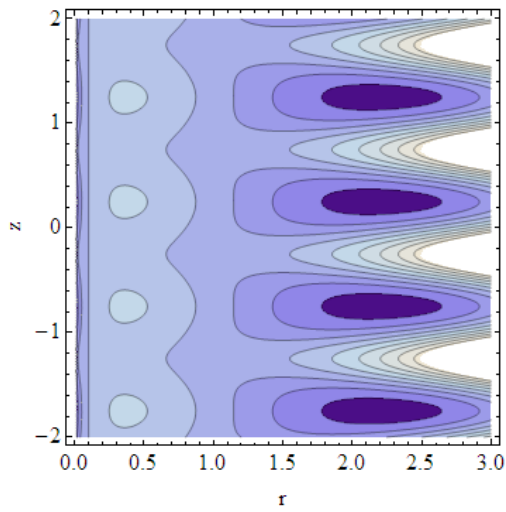$Figs.$ 4.28(a, b, c), Streamlines for Gold nanoparticle with shape factor of cylinders for distinct values of (**a**) $\phi = 0.03$, (**b**) $\phi = 0.05$, (**c**) $\phi = 0.07$.

(a)

(b)

(c)

Figs. 4.29(a, b, c), Streamlines for Gold nanoparticle with shape factor of platelets for distinct values of (**a**) $\phi = 0.03$, (**b**) $\phi = 0.05$, (**c**) $\phi = 0.07$.

(a)

(b)

(c)

$Figs.$ 4.30(a, b, c), Streamlines for Gold nanoparticle with shape factor of bricks for distinct values of (**a**) $d = 0.008$, (**b**) $d = 0.009$, (**c**) $d = 0.01$.

113

(a)

(b)

(c)

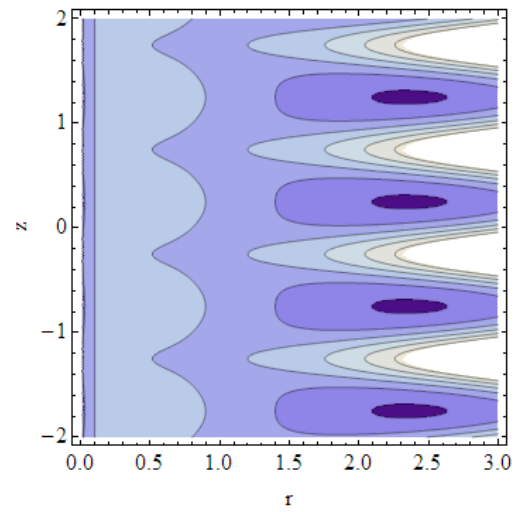$Figs.$ $4.31(a, b, c)$, Streamlines for Gold nanoparticle with shape factor of cylinders for distinct values of (**a**) $d = 0.008$, (**b**) $d = 0.009$, (**c**) $d = 0.01$.
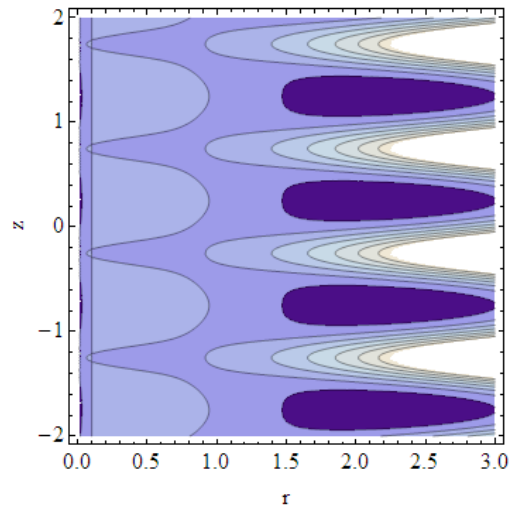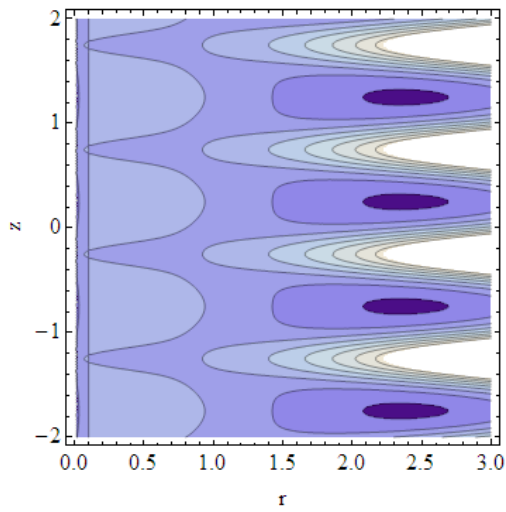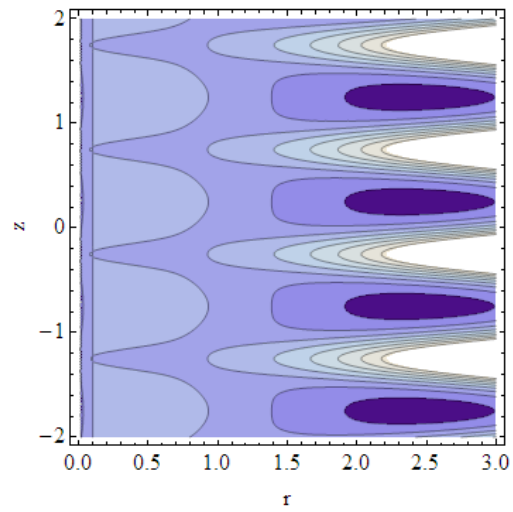
$Figs.$ 4.32(a, b, c), Streamlines for Gold nanoparticle with shape factor of platelets for distinct values of (**a**) $d = 0.008$, (**b**) $d = 0.009$, (**c**) $d = 0.01$.

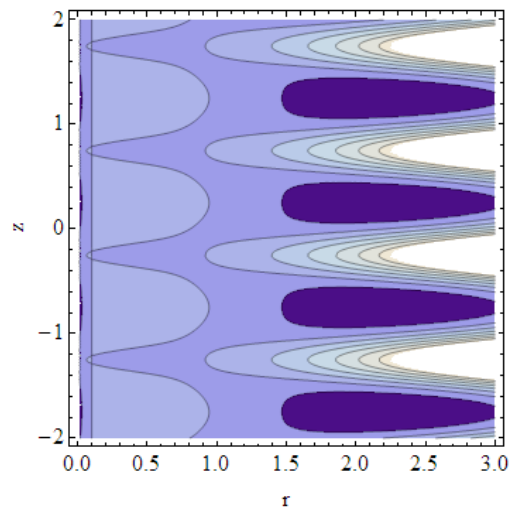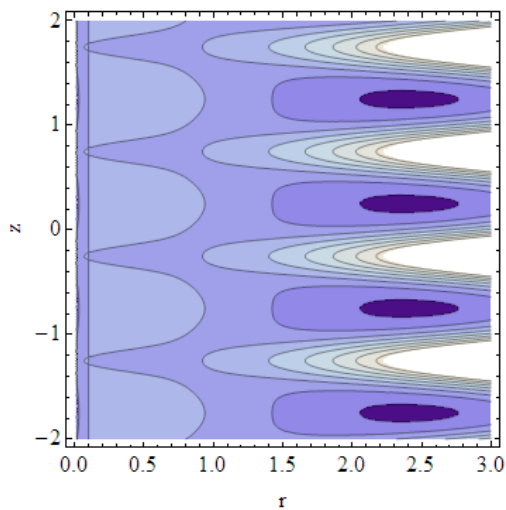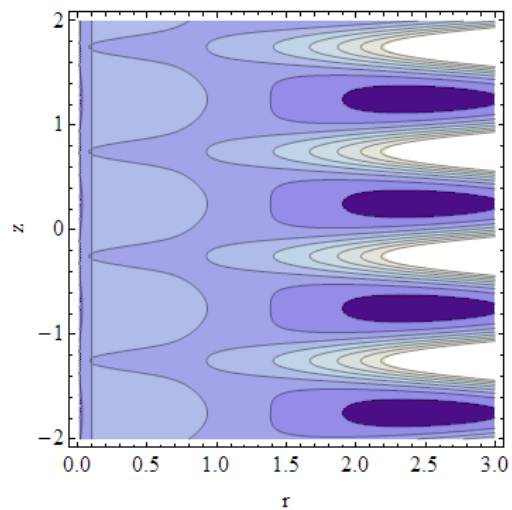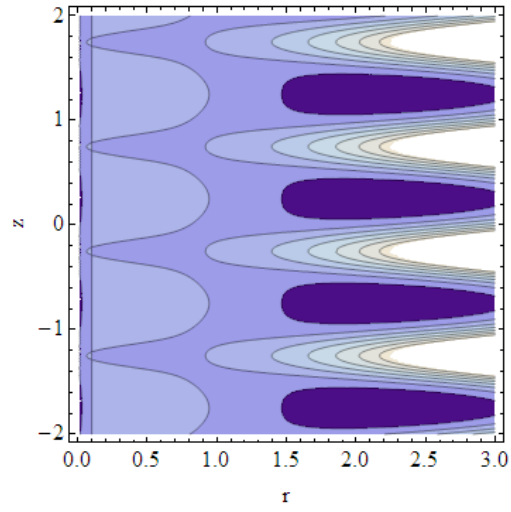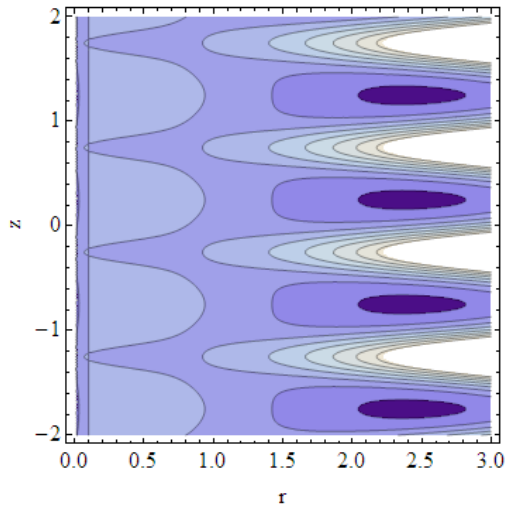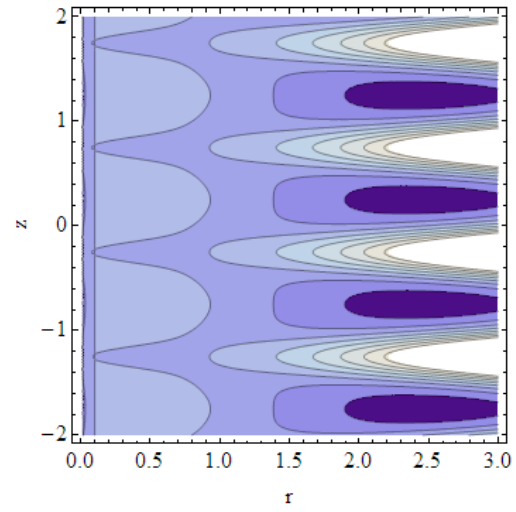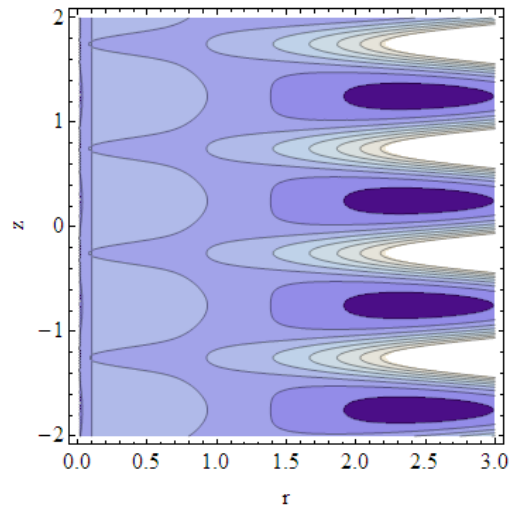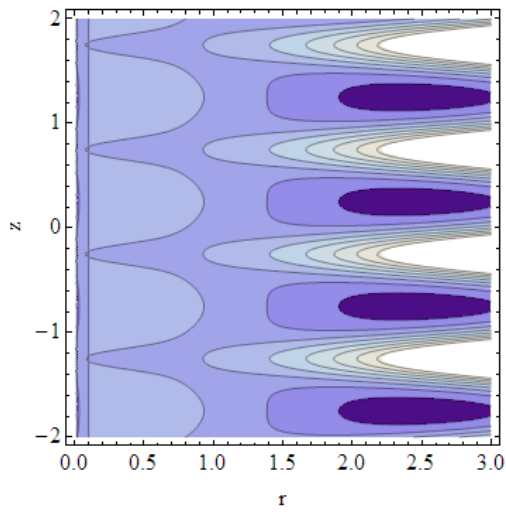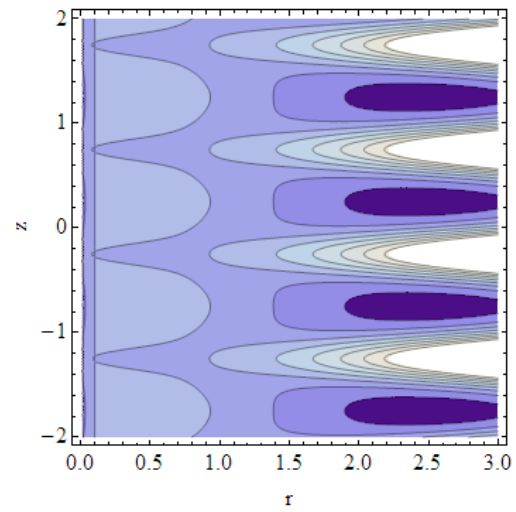$Figs.$ $4.33(a, b, c)$, Streamlines for Gold nanoparticle with shape factor of (**a**) Bricks $(m = 3.7)$, (**b**) Cylinders $(m = 4.9)$, (**c**) Platelets $(m = 5.7)$.

"r"	"Bricks"	"Cylinders"	"Platelets"
	m=3.7	m=4.9	m=5.7
r_1=0.1	1.000000	1.000000	1.000000
0.2	0.728822	0.726736	0.72535
0.3	0.567964	0.564896	0.562856
0.4	0.451209	0.447691	0.445353
0.5	0.357893	0.354280	0.351878
0.6	0.278823	0.275388	0.273105
0.7	0.209097	0.206070	0.204058
0.8	0.145791	0.143375	0.141769
0.9	0.087193	0.0854003	0.0843241
"h"=1	0.03149	0.0308495	0.0304187

Table. 4.1, Variation of temperature profile for different shape factor m with curvature $\zeta = 0.1$.

"r"	"Bricks"	"Cylinders"	"Platelets"
	m=3.7	m=4.9	m=5.7
r_1=0.1	1.000000	1.000000	1.000000
0.2	0.71079	0.708674	0.707268
0.3	0.542328	0.539252	0.537206
0.4	0.422296	0.418808	0.416489
0.5	0.328471	0.324928	0.322572
0.6	0.251008	0.247677	0.245462
0.7	0.184667	0.181764	0.179834
0.8	0.1263260	0.124036	0.122513
0.9	0.0739822	0.0724649	0.0714563
"h"=1	0.0262754	0.256751	0.0252761

Table. 4.2, Variation of temperature profile for different shape factor m with curvature $\zeta = 0.5$.

4.4 Conclusions

A detailed mathematical analysis has been done for impact of Ag nanoparticles on the peristaltic flow through a curved tube with an endoscope inserted in it. Some observations of the present study made on the basis of graphical results are highlighted below

- Temperature profile of the nanofluid decreases with the increase in shape factor m of nanoparticles.

- With an increment in curvature parameter, temperature of nanofluid recedes.

- Pressure gradient exhibits higher results with larger Darcy's number.

- Axial velocity elevates as we move from endoscope to the center of annular region.

- For greater Grashoff's number G_r and Darcy's number d, axial velocity is larger.

- The inner bolus grows larger with increasing Darcy's number.

- The trapping phenomena reveals that the size of inner bolus appears larger for Platelet nanoparticles as compared to Brick and Cylinder nanoparticles.

4.5 Appendix

$$C_1 = -\frac{4 + \gamma\frac{K_f}{K_{nf}}r_1^2 - \gamma\frac{K_f}{K_{nf}}r_2^2}{4\left(\ln r_1 - \ln r_2\right)}, C_2 = -\left(\frac{4\ln r_2 + \gamma\frac{K_f}{K_{nf}}r_1^2\ln r_2 - \gamma\frac{K_f}{K_{nf}}r_2^2\ln r_1}{4\left(\ln r_1 - \ln r_2\right)}\right),$$

$$C_3 = \frac{1}{16(r_1^2 - r_2^2)}(-4C_1r_1^2 + 8C_1r_1^2\ln r_1 - \gamma\frac{K_f}{K_{nf}}r_1^4 + 4C_1r_2^2 - +8C_1r_2^2\ln r_2 - \gamma\frac{K_f}{K_{nf}}r_2^4),$$

$$C_4 = -\frac{r_2^2}{16(r_1^2 - r_2^2)}(8C_1r_1^2\ln r_1 - 8C_1r_1^2\ln r_2 - \gamma\frac{K_f}{K_{nf}}r_1^4 + \gamma\frac{K_f}{K_{nf}}r_1^2r_2^2),$$

$$C_5 = \frac{1}{a_6}(a_4 + \frac{1}{\frac{\zeta\cos\theta}{1+\zeta r\cos\theta}}(\frac{\alpha}{\sqrt[2]{d}}a_4 - a_5)), C_6 = -1 - a_3 - \frac{\ln r_1}{a_6}(a_4 + \frac{1}{\frac{\zeta\cos\theta}{1+\zeta r\cos\theta}}(\frac{\alpha}{\sqrt[2]{d}}a_4 - a_5)),$$

$$C_7 = \frac{a_{11}}{a_{12}}, C_8 = -r_1(a_7 + r_1\frac{a_{11}}{a_{12}}), b_1 = -S(\frac{C_2r_2}{2} - \frac{Br_2^3}{16} + C_1(-\frac{r_2}{4} + \frac{r_2\ln r_2}{2})), b_2 = -S(\frac{C_2r_1^2}{4}$$

$$-\frac{Br_2^4}{64} + \frac{C_1}{2}(-\frac{r_2^2}{2} + \frac{r_2^2\ln r_2}{2})), b_3 = -S(\frac{C_2r_1^2}{4} - \frac{Br_1^4}{64} + \frac{C_1}{2}(-\frac{r_1^2}{2} + \frac{r_1^2\ln r_1}{2})),$$

$$b_7 = S(-\frac{Br_1^4}{32} + C_1(-\frac{r_1^2}{4} + \frac{r_1^2\ln r_1}{2}) + \frac{C_2r_1^2}{4} - \frac{C_3r_1^2}{2} - C_4\ln r_1),$$

$$b_8 = S(-\frac{Br_1^6}{48} + C_1(-\frac{3r_1^4}{16} + \frac{r_1^4\ln r_1}{4}) + \frac{C_2r_1^4}{8} - \frac{C_3r_1^4}{4} - \frac{C_4}{2}r_1^2),$$

$$b_9 = S(-\frac{Br_2^4}{32} + C_1(-\frac{r_2^2}{4} + \frac{r_2^2\ln r_2}{2}) + \frac{C_2r_2^2}{4} - \frac{C_3r_2^2}{2} - C_4\ln r_2), \ b_{10} = S(-\frac{Br_2^6}{48}$$

$$+C_1(-\frac{3r_2^4}{16}+\frac{r_2^4\ln r_2}{4})+\frac{C_2 r_2^4}{8}-\frac{C_3 r_2^4}{4}-\frac{C_4}{2}r_2^2),\ b_{11}=S(-\frac{5Br_2^4}{32}+\frac{C_1}{2}\left(-r_2^2+3r_2^2\ln r_2\right)$$

$$-\frac{3C_1 r_2^2}{4}+\frac{3C_2 r_2^2}{4}-\frac{3C_3 r_2^2}{2}-C_4(\ln r_2+1),\ b_{12}=S(-\frac{5Br_2^4}{48}+\frac{C_1}{4}\left(r_2^2+3r_2^2\ln r_2\right)$$

$$-\frac{9C_1 r_2^2}{16}+\frac{3C_2 r_2^2}{8}-\frac{3C_3 r_2^2}{4}-\frac{C_4}{2}),\ b_{13}=1+\zeta r_2\cos\theta,\ b_{14}=\frac{\zeta\cos\theta}{1+\zeta r_2\cos\theta},$$

$$a_1=b_1+\frac{Lr_2}{2A},\ a_2=b_2+\frac{Lr_2^2}{4A},\ a_3=b_3+\frac{Lr_1^2}{4A}, a_4=a_2-a_3,\ a_5=a_1-1-\frac{AdL}{b_{13}},$$

$$a_6=(\ln r_1-\ln r_2)(1+\frac{\zeta r_2\cos\theta\alpha}{\zeta\cos\theta\sqrt[2]{d}})+\frac{1+\zeta r_2\cos\theta}{\zeta r_2\cos\theta},\ a_7=\frac{r_1}{2}(-\frac{3Lr_1^2}{4A}+b_7-C_5\ln r_1)$$

$$-\frac{1}{2r_1}(-\frac{3Lr_1^4}{8A}+b_8-\frac{C_5 r_1^2}{2}),\ a_8=\frac{r_2}{2}(-\frac{3Lr_2^2}{4A}+b_9-C_5\ln r_2)-\frac{1}{2r_2}(-\frac{3Lr_2^4}{8A}+b_{10}-\frac{C_5 r_2^2}{2}),$$

$$a_9=\frac{1}{2}(-\frac{9Lr_2^2}{4A}+b_{11}-\frac{C_5}{r_2})-\frac{1}{2}(-\frac{9Lr_2^4}{4A}+b_{12}-\frac{C_5}{2}),\ a_{10}=-1-\frac{AdL}{b_{13}},\ a_{11}=-a_8+\frac{r_1}{r_2}a_7$$

$$\frac{\sqrt[2]{d}}{\alpha}(-r_1a_7\ln r_2+a_9-b_{14}a_8+\frac{b_{14}a_7}{r_2}-b_{14}+a_{10}),\ a_{12}=r_2-\frac{r_1^2}{r_2}-\frac{\sqrt[2]{d}}{\alpha}+r_1^2\ln r_2\frac{\sqrt[2]{d}}{\alpha}$$

$$+\frac{\sqrt[2]{d}}{\alpha}\frac{r_2\zeta\cos\theta}{1+\zeta r_2\cos\theta}-\frac{\sqrt[2]{d}}{\alpha}\frac{r_1^2\zeta\cos\theta}{r_2\left(1+\zeta r_2\cos\theta\right)}.$$

Chapter 5

Physiological study of nanofluid flow for Hamilton and Crosser model with variable viscosity

Nanofluids are classified as a class of fluids that enhance the thermal conductivity and serve as a modern drug delivery technique. The main objective of this chapter is to present the effects of variable viscosity on peristaltic flow of Au-nanoparticles. The geometry under consideration is a curved tube with an endoscope inserted into it. The constructed mathematical differential system is solved by perturbation method. The comparison between curvature and non-curvature tube over velocity, pressure gradient and pressure rise are visualized through graphs. For better comprehension of flow and heat characteristics, streamlines for flow and contour map for temperature are plotted. We perceive from the present analysis that non-curvature tube exhibits larger velocity, pressure gradient and pressure rise in the presence of nanoparticles.

5.1   Mathematical formulation

We are interested to examine the peristaltic transport of incompressible, laminar and viscous nanofluid in the region between two curved annular tubes. A sinusoidal type wave with speed c travels down the outer wall of tube with wave amplitude b and wavelength λ. Inner tube is considered to be rigid and have constant temperature T_o while outer tube maintains temperature

T_1. The mathematical formulation model for curved tube is, an inflexible circular tube of radius a_2 wrapped as a circle having radius k and endoscope in the form of coaxial tube of radius a_1. Due to the curviness of tube, curvature parameter is also taken into account. Gold nanoparticles with shape factor of spheres are considered along with blood.

Mathematically, two wall surfaces can be written as

$$\bar{R}_1 = a_1,$$
$$\bar{R}_2 = a_2 + b\sin\left[\frac{2\pi}{\lambda}(Z - ct)\right].$$

(5.1)

For incompressible fluid, continuity equation is given as

$$\frac{\partial \bar{U}}{\partial \bar{R}} + \frac{\bar{U}}{\bar{R}} + \frac{1}{\bar{R}}\frac{\partial \bar{V}}{\partial \bar{\theta}} + \frac{\bar{U}\cos\bar{\theta} - \bar{V}\sin\bar{\theta}}{k + \bar{R}\cos\bar{\theta}} + \frac{k}{k + \bar{R}\cos\bar{\theta}}\frac{\partial \bar{W}}{\partial \bar{Z}} = 0.$$

(5.2)

The components of momentum equation for variable viscosity using toroidal coordinate are given as

$$\rho_{nf}\left(\frac{\partial \bar{U}}{\partial \bar{t}} + \bar{U}\frac{\partial \bar{U}}{\partial \bar{R}} + \frac{\bar{V}}{\bar{R}}\frac{\partial \bar{U}}{\partial \bar{\theta}} + \frac{k\bar{W}}{k + \bar{R}\cos\bar{\theta}}\frac{\partial \bar{U}}{\partial \bar{Z}} - \frac{\bar{V}^2}{\bar{R}} - \frac{\bar{W}^2\cos\bar{\theta}}{k + \bar{R}\cos\bar{\theta}}\right)$$
$$= \frac{k}{\bar{R}(k + \bar{R}\cos\bar{\theta})}\left(\frac{\partial}{\partial \bar{Z}}\left(\mu_{nf}(\bar{R})\bar{R}\left(\frac{k}{k + \bar{R}\cos\bar{\theta}}\frac{\partial \bar{U}}{\partial \bar{Z}} + (k + \bar{R}\cos\bar{\theta})\frac{\partial}{\partial \bar{R}}\left(\frac{\bar{W}}{k + \bar{R}\cos\bar{\theta}}\right)\right)\right)$$
$$+ \frac{\partial}{\partial \bar{R}}\left(2\mu_{nf}(\bar{R})\bar{R}\left(\frac{k + \bar{R}\cos\bar{\theta}}{k}\right)\frac{\partial \bar{U}}{\partial \bar{Z}}\right) + \left(\frac{\partial}{\partial \bar{\theta}}\mu_{nf}(\bar{R})\left(\frac{k + \bar{R}\cos\bar{\theta}}{k}\right)\right)$$
$$\left(\frac{\partial \bar{V}}{\partial \bar{R}} - \frac{\bar{V}}{\bar{R}} + \frac{1}{\bar{R}}\frac{\partial \bar{U}}{\partial \bar{\theta}}\right)\right) + \frac{2\mu_{nf}(\bar{R})}{\bar{R}}\left(\frac{1}{\bar{R}}\frac{\partial \bar{V}}{\partial \bar{\theta}} + \frac{\bar{U}}{\bar{R}}\right) - \frac{2\mu_{nf}(\bar{R})\cos\bar{\theta}}{k + \bar{R}\cos\bar{\theta}}\left(\frac{k}{k + \bar{R}\cos\bar{\theta}}\frac{\partial \bar{W}}{\partial \bar{Z}}\right)$$
$$+ \frac{\bar{U}\cos\bar{\theta} - \bar{V}\sin\bar{\theta}}{k + \bar{R}\cos\bar{\theta}}\right) - \frac{\partial \bar{P}}{\partial \bar{R}},$$

(5.3)

$$\rho_{nf}\left(\frac{\partial\bar{V}}{\partial\bar{t}}+\bar{U}\frac{\partial\bar{V}}{\partial\bar{R}}+\frac{\bar{V}}{\bar{R}}\frac{\partial\bar{V}}{\partial\bar{\theta}}+\frac{k\bar{W}}{k+\bar{R}\cos\bar{\theta}}\frac{\partial\bar{V}}{\partial\bar{Z}}+\frac{\bar{U}\bar{V}}{\bar{R}}+\frac{\bar{W}^2\cos\bar{\theta}}{k+\bar{R}\cos\bar{\theta}}\right)$$

$$=\frac{k}{\bar{R}(k+\bar{R}\cos\bar{\theta})}\left(\frac{\partial}{\partial\bar{Z}}\left(\mu_{nf}(\bar{R})\bar{R}\left((k+\bar{R}\cos\bar{\theta})\frac{\partial}{\partial\bar{\theta}}\left(\frac{\bar{W}}{k+\bar{R}\cos\bar{\theta}}\right)+\frac{k}{k+\bar{R}\cos\bar{\theta}}\frac{\partial\bar{V}}{\partial\bar{Z}}\right)\right)$$

$$+\frac{\partial}{\partial\bar{R}}\left(\mu_{nf}(\bar{R})\bar{R}\left(\frac{k+\bar{R}\cos\bar{\theta}}{k}\right)\left(\frac{1}{\bar{R}}\frac{\partial\bar{U}}{\partial\bar{\theta}}+\frac{\partial\bar{V}}{\partial\bar{R}}-\frac{\bar{V}}{\bar{R}}\right)\right)+\frac{\partial}{\partial\bar{\theta}}\left(2\mu_{nf}(\bar{R})\left(\frac{k+\bar{R}\cos\bar{\theta}}{k}\right)\right.$$

$$\left.\left(\frac{1}{\bar{R}}\frac{\partial\bar{V}}{\partial\bar{\theta}}+\frac{\bar{U}}{\bar{R}}\right)\right)\right)+\frac{\mu_{nf}(\bar{R})}{\bar{R}}\left(\frac{1}{\bar{R}}\frac{\partial\bar{U}}{\partial\bar{\theta}}+\frac{\partial\bar{V}}{\partial\bar{R}}-\frac{\bar{V}}{\bar{R}}\right)+\frac{2\mu_{nf}(\bar{R})\sin\bar{\theta}}{k+\bar{R}\cos\bar{\theta}}\left(\frac{k}{k+\bar{R}\cos\bar{\theta}}\frac{\partial\bar{W}}{\partial\bar{Z}}\right.$$

$$\left.+\frac{(\bar{U}\cos\bar{\theta}-\bar{V}\sin\bar{\theta})}{k+\bar{R}\cos\bar{\theta}}\right)-\frac{1}{\bar{R}}\frac{\partial\bar{P}}{\partial\bar{\theta}}, \tag{5.4}$$

$$\rho_{nf}\left(\frac{\partial\bar{W}}{\partial\bar{t}}+\bar{U}\frac{\partial\bar{W}}{\partial\bar{R}}+\frac{\bar{V}}{\bar{R}}\frac{\partial\bar{W}}{\partial\bar{\theta}}+\frac{k\bar{W}}{k+\bar{R}\cos\bar{\theta}}\frac{\partial\bar{W}}{\partial\bar{Z}}+\frac{\bar{W}\left(\bar{U}\cos\bar{\theta}-\bar{V}\sin\bar{\theta}\right)}{k+\bar{R}\cos\bar{\theta}}\right)$$

$$=\frac{k}{\bar{R}(k+\bar{R}\cos\bar{\theta})}\left(\frac{\partial}{\partial\bar{Z}}\left(2\mu_{nf}(\bar{R})\bar{R}\left(\frac{k}{k+\bar{R}\cos\bar{\theta}}\frac{\partial\bar{W}}{\partial\bar{Z}}+\frac{(\bar{U}\cos\bar{\theta}-\bar{V}\sin\bar{\theta})}{k+\bar{R}\cos\bar{\theta}}\right)\right)$$

$$+\frac{\partial}{\partial\bar{R}}\left(\mu_{nf}(\bar{R})\bar{R}\left(\frac{k+\bar{R}\cos\bar{\theta}}{k}\right)\left(\frac{k}{k+\bar{R}\cos\bar{\theta}}\frac{\partial\bar{U}}{\partial\bar{Z}}+(k+\bar{R}\cos\bar{\theta})\frac{\partial}{\partial\bar{R}}\left(\frac{\bar{W}}{k+\bar{R}\cos\bar{\theta}}\right)\right)\right)$$

$$+\frac{\partial}{\partial\bar{\theta}}\left(\mu_{nf}(\bar{R})\left(\frac{k+\bar{R}\cos\bar{\theta}}{k}\right)\left(\frac{k+\bar{R}\cos\bar{\theta}}{k}\frac{\partial}{\partial\bar{\theta}}\left(\frac{\bar{W}}{k+\bar{R}\cos\bar{\theta}}\right)+\frac{k}{k+\bar{R}\cos\bar{\theta}}\frac{\partial\bar{V}}{\partial\bar{Z}}\right)\right)\right)$$

$$+\mu_{nf}(\bar{R})\frac{\cos\bar{\theta}}{k+\bar{R}\cos\bar{\theta}}\left(\frac{k}{k+\bar{R}\cos\bar{\theta}}\frac{\partial\bar{U}}{\partial\bar{Z}}+\frac{k}{k+\bar{R}\cos\bar{\theta}}\frac{\partial}{\partial\bar{R}}\left(\frac{\bar{W}}{k+\bar{R}\cos\bar{\theta}}\right)\right)$$

$$-\mu_{nf}(\bar{R})\frac{\sin\bar{\theta}}{k+\bar{R}\cos\bar{\theta}}\left(\frac{k}{k+\bar{R}\cos\bar{\theta}}\frac{\partial\bar{V}}{\partial\bar{Z}}+\frac{k}{k+\bar{R}\cos\bar{\theta}}\frac{\partial}{\partial\bar{\theta}}\left(\frac{\bar{W}}{k+\bar{R}\cos\bar{\theta}}\right)\right)$$

$$+(\rho\beta)_{nf}g(T-T_1)-\frac{k}{k+\bar{R}\cos\bar{\theta}}\frac{\partial\bar{P}}{\partial\bar{Z}}. \tag{5.5}$$

Energy equation with heat generation for nanofluid is given as

$$(\rho c_p)_{nf}\left(\frac{\partial\bar{T}}{\partial\bar{t}}+\bar{U}\frac{\partial\bar{T}}{\partial\bar{R}}+\frac{k\bar{W}}{k+\bar{R}\cos\bar{\theta}}\frac{\partial\bar{T}}{\partial\bar{Z}}+\frac{\bar{U}}{\bar{R}}\frac{\partial\bar{T}}{\partial\bar{\theta}}\right)=K_{nf}\left(\frac{\partial^2\bar{T}}{\partial\bar{R}^2}+\frac{1}{\bar{R}}\frac{\partial\bar{T}}{\partial\bar{R}}+\frac{\cos\bar{\theta}}{k+\bar{R}\cos\bar{\theta}}\frac{\partial\bar{T}}{\partial\bar{R}}\right.$$

$$+\frac{1}{\bar{R}^2}\frac{\partial^2\bar{T}}{\partial\bar{\theta}^2}+\frac{k^2}{(k+\bar{R}\cos\bar{\theta})^2}\frac{\partial^2\bar{T}}{\partial\bar{Z}^2}$$

$$\left.-\frac{\sin\bar{\theta}}{k+\bar{R}\cos\bar{\theta}}\frac{\partial\bar{T}}{\partial\bar{\theta}}\right)+Q_0. \tag{5.6}$$

For the fixed frame, the boundary condition is given as

$$
\begin{aligned}
\bar{W} &= 0, \ \bar{T} = \bar{T}_0, \ \text{at} \quad \bar{R} = \bar{R}_1 = a_1, \\
\bar{W} &= 0, \ \bar{T} = \bar{T}_1, \ \text{at} \quad \bar{R} = \bar{R}_2 = a_2 + b \sin\left[\frac{2\pi}{\lambda}\left(\bar{Z} - ct\right)\right],
\end{aligned}
\tag{5.7}
$$

where $\bar{T}_1$ and $\bar{T}_0$ are representing the temperature of the outer and inner tube as suggested in [29]

For this present nanofluid model, μ_{nf} is the variable nanofluid viscosity and the variation of viscosity from Brinkman [33] and Srivastava et al. [34] is as follows

$$
\bar{\mu}_{nf} = \frac{\mu_f(\bar{R})}{(1-\varphi)^{2.5}},
\tag{5.8}
$$

where μ_f is the base fluid viscosity. Also viscosity of the base fluid is assorted according to the following relation

$$
\mu_f(\bar{R}) = \mu_o e^{-\alpha\bar{R}} = \frac{\mu_o}{1+\alpha\bar{R}}.
\tag{5.9}
$$

Here μ_o is the blood viscosity and α is representing variable viscosity parameter ($\alpha << 1$). From Eqs. (5.8), (5.9) the effective viscosity of the nanofluid is given as

$$
\bar{\mu}_{nf} = \frac{\mu_o}{(1-\varphi)^{2.5}\left(1+\alpha\bar{R}\right)},
\tag{5.10}
$$

It is evident from the equation discussed above that for $\alpha = 0$, Brinkman's viscosity model (i.e., the effective viscosity independent of $\bar{R}$) is going to be retrieved. Also for $\varphi = 0$, we can get fluid viscosity independent of the nanoparticles.

For this stated nanofluid model, specific heat, density and the nanofluid viscosity μ_{nf} are defined as

$$
\begin{aligned}
(\rho c_p)_{nf} &= \varphi(\rho c_p)_s + (\rho c_p)_f\left(1-\varphi\right), \ \alpha_{nf} = \frac{K_{nf}}{(\rho C_p)_{nf}}, \\
(\rho\beta)_{nf} &= \varphi(\rho\beta)_s + (1-\varphi)\left(\rho\beta\right)_f, \ \rho_{nf} = \varphi\rho_s + (1-\varphi)\rho_f.
\end{aligned}
\tag{5.11}
$$

123

Hamilton and Crosser [36] gave the most frequent utilized thermal conductivity equation (11) for the mixtures of micrometer size particles, it is believed that this equation can be used for the nanofluids.

$$\frac{K_{nf}}{K_f} = \frac{(n-1)k_f + k_s - (n-1)(k_f - k_s)\varphi}{k_s + (n-1)k_f + \varphi(k_f - k_s)}. \tag{5.12}$$

In the above stated equation, n is used to represent the shape factor and for spherical nanoparticles $n = 3$. This relation accurately speculates the thermal conductivity of nanofluids as shown by Zhang et al. [35].

As axial velocity is efficacious velocity component, so we assume the velocity of the form $(0, 0, \bar{W})$. Further we used following transformation to shift from fixed frame $(\bar{R}, \bar{Z}, \bar{t})$ to wave frame $(\bar{r}, \bar{z})$,

$$\bar{z} = \bar{Z} - c\bar{t}, \ \bar{r} = \bar{R}, \ \bar{w} = \bar{W} - c, \ \bar{u} = \bar{U}, \ \bar{p}(\bar{z}, \bar{r}) = \bar{P}(\bar{Z}, \bar{R}, \bar{t}), \tag{5.13}$$

here $\bar{u}$, $\bar{w}$ and $\bar{p}$ are velocity components and pressure in wave frame respectively.

Following are the dimensionless quantities

$$
\begin{aligned}
w &= \frac{\bar{w}}{c}, \ r = \frac{\bar{r}}{a_2}, \ u = \frac{\lambda \bar{u}}{a_2 c}, \ z = \frac{\bar{z}}{\lambda}, \ r_2 = \frac{\bar{r}_2}{a_2} = 1 + \varepsilon \sin(2\pi z), \\
\varepsilon &= \frac{b}{a_2}, \ t = \frac{c\bar{t}}{\lambda}, \ \tilde{\theta} = \frac{T - T_1}{T_0 - T_1}, \ \bar{\theta} = \theta, \ G_r = \frac{a_2^2(T_1 - T_0)\rho_f \beta_f g(1 - \varphi)^{2.5}}{c\mu_o}, \\
\zeta &= \frac{a_2}{k}, \ r_1 = \frac{\bar{r}_1}{a_2} = \epsilon, \ \gamma = \frac{a_2^2 Q_0}{(T_1 - T_0)k_f}, \ R_e = \frac{a_2 c\rho_f}{\mu_f}, \ \delta = \frac{a_2}{\lambda}, \\
p &= \frac{a_2^2 \bar{p}}{c\lambda \mu_f}, \ d = \frac{\kappa^*}{a_2^2}.
\end{aligned} \tag{5.14}
$$

After employing the approximations, Eqs. $(5.2) - (5.6)$ are written as

$$\frac{\partial p}{\partial r} = 0, \tag{5.15}$$

$$\frac{\partial p}{\partial \theta} = 0, \tag{5.16}$$

124

$$\frac{1}{1+\zeta r \cos\theta}\frac{\partial p}{\partial z} = \frac{(1-\varphi)^{2.5}}{\mu_o}\left(\frac{1}{r(1+\zeta r \cos\theta)}\left(\frac{\partial}{\partial r}\left(r(1-\alpha r)(1+\zeta r \cos\theta)^2\frac{\partial}{\partial r}\frac{(w+1)}{(1+\zeta r \cos\theta)}\right)+\right.$$
$$\frac{\partial}{\partial\theta}\left((1-\alpha r)\frac{(1+\zeta r \cos\theta)^2}{r}\frac{\partial}{\partial\theta}\frac{(w+1)}{(1+\zeta r \cos\theta)}\right)\right)+\frac{\mu_o\zeta\cos\theta}{(1-\varphi)^{2.5}}\frac{\partial}{\partial r}\left(\frac{w+1}{1+\zeta r \cos\theta}\right)$$
$$\left.-\frac{\mu_o}{(1-\varphi)^{2.5}}\frac{\zeta\sin\theta}{r}\frac{\partial}{\partial\theta}\left(\frac{w+1}{1+\zeta r \cos\theta}\right)+G_r\frac{(\rho\beta)_{nf}}{(\rho\beta)_f}\frac{\mu_o}{(1-\varphi)^{2.5}}\tilde{\theta}\right) \qquad (5.17)$$

$$\frac{\partial^2\tilde{\theta}}{\partial r^2}+\frac{1}{r}\frac{\partial\tilde{\theta}}{\partial r}+\frac{\zeta\cos\theta}{1+\zeta r \cos\theta}\frac{\partial\tilde{\theta}}{\partial r}+\frac{1}{r^2}\frac{\partial^2 w}{\partial\theta^2}+\gamma\frac{K_f}{K_{nf}}=0. \qquad (5.18)$$

In wave frame, the boundary conditions take the form

$$w=-1,\ \tilde{\theta}=1, \qquad \text{at} \quad r=r_1=\epsilon,$$

$$w=-1,\ \tilde{\theta}=0,\ \text{at} \quad r=r_2=1+\varepsilon\sin(2\pi z). \qquad (5.19)$$

The volume flow rate in the dimensionless form is given as

$$q=F+\frac{1}{2}-\frac{\epsilon^2}{2}+\frac{\varepsilon^2}{4}, \qquad (5.20)$$

$$F=\int_{r_1}^{r_2} rwdr. \qquad (5.21)$$

5.2   Solution of the problem

In order to get the expression for velocity and temperature according to the given boundary condition, we consider the following

$$\tilde{\theta}(r(z,t),\ \theta) = \tilde{\theta}_0(r)+\zeta\cos(\theta)\tilde{\theta}_1(r)+...$$
$$w(r(z,t),\ \theta) = w_0(r)+\zeta\cos(\theta)w_1(r)+... \qquad (5.22)$$

125

Using Eq. (5.21) into Eqs. (5.16) to (5.18) and equating like powers of $\zeta \cos(\theta)$, we obtain the written below systems

5.2.1 Zeroth order system

$$\frac{\partial^2 \tilde{\theta}_0}{\partial r^2} + \frac{1}{r}\frac{\partial \tilde{\theta}_0}{\partial r} + \gamma\frac{K_f}{K_{nf}} = 0, \tag{5.23}$$

$$(1 - \alpha r)\frac{\partial^2 w_0}{\partial r^2} + \left(\frac{1}{r} - 2\alpha\right)\frac{\partial w_0}{\partial r} + G_r\frac{(\rho\beta)_{nf}}{(\rho\beta)_f}\frac{\mu_o}{(1-\varphi)^{2.5}}\tilde{\theta}_0 = \frac{\mu_o}{(1-\varphi)^{2.5}}\frac{dp}{dz}, \tag{5.24}$$

$$\tilde{\theta}_0(r_1) = 1, \ w_0(r_1) = -1,$$

$$\tilde{\theta}_0(r_2) = 0, \ w_0(r_2) = -1. \tag{5.25}$$

5.2.2 First order system

$$\frac{\partial^2 \tilde{\theta}_1}{\partial r^2} + \frac{1}{r}\frac{\partial \tilde{\theta}_1}{\partial r} - \frac{\tilde{\theta}_1}{r^2} + r\gamma\frac{K_f}{K_{nf}} + r\frac{\partial^2 \tilde{\theta}_0}{\partial r^2} + 2\frac{\partial \tilde{\theta}_0}{\partial r} = 0 , \tag{5.26}$$

$$(1 - \alpha r)\frac{\partial^2 w_1}{\partial r^2} + \frac{(1-\alpha r)}{r}\frac{\partial w_1}{\partial r} - \frac{(1-\alpha r)}{r^2}w_1 + r(1-\alpha r)\frac{\partial^2 w_0}{\partial r^2}$$

$$+ 2(1-\alpha r)\frac{\partial w_0}{\partial r} + \alpha w_0 + G_r\frac{(\rho\beta)_{nf}}{(\rho\beta)_f}\frac{\mu_o}{(1-\varphi)^{2.5}}(r\tilde{\theta}_0 + \tilde{\theta}_1) = 0, \tag{5.27}$$

$$\tilde{\theta}_1(r_1) = 0, \ w_1(r_1) = 0,$$

$$\tilde{\theta}_1(r_2) = 0, \ w_1(r_2) = 0. \tag{5.28}$$

Solution of equation (5.23) and (5.26) is obtained as [37] and Eqs. (24, 27) are solved with the help of inbuilt program of Mathematica.

Pressure gradient is defined as

$$\frac{dp}{dz} = \frac{F - t_1}{t_2}, \tag{5.29}$$

where t_1 and t_2 can be easily calculated through Mathematica.

5.3   Results and discussion

Individual effects of Grashoff's number, heat source parameter, amplitude ratio and variable viscosity on the dimensionless velocity, pressure gradient and pressure rise are illustrated in Figs $5.1 - 5.12$. Furthermore, streamlines for these parameters are depicted in Figs $5.13 - 5.16$ and thermal graphs are also portrayed in Figs $5.17 - 5.18$.

The effects of Grashoff's number G_r on dimensionless velocity w are presented in Fig 5.1 for nanofluid. It is important to note that an increase in Grashoff's number represents an increase in nanofluid velocity. From Fig 5.2, we observed that as heat source/sink parameter γ increases, the velocity starts to become shallow. Physically, this is due to the increase in the temperature. Fig 5.3 depicts the effects of amplitude ratio on velocity profile. It is found that a higher amplitude ratio φ, results in higher velocity i.e. with large amplitude of propagated wave the resultant velocity is higher. Fig 5.4 is pictorial representation of effects of variable viscosity α for dimensionless velocity. As the values of this parameter increases, velocity in response ascends. Moreover, in the absence of curvature parameter that is for non-curvature tube, the dimensionless velocity profile is higher as compared to velocity of nanofluid in curvature tube. Thus one can conclude that , in the curved tube velocity is observed to be lower or the cravenness results in a decrease of velocity. Apart from the attitude of velocity curve all the parameters have identical behavior both in the presence and absence of curvature parameter.

Figs $5.5 - 5.8$ are sketched to illustrate the change in pressure gradient for parameters such as G_r, γ, φ and α. A sinusoidal curve is observed for pressure gradient and this is due to the fact that wave propagated along the walls is sinusoidal, thus the curve for pressure gradient behaves likewise. Fig 5.5 depicts the behavior of pressure gradient due to the variation of Grashoff's number G_r. It is observed that the growth of buoyancy forces results in increase of pressure gradient. For both the situations, curved and non-curved tube, similar trend is witnessed whereas curve amplitude of dp/dz for non-curvature tube is higher in comparison to amplitude of curved tube. Fig 5.6 is used for the graphical representation of heat source/sink parameter γ on pressure gradient. It is clear from the figure that with a rise in this parameter, a decrease in dp/dz is happening. Variational change in pressure gradient due to amplitude ratio φ are shown in Fig 5.7. Here as we elevate the values of this parameter, pressure gradient appears to have a increasing trend in the narrow part of tube while opposite behavior near

the wider part of tube is seen. Fig 5.8 is plotted to give the influence of variable viscosity on dp/dz. An increase in α give rise to the amplitude of pressure gradient. Non-curvature tube have higher pressure gradient than curvature tube.

To explain the pumping properties it is important to know pressure rise per wavelength. Thus Figs $5.9 - 5.12$ are plotted to give the pressure rise for varying different parameters such as Grashoff's number G_r, source parameter γ, amplitude ratio φ and variable viscosity α.With expansion in flow rate,a similar observation from these figures is that pressure rise per wavelength declines. Fig 5.9 is depicted to study the behavior of pressure rise for various values of G_r. Pressure rise elevates with a rise in G_r in the retrograde pumping region whereas it declines in the augmented region. Effects of heat source parameter are plotted in Fig 5.10. With the increase in this parameter, Δp drops for retrograde pumping region and rise in augmented pumping region. Fig 5.11 is giving the pictorial presentation of pressure rise for variation of amplitude ratio φ. Initially an increase in observed for growing values of φ but, in augmented pumping region opposite trend is seen. Variation of variable viscosity for Δp is plotted in Fig 5.12 and we witness elevating behavior in retrograde region and a decline is captured in augmented pumping region.

An engrossing phenomena of trapping for peristaltic flow with an endoscope is described in Figs $(5.13 - 5.16)$. Au nanoparticles are taken into consideration for this discussion. Pattern of flow in the region enclosed by catheter and curved tube is studied by plotting streamlines. Increase in number of enclosed bolus is observed for variation of G_r along with closed streamlines and is portrayed in Figs 5.13. From figure it is seen that the quantity of trapped bolus increases when G_r shifts from 1.5 to 1.75 and size is also observed to increase as G_r further changes from 1.75 to 2. Effects of γ over trapping phenomena is studied in Fig 5.14. It is witnessed that as γ changes from 0.1 to 0.5, magnitude of trapped bolus decreases and than increases as γ jumps to 0.9 from 0.5. Fig 5.15 is used to show the impact of φ over trapping phenomena. As φ is increased from 0.11 to 0.12, number of bolus increases and on further increasing φ from 0.12 to 0.13 same trend is witnessed. Variation of variable viscosity α is studied in Figs 5.16. Initially, number of trapped bolus increases for increasing α then their size also increases with similar trend of α.

Figs $(5.17 - 5.18)$ are responsible for the variation of temperature contour maps for different

128

parameters. In Figs 5.17, we see that as heat source parameter increases, initially the quantity of trapped bolus reduces and on additional increase of γ the size is also seen to recedes. For the variation of curvature,it is portrayed in Figs 5.18 that first the size of bolus increases and on additional increment of ζ number of trapped bolus elevates.
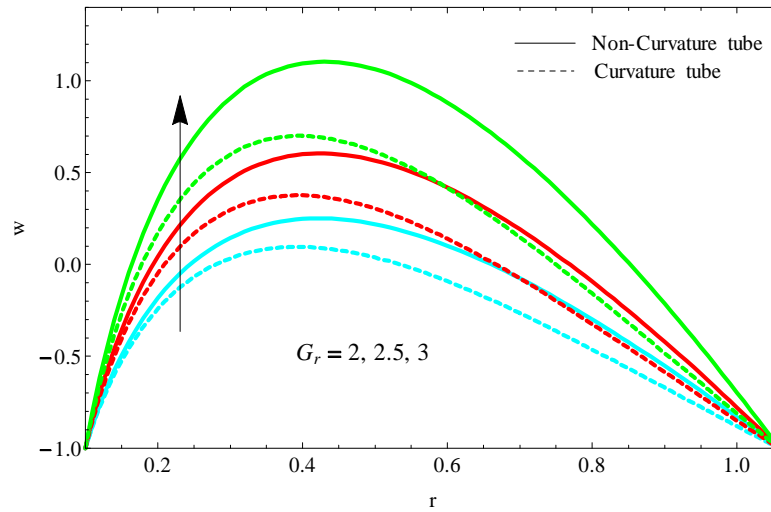

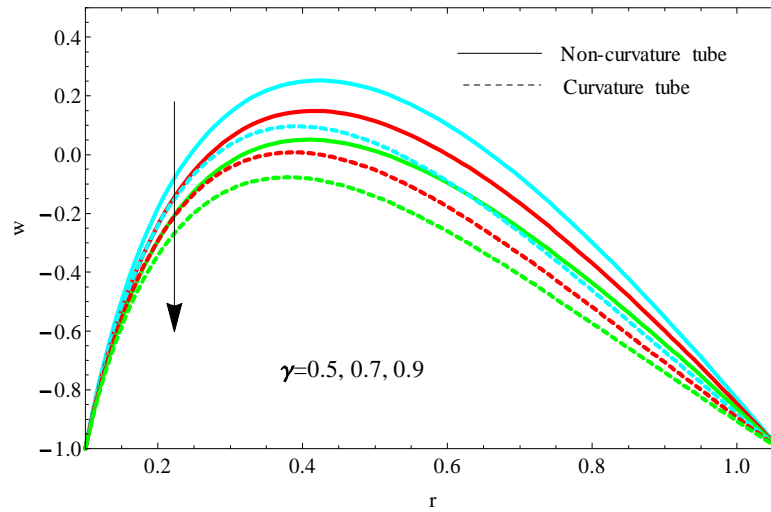$Fig.$ 5.1, Variation of velocity for distinct Grashroff number G_r.

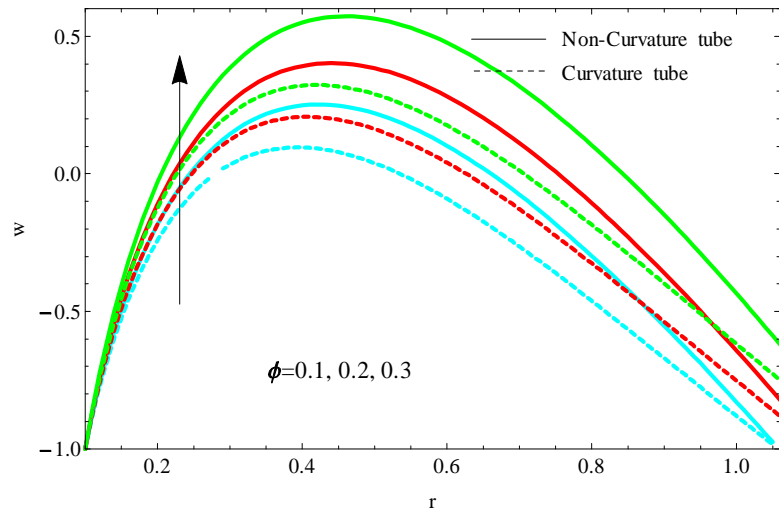$Fig.$ 5.2, Variation of velocity for distinct heat source(sink) parameter γ.

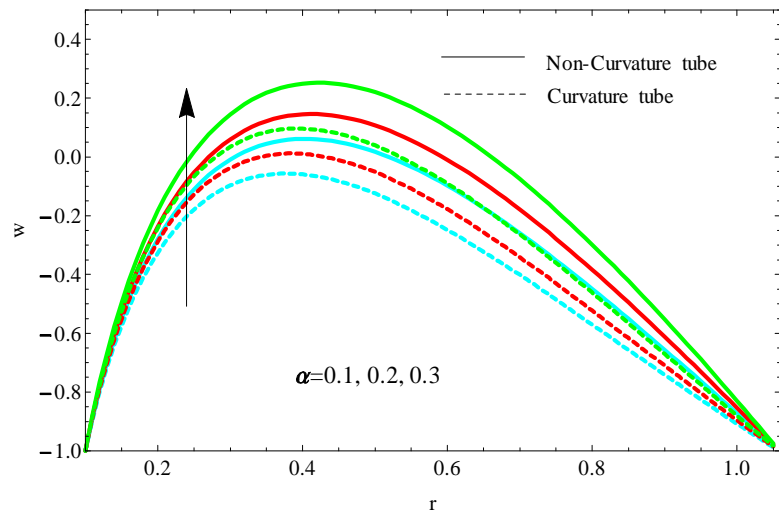*Fig.* 5.3, Variation of velocity for distinct amplitude ratio φ.

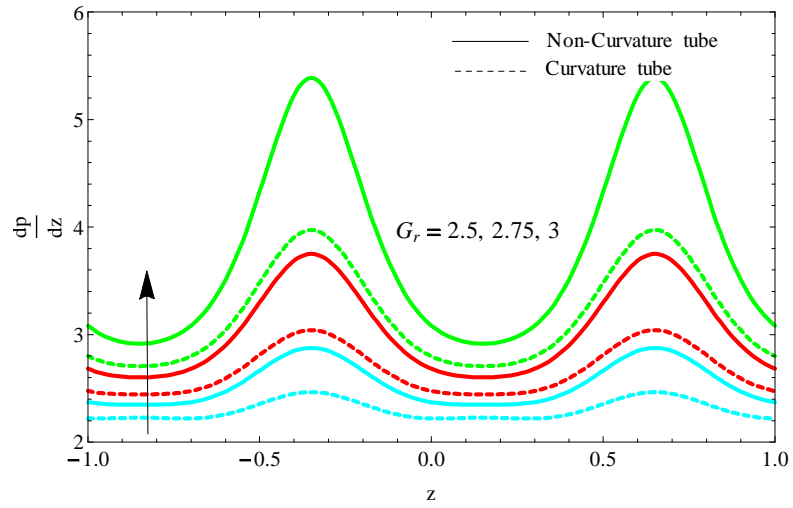*Fig.* 5.4, Variation of velocity for distinct variable viscosity α.

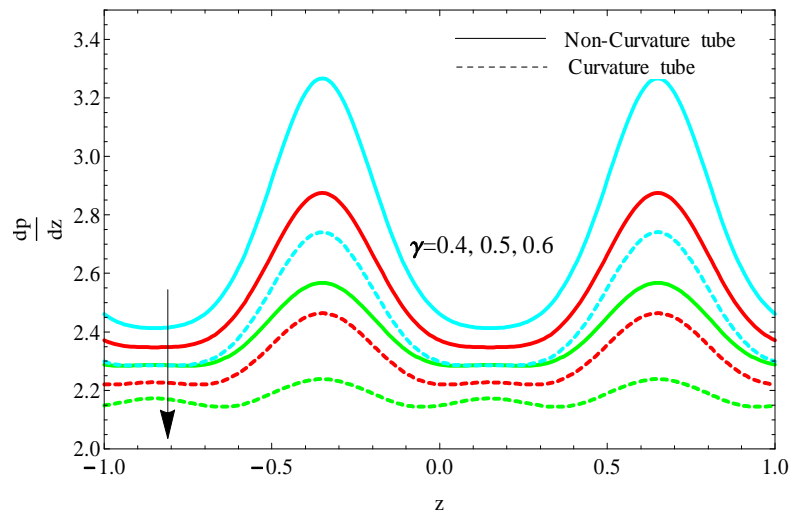$Fig.$ 5.5, Pressure gradient for variation of Grashroff number G_r.

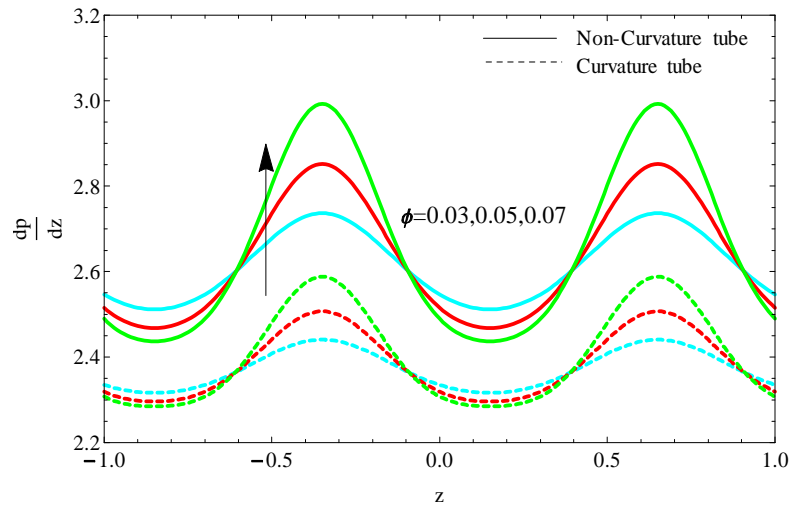$Fig.$ 5.6, Pressure gradient for variation of heat source(sink) parameter γ.

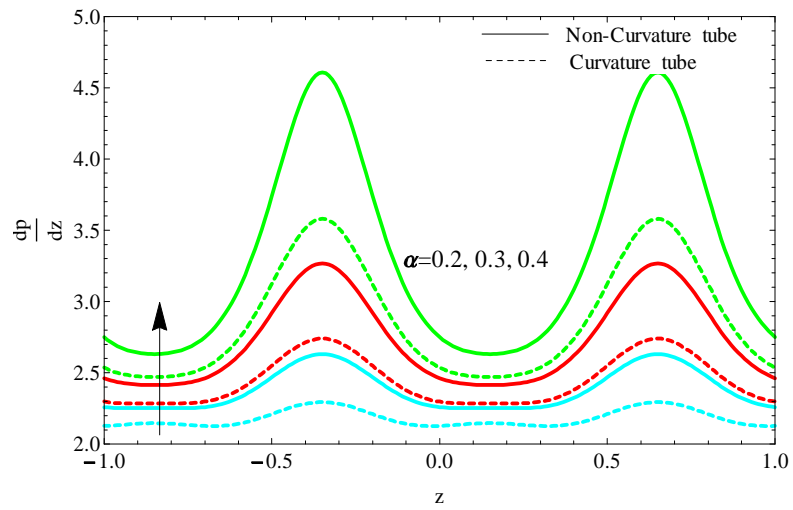*Fig.* 5.7, Pressure gradient for variation of amplitude ratio φ.

Fig. 5.8, Pressure gradient for variation of variable viscosity α.
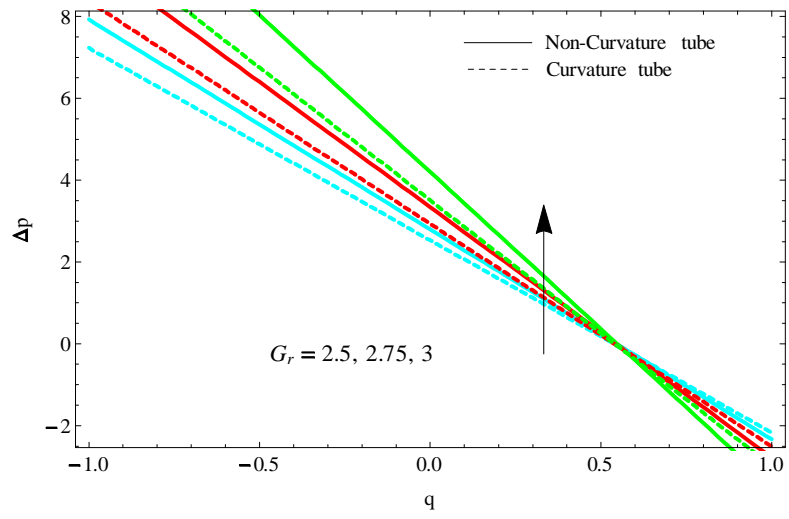
$Fig.$ 5.9, Pressure rise for different values of Grashroff number G_r.
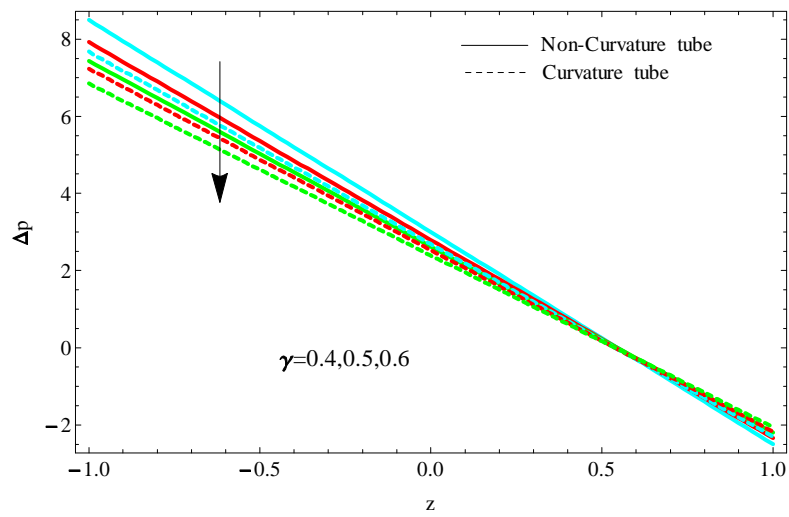
$Fig.$ 5.10, Pressure rise for different values of heat source (sink) parameter γ.
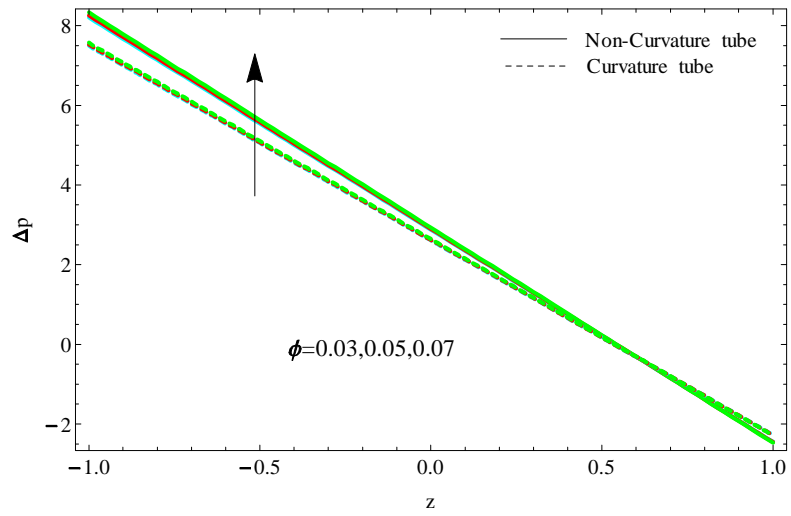
Fig. 5.11, Pressure rise for distinct values of amplitude ratio φ.
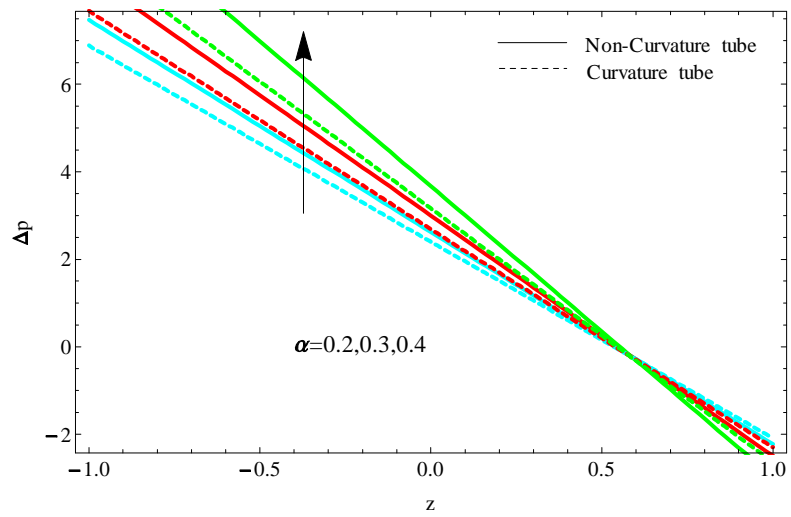
Fig. 5.12, Pressure rise for distinct values of variable viscosity α.
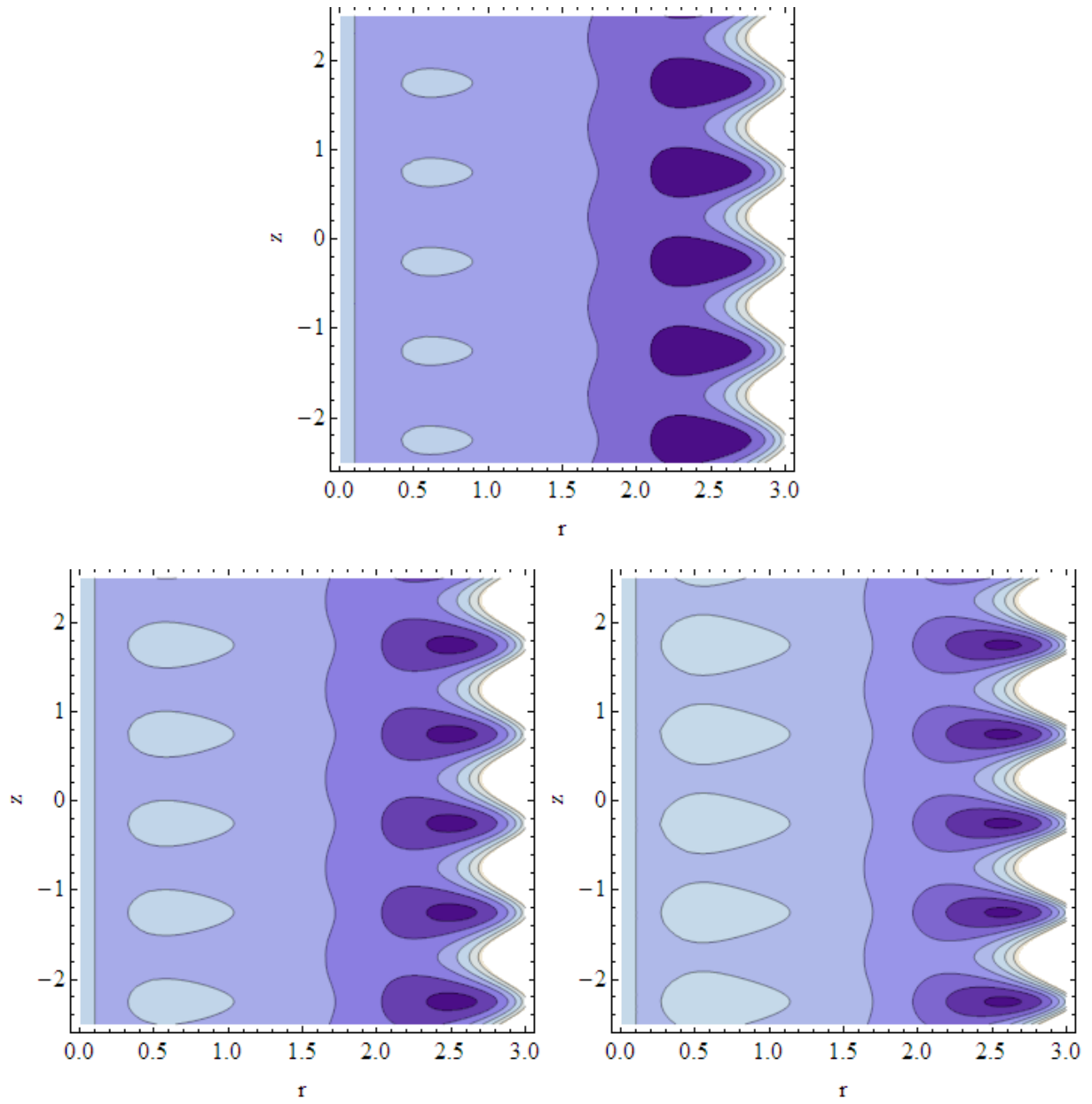
Figs. 5.13, Streamlines for Grashoff's number (**a**) $G_r = 1.5$, (**b**) $G_r = 1.75$, (**c**) $G_r = 2$.
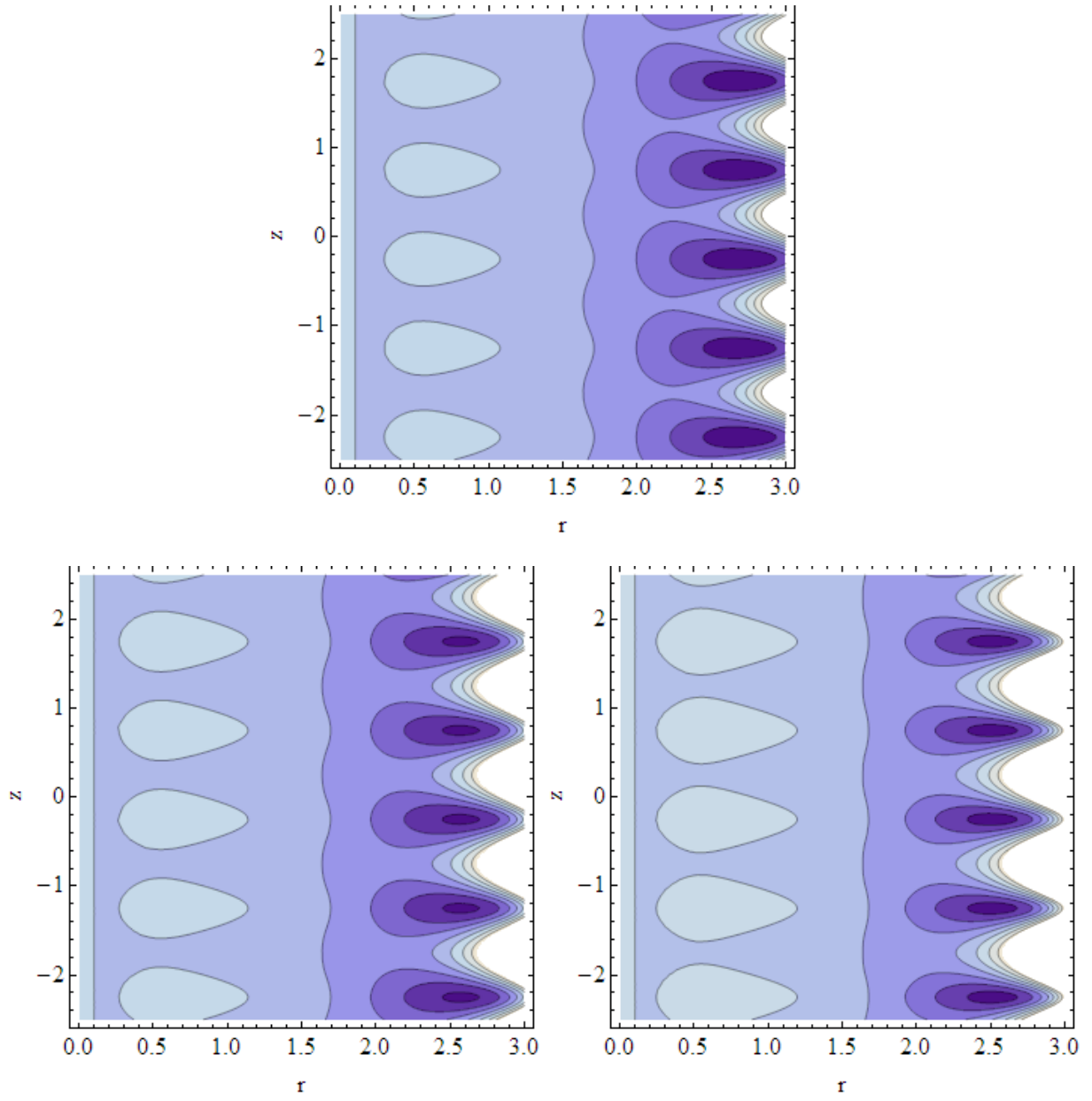
Figs. 5.14, Streamlines for distinct values of heat source (sink) parameter (**a**) $\gamma = 0.1$, (**b**) $\gamma = 0.5$, (**c**) $\gamma = 0.9$.
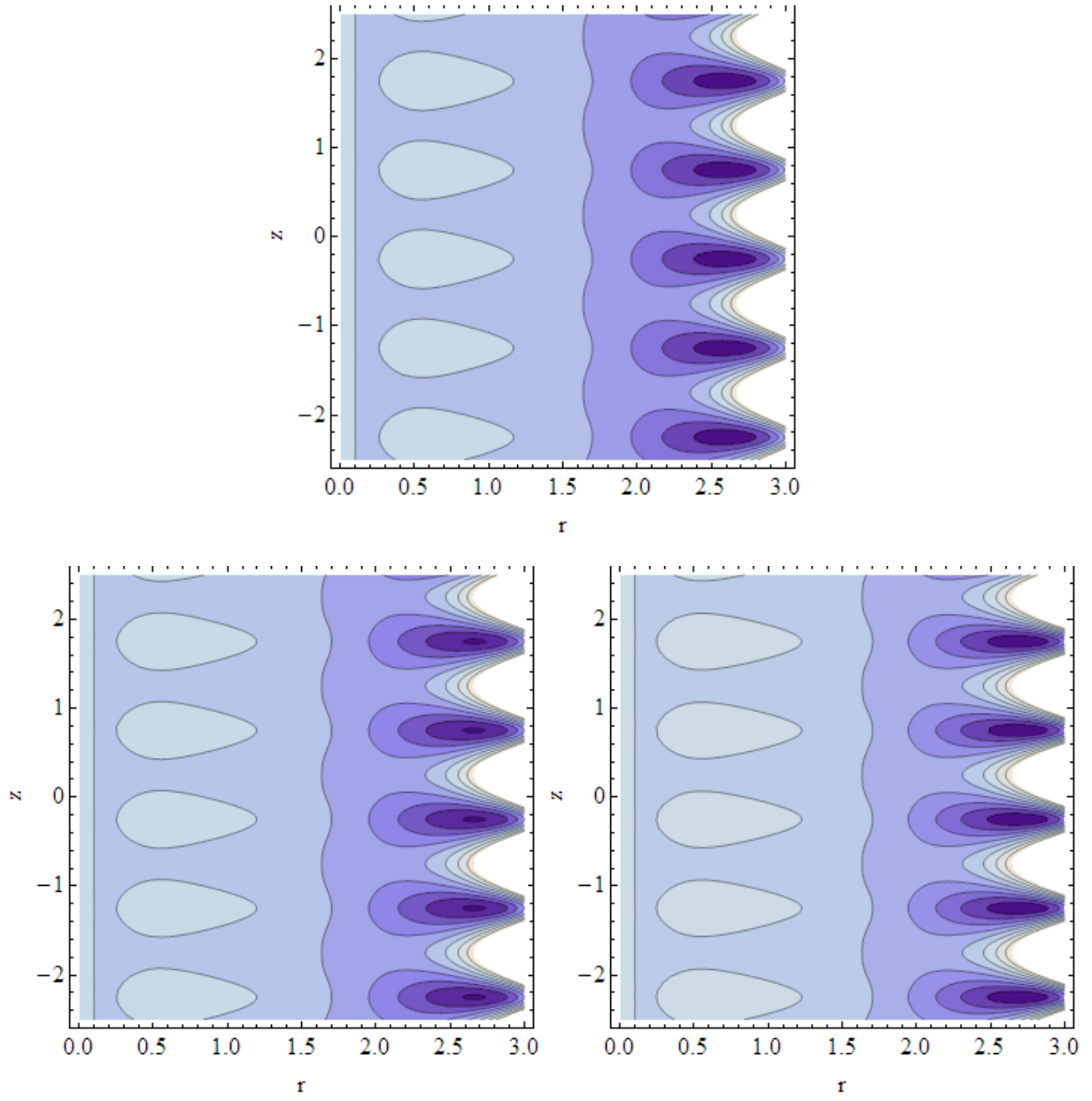
Figs. 5.15, Streamlines for distinct values of amplitude ratio(**a**) $\varphi = 0.11$, (**b**) $\varphi = 0.12$, (**c**) $\varphi = 0.13$.
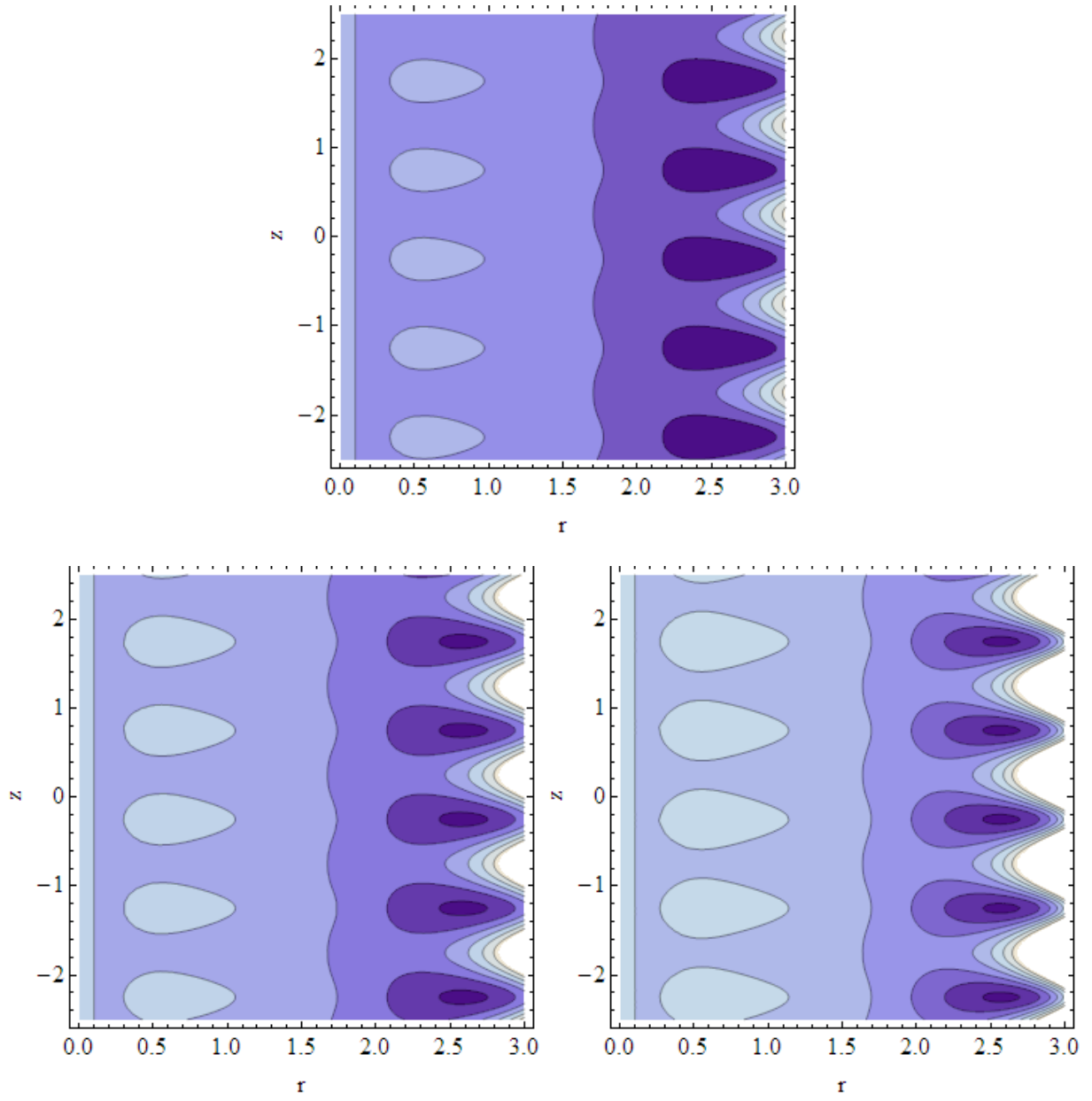
Figs. 5.16, Streamlines for distinct values of variable viscosity (**a**) $\alpha = 0.1$, (**b**) $\alpha = 0.2$, (**c**) $\alpha = 0.3$.
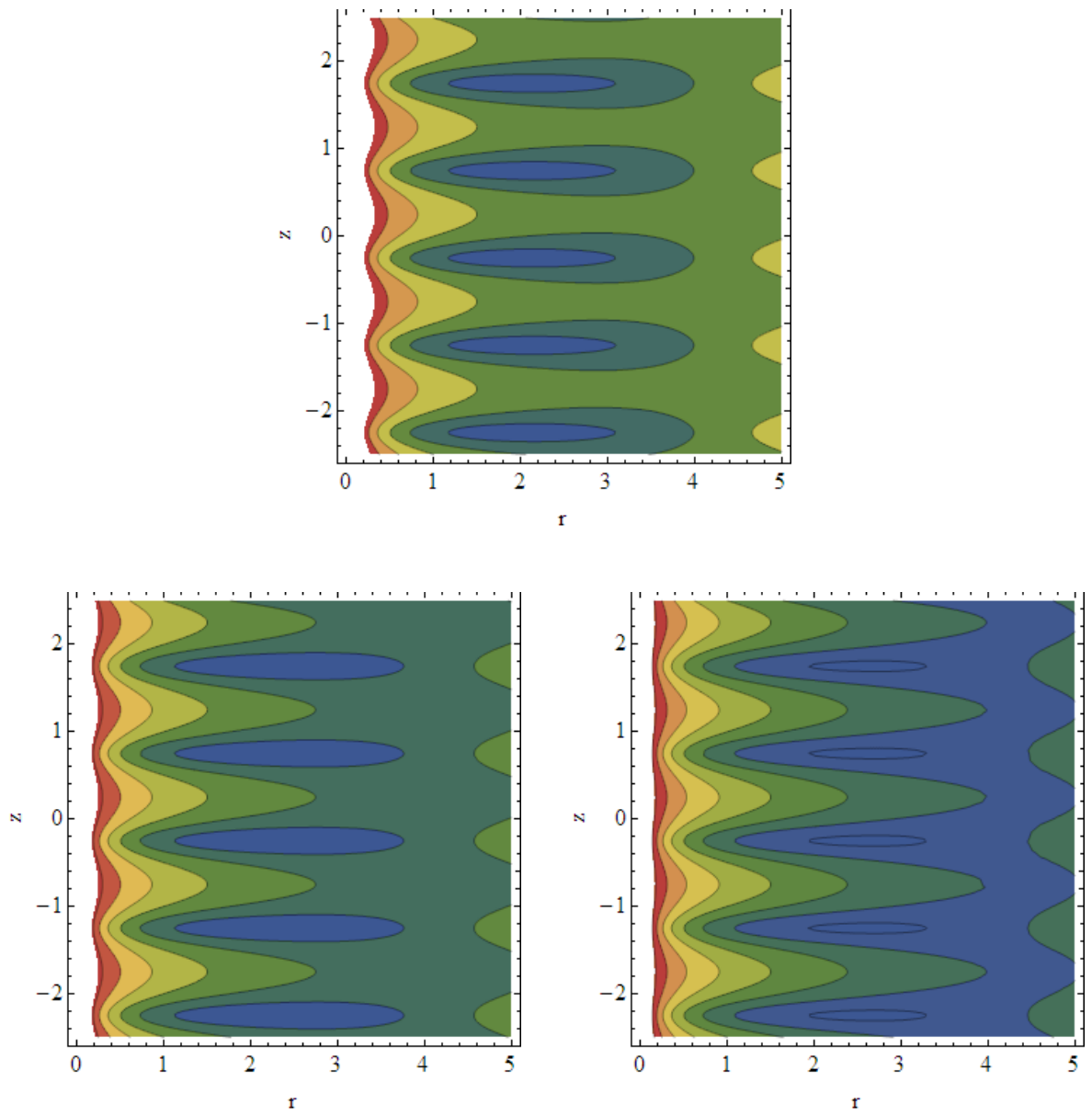
Figs. 5.17, Temperature contour maps for distinct values of heat source parameter (**a**)

$\gamma = 0.1$, (**b**) $\gamma = 0.2$, (**c**) $\gamma = 0.3$.
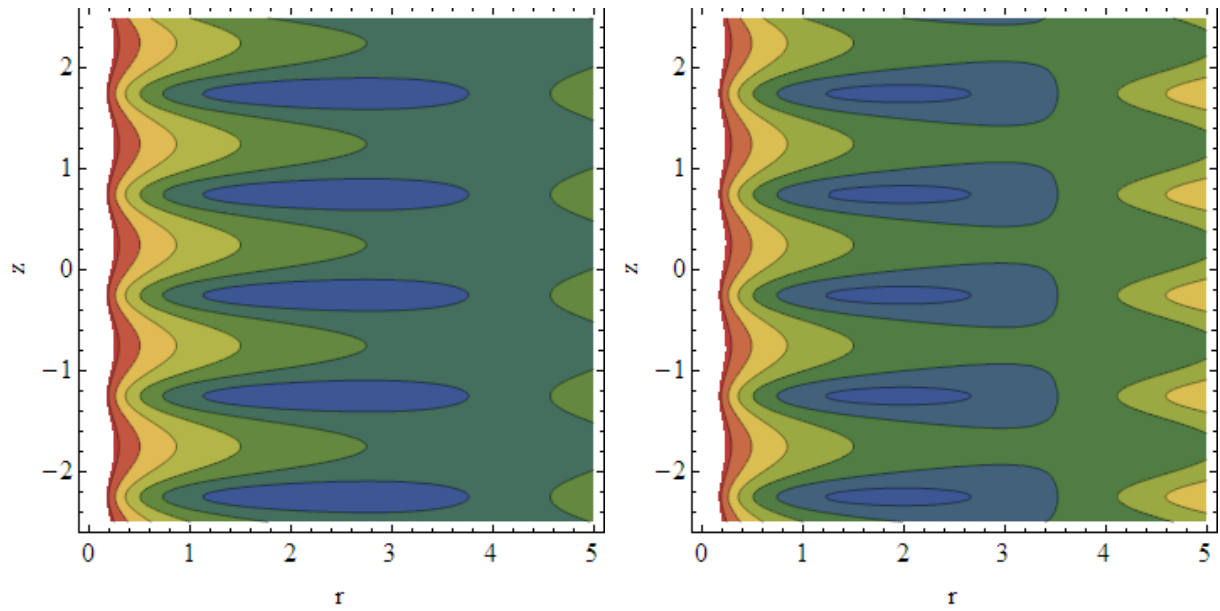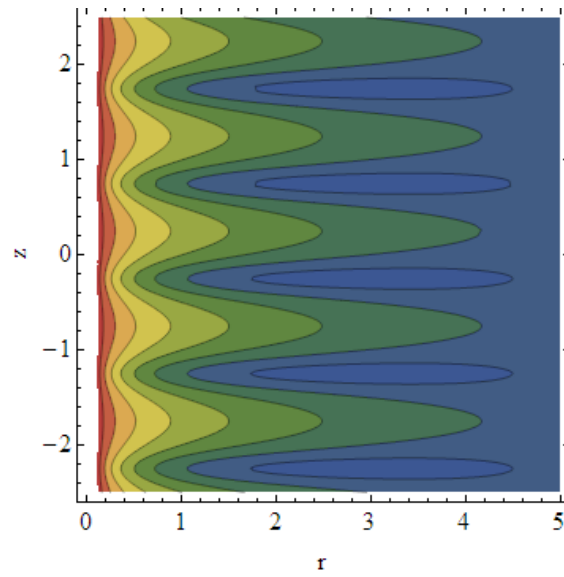
Figs. 5.18, Temperature contour maps for distinct values of curvature parameter (**a**) $\zeta = 0.4$, (**b**) $\zeta = 0.5$, (**c**) $\zeta = 0.6$.

5.4   Summary of the work

A detailed mathematical analysis has been done for impact of Au nanoparticles on the peristaltic flow through a curved tube with an endoscope inserted in it. Some observations of the present study made on the basis of graphical results are highlighted below

- With an increment in curvature parameter, velocity of nanofluid recedes.

- Pressure gradient exhibits higher results with larger variable viscosity α.

- Axial velocity elevates as we move from endoscope to the center of annular region.

- For greater Grashoff's number G_r and variable viscosity α, axial velocity is larger.

- The inner bolus for streamlines grows larger with increasing variable viscosity parameter.

- Bolus in temperature contour map increases in size with increase in curvature parameter.

Chapter 6

Impact of hybrid nanoparticles on peristaltic flow in curved tube

Hybrid nanofluid is considered to be a new class of nanofluids which is getting famous due to its thermal properties and possible utilities to further ameliorates the heat transfer rate. Main objective of this analysis is to represent a comparison between conventional nanofluid and hybrid nanofluid when fluid is passed through curved tube with an endoscope inserted in it while flow behavior is peristaltic. Cu/water nanofluid and $Cu - Fe_2O_4$/water hybrid nanofluid are considered for this problem. Results for pressure gradient,velocity, pressure rise and streamlines are given graphically. Tables for temperature and heat transfer rate are also mentioned. Present study concludes that heat transfer rate for hybrid nanofluid is greater in comparison to nanofluid.

6.1 Formulation of the problem

We are interested to examine the transport of incompressible, laminar and viscous nanofluid in the region between two curved annular tubes. A sinusoidal type of wave with velocity c travels down the walls of tube with wave amplitude b and wavelength λ. Inner tube is considered to be inflexible. The mathematical formulation model for curved tube is , an inflexible circular tube having radius a_2 wrapped as circular coil of radius k and endoscope as coaxial tube of radius a_1. Because of the bending of tube, curvature parameter is also taken into account. Copper

nanoparticles along with iron oxide are taken under consideration

Mathematically, two wall surfaces can be written as

$$\bar{R}_1 = a_1,$$
$$\bar{R}_2 = b \sin \left[\frac{2\pi}{\lambda} (Z - ct) \right] + a_2. \tag{6.1}$$

Toroidal coordinates system (r, θ, φ) is utilized to investigate the flow field in the geometry discussed above. Flow geometry is considered to lie in a plane so torsion impact is ignored.

The continuity equation for considered incompressible fluid in the toroidal coordinates is given as

$$\frac{\partial \bar{U}}{\partial \bar{R}} + \frac{\bar{U}}{\bar{R}} + \frac{\bar{U} \cos \bar{\theta} - \bar{V} \sin \bar{\theta}}{\bar{R} \cos \bar{\theta} + k} + \frac{1}{\bar{R}} \frac{\partial \bar{V}}{\partial \bar{\theta}} + \frac{k}{\bar{R} \cos \bar{\theta} + k} \frac{\partial \bar{W}}{\partial \bar{Z}} = 0. \tag{6.2}$$

The component form of momentum equation using toroidal coordinate are written as

$$\rho_{hnf} \left(\frac{\partial \bar{U}}{\partial \bar{t}} + \frac{\bar{V}}{\bar{R}} \frac{\partial \bar{U}}{\partial \bar{\theta}} + \bar{U} \frac{\partial \bar{U}}{\partial \bar{R}} + \frac{k \bar{W}}{\bar{R} \cos \bar{\theta} + k} \frac{\partial \bar{U}}{\partial \bar{Z}} - \frac{\bar{W}^2 \cos \bar{\theta}}{\bar{R} \cos \bar{\theta} + k} - \frac{\bar{V}^2}{\bar{R}} \right)$$
$$= \mu_{hnf} \left(\left(\frac{1}{\bar{R}^2} \frac{\partial^2 \bar{U}}{\partial \bar{\theta}^2} + \frac{\partial^2 \bar{U}}{\partial \bar{R}^2} + \frac{1}{\bar{R}} \frac{\partial \bar{U}}{\partial \bar{R}} \right) + \frac{k^2}{(\bar{R} \cos \bar{\theta} + k)^2} \frac{\partial^2 \bar{U}}{\partial \bar{Z}^2} - \frac{\bar{U}}{\bar{R}^2} \right.$$
$$- \frac{2}{\bar{R}^2} \frac{\partial \bar{V}}{\partial \bar{\theta}} + \frac{1}{\bar{R} \cos \bar{\theta} + k} \left(\cos \bar{\theta} \frac{\partial \bar{U}}{\partial \bar{R}} + \frac{\bar{V} \sin \bar{\theta}}{\bar{R}} - \frac{\sin \bar{\theta}}{\bar{R}} \frac{\partial \bar{U}}{\partial \bar{\theta}} \right)$$
$$\left. + \frac{2k \sin \bar{\theta}}{(\bar{R} \cos \bar{\theta} + k)^2} \frac{\partial \bar{W}}{\partial \bar{Z}} - \frac{\cos \bar{\theta}}{(\bar{R} \cos \bar{\theta} + k)^2} \left(\bar{U} \cos \bar{\theta} - \bar{V} \sin \bar{\theta} \right) \right) - \frac{\partial \bar{P}}{\partial \bar{R}}, \tag{6.3}$$

$$\rho_{hnf} \left(\frac{\partial \bar{V}}{\partial \bar{t}} + \bar{U} \frac{\partial \bar{V}}{\partial \bar{R}} + \frac{k \bar{W}}{\bar{R} \cos \bar{\theta} + k} \frac{\partial \bar{V}}{\partial \bar{Z}} + \frac{\bar{V}}{\bar{R}} \frac{\partial \bar{V}}{\partial \bar{\theta}} + \frac{\bar{W}^2 \cos \bar{\theta}}{\bar{R} \cos \bar{\theta} + k} + \frac{\bar{U} \bar{V}}{\bar{R}} \right)$$
$$= \mu_{hnf} \left(\left(\frac{1}{\bar{R}^2} \frac{\partial^2 \bar{V}}{\partial \bar{\theta}^2} + \frac{\partial^2 \bar{V}}{\partial \bar{R}^2} + \frac{1}{\bar{R}} \frac{\partial \bar{V}}{\partial \bar{R}} \right) + \frac{k^2}{(\bar{R} \cos \bar{\theta} + k)^2} \frac{\partial^2 \bar{V}}{\partial \bar{Z}^2} + \frac{2}{\bar{R}^2} \frac{\partial \bar{U}}{\partial \bar{\theta}} - \frac{\bar{V}}{\bar{R}^2} \right.$$
$$+ \frac{\cos \bar{\theta}}{\bar{R} \cos \bar{\theta} + k} \frac{\partial \bar{V}}{\partial \bar{R}} - \frac{\sin \bar{\theta}}{\bar{R} \cos \bar{\theta} + k} \left(\frac{\bar{U}}{\bar{R}} + \frac{1}{\bar{R}} \frac{\partial \bar{V}}{\partial \bar{\theta}} \right) + \frac{2k \sin \bar{\theta}}{(\bar{R} \cos \bar{\theta} + k)^2} \frac{\partial \bar{W}}{\partial \bar{Z}}$$
$$\left. + \frac{\sin \bar{\theta}}{(\bar{R} \cos \bar{\theta} + k)^2} \left(\bar{U} \cos \bar{\theta} - \bar{V} \sin \bar{\theta} \right) \right) - \frac{1}{\bar{R}} \frac{\partial \bar{P}}{\partial \bar{\theta}}, \tag{6.4}$$

$$
\rho_{hnf}\left(\frac{\partial \bar{W}}{\partial \bar{t}}+\bar{U}\frac{\partial \bar{W}}{\partial \bar{R}}+\frac{\bar{V}}{\bar{R}}\frac{\partial \bar{W}}{\partial \bar{\theta}}+\frac{k\bar{W}}{\bar{R}\cos\bar{\theta}+k}\frac{\partial \bar{W}}{\partial \bar{Z}}-\frac{\bar{W}\left(\bar{V}\sin\bar{\theta}-\bar{U}\cos\bar{\theta}\right)}{\bar{R}\cos\bar{\theta}+k}\right)
$$
$$
=\ \mu_{hnf}\left(\left(\frac{1}{\bar{R}^2}\frac{\partial^2 \bar{W}}{\partial \bar{\theta}^2}+\frac{\partial^2 \bar{W}}{\partial \bar{R}^2}+\frac{1}{\bar{R}}\frac{\partial \bar{W}}{\partial \bar{R}}\right)+\frac{k^2}{(\bar{R}\cos\bar{\theta}+k)^2}\frac{\partial^2 \bar{W}}{\partial \bar{Z}^2}-\frac{\bar{W}}{(\bar{R}\cos\bar{\theta}+k)^2}\right.
$$
$$
-\frac{1}{\bar{R}\cos\bar{\theta}+k}\left(\frac{\sin\bar{\theta}}{\bar{R}}\frac{\partial \bar{W}}{\partial \bar{\theta}}-\cos\bar{\theta}\frac{\partial \bar{W}}{\partial \bar{R}}\right)+\left(\cos\bar{\theta}\frac{\partial \bar{U}}{\partial \bar{Z}}-\sin\bar{\theta}\frac{\partial \bar{V}}{\partial \bar{Z}}\right)\frac{2k\sin\bar{\theta}}{(\bar{R}\cos\bar{\theta}+k)^2}\right)
$$
$$
+(\rho\beta)_{hnf}g(T-T_1)-\frac{k}{\bar{R}\cos\bar{\theta}+k}\frac{\partial \bar{P}}{\partial \bar{Z}}. \tag{6.5}
$$

Energy equation in the occupancy of heat generation for a hybrid nanofluid is written as,

$$
(\rho c_p)_{hnf}\left(\frac{\partial \bar{T}}{\partial \bar{t}}+\bar{U}\frac{\partial \bar{T}}{\partial \bar{R}}+\frac{k\bar{W}}{\bar{R}\cos\bar{\theta}+k}\frac{\partial \bar{T}}{\partial \bar{Z}}+\frac{\bar{U}}{\bar{R}}\frac{\partial \bar{T}}{\partial \bar{\theta}}\right)\ =\ K_{hnf}\left(\frac{1}{\bar{R}}\frac{\partial \bar{T}}{\partial \bar{R}}+\frac{\partial^2 \bar{T}}{\partial \bar{R}^2}+\frac{\cos\bar{\theta}}{\bar{R}\cos\bar{\theta}+k}\frac{\partial \bar{T}}{\partial \bar{R}}\right.
$$
$$
+\frac{1}{\bar{R}^2}\frac{\partial^2 \bar{T}}{\partial \bar{\theta}^2}+\frac{k^2}{(\bar{R}\cos\bar{\theta}+k)^2}\frac{\partial^2 \bar{T}}{\partial \bar{Z}^2}
$$
$$
\left.-\frac{\sin\bar{\theta}}{\bar{R}\cos\bar{\theta}+k}\frac{\partial \bar{T}}{\partial \bar{\theta}}\right)+Q_0. \tag{6.6}
$$

For the fixed frame, the boundary condition is given as

$$
\bar{W}\ =\ 0,\ \bar{T}=\bar{T}_0,\ \text{at}\quad \bar{R}=\bar{R}_1=a_1,
$$
$$
\bar{W}\ =\ 0,\ K_{hnf}\frac{\partial \bar{T}}{\partial \bar{R}}=-B(\bar{T}-\bar{T}_1),\ \text{at}\quad \bar{R}=\bar{R}_2=a_2+b\sin\left[\frac{2\pi}{\lambda}\left(\bar{Z}-ct\right)\right]. \tag{6.7}
$$

As the axial velocity is effective velocity component so we suppose the vector form as $(0,0,\bar{W})$. The written below relation is utilized to switch from $(\bar{R},\bar{Z},\bar{t})$ fixed frame to wave frame (r,z),

$$
\bar{z}=\bar{Z}-c\bar{t},\ \bar{p}(\bar{z},\bar{r})=\bar{P}(\bar{Z},\bar{R},\bar{t}),\ \bar{u}=\bar{U},\ \bar{r}=\bar{R},\ \bar{w}=\bar{W}-c. \tag{6.8}
$$

Introducing the following dimensionless quantities

$$
\begin{aligned}
w &= \frac{\bar{w}}{c}, \ r = \frac{\bar{r}}{a_2}, \ t = \frac{c\bar{t}}{\lambda}, \ u = \frac{\lambda\bar{u}}{a_2 c}, \ r_2 = 1 + \varepsilon\sin(2\pi z), \ z = \frac{\bar{z}}{\lambda}, \\
\varepsilon &= \frac{b}{a_2}, \ G_r = \frac{a_2^2(T_1 - T_0)\rho_f\beta_f g}{c\mu_f}, \ \tilde{\theta} = \frac{T - T_1}{T_0 - T_1}, \ \bar{\theta} = \theta, \ \zeta = \frac{a_2}{k}, \\
r_1 &= \frac{\bar{r}_1}{a_2} = \epsilon, \ \gamma = \frac{a_2^2 Q_0}{(T_1 - T_0)k_f}, \ R_e = \frac{a_2 c\rho_f}{\mu_f}, \ \delta = \frac{a_2}{\lambda}, \ p = \frac{a_2^2\bar{p}}{c\lambda\mu_f}.
\end{aligned}
\tag{6.9}
$$

Mentioned above expressions are representing p as the pressure, G_r as the Grashrof number, $\tilde{\theta}$ as the temperature, R_e is the Reynolds number, γ is dimensionless heat source parameter, ζ is the curvature parameter and δ represent wave number. Employing the lubrication approach, Eqs. $(6.2) - (6.6)$ are now written as

$$
\frac{\partial p}{\partial r} = 0,
\tag{6.10}
$$

$$
\frac{\partial p}{\partial \theta} = 0,
\tag{6.11}
$$

$$
\begin{aligned}
\frac{1}{1 + \zeta r\cos\theta}\frac{\partial p}{\partial z} &= \frac{\mu_{hnf}}{\mu_f}\left(\frac{\partial^2 w}{\partial r^2} + \frac{1}{r}\frac{\partial w}{\partial r} + \frac{\zeta\cos\theta}{1 + \zeta r\cos\theta}\frac{\partial w}{\partial r} + \frac{1}{r^2}\frac{\partial^2 w}{\partial\theta^2} - \frac{\zeta^2(w+1)}{(1 + \zeta r\cos\theta)^2}\right. \\
&\left. - \frac{\zeta\sin\theta}{r(1 + \zeta r\cos\theta)}\frac{\partial w}{\partial\theta} + G_r\frac{(\rho\beta)_{hnf}}{(\rho\beta)_f}\frac{\mu_f}{\mu_{hnf}}\tilde{\theta}\right),
\end{aligned}
\tag{6.12}
$$

$$
\frac{\partial^2\tilde{\theta}}{\partial r^2} + \frac{1}{r}\frac{\partial\tilde{\theta}}{\partial r} + \frac{\zeta\cos\theta}{1 + \zeta r\cos\theta}\frac{\partial\tilde{\theta}}{\partial r} + \frac{1}{r^2}\frac{\partial^2 w}{\partial\theta^2} + \gamma\frac{K_f}{K_{hnf}} = 0.
\tag{6.13}
$$

In wave frame, the pertinent boundary conditions are given as

$$
\begin{aligned}
&\tilde{\theta} = 1, \ w = -1, &&\text{at} \quad r = r_1 = \epsilon, \\
&\frac{\partial\tilde{\theta}}{\partial r} + B_i\frac{K_f}{K_{hnf}}\tilde{\theta} = 0, \ w = -1, &&\text{at} \quad r = r_2 = 1 + \varepsilon\sin(2\pi z),
\end{aligned}
\tag{6.14}
$$

Dimensionless volume flow rate is given as

$$
q = F + \frac{1}{2} - \frac{\epsilon^2}{2} + \frac{\varepsilon^2}{4},
\tag{6.15}
$$

where

$$F = \int_{r_1}^{r_2} rw dr. \tag{6.16}$$

6.2   Solution of the problem

In order to get the expression for velocity and temperature according to the given boundary condition,we consider the following

$$\begin{aligned}
\tilde{\theta}(r(z,t),\ \theta) &= \tilde{\theta}_0(r) + \zeta \cos(\theta)\tilde{\theta}_1(r) + \dots \\
w(r(z,t),\ \theta) &= w_0(r) + \zeta \cos(\theta)w_1(r) + \dots
\end{aligned} \tag{6.17}$$

Substituting Eq. (6.17) into Eqs. (6.12) to (6.14) and equating same powers of $\zeta \cos(\theta)$, we obtain the written below systems and their solutions

6.2.1   Zeroth order system

$$\frac{\partial^2 \tilde{\theta}_0}{\partial r^2} + \frac{1}{r}\frac{\partial \tilde{\theta}_0}{\partial r} + \gamma \frac{K_f}{K_{hnf}} = 0, \tag{6.18}$$

$$\frac{\partial^2 w_0}{\partial r^2} + \frac{1}{r}\frac{\partial w_0}{\partial r} + G_r \frac{(\rho\beta)_{hnf}}{(\rho\beta)_f}\frac{\mu_f}{\mu_{hnf}}\tilde{\theta}_0 = \frac{\mu_f}{\mu_{hnf}}\frac{dp}{dz}, \tag{6.19}$$

$$\tilde{\theta}_0(r_1) = 1,\ w_0(r_1) = -1, \tag{6.20}$$

$$(\frac{\partial \tilde{\theta}_0}{\partial r} + B_i \frac{K_f}{K_{hnf}}\tilde{\theta}_0)\ |_{r=r_2} = 0,\ w_0(r_2) = -1. \tag{6.21}$$

The exact solution at this order is given as

$$\tilde{\theta}_0(r) = C_1 \ln r + C_2 - \frac{\gamma \frac{K_f}{K_{hnf}}}{4}r^2, \tag{6.22}$$

146

$$w_0(r) = \frac{\frac{dp}{dz}}{4\frac{\mu_{hnf}}{\mu_f}}r^2 - G_r\frac{(\rho\beta)_{hnf}}{(\rho\beta)_f}\frac{\mu_f}{\mu_{hnf}}\left(-\frac{\gamma\frac{K_f}{K_{hnf}}}{64}r^4 + \frac{C_1}{2}\left(\frac{r^2\ln r}{2} - \frac{r^2}{2}\right) + \frac{C_2}{4}r^2\right)$$
$$+C_5\ln r + C_6. \tag{6.23}$$

6.2.2   First order system

$$\frac{\partial^2\tilde{\theta}_1}{\partial r^2} + \frac{1}{r}\frac{\partial\tilde{\theta}_1}{\partial r} - \frac{\tilde{\theta}_1}{r^2} + r\frac{\partial^2\tilde{\theta}_0}{\partial r^2} + 2\frac{\partial\tilde{\theta}_0}{\partial r} + r\gamma\frac{K_f}{K_{hnf}} = 0 \ , \tag{6.24}$$

$$\frac{\partial^2 w_1}{\partial r^2} + \frac{1}{r}\frac{\partial w_1}{\partial r} - \frac{w_1}{r^2} + r\frac{\partial^2 w_0}{\partial r^2} + 2\frac{\partial w_0}{\partial r} + G_r\frac{(\rho\beta)_{hnf}}{(\rho\beta)_f}\frac{\mu_f}{\mu_{hnf}}(r\tilde{\theta}_0 + \tilde{\theta}_1) = 0, \tag{6.25}$$

$$\tilde{\theta}_1(r_1) = 0, \ w_1(r_1) = 0, \tag{6.26}$$

$$(\frac{\partial\tilde{\theta}_1}{\partial r} + B_i\frac{K_f}{K_{hnf}}\tilde{\theta}_1)\,|_{r=r_2}= 0, \ w_1(r_2) = 0. \tag{6.27}$$

Solution is obtained by using Eqs. (6.22, 6.23) into Eqs. (6.24, 6.25) and is given as follow

$$\tilde{\theta}_1(r) = rC_3 + \frac{C_4}{r} + r\left(\frac{\gamma\frac{K_f}{K_{hnf}}r^2}{8} - \frac{C_1\ln r}{2}\right) - \frac{1}{r}\left(\gamma\frac{K_f}{K_{hnf}}\frac{r^4}{16} - \frac{C_1r^2}{4}\right), \tag{6.28}$$

$$w_1(r) = rC_7 + \frac{C_8}{r} + \frac{r}{2}\left(-\frac{3\frac{dp}{dz}}{4\frac{\mu_{hnf}}{\mu_f}}r^2 + G_r\frac{(\rho\beta)_{hnf}}{(\rho\beta)_f}\frac{\mu_f}{\mu_{hnf}}\left(-\frac{\gamma\frac{K_f}{K_{hnf}}}{32}r^4 + \frac{C_1}{2}r^2\ln r - \frac{C_1}{4}r^2\right.\right.$$

$$\left.+\frac{C_2}{4}r^2 - \frac{C_3}{2}r^2 - C_4\ln r\right) - C_5\ln r\bigg) - \frac{1}{2r}\left(-\frac{3\frac{dp}{dz}}{8\frac{\mu_{hnf}}{\mu_f}}r^4 + G_r\frac{(\rho\beta)_{hnf}}{(\rho\beta)_f}\frac{\mu_f}{\mu_{hnf}}\right.$$

$$\left.-\frac{\gamma\frac{K_f}{K_{hnf}}}{48}r^6 + \frac{C_1}{4}r^4\ln r - \frac{3C_1}{16}r^4 + \frac{C_2}{8}r^4 - \frac{C_3}{4}r^4 - \frac{C_4}{2}r^2\right) - \frac{C_5}{2}r^2\bigg) \tag{6.29}$$

here all the C's are constants and defined in appendix.

The pressure gradient is defined as

$$\frac{dp}{dz} = \frac{F - t_1}{t_2}, \tag{6.30}$$

where t_1 and t_2 are calculated by Mathematica.

The thermophysical properties of stated nanofluid model and hybrid nanofluid are defined as mentioned in [70]

Properties	Nanofluid	Hybrid nanofluid
Viscosity	$\mu_{nf} = \dfrac{\mu_f}{(1-\varphi)^{2.5}}$	$\mu_{hnf} = \dfrac{\mu_f}{(1-\varphi_1)^{2.5}(1-\varphi_2)^{2.5}}$
Density	$\rho_{nf} = \varphi\rho_s + (1-\varphi)\rho_f.$	$\rho_{hnf} = \varphi_1\rho_{s_1} + \varphi_2\rho_{s_2} + (1-\varphi_1)(1-\varphi_2)\rho_f.$
Heat Capacity	$(\rho c_p)_{nf} = \varphi(\rho c_p)_s + (1-\varphi)(\rho c_p)_f$	$(\rho c_p)_{hnf} = \varphi_1(\rho c_p)_{s_1} + \varphi_2(\rho c_p)_{s_2} + (1-\varphi_1)(1-\varphi_2)(\rho c_p)_f$
Thermal Conductivity	$\dfrac{K_{nf}}{K_f} = \dfrac{(n-1)k_f+k_s-(n-1)(k_f-k_s)\varphi}{k_s+(n-1)k_f+\varphi(k_f-k_s)}$	$\dfrac{K_{hnf}}{K_{bf}} = \dfrac{(n-1)k_{bf}+k_{s_2}-(n-1)(k_{bf}-k_{s_2})\varphi_2}{k_{s_2}+(n-1)k_{bf}+\varphi_2(k_{bf}-k_{s_2})}$ where $\dfrac{K_{bf}}{K_f} = \dfrac{(n-1)k_f+k_{s_1}-(n-1)(k_f-k_{s_1})\varphi_1}{k_{s_1}+(n-1)k_f+\varphi_1(k_f-k_{s_1})}$

Here n signify shape factor of nanoparticles given by $3/\psi$, where ψ represents sphericity of the particle and is determined by the formation of nanoparticle. For cylindrical nanoparticle $n = 6$ or $\psi = 1/2$ while for spherical nanoparticle $\psi = 1$ or $n = 6$. Here, in this investigation we have taken $n = 6$ i.e. considered spherical shape.

Thermophysical properties	Fluid Phase(water)	Cu	Fe_2O_4
$C_p(j/kg)K$	4179	385	670
$\rho(kg/m^3)$	997.1	3970	5180
$k(W/mK)$	0.613	40	9.7

6.3   Results and discussion

In the present study, parameters that we considered are φ_2, B_i, G_r, ζ and $\varphi_1 = 0.1$ is fixed. The physical situation is modeled in terms of partial differential equation and then perturbation method is used to solve these equations. Results obtained, are represented through graphs and tables.

Figures depict the effects of parameters on velocity profile, pressure gradient, pressure rise and streamlines for both hybrid nanofluid and nanofluid. Particularly, Figs $6.1 - 6.5$ portray the behavior of velocity profile for the variation of G_r, γ, B_i, ζ and φ_2 respectively. It is clear from Fig 6.1 that with a rise in G_r, decrease is observed in the region $[0.1 - 0.5]$ and for the region $[0.5 - 1]$ an increase is witnessed. It is eminent that velocity for nanofluid is higher in first region as compared to hybrid nanofluid and opposite trend is seen in second region. Fig

6.2 explains the effect of γ on velocity profile. Initially with an increase in γ, velocity profile declines but in the region $[0.5-1]$ increase is observed for this parameter. Hybrid nanofluid velocity is smaller in first region while in the second region we see that velocity for hybrid nanofluid is higher then nanofluid.

Influence of Biot number on velocity is displayed in Fig 6.3. We can see the similar behavior for this parameter as we observed for γ in both cases of nanofluid and hybrid nanofluid. Influence of curvature ζ is seen in Fig 6.4. As the bending of the tube increases, we see a decline in velocity near the mid of tube while towards the sides of tube, velocity is higher. Hybrid nanofluid velocity is greater then nanofluid velocity in first half region. Fig 6.5 is giving the visual display of variation of volume fraction φ_2. The outcome of this observation is that in the first region velocity decreases as we increase the volume fraction but it increases in second half.

For peristaltic transportation pressure gradient plays a vital role. So Figs $6.6-6.10$ are drawn to depict the impact of different parameters on pressure gradient for hybrid nanofluid and nanofluid. Increasing G_r results in increase of pressure gradient, also dp/dz for hybrid nanofluid is higher in comparison to nanofluid and this can be seen in Fig 6.6. Heat source/sink parameter gives the similar effect as of Grashoff's number on pressure gradient i.e. by elevating γ an increase is observed for dp/dz. Fig 8 also shows that pressure gradient for hybrid nanofluid is larger then nanofluid.

Fig 6.8 is sketched to give the effect of Biot number on dp/dz. With higher B_i ,pressure gradient is observed to be higher and amplitude for hybrid nanofluid is larger then nanofluid's curve. Visual evidence for the fluctuation of curvature parameter is given in Fig 6.9. Larger curvature results in higher pressure gradient for both hybrid nanofluid and nanofluid, while dp/dz for hybrid nanofluid remains greater then dp/dz of nanofluid. Fig 6.10 is an observation for the variation of volume fraction and it illustrates that as we gradually increase the concentration of Fe_2O_4 in water, pressure gradient elevates.

Figs $6.11-6.15$ are pictorial representations of pressure rise for both hybrid nanofluid and nanofluid under the influence of several parameters. Describing precisely, Fig 6.11 is effect of G_r and as it begin to increase we see an increase in pressure rise as well. Fig 6.12 is representing variation of γ and with larger values of γ, we get greater pressure rise. Fluctuation of Biot number is sketched in Fig 6.13 and it results in increased pressure rise for larger values. More

curvature has an increasing effect on Δp but opposite behavior is seen towards the end of region which is clearly visible in Fig 6.14. One more observation for these figures is that pressure rise for hybrid nanofluid is greater than Δp for nanofluid. Fig 6.15 is also advocating this behaviour where distinct φ_2 are taken under consideration.

Streamlines give the flow pattern and we have drawn these flow patterns for hybrid nanofluid in Fig $6.16 - 6.20$. It is noted that for variation of Grashoff's number, initially number of trapped bolus decreases but for further variation we observe an increase in these bolus which is evident in Fig 6.16. Number and size of trapped bolus has clearly reduced in Fig 6.17 which is the result of larger heat source parameter. Fig 6.18 is describing that with an increase in volume fraction φ_2 well distinct bolus are seen and eventually they increase in number as well. Streamlines for variation of B_i are given in Fig 6.19 and it is witnessed that magnitude and quantity of trapped bolus are intensified. For greater curvature parameter i.e for a more curved tube we see a significant increase in number of bolus and is clear in Fig 6.20.

Temperature profile for curved channel with $Cu/water$ and $Cu - Fe_2O_4/water$ is presented in Table 6.1. It is declared that temperature source parameter contributes positively for temperature profile i.e. for larger values of γ we get higher temperature. Similar behaviour is testified for Biot number whereas curvature parameter acts oppositely, for larger curvature we get low temperature. It is clear from the table that temperature for hybrid nanofluid is higher than temperature of nanofluid. Also it is interesting to see the variation in concentration effects the temperature profile. Higher concentration of Fe_2O_4 in base fluid results in higher temperature. Table 6.2 is bearing the data for heat transfer rate of peristaltic transport in curved tube with $Cu/water$ and $Cu - Fe_2O_4/water$. Heat source parameter and Biot number are responsible for higher heat transfer rate for both nanofluid and hybrid nanofluid. Curvature parameter has deteriorating impact on heat transfer rate i.e. with a rise in ζ it decreases. Greater volume

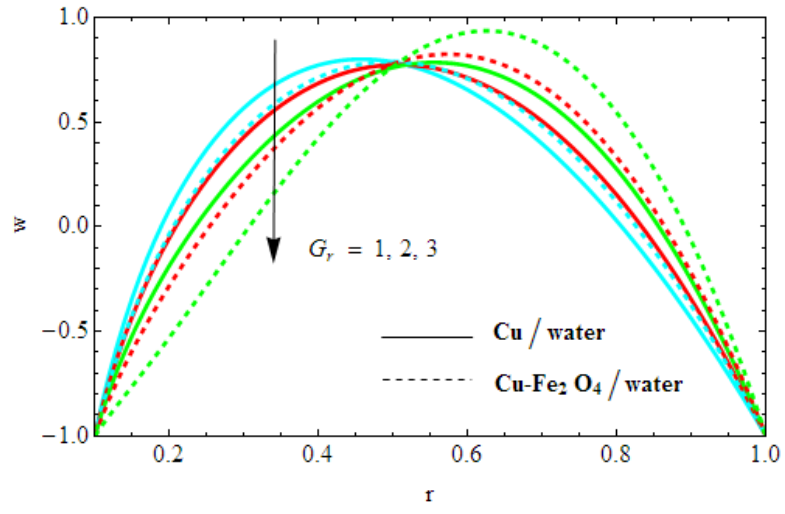fraction φ_2 results in higher transfer rate.

$Fig.$ 6.1, Effects of distinct values of Grashroff number G_r on velocity profile.
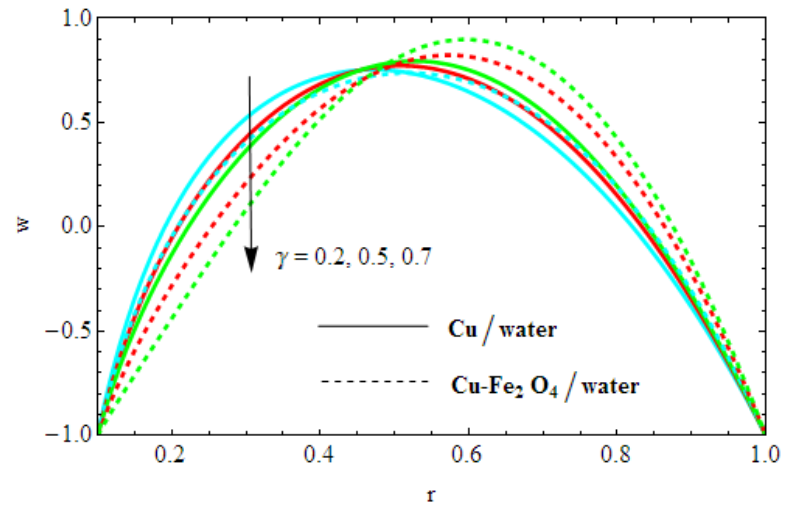

$Fig.$ 6.2, Effects of heat source parameter γ on velocity profile.
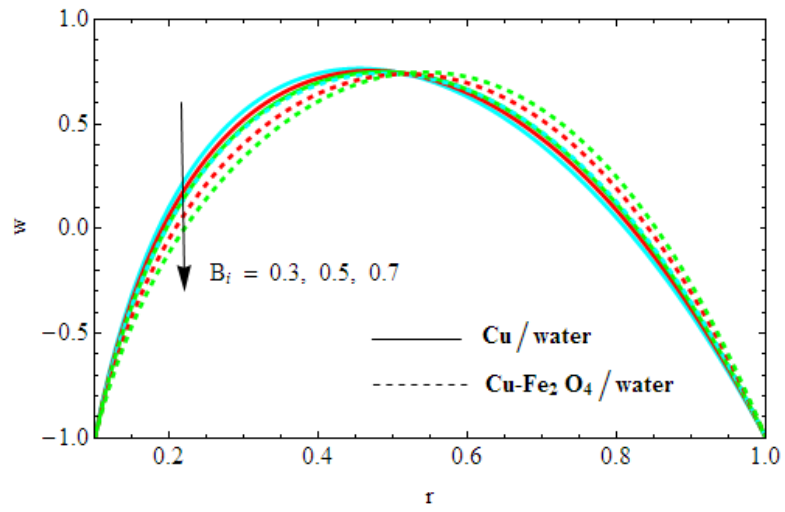
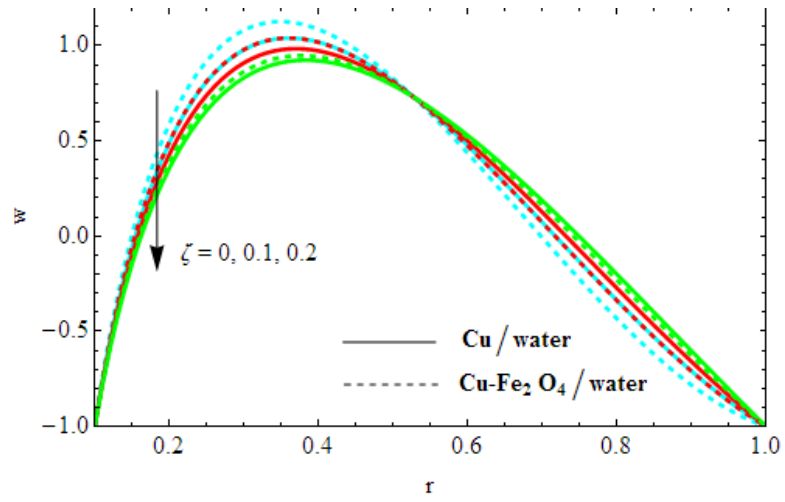*Fig.* 6.3, Effects of Biot number B_i on velocity profile.

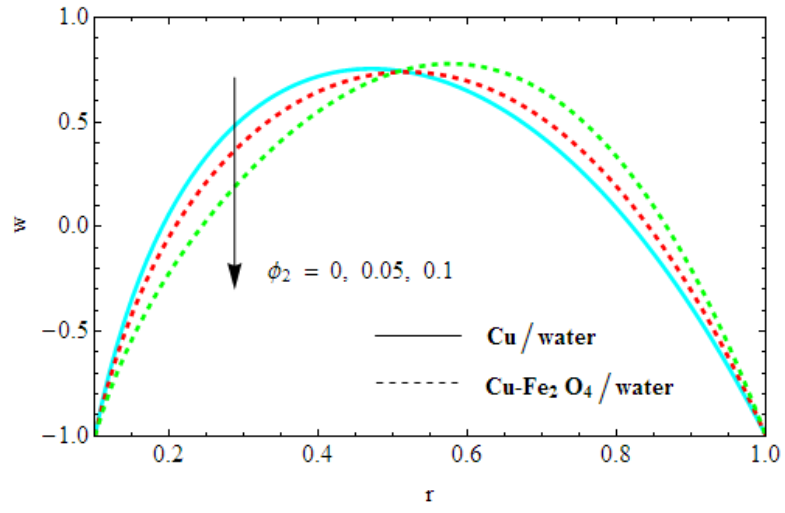*Fig.* 6.4, Effects of curvature parameter ζ on velocity profile.

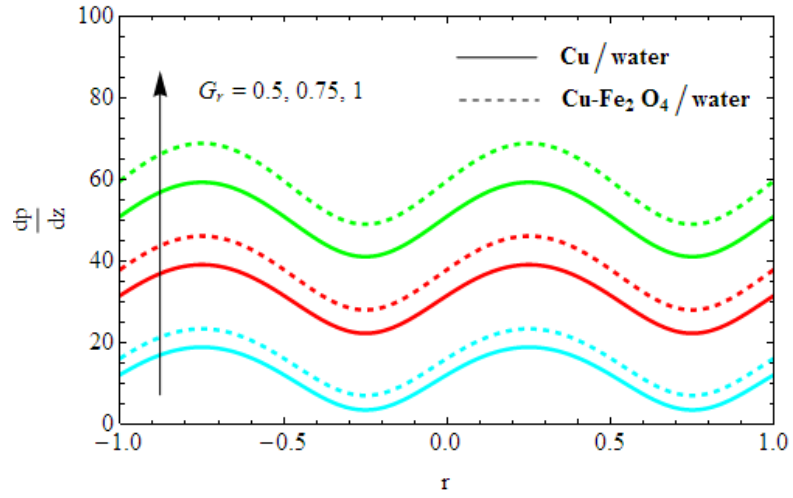$Fig.$ 6.5, Effects of nanoparticle volume fraction ϕ_2 on velocity profile.
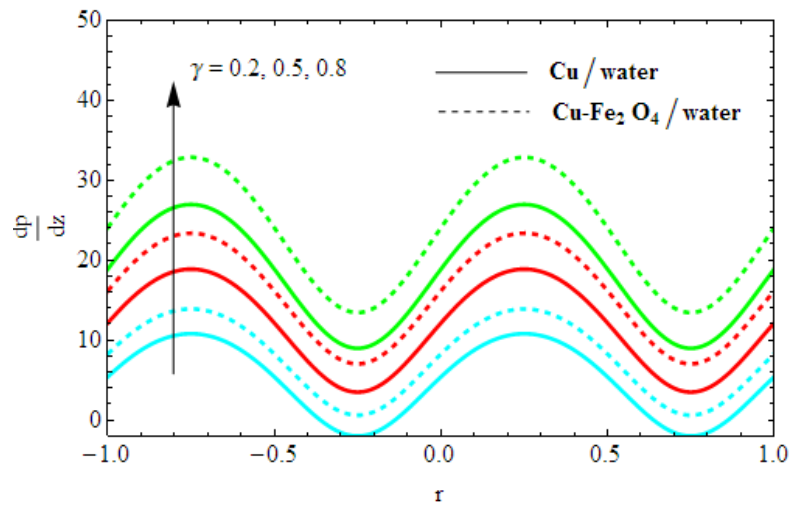

$Fig.$ 6.6, Variations of pressure gradient for G_r.
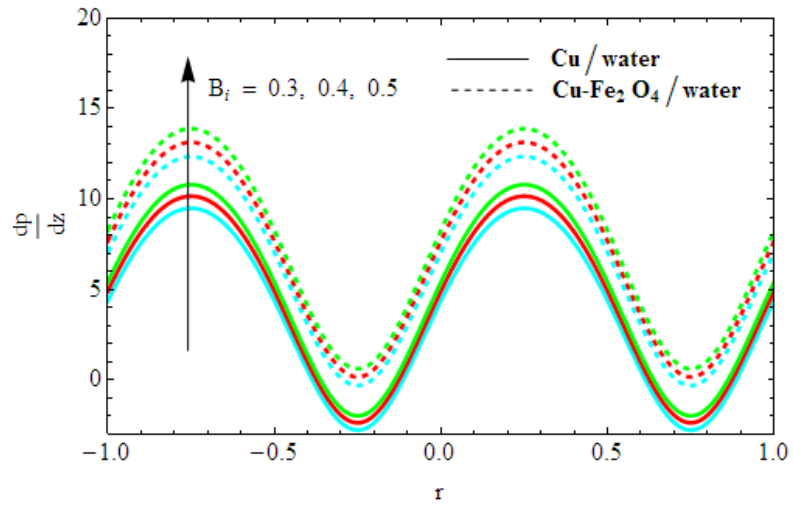
Fig. 6.7, Variations of pressure gradient for γ.

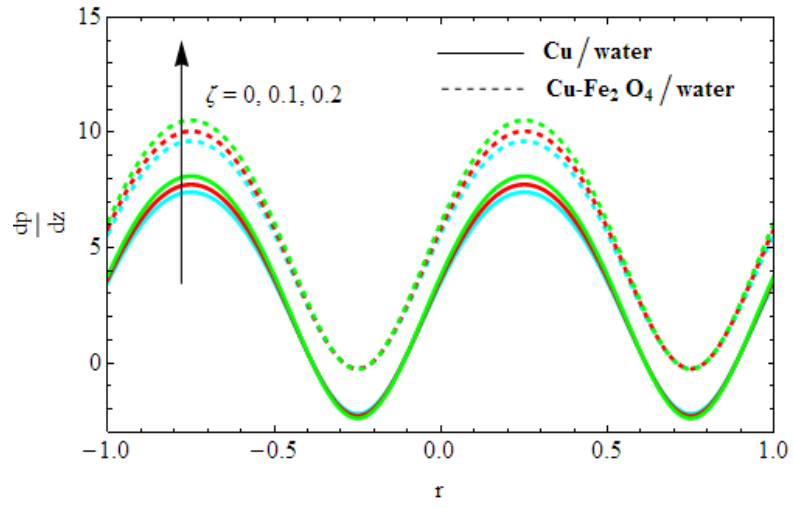*Fig.* 6.8, Variations of pressure gradient for B_i.

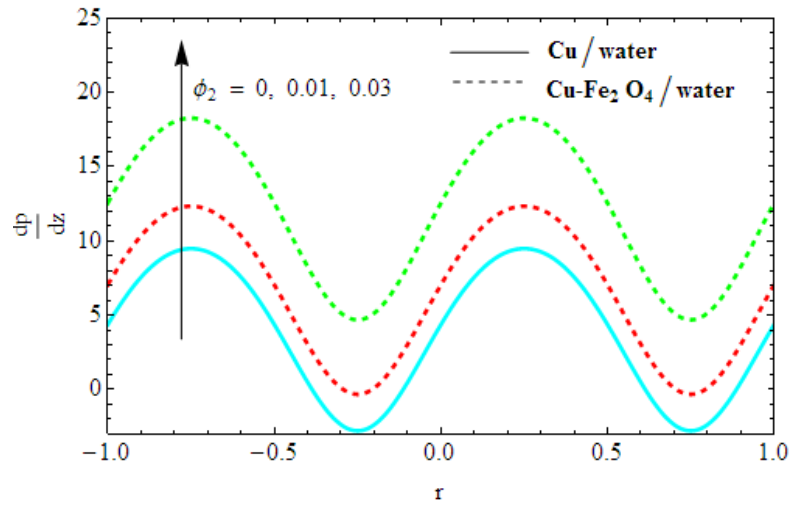*Fig.* 6.9, Variations of pressure gradient for ζ.
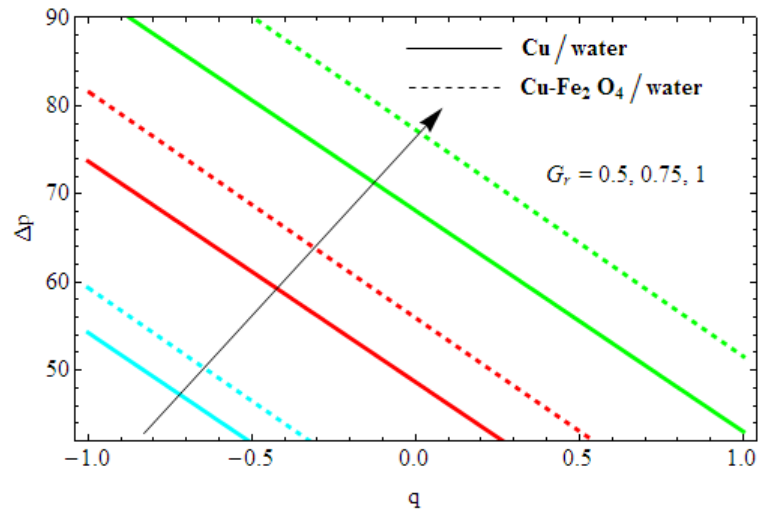

Fig. 6.10, Variations of pressure gradient for ϕ_2.

Fig. 6.11, Distinct G_r for nanofluid and hybrid nanofluid pressure rise.

Fig. 6.12, Distinct γ for nanofluid and hybrid nanofluid pressure rise.

Fig. 6.13, Distinct B_i for nanofluid and hybrid nanofluid pressure rise.

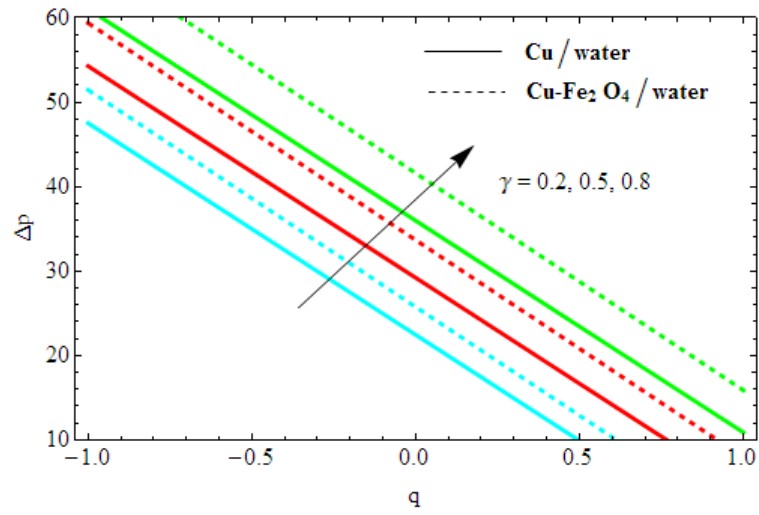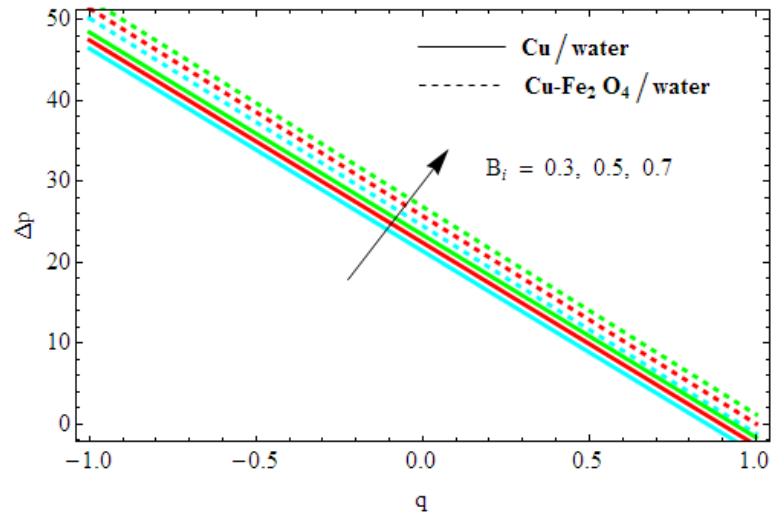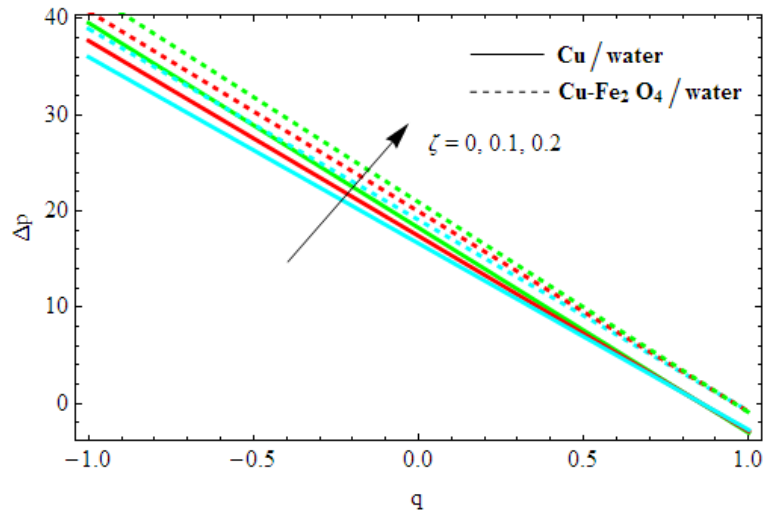*Fig.* 6.14, Distinct ζ for nanofluid and hybrid nanofluid pressure rise.
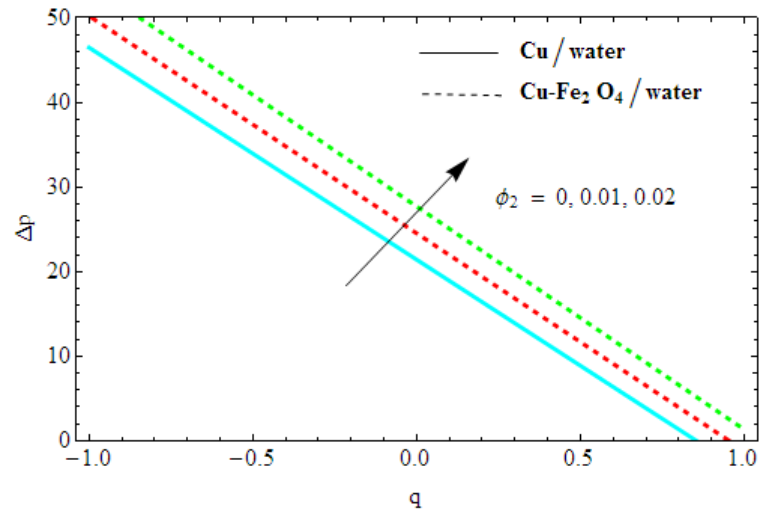
$Fig.$ 6.15, Distinct ϕ_2 for nanofluid and hybrid nanofluid pressure rise.
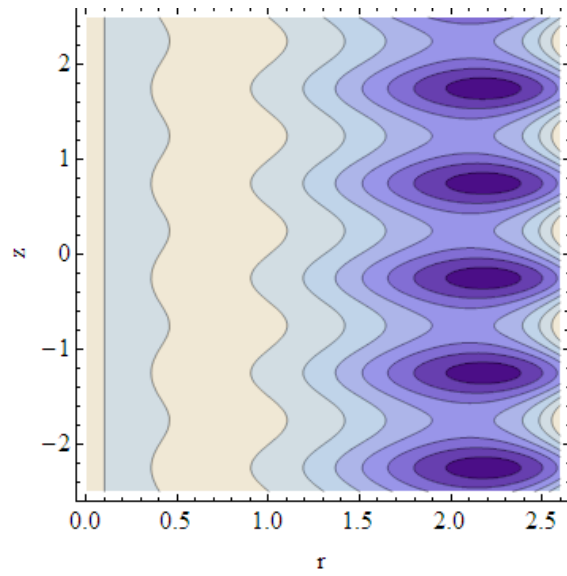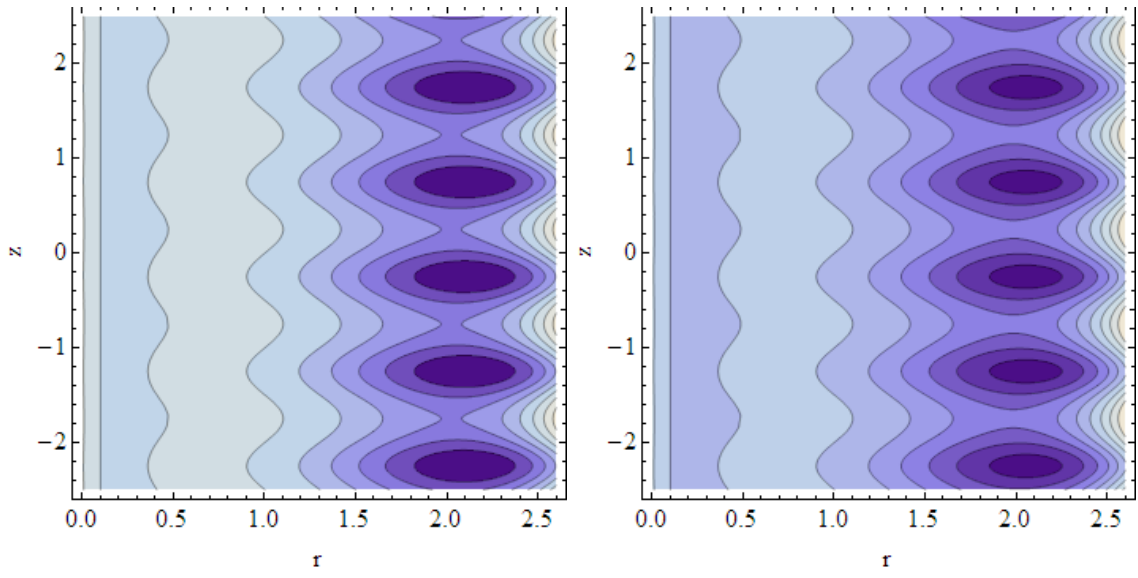
Figs. 6.16 (a, b, c), Streamlines for variation of G_r for hybrid nanofluid.
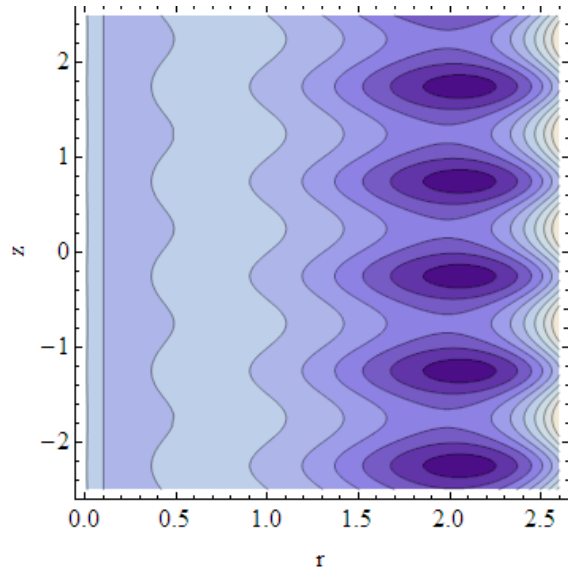
Figs. 6.17 (a, b, c), Streamlines for variation of γ for hybrid nanofluid.
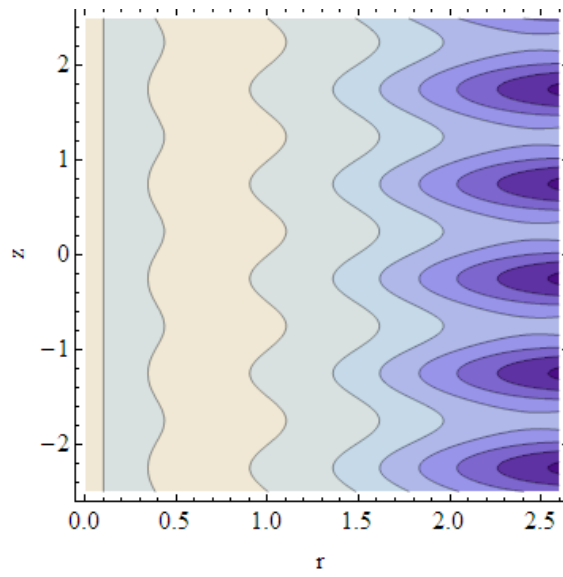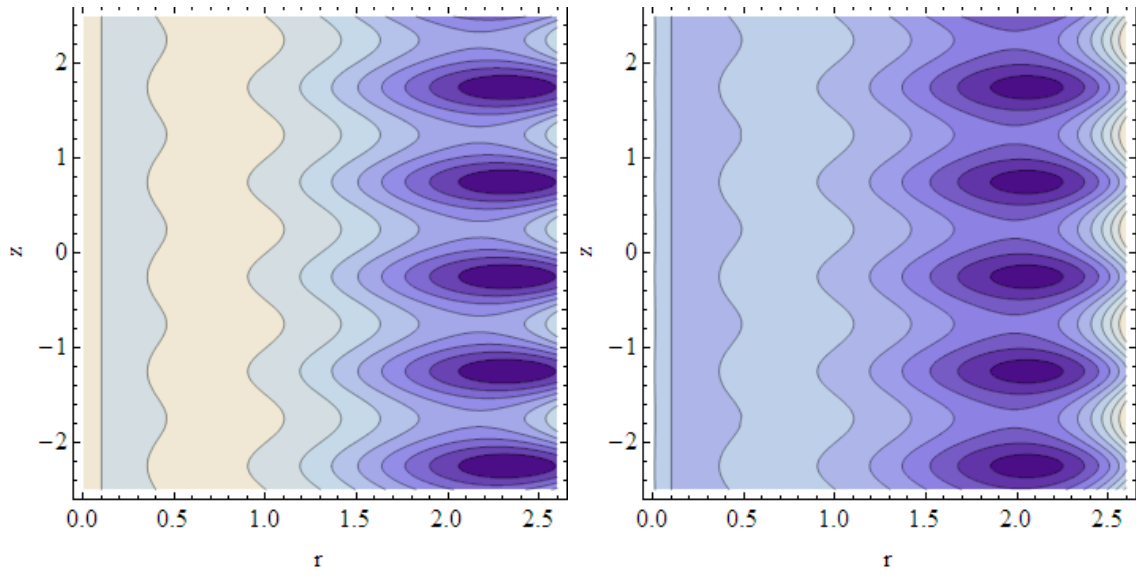
Figs. 6.18 (a, b, c), Streamlines for variation of ϕ_2 for hybrid nanofluid.
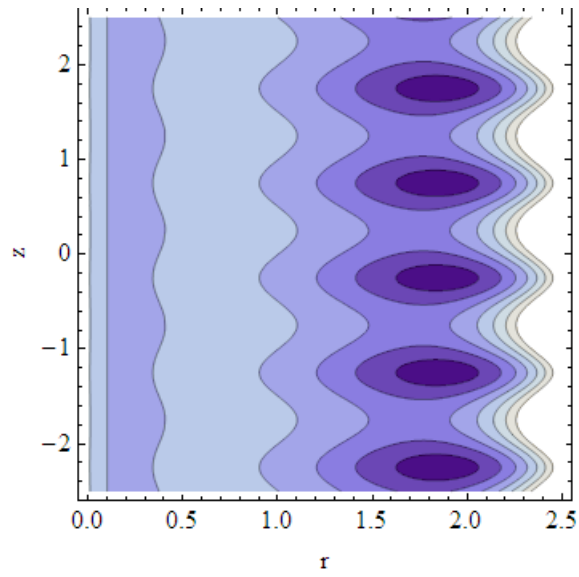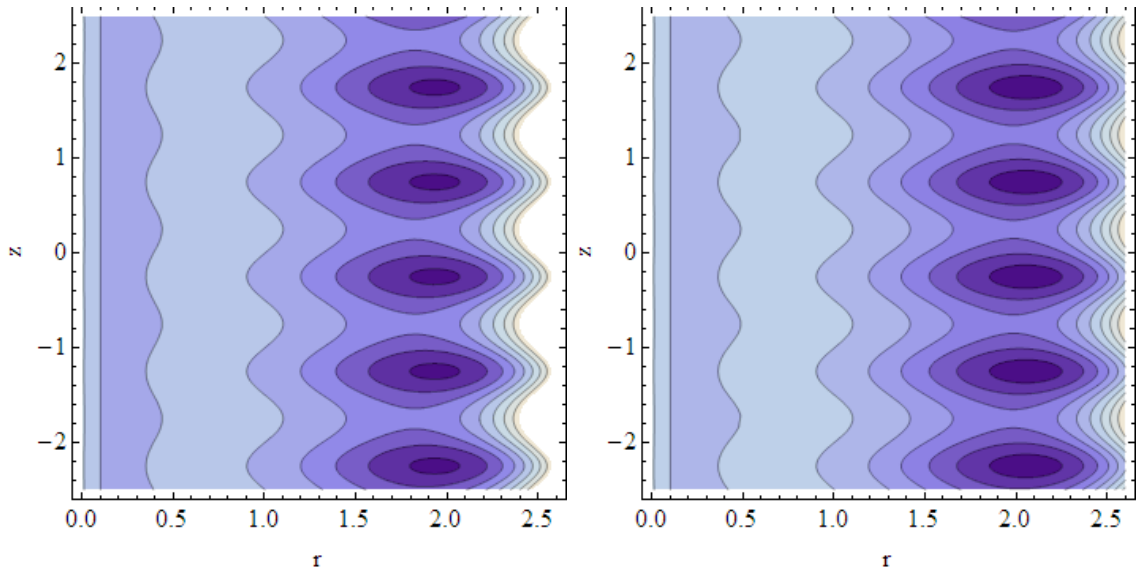
$Figs.$ 6.19 (a, b, c), Streamlines for variation of B_i for hybrid nanofluid.
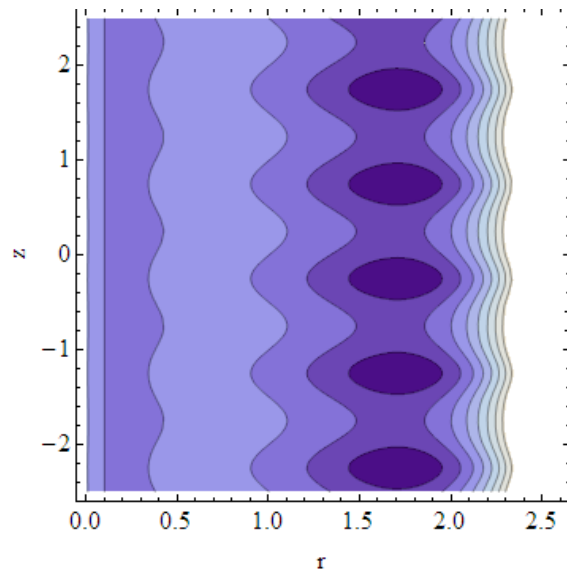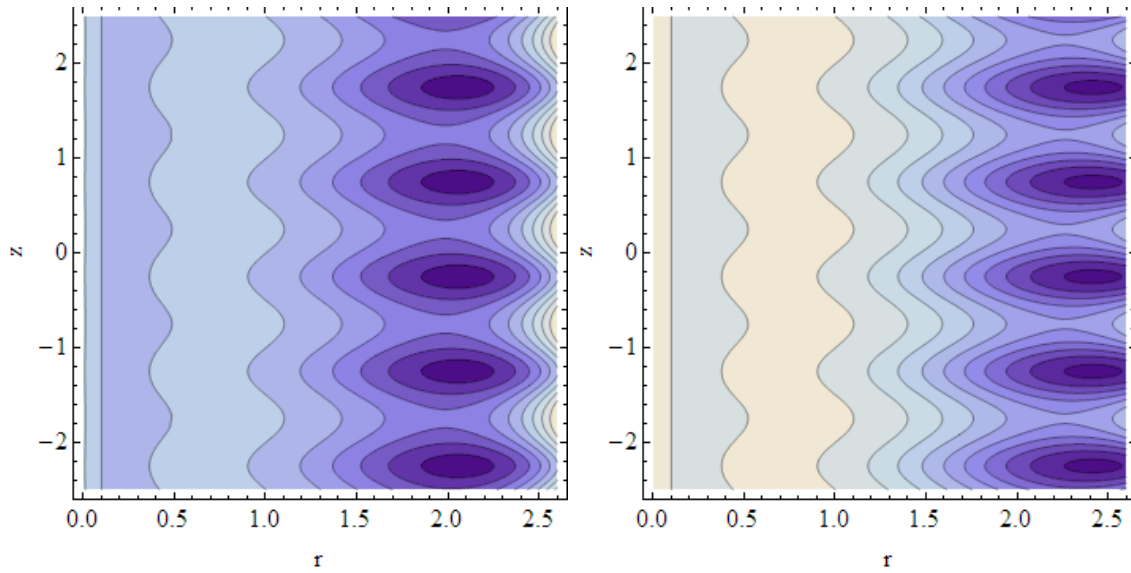
Figs. 6.20 (a, b, c), Streamlines for variation of ζ for hybrid nanofluid.

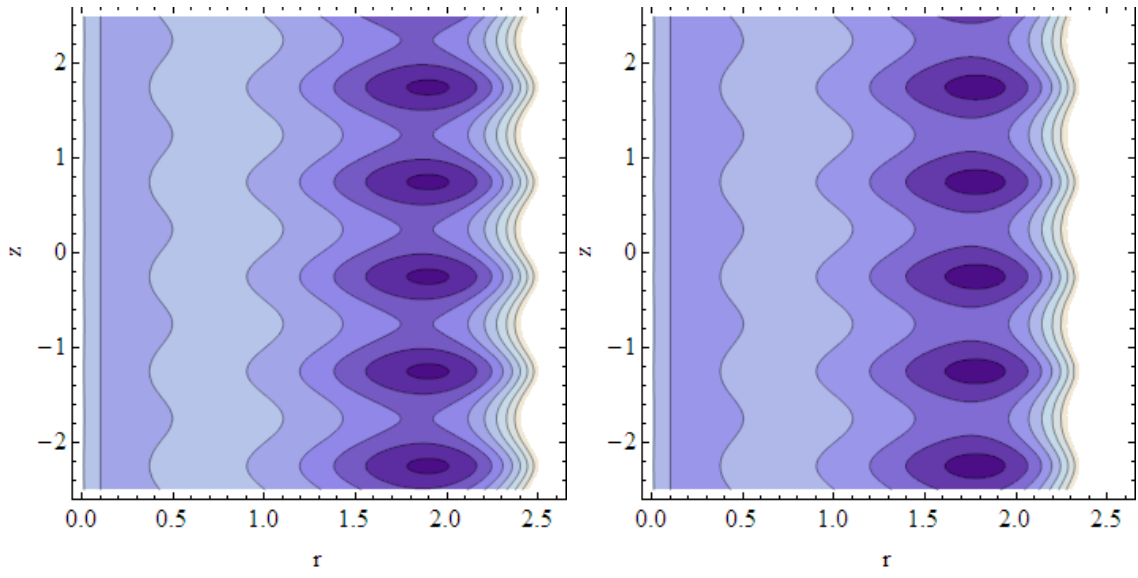| "r"	"γ"	"B_i"	"ζ"	"φ_2"	"$Cu/water$"	"$Cu - Fe_2O_4/water$"
0.1	0.2	0.5	0.5	0.05	1	1
0.3					0.718686	0.750885
0.5					0.579443	0.623342
0.3	0.2				0.718686	0.750885
	0.5				0.843552	0.922428
	0.7				0.926796	1.03679
	0.2	0.4			0.711517	0.740233
		0.5			0.718686	0.750885
		0.6			0.725635	0.761278
		0.5	0		0.748035	0.777608
			0.1		0.742165	0.772263
			0.2		0.736295	0.766919
			0.5	0.01	-	0.723957
				0.02	-	0.729733
				0.05	-	0.750885

Table. (6.1), Variation in temperature profile for both nanofluid and hybrid nanofluid.

"r"	"γ"	"B_i"	"ζ"	"φ_2"	"Cu/water"	"$Cu-Fe_2O_4/water$"
0.1	0.2	0.5	0.5	0.05	-1.39812	-0.977032
0.3					-0.481258	-0.344830
0.5					-0.312859	-0.233073
0.3	0.2				-0.481258	-0.344830
	0.5				-0.308248	-0.152668
	0.7				-0.192909	-0.024560
	0.2	0.4			-0.493711	-0.359271
		0.5			-0.481258	-0.344830
		0.6			-0.469308	-0.330861
		0.5	0		-0.437218	-0.312498
			0.1		-0.446026	-0.318964
			0.2		-0.454834	-0.325431
			0.5	0.01	-	-0.453449
				0.02	-	-0.425930
				0.05	-	-0.344830

Table. (6.2), Variation in heat transfer rate for nanofluid and hybrid nanofluid.

6.4   Conclusions

A detailed mathematical analysis has been done for hybrid nanofluid peristaltic flow through a curved tube with an endoscope inserted in it. Some observations of the present study made on the basis of graphical results are highlighted below

- Axial velocity elevates as we move from endoscope to the center of annular region.

- Pressure gradient exhibits higher results for hybrid nanofluid in comparison to nanofluid.

- Pressure rise shows positive attitude towards volume fraction.

- Higher concentration of Fe_2O_4 in base fluid results in higher temperature.

- Heat transfer rate is greater for hybrid nanofluid than nanofluid.

- Significant increase in the number of trapped bolus is observed for larger φ_2.

164

6.5 Appendix

$$C_1 = \frac{r_2(-4 - \gamma\frac{k_f}{k_{hnf}}r_1^2 + 2\gamma\frac{k_f}{k_{hnf}}r_2 + \gamma(\frac{k_f}{k_{hnf}})^2 B_i r_2^2)}{4(-1 + r_2\log r_1 - r_2\log r_2)}, C_2 = \frac{1}{4}(4 + \gamma\frac{k_f}{k_{hnf}}r_1^2) +$$

$$\frac{r_2\log\ r(-4 - \gamma\frac{k_f}{k_{hnf}}r_1^2 + 2\gamma\frac{k_f}{k_{hnf}}r_2 + \gamma(\frac{k_f}{k_{hnf}})^2 B_i r_2^2)}{4(-1 + r_2\log\ r_1 - r_2\log r_2)},$$

$$C_3 = -(-(\frac{C_1 r_1}{4} - \frac{1}{2}C_1 r_1\log\ r_1 + \frac{\gamma\frac{k_f}{k_{hnf}}r_1^3}{16})(-\frac{1}{r_2^2} + \frac{B_i\frac{k_f}{k_{hnf}}}{r_2}) +$$

$$\frac{-\frac{C_1}{4} - \frac{1}{2}\log\ r_2 + \frac{1}{4}C_1 B_i\frac{k_f}{k_{hnf}}r_2 - \frac{1}{2}C_1 B_i\frac{k_f}{k_{hnf}}r_2\log\ r_2 + \frac{1}{16}\gamma\frac{k_f}{k_{hnf}}r_2^2(3 + B_i\frac{k_f}{k_{hnf}}r_2)}{r_1}$$

$$)/(-r_1(-\frac{1}{r_2^2} + \frac{B_i\frac{k_f}{k_{hnf}}}{r_2}) + \frac{1 + B_i\frac{k_f}{k_{hnf}}r_2}{r_1}),$$

$$C_4 = -(-8C_1 r_1^2 r_2^2 + 8C_1 r_1^2 r_2^2\log\ r_1 - 8C_1 r_1^2 r_2^2\log\ r_2 - r_1^4 r_2^2\gamma\frac{k_f}{k_{hnf}} + 8C_1 r_1^2 r_2^3\log\ r_1 B_i\frac{k_f}{k_{hnf}}$$

$$-8C_1 r_1^2 r_2^3\log\ r_2 B_i\frac{k_f}{k_{hnf}} - r_1^4 r_2^3\gamma B_i(\frac{k_f}{k_{hnf}})^2 + 3\gamma\frac{k_f}{k_{hnf}}r_1^2 r_2^4 + \gamma B_i(\frac{k_f}{k_{hnf}})^2 r_1^2 r_2^5)/(16$$

$$(-r_1^2 + B_i(\frac{k_f}{k_{hnf}})r_1^2 r_2 - r_2^2 - B_i(\frac{k_f}{k_{hnf}})r_2^3)),$$

$$C_5 = -(-4AS[\frac{1}{4}(-C_1 + C_2 + C_1 r_1^2\log\ r_1 - \frac{\gamma\frac{k_f}{k_{hnf}}r_1^4}{64}] + 4AS[\frac{1}{4}(-C_1 + C_2 + C_1 r_2^2\log\ r_2 - \frac{\gamma\frac{k_f}{k_{hnf}}r_2^4}{64}]$$

$$+\frac{dp}{dz}r_1^2 - \frac{dp}{dz}r_2^2)/(4A(\log\ r_1 - \log\ r_2)),$$

$$C_6 = -(4A\log\ r_1 - 4A\log\ r_2 + 4A\log\ r_2 S[\frac{1}{4}(-C_1 + C_2 + C_1 r_1^2\log\ r_1 - \frac{\gamma\frac{k_f}{k_{hnf}}r_1^4}{64}] - 4A\log\ r_1 S$$

$$[\frac{1}{4}(-C_1 + C_2 + C_1 r_1^2\log\ r_1 - \frac{\gamma\frac{k_f}{k_{hnf}}r_1^4}{64}] - \frac{dp}{dz}r_1^2\log\ r_2 + \frac{dp}{dz}r_1^2\log\ r_2)/(4A(\log\ r_1 - \log\ r_2)),$$

$$C_7 = -\frac{1}{-\frac{r_1}{r_2} + \frac{r_2}{r_1}}(-1/r_2(\frac{C_5 r_1}{4} + \frac{C_4 S r_1}{4} - \frac{1}{2}(C_5 + C_4 S)r_1\log\ r_1 - \frac{1}{32A}(6\frac{dp}{dz} + A(C_1 - 2C_2 + 4C_3)S$$

$$-4AC_1 S r_1^3\log r_1 - \frac{1}{192}S\gamma\frac{k_f}{k_{hnf}}r_1^5) + 1/r_1((\frac{C_5 r_2}{4} + \frac{C_4 S r_2}{4} - \frac{1}{2}(C_5 + C_4 S)r_2\log\ r_2 - \frac{1}{32A}(6\frac{dp}{dz}$$

$$+A(C_1 - 2C_2 + 4C_3)S - 4AC_1 S r_2^3\log r_2 - \frac{1}{192}S\gamma\frac{k_f}{k_{hnf}}r_2^5),$$

$$C_8 = \frac{1}{192A(r_1^2 - r_2^2)}r_1^2(96AC_5 r_2^2\log r_1 + 96ASC_4 r_2^2\log r_1 - 96AC_5 r_2^2\log r_2 - 96ASC_4 r_2^2\log r_2 + 36\frac{dp}{dz}r_1^2 r_2^2$$

$$+6AC_1 S r_1^2 r_2^2 - 12AC_2 S r_1^2 r_2^2 + 24AC_3 S r_1^2 r_2^2 - 24AC_1 S r_1^2 r_2^2\log r_1 + AS\gamma\frac{k_f}{k_{hnf}}r_1^4 r_2^2 - 36\frac{dp}{dz}r_2^4 - 6AC_1 S$$

$$+12AC_2 S r_2^4 - 24AC_3 S r_2^4 + 24AC_1 S r_2^4\log r_2 - A\gamma\frac{k_f}{k_{hnf}}S r_2^6).$$

References

[1] T. W. Latham, Fluid motion in a peristaltic pumps, MS. Thesis, Massachusetts Institute of Technology, Cambridge, 1966.

[2] A. H. Shapiro, M. Y. Jafferian and S. L. Weinberg, Peristaltic pumping with long wavelengths at low Reynolds number, J. Fluid. Mech. 37 (1969) 799-825.

[3] R. A. Ramachandra and S. Usha, Peristaltic transport of two immiscible viscous fluids in a circular tube, J. Fluid Mech. 298 (1995) 271-285.

[4] A. Yildirim and S. A. Sezer, Effects of partial slip on the peristaltic flow of a MHD Newtonian fluid in an asymmetric channel, Math. C omput. Model, 52 (2010) 618-625.

[5] Y. A. Elmaboud, Influence of induced magnetic field on peristaltic flow in an annulus, Commun. Nonlinear. Sci. Numer. Simulat, 17 (2012) 685-698.

[6] H. Sato, T. Kawai, T. Fujia and M. Okabe, Two dimensional peristaltic flow in curved channels, Trans. Jpn. Soc. Mech. En. B, 66 (2000) 679-685.

[7] A. Kalantari, K. Sadeghy and S. Sadeqi, Peristaltic flow of non-Newtonian fluids through curved channels: a numerical stusy, Annual Transactions - The Nordic Rheology Society, 21 (2013) 163-170.

[8] N. Ali, M. Sajid, T. Javed and Z. Abbas, An analysis of peristatic flow of a micropolar fluid in a curved channel. Chin. Phys. Lett., 28 (2011) 014704.

[9] T. Hayat, M. Iqbal, H. Yasmin and F. Alsaad, Hall effects on peristaltic flow of couple stress fluid in an inclined asymmetric channel, Int. J. Biomath., 7 (2014) 1450057.

[10] P. U. Singh, R. S. Gupta, V. K. Kapur, On the steady performance of annular hydrostatic thrust bearing: Rabinowitsch fluid model, ASME J Tribol., 134 (2012) 1341.

[11] S. Jothi, A. R. Prasad, M. V. S. Reddy, Peristaltic flow of a Prandtl fluid in a symmetric channel under the effect of a magnetic field, Adv. Appl. Sci. Res., 3 (2012) 2108-2119.

[12] S. Nadeem and E.N. Maraj, The mathematical analysis for peristaltic flow of hyperbolic tangent fluid in a curved channel, Commun. Theor. Phys., 59 729 (2013).

[13] S. Nadeem, S. Ashiq, N. S. Akbar and C. Lee, Peristaltic flow of hyperbolic tangent fluid in a diverging tube with heat and mass transfer, J. Energy Engineering, 139 (2013) 94.

[14] A. Abbasi, I. Ahmad, N. Ali, and T. Hayat, An analysis of peristaltic motion of compressible convected Maxwell fluid, AIP Advances, 6 (2016) 015119.

[15] S. Nadeem, S. Ahmed, T. Mustafa and N. Muhammad, Chemically reactive species in the flow of a Maxwell fluid, Results in Physics, 7 (2017) 2607-2613.

[16] Carlton JMR, Yowell CA, Sturrock KA, Dame JB. Biomagnetic separation of contaminating host leukocytes from plasmodium-infected erythrocytes. Exp Parasitol 2001; 97 : $111 - 4$.

[17] Fuh CB, Lin LY, Lai MH. Analytical magnetapheresis of magnetically susceptible particles. J Chromatogr A 2000; 874 : $131 - 42$.

[18] Voltairas PA, Fotiadis DI, Michalis LK. Hydrodynamics of magnetic drug targeting. J Biomech 2002; 35 : $813 - 21$.

[19] Haik Y, Pai V, Chen CJ. Development of magnetic device for cell separation. J Magn Magn Mater 1999; 194 : $254 - 61$.

[20] Badescou V, Rotariu O, Murariu V, Rezlescu N. Transverse high gradient magnetic filter cell with bounded flow field. IEEE Trans Magn1997; 33(6) : $4439 - 44$.

[21] Ruuge EK, Rusetski AN. Magnetic fluid as drug carriers: targeted transport of drugs by a magnetic field. J Magn Magn Mater 1993; 122 : $335 - 9$.

[22] Plavins J, Lauva M. Study of colloidal magnetite binding erythrocytes: prospects for cell separation. J Mag Magn Mater 1993; 122 : $349 - 53$.

[23] V.I. Vishnyakov and K.B. Pavlov, "Peristaltic flow of a conductive fluid in a transverse magnetic field," Translated from Magnitnaya Gidrodinamika8, $174 - 178$ (1972).

[24] G. S. Beavers and D. D. Joseph, Boundary conditions at a naturally permeable wall, J. Fluid Mech., 30 (1967)197-207.

[25] P. D. Verma and H. K. Vyas, Viscous flow down and open inclined channel with naturally permeable bed, Indian J. Pure Appl. Math. 11 (1980) 165-172.

[26] N. S. Akbar, S. U. Rahman, R. Ellahi and S. Nadeem, Nanofluid flow in tapering stenosed arteries with permeable walls, Int. J. Therm. Sci., 85 (2011) 54-61.

[27] A. Rapits, N. Kafousias and C. Massalas, Free convection and mass transfer flow through a porous medium bounded by an infinite vertical porous plate with constant heat flux, Z. Angew. Math. Mech., 62 (1982) 489-491.

[28] C. Vasudev, U. R. Rao, G. P. Rao and M. V. S. Reddy, Peristaltic flow of a Newtonian fluid through a porous medium in a vertical tube under the effect of a magnetic field, Int. J. Cur. Sci., 3 (2011) 105-110.

[29] Kh. S. Mekheimer, Non-linear peristaltic transport through a porous medium in an inclined planar channel, J. Porous Medium, 6 (2003) 189-201.

[30] H. Sato, T. Kawai, T. Fujita, M. Okabe, Two dimensional peristaltic flow in curved channels, Trans. Jpn. Soc. Mech. Eng. B, 66 (2000), pp. 679-685.

[31] N. Ali, K. Javid, M. Sajid, O.A. Bég, Numerical simulation of peristaltic flow of a biorheological fluid with shear-dependent viscosity in a curved channel, Comput. Methods Biomech. Biomed. Eng., 19 (2016), pp. 614-627.

[32] C. Davies, P.W. Carpenter, Instabilities in a plane channel flow between compliant walls, J. Fluid Mech., 352 (1997), p. 205.

[33] A. Riaz, R. Ellahi, S. Nadeem, Peristaltic transport of Carreau fluid in a compliant rectangular duct, Alex. Eng. J., 53 (2014), pp. 475-484.

[34] S. Srinivas, M. Kothandapani, The influence of heat and mass transfer on MHD peristaltic flow through a porous space with compliant walls, Appl. Math. Comput., 213 (2009), pp. 197-208.

[35] M. O. Kramer, J. Readers Forum, Aerospace Sci., 68 (1960) 27.

[36] M. O. Kramer, Boundary layer stabilization by distributed damping, J. Amer. Soc. Nav. Engrs., 27 (1960) 69-69.

[37] T. K. Mittra and S. N. Prasad, On the influence of wallproperties and Poiseuille flow in peristalsis, J. Biomech., 6 (1973) 681-693.

[38] G. S. Dheia and M. A. Ahmed, Effects of wall properties and heat transfer on the peristaltic transport of a Jeffrey fluid through porous medium channel, Math. Theory Model., 4 (2014) 86-99.

[39] S. Sreenadh, C. U. Shankar and A. R. Pallavi, Effects of wall properties and heat transfer on the peristaltic transport of food bolus through oesophagus a mathematical model, Int. J. of Appl. Math and Mech., 8(2012)108.

[40] S. Srinivas, R. Gayathri and M. Kothandapani, The influence of slip conditions, wall properties and heat transfer on MHD peristaltic transport, Comp. Ph. Comm., 180 (2009) 2115-2122.

[41] G. Radhakrishnamacharya and Ch. Srinivasulu, Influence of wall properties on peristaltic transport with heat transfer, Comp. Red. Rend. Meca., 335 (2007) 369-373.

[42] S. Nadeem and E. N. Maraj and N. S. Akbar, Investigation of peristaltic flow of Williamson nanofluid in a curved channel with compliant walls, Appl. Nanosci., 4 (2014) 511-521.

[43] A. Ebaid, A new numerical solution for the MHD peristaltic flow of a bio-fluid with variable viscosity in a circular cylinderical tube via Adomian decomposition method, Phys. Let. A, 372 (2008) 5321-5328.

[44] S. Nadeem and N. S. Akbar, Influence of temperature dependent viscosity on peristaltic transport of a Newtonian fluid: Application of an endoscope, Appl. Math. Comput., 216 (2010) 3606-3619.

[45] A. Khan, R. Ellahi and K. Vafai, Peristaltic transport of a Jeffery fluid with variable viscosity through a porous medium in an asymmetric channel, Adv. Math. Phys., 2012 (2012) 169642.

[46] A. E. Hakeem, A. E. Naby, M. E. Misiery and Shamy, Hydromagnetic flow of fluid with variable viscosity in a uniform tube with peristalsis, J. Phys. A: Math. Gen., 36 (2003) 8585.

[47] F. M. Abbasi, T. Hayat, S. A. Shehzad, F. Alsaadi and Naif Altoaibi, Hydromagnetic peristaltic transport of copper-water nanofluid with temperature-dependent effective viscosity, Particuology, 27 (2016) 133-140.

[48] Kh. S. Mekheimer and Y.A. elmaboud, Peristaltic flow of a couple stress fluid in an annulus: application of an andoscope, Physica A, 387 (2008) 2403-2415.

[49] Kh. S. Mekheimer, Y.A. elmaboud, The influence of heat transfer and magnetic field on peristaltic transport of a Newtonian fluid in a vertical annulus: application of an endoscope, Phys. Lett. A., 372 (2008) 1657-1665.

[50] D. Tripathi, Peristaltic transport of fractional Maxwell fluids in uniform tubes, Applications in endoscopy, Comput. Math. Appls., 62 (2011)1116-1126.

[51] N. S. Akbar and S. Nadeem, Characteristics of heating scheme and mass transfer on the peristaltic flow for an Erying-Powell fluid in an endoscope, Int. J. Heat Mass Trans., 55 (2012) 375-383.

[52] I. C. Walton and S. H. Bittleston, The axial flow of a Bingham plastic in a narrow eccentric annulus, J. Fluid Mech., 222 (1991) 39-60.

[53] Kh. S. Mekheimer, Y. Abd elmaboud and A. I. Abdellateefe, Peristaltic transport through eccentric cylinders: mathematical model, Appl. Bionic Biomech., 10 (2013) 19-27.

[54] R. Ellahi, A. Riaz and S. Nadeem, Series solutions of magnetohydrodynamic peristaltic flow of a Jeffrey fluid in eccentric cylinders, Appl. Math. Inf. Sci., 7 (2013) 1441-1449.

[55] N. T. Eldabe, S. M. Elshaboury and A. H. Alfaisal, MHD peristaltic flow of a couple stress fluids with heat and mass transfer through a porous medium, Inno. Syst. Desi. Engin., 3 (2012) 51-67.

[56] A. Sinha, G. C. Shit and N. K. Ranjit, Peristaltic transport of MHD flow and heat transfer in an asymmetric channel: Effexts of variable viscosity, velocity slip and temperature jump, Alex. Eng. J., 54 (2015) 691-704.

[57] S. U. S. Choi and J. A. Eastman, Enhancing thermal conductivity of fluids with nanoparticles, Int. Mech. Eng. Cong. Expos., 66 (1995) 99-105.

[58] J. Buongiorno, Convective transport in nanofluids, ASME J. Heat Transf., 128 (2005) 240-250.

[59] C.T. Nguyen, G. Roy, C. Gauthier, N. Galanis, Heat transfer enhancement using Al2O3–water nanofluid for an electronic liquid cooling system. Applied Thermal Engineering 27, 8-9(2007) 1501-1506.

[60] N. A. Roberts, D. G Walker, Convective performance of nanofluids in commercial electronics cooling systems, Appl. Therm. Eng. 30, 16 (2010) 2499-2504.

[61] O. Mahian, A Kianifar, S. A. Kalogirou, I. Pop, S. Wongwises. A review of the applications of nanofluids in solar energy, Int. J. Heat Mass Transfer., 57, 2 (2013) 582-594.

[62] A. Ebaid, E. H. Aly, Exact analytical solution of the peristaltic nanofluids flow in an asymmetric channel with flexible walls and slip condition: application to the cancer treatment, Comput Math Methods Med (2013).

[63] O. Eytan, A. J. Jaffa, and D. Elad, Peristaltic flow in a tapered channel: application to embryo transport within the uterine cavity, Med Eng Phys, 23(2001) 473–482.

[64] Q. A. Pankhurst, J. Connolly, S. K. Jones, and J. Dobson, Applications of magnetic nanoparticles in biomedicine, J. Phys. D, 13(2003) R167.

[65] E. V. Timofeeva, J. L. Routbort and D. Singh, Particle shape effects on thermophysical properties of aluminna nanofluids, J. Appl. Phy., 106 (2009) 014304-10.

[66] V. V. Mody, A. Cox, S. Shah, A. Singh, W. Bevins and H. Parihar, Magneticnanoparticle drug delivery systems for targeting tumor. Appl. Nanosci., 4 (2014) 385-392.

[67] F. M. Abbasi, T. Hayat, S. A. Shehzad, F. Alsaadi and N. Altoaibi, Hydromagnetic peristaltic transport of copper-water nanofluid with temperature-dependent effective viscosity, Particuology, 27 (2016) 133-140.

[68] J. H. He, Homotopy perturbation technique, a new nonlinear analyical technique, Comput. Methods Appl., 135 (2013) 73-79.

[69] J. H. He, Application of homopoty perturbation method to nonlinear wave equations, Cha. Solit. Fractals, 26 (2015) 695-700.

[70] S. Nadeem, N. Abbas, On both MHD and slip effect in Micropolar hybrid nanofluid past a circular cylinder under stagnation point region, Canadian Journal of Physics, 97(2018) 392-399.

172

Turnitin Originality Report

Mathematical Observation for Peristaltic flows of Nanofluid in an Endoscope   by Nuzhat turnitin
Irshad .

From DRSM (DRSM L)

- Processed on 27-Jan-2021 10:09 PKT
- ID: 1495127052
- Word Count: 26782

Similarity Index
19%
Similarity by Source

Internet Sources:
7%
Publications:
14%
Student Papers:
10%

Focal Person (Turnitin)
Quaid-i-Azam University
Islamabad

sources:

1 5% match (student papers from 22-Dec-2017)
Submitted to Higher Education Commission Pakistan on 2017-12-22

2 1% match (publications)
Iqra Shahzadi, S. Nadeem. "Role of Inclined Magnetic Field and Copper Nanoparticles on
Peristaltic Flow of Nanofluid through Inclined Annulus. Application of the Clot Model",
Communications in Theoretical Physics, 2017

3 1% match (publications)
Behrouz Takabi, Hossein Shokouhmand. " Effects of – /water hybrid nanofluid on heat transfer
and flow characteristics in turbulent regime ", International Journal of Modern Physics C, 2015

4 1% match (Internet from 06-Aug-2020)
https://www.eurekaselect.com/160915/article

5 < 1% match (publications)
Iqra Shahzadi, S. Nadeem, Faranak Rabiei, "Simultaneous effects of single wall carbon
nanotube and effective variable viscosity for peristaltic flow through annulus having permeable
walls", Results in Physics, 2017

6 < 1% match (publications)
Iqra Shahzadi, S Nadeem. "Analysis of Ag/blood-mediated transport in curved annulus with
exclusive nature of convective boundary", Physica Scripta, 2019

7 < 1% match (student papers from 19-Jan-2017)
Submitted to Higher Education Commission Pakistan on 2017-01-19

8 < 1% match (student papers from 18-Dec-2017)
Submitted to Universiti Teknologi Malaysia on 2017-12-18

9 < 1% match (publications)